Pharmacological characterisation of the fatty acid receptors GPR120 and FFA1

Sarah-Jane Watson, BSc.

Thesis submitted to the University of Nottingham

for the degree of Doctor of Philosophy

NOVEMBER 2013

Abstract

In recent years, two G protein coupled receptors have been de-orphanised which respond to long chain free fatty acids (FFAs), and so are able to mediate the signalling of these important nutrient molecules. FFA1 (GPR40) is predominantly expressed in pancreatic β-cells, while the expression profile of GPR120 includes gut endocrine cells and adipose tissue. These distributions, together with the potential of both receptors to stimulate insulin and incretin hormone secretion, singled them out as potential drug targets for type 2 diabetes and obesity. The aim of this thesis was to evaluate the pharmacology of these receptors and their signalling properties, including the development of fluorescent FFA receptor ligands to evaluate agonist binding using imaging techniques.

GPR120 has been identified to exist as two splice isoforms in humans, differing by a short insertion in the third intracellular loop, but no full isoform specific characterisation of receptor signalling and trafficking had been undertaken. This work therefore studied the GPR120S and GPR120L isoforms in terms of both G protein dependent and β–arrestin dependent signalling, and trafficking. It was found that the long GPR120L isoform exhibited reduced G protein signalling, but similar β-arrestin recruitment and lysosomal intracellular trafficking profiles as GPR120S. Potentially, expression of the long GPR120 isoform provides a mechanism to direct signalling to the β-arrestin pathway, for example to produce anti-inflammatory effects in macrophages. As the expression profile of GPR120 overlaps with that of FFA1, for example in

colonic endocrine cells, a series of constrained GPR120 homo-dimers and GPR120:FFA1 heterodimers were created using irreversible bimolecular fluorescence complementation, and the potential for novel pharmacology was investigated by monitoring dimer internalisation. However, there was no evidence that such dimerisation altered the pharmacology of the ligands tested. Second, a model of the GPR120S ligand binding site was tested using point mutagenesis of the receptor. This mutagenesis validated key features of the model, including the role of Arg99 in co-ordinating the agonist carboxylate group, and interactions of the agonists with the conserved transmembrane VI Trp "toggle-switch" involved in receptor activation. Another mutation (Asn215) provided evidence for ligand-specific binding modes within the pocket. This study showed the complexity of testing mutants designed to interfere with ligand binding indirectly through signalling assays and highlighted the requirement for a FFA receptor binding assay to measure ligand affinity directly.

In the absence of radioligands of suitable selectivity and affinity, a novel fluorescent ligand, based on the FFA1/GPR120 agonist GW9508, was used to successfully develop a whole cell FFA1 competition binding assay for the first time, obtaining FFA1 affinity estimates for a range of synthetic ligands. Fluorescent ligand binding was further investigated using fluorescence correlation spectroscopy and photon counting histogram analysis, defining the diffusion characteristics of FFA1 receptors in the membrane of single living cells, and providing preliminary evidence for their dimerisation.

Acknowledgements

I would like to thank Dr Nick Holliday and Dr Steve Hill for the great opportunity to do this PhD project. I am especially grateful to Nick, for letting me briefly escape to New Zealand when I should have been writing my thesis!

I would also like to thank CellAura, Nottingham for synthesis of 40Ag-Cy5; and both the EPSRC and AstraZeneca for financial support. Thanks also to my industrial supervisor Alastair Brown for hosting my times at Alderley Park, Graeme Robb for his model of the GPR120 binding site and both for helpful discussions of my data.

I have especially enjoyed my time being part of the Institute of Cell Signalling, not least for the many cakes over the years! Thanks to all the ICS members, past and present, for scientific support and for the great times had at home and away at conferences overseas. Special thank-yous go to Laura Kilpatrick for answering every little question I have ever had; Dr Leigh Stoddart for being my point of reference for FFA receptors; Dr Rachel Thomas for her supportive pep talks; Marleen Groenen for her assistance, Dr Steve Briddon for his help with FCS and Tim Self for his training and expertise when using the microscopes.

I would also like to thank my family and my friends outside of science, who still have no idea what I do, but are supportive nonetheless.

Avslutningsvis vill jag tacka mina svenska vänner Josie Gilbert, Lars Bergström, och speciellt Jens Haapalahti… ***tack så mycket!***

Papers

Watson SJ, Brown AJ, Holliday ND (2012) Differential signaling by splice variants of the human free fatty acid receptor GPR120 *Mol Pharmacol*. **81**(5):631-42

Holliday ND, Watson SJ, Brown AJ (2012) Drug discovery opportunities and challenges at G protein-coupled receptors for long chain free Fatty acids *Front Endocrinol (Lausanne)* **3**;2:112

Abbreviations

2-APB	2-aminoethoxydiphenyl borate
AF	AlexaFluor
β_2AR	β_2 adrenoceptor
BG	benzyl guanine
BRET	bioluminescence resonance energy transfer
BSA	bovine serum albumin
CCK	cholecystokinin
cAMP	adenosine-3',5' cyclic monophosphate
DHA	docosahexaenoic acid
DMEM	Dulbecco's modified Eagle's medium
DMSO	dimethyl sulphoxide
EC_{50}	concentration for 50% maximal response
ECL	extracellular loop
ERK	extracellular signal-related protein kinase
FBS	foetal bovine serum
FCS	fluorescence correlation spectroscopy
FFA	free fatty acid
FRET	fluorescence resonance energy transfer
GDP	guanosine diphosphate
GEF	guanine nucleotide exchange factor
GFP	green fluorescent protein
GI	gastrointestinal

GIP	glucose-dependent insulinotropic peptide
GLP-1	glucagon-like peptide-1
GPCR	G protein-coupled receptor
GRK	GPCR related kinase
GSIS	glucose stimulated insulin secretion
GTP	guanosine 5’ triphosphate
HBSS	Hepes buffered saline solution
HEK	human embryonic kidney
IC_{50}	concentration for 50% inhibition
ICL	intracellular loop
IP_3	inositol 1,4,5-trisphosphate
JNK	c-Jun N-terminal kinase
Ki	equilibrium dissociation constant
LB	Luria Bertani
MAPK	mitogen activated protein kinase
Met36	Metabolex compound 36
PP2A	protein phosphatase 2A
PPAR	perioxisome proliferator-activated receptor
PBS	phosphate buffered saline
PCH	photon counting histogram
PDE	phosphodiesterase
PIP_2	phosphatidylinositol 4,5-bisphosphate
PLC	phospholipase C

PTx	*Pertussis* toxin
PUFA	polyunsaturated fatty acid
PKA/C	Protein kinase A or C
S1P	sphingosine-1-phosphate
SOCE	store operated calcium entry
TM	transmembrane helix
TZD	thiazolidinedione
vYFP	venus yellow fluorescent protein
vYC	carboxyl fragment (173-238) venus yellow fluorescent protein
vYN	amino fragment (2-172) venus yellow fluorescent protein
WT	wild type

Table of contents

Chapter One: Introduction

1.1 Fatty acids

Fatty acid nutrients are classically seen as an important energy source, as their β oxidation in the mitochondria yields energy (Yaney and Corkey, 2003). Fatty acids are also central to the synthesis and composition of other cellular lipids, for example the phospholipids that make up the plasma membrane (Williams et al., 2012).

Increasingly however, free fatty acids (FFAs), where "free" refers to fatty acids that are not bound to carrier proteins such as albumin in plasma, have been shown to play diverse roles in intracellular signalling. Originally, these signalling roles were thought to be fulfilled indirectly via effects on metabolism and through nuclear localised peroxisome proliferator-activated receptors (PPARs) (Michalik et al., 2006). More recently, this signalling has also been shown to be elicited through membrane localised receptors, such as the fatty acid receptor family of G protein-coupled receptors (GPCRs) (Stoddart et al., 2008).

Understanding these FFA signalling pathways is critical in unravelling the complex picture of the roles different types of FFA play in nutrition, and in targeting such pathways therapeutically. Some dietary fatty acids are seen as "beneficial", such as ω-3 polyunsaturated fatty acids in fish oils, for example in having a neuroprotective effect in Alzheimer's disease (the nomenclature of fatty acids is covered in section 1.4.1). Unfortunately, evidence can be either

for (Hashimoto and Hossain, 2011), or against increasing ω-3 fatty acids in the diet (Yip et al., 2013). Other FFAs are seen as damaging, for example supplementing the diet with ω-6 unsaturated fatty acids such as linoleic acid has been shown to increase the risk of cardiovascular disease mortality (Ramsden et al., 2013). Some work has suggested that the ratio of dietary FFAs (e.g. ω-3:ω-6 unsaturated FFAs) is key for a beneficial effect upon fertility (Yan et al., 2013). Equally the dual action of different types of fatty acids as nutrients and as signalling molecules is linked to the pathogenesis and possible treatment of metabolic diseases, for example obesity (Buckley and Howe, 2010) and type II diabetes (Petit et al., 2012). In this introduction, the different mechanisms by which FFAs elicit intracellular signalling are briefly reviewed, before focusing on the potential physiological roles and signalling mechanisms of the recently identified FFA GPCRs, which are the subject of this thesis.

1.2 Types of FFA signalling

1.2.1 Effects via metabolism and as signalling precursors

β oxidation in the mitochondria is the process which breaks down fatty acids into acetyl-Coenzyme A (CoA) for entry into the tricarboxylic acid cycle. This yields reduced NADH (nicotinamide adenine dinucleotide) and $FADH_2$ (flavin adenine dinucleotide) which can then enter the electron transport chain to generate energy in the form of adenosine triphosphate (ATP) (Porter and Brand, 1995). The ratio of acetyl-CoA to CoA fluctuates depending on the metabolic status of the cell, and therefore signals the nutrient status of the

cell. For example if there is a high level of nutrients, there will be a higher level of acetyl-CoA. Acetylation has also been shown to regulate both the activity of metabolic enzymes and the expression of their genes (Wellen and Thompson, 2012). Meanwhile, malonyl-CoA is produced from the carboxylation of acetyl-CoA, and regulates the activity of carnitine acyltransferase, preventing long chain fatty acids being taken up into the mitochondria for β oxidation (Graciano et al., 2011).

The relationship between the cellular uptake and β-oxidation of fatty acids must be balanced, as intracellular accumulation outweighing β-oxidation can lead to the engagement of alternative metabolic pathways which for example, may contribute to insulin resistance (Zhang et al., 2010a). One such process in skeletal muscle cells involved the metabolism of the saturated FFA palmitate into the inflammatory molecule ceramide (Sabin et al., 2007). Free fatty acids are also precursors which can affect production of many other lipophilic signalling molecules, such as cannabinoids (Kim et al., 2011), prostaglandins (Hellmann et al., 2013), leukotrienes (Norris and Dennis, 2012), and sphingosine (Huwiler and Pfeilschifter, 2009).

1.2.2 The influence of FFAs on cellular membranes

The plasma membrane is made up of a phospholipid bilayer, formed due to the nature of the phospholipids. They are made up of a hydrophilic phosphate headgroup (orientated towards the aqueous environment) and two hydrophobic fatty acid tails. The different types of fatty acids incorporated into phospholipids present in the plasma membrane can influence membrane

fluidity. Phospholipids containing saturated fatty acids (rigid, lacking double bonds) can aggregate in lipid rafts (that also contain the lipid cholesterol), whilst unsaturated fatty acid tails have rotation around their double bonds, and form a more fluid membrane excluding cholesterol (the structures of FFAs are covered in section 1.4.1) (Williams et al., 2012). Saturated lipid rafts have received attention as "microdomains" within the plasma membrane that might organise protein signalling complexes, for example containing G protein coupled receptors (Bjork and Svenningsson, 2011).

There are several examples of how different fatty acids can have a modulatory role upon membrane receptors, by their incorporation into lipids to influence the plasma membrane environment. It was found that a higher concentration of phosphatidylcholine containing ω-6 fatty acid (compared to ω-3) in the plasma membrane caused a reduction in G protein-coupled signalling from the light receptor rhodopsin. This was thought to be due to the double bond at ω-6 docosapentaenoic acid (DPA) instead of at ω-3 docosahexaenoic acid (DHA), that appears to directly impact the conformation changes associated with rhodopsin activation (Mitchell et al., 2012) Also, DHA and DPA supplementation of cells expressing Toll-like receptor (TLR)-4, found that the subsequent activation of TLR-4 led to the increased release of fatty acids from membrane lipids (via lipase activity) that selectively inhibited cyclooxygenase pathways, therefore having an anti-inflammatory effect (Norris and Dennis, 2012). It has also been found that fatty acids can modulate the activity of potassium and sodium ion channels and that this can be exploited therapeutically in the treatment of epilepsy. The presence of polyunsaturated

fatty acids (PUFAs) in the diet, such as DHA, resulted in the hyperpolarisation of the plasma membrane in isolated pyramidal neurones, preventing the hyper excitability associated with epileptic seizures (Tigerholm et al., 2012). ω-3 fatty acids have also been shown to play a direct and indirect signalling role upon transient receptor potential (TRP) channels in neurodegeneration (Leonelli et al., 2011). Interestingly, FFAs have a diverse range of effects upon TRP channels. They can act both directly upon these channels or can modulate TRP activity indirectly by having an effect upon the plasma membrane lipids. For example DHA was found to be a potent agonist, whilst linolenic acid was an antagonist directly at TRPV1 (Matta et al., 2007). On the other hand, these effects could be mediated by the fact that PUFAs alter the composition of plasma membrane lipids around the receptor (Bruno et al., 2007).

In addition to the plasma membrane, the presence of different dietary FFAs can alter the composition of other cellular membrane bilayers with functional significance. For example cardiolipin is a dimeric phospholipid (with four acyl fatty acid tails) found in the inner mitochondrial membrane. It is thought to be required for various mitochondria functions, and that its effects can be regulated by cardiolipin remodelling with different fatty acids. For example supplementation of DHA has been shown to have a positive effect in preventing mitochondrial cell death, thought to be due to it having an unsaturating effect upon cardiolipin composition (Khairallah et al., 2012). Potentially, this could be used in treating mitochondrial dysfunction in various disorders, such as Parkinson's (Chao et al., 2012), Alzheimer's (Eckert et al., 2012) and cardiovascular disease (Stanley et al., 2012).

1.2.3 The PPAR family of nuclear receptors

The PPAR family of receptors are ligand activated transcription factors. Arguably, they were the first free fatty acid receptors to be identified, responding intracellularly to the fatty acids and their derivatives. Following activation by lipid ligands in the cytoplasm, PPARs translocate to the nucleus and form heterodimers with the retinoid x receptor. Using a de-repression mechanism, these heterodimers then activate the expression of genes related to lipid homeostasis and metabolism, which lower circulating lipid levels and increase insulin sensitivity. They activate or suppress genes involved in metabolism, but the activity of which specific genes they modulate depends on the subtype in question, of which there are 3: α, β/δ and γ (Sugden and Holness, 2008).

The endogenous ligands for the PPAR**α** subtype include fatty acids and other mediators such as prostaglandins. This subtype plays a role in regulating β-oxidation of fatty acids in the liver and skeletal muscle, adapting metabolism in response to a change in nutrition. These genes are involved in lipid catabolism and homeostasis, and their activation results in increasing the oxidation and uptake of fat, and decreasing the synthesis of fatty acids (Cook et al., 2000). It is a clinical target for dyslipidaemia (Nicholls and Uno, 2012), using synthetic agonists such as clofibric acid, and was also surprisingly found to be a modulator of inflammation (Belfort et al., 2010).

The PPAR**β/δ** subtype is found in all tissues, but the least is known about this subtype. Its activation represses genes involved in lipid metabolism to

increase fat oxidation (Roberts et al., 2011). Selective agonists suggest a clinical role in improving insulin sensitivity and perhaps a use in the treatment of diabetes (Salvado et al., 2012).

There are two subtypes of PPAR**γ** found in pancreas and skeletal muscle, and adipose tissue. Its activation modulates genes involved in insulin signalling, glucose and lipid homeostasis (Herzig et al., 2003) and lipid storage, playing a role in adipocyte differentiation (Floyd and Stephens, 2012; Roberts et al., 2011; Virtue et al., 2012). Its activation also has an anti-inflammatory effect (Liao et al., 2007). PPARγ agonists, such as thiazolidinediones (TZDs) have been used in the past as insulin sensitisers in type II diabetes, but recently these have also been associated with an increased cardiovascular risk (see section 1.4.4.1.1.4).

1.2.4 Fatty acid receptor family of GPCRs

More recently, FFA mediated signalling has also been shown to be elicited through plasma membrane localised GPCRs (Stoddart et al., 2008). One FFA family of GPCRs is found in a cluster present on chromosome 19q13.1. This cluster contains GPR40, also known as **f**ree **f**atty **a**cid receptor **1** (FFA1) along with GPR41 (FFA3), GPR42 (an inactive pseudogene in man) and GPR43 (FFA2). FFA2 and FFA3 are activated by short chain FFAs (Brown et al., 2003; Le Poul et al., 2003; Nilsson et al., 2003). FFA2 is expressed in the immune cells (Le Poul et al., 2003), adipose tissue (Brown et al., 2003; Nilsson et al., 2003) and the gastrointestinal (GI) tract (Karaki et al., 2006; Karaki et al., 2008). FFA2 plays a role in the stimulation of adipogenesis and inhibition of

lipolysis (Ge et al., 2008; Hong et al., 2005). Meanwhile, FFA3 is also expressed in the adipose tissue (Brown et al., 2003), the immune cells (Brown et al., 2003; Le Poul et al., 2003) and the GI tract (Tazoe et al., 2009), and has been shown to be involved in the production of the anorexigenic hormone, leptin (Xiong et al., 2004).

FFA1 receptors (Briscoe et al., 2003; Itoh et al., 2003; Kotarsky et al., 2003), together with the distantly related GPR120 found on chromosome 10q23.33 (Fredriksson et al., 2003a), are activated by medium to long chain FFAs (Hirasawa et al., 2005). FFA1 is predominantly expressed in pancreatic β cells and GI tract (Briscoe et al., 2003; Itoh et al., 2003; Kotarsky et al., 2003) and one of its key roles is the potentiation of glucose stimulated insulin secretion (GSIS) from β cells (Briscoe et al., 2003). GPR120 is predominantly expressed in intestinal enteroendocrine cells (e.g. L cells), as well as in the lungs and adipose tissue (Gotoh et al., 2007; Hirasawa et al., 2005) and is thought to play a role in the secretion of satiety gut hormones, also known as incretins, such as cholecystokinin (CCK) (Tanaka et al., 2008a) and glucagon-like peptide-1 (GLP-1) (Tanaka et al., 2008b). These two receptors will be discussed in more detail later in the introduction (section 1.4).

There are two more unrelated receptors which respond to fatty acids or their close derivatives: GPR84 and GPR119. GPR84 is expressed on macrophages, and has been postulated to be a pro-inflammatory receptor (Suzuki et al., 2013). It is activated by medium chain fatty acids (C9-14) (Nagasaki et al., 2012), and this amplifies the production of pro-inflammatory cytokines, for

example in macrophages (Suzuki et al., 2013). Tumour necrosis factor (TNF) α has been shown to upregulate expression of GPR84 in adipocytes, suggesting its participation in metabolic inflammation contributing to the vicious cycle between obesity and type II diabetes (Nagasaki et al., 2012).

GPR119, on the other hand, responds to ethanolamide derivatives of fatty acids and phospholipids (Soga et al., 2005). It is expressed in the pancreatic β cell (Soga et al., 2005) and in intestinal endocrine L cells in the GI tract (Lauffer et al., 2009). Its activation in the pancreatic β cell leads to glucose dependent insulin secretion, through coupling to Gs to cause an increase in cyclic adenosine monophosphate (cAMP) levels (Soga et al., 2005), whilst activation in the L cell leads to the release of GLP-1 and other peptide hormones (Lauffer et al., 2009). Both oleoylethanolamide and a synthetic agonist at GPR119 were found to suppress food intake and reduce body weight in rodents (Overton et al., 2006). A summary of the ligands of FFAs at the FFA family of receptors is shown in Figure 1.1.

There are also other families of lipid GPCRs which are not phylogenetically related, but can still share related agonist pharmacology, for example the cannabinoid receptors and the sphingosine-1-phosphate receptor subtypes. There are two cannabinoid receptors, CB1 and CB2. CB2 is involved in immune responses, whilst CB1 is expressed both centrally and peripherally, and is involved in glucose and lipid metabolism (Cavuoto et al., 2007). They are activated by lipid derived endocannabinoids such as anandamide (also shown in Figure 1.1), which are endogenously produced from phospholipids

containing arachidonic acid present in the plasma membrane of cells (Newman et al., 2007). In relation to the therapeutic opportunities presented by other fatty acid receptors (discussed in section 1.4.4), the CB1 receptor has been a target for obesity treatments (the inverse agonist rimonabant, now withdrawn for its depressant side effects (Despres et al., 2005)), as centrally expressed receptors play a role in controlling appetite (Kim et al., 2013b). The five sphingosine-1-phosphate (S1P) receptor subtypes are activated by S1P and lysophosphatidic acid (Rosen et al., 2009). S1P is a lipid mediator generated from sphingomyelin, thought to play in a role in the positive cardiovascular effects of high density lipoprotein (HDL) (Rodriguez et al., 2009). Interestingly, blockade of S1P receptor signalling was also found to slow the onset of streptozotocin induced diabetes (Imasawa et al., 2010). Also, treatment with immunomodulatory drug fingolimod (FTY720; an S1P receptor 1 agonist following its phosphorylation by sphingosine kinase), prevented weight gain and increased insulin sensitivity in mice, implicating this receptor as another possible therapeutic target in type II diabetes (Kendall and Hupfeld, 2008).

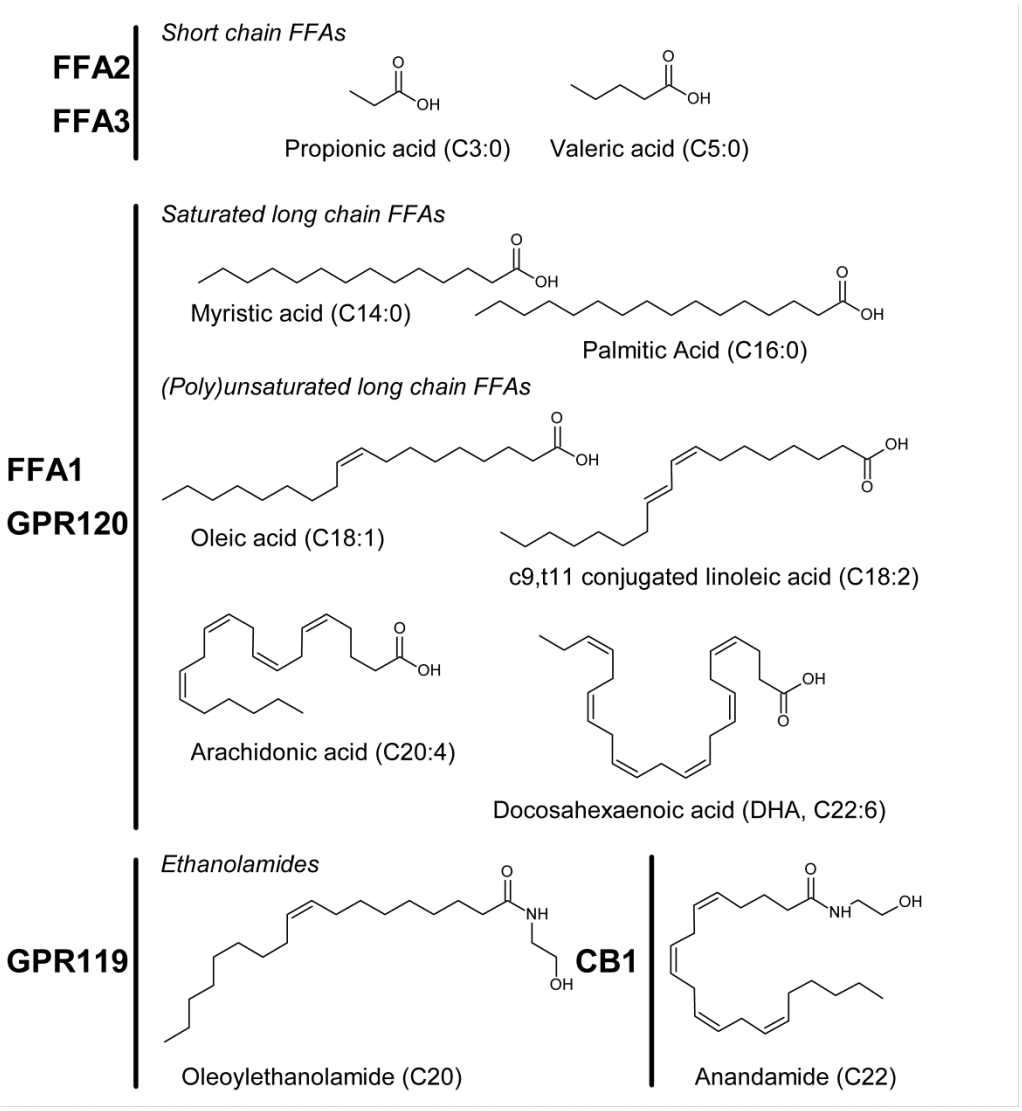

Figure 1.1 Structures of ligands at fatty acid receptors

Structures of the various ligands at members of the FFA receptor family. Short chain FFAs at FFA2 and FFA3; medium to long chain FFAs at FFA1 and GPR120; and FFA derivatives at GPR119. Also included is anandamide, the agonist for the cannabinoid receptor, CB1. The ω-x nomenclature for unsaturated FFAs derives from the first position of the double bond(s) relative to the terminal methyl of the acyl chain; i.e. ω-3 (3rd bond, such as DHA), ω-6 (6th bond; arachidonic acid, linoleic acid), ω-9 (9th bond; oleic acid).

1.3 G protein-coupled receptors

The FFA plasma membrane GPCRs are part of a receptor family of more than 800 distinct proteins, contributing to approximately 1-2 % of the human genome (Fredriksson et al., 2003b). This great number of GPCRs allows for them as a whole to respond to a great variety of ligands such as photons, amino acids, peptides, proteins, lipids, carbohydrates and other small organic compounds (Lagerstrom and Schioth, 2008). Thus GPCRs play a fundamental role in cell to cell communication between different cell types in the body, essential for whole body homeostasis. GPCRs are also already well-represented as drug targets. They are the object of 25-30 % of current drugs (Overington et al., 2006), though these only target only a small number of GPCRs, ~30 (Wise et al., 2004). As a group, GPCRs have similarities, but also contain differences which allow for their division into families by functional and structural similarity.

1.3.1 Classification

The first attempt to classify GPCRs assigned them into six groups, A - F (Kolakowski, 1994). This classification system has been further embellished over the years, condensing into five groups (Bockaert and Pin, 1999; Fredriksson et al., 2003b). This latest classification system is called the GRAFS system and relates to the non-sensory GPCRs, giving families based on phylogenetic analysis: glutamate (also called class C), rhodopsin (class A), adhesion, frizzled and secretin (class B) (Fredriksson et al., 2003b).

Class A comprises of rhodopsin-like GPCRs, which is the largest group, containing almost 700 GPCRs (~400 olfactory GPCRs, with the other ~300 being non-sensory GPCRs). Receptors within this group typically have short amino termini and are activated by the ligand binding within the TM helices or the extracellular loops (Bockaert and Pin, 1999). This group can be further split into 4 smaller groups. The α subgroup contains many pharmaceutically relevant monoamine receptors, such as the β adrenoceptors, the muscarinic receptors, the histamine receptors, the dopamine receptors and the serotonin receptors. The small amine ligands bind within the transmembrane (TM) helices of these receptors (Rosenbaum et al., 2007). The fatty acid receptors also belong to this group. The β subgroup predominantly contains peptide receptors such as the neuropeptide Y family of receptors, the oxytocin receptor and the neurokinin-1 receptor. These peptide ligands also bind within the TM helices, but with additional involvement from the extracellular loops (ECLs) (Fong et al., 1992). Meanwhile, the γ subgroup includes both peptide receptors and lipid receptors such as the opioid receptors and the chemokine receptors; whilst glycoprotein and olfactory receptors belong to the δ sub-group (Fredriksson et al., 2003b).

Class B is an amalgamation of the secretin-like group of receptors and the adhesion group of receptors. The secretin-like peptide receptors include the secretin receptor, the glucagon receptor, the glucagon-like peptide receptor and the gastric inhibitory polypeptide receptor. They typically contain a large amino terminus which contain six cysteine residues that form disulphide bridges, thought to be key for forming the ligand binding domain for peptide

hormones (Grace et al., 2004; Lisenbee et al., 2005). Meanwhile, the adhesion receptors also have a large amino terminus (Bjarnadottir et al., 2004), but differ from the secretin receptors by the fact their amino termini may contain proteolytic domains, and that they also bind extracellular matrix molecules (Krasnoperov et al., 2002).

Class C receptors are the metabotropic receptors, that respond to neurotransmitters glutamate and **γ**-**a**mino**b**utyric **a**cid (GABA), calcium, and to sweet and unami taste molecules. They also contain a large globular amino terminus motif called a Venus fly trap (VFT) motif, containing two domains that in between them form a cleft. Once the agonist binds within, the two domains close together, not too dissimilar to a Venus fly trap (Kunishima et al., 2000); these receptors are also known for characteristically forming dimers, in part via interactions through the VFT domains (see section 1.6.5).

The final class of receptors is known as the frizzled/taste2 group, which contains the group of 10 frizzled receptors (FZD 1-10) and the smoothened (SMO) receptor (Davies et al., 2007; Kolakowski, 1994), both of which are involved in development. Frizzled receptors respond to secreted glycoproteins associated with Wnt signalling (Malbon, 2004). Meanwhile, SMO is involved in sonic hedgehog (SH) signalling, for example during developmental responses (Polizio et al., 2011).

1.4 Long chain fatty acid GPCRs, FFA1 and GPR120

The fatty acid receptors described in 1.2.4 are all class A GPCRs. FFA1 is an intron-less gene (Sawzdargo et al., 1997), whilst GPR120 contains four exons and has two splice variants (Figure 1.2). The short isoform contains 361 residues, whilst the long isoform contains 16 additional residues between positions 231 and 247 in intracellular loop (ICL) 3.

1.4.1 FFA GPCR pharmacology

As a group, FFA GPCRs are distinguished predominantly by their selectivity for endogenous FFAs of different chain length. FFA2 and FFA3 are both activated by C2-6 short chain fatty acids (Brown et al., 2003; Le Poul et al., 2003; Nilsson et al., 2003), but differ in their order of potency: FFA2 is C3>C4=C2>C6>C5, whilst FFA3 is C3>C4>C6>C5>C2 (Le Poul et al., 2003). GPR120 is activated by long chain fatty acids: C14-18 saturated, C16-22 mono- and poly-unsaturated (Hirasawa et al., 2005). FFA1 is activated by medium to long chain fatty acids: C6-18 saturated and C10–22 unsaturated (Briscoe et al., 2003; Itoh et al., 2003; Kotarsky et al., 2003). As discussed above, GPR119 is activated by ethanolamide derivatives of fatty acids and phospholipids rather than fatty acids themselves (Soga et al., 2005), and most potently by oleoylethanolamide (Overton et al., 2006); thus unlike FFA1 and GPR120, free carboxylic acid groups present in FFAs are not required for GPR119 activity.

FFA1 and GPR120 are activated by all types of fatty acids including saturated, unsaturated, polyunsaturated and conjugated fatty acids. Saturated fatty acids contain no double bonds i.e. they are *saturated* with hydrogens, whilst

unsaturated fatty acids contain one double bond. PUFAs contain multiple double bonds, and conjugated fatty acids contain a pair of double bonds that are separated by only one single bond (Figure 1.1). Fatty acids can also be named for the position of the double bond, for example ω-3 fatty acids are named such because the double bond is placed at the third carbon from the terminal methyl of the carbon chain (the opposite end of the fatty acid from the carboxyl group).

Additionally, both FFA1 and GPR120 are activated by the synthetic agonist GW9508, whilst only FFA1 is inhibited by the antagonist GW1100 (Briscoe et al., 2006). These and other synthetic ligands will be discussed in more depth in chapter 4.

1.4.2 Polymorphisms found in FFA1 and GPR120

Three single nucleotide polymorphisms of FFA1 have been identified in humans: D175N found in ECL2 (Hamid et al., 2005); R211H found in ICL3 (Haga et al., 2002; Hamid et al., 2005; Ogawa et al., 2005) and G180S found in TM 5 (Vettor et al., 2008). These polymorphisms have principally been explored as risk factors for type II diabetes (see also section 1.4.3).

Both D175A and R211H are caused by guanine to adenine substitutions. Studies on both Danish (Hamid et al., 2005) and Italian subjects (Vettor et al., 2008) found that these mutations had no effect upon markers for type II diabetes. *In vitro* signalling studies found both R211H and D175N mutants to have similar agonist potency values to FFA1 wild type (WT), but D175N had a maximum efficacy lower than WT and R211H (Hamid et al., 2005). Conversely

however, a study on Japanese subjects found a sliding scale of phenotype. The Arg homozygotes had the lowest measurements, in terms of levels of insulin secretion and values determined using the homeostasis models of insulin resistance and β-cell function, whilst the His homozygotes had the highest, and the heterozygotes were intermediate. They postulated that the H211 FFA1 phenotype predisposes to insulin resistance (Ogawa et al., 2005).

Interestingly, the prevalence of the FFA1 G180S mutation increased with body mass index, suggesting a link between the mutation, and the likelihood to become obese. Carriers of the Ser allele were found to have significantly lower insulin secretion in response to lipids. Additionally, *in vitro* studies also found the Ser180 FFA1 receptors to have a significantly lower signalling response to fatty acids (Vettor et al., 2008). However, more recent work on these mutations using recombinant cell lines found no difference in signalling or potency to agonists (Smith et al., 2009).

A recent study has also found a human GPR120 polymorphism present in European populations. R270H was found to inhibit intracellular signalling mediated by long chain fatty acids and increased the risk of obesity in both mice and humans (Ichimura et al., 2012).

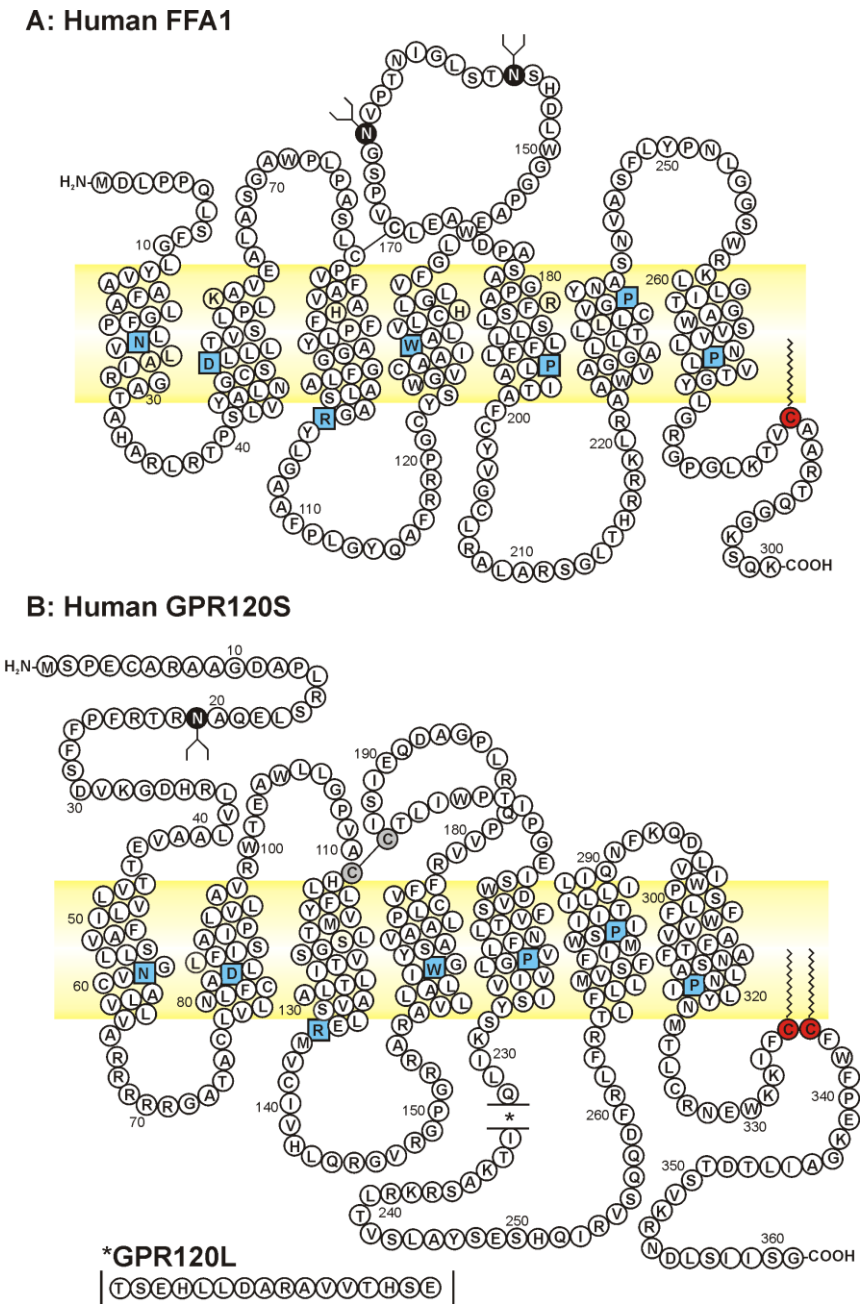

Figure 1.2 Structures of FFA1 and GPR120.

Structures of FFA1 and GPR120, with the site of the 16 residue insert in the long isoform of GPR120 also shown (*). The most conserved residue in each TM helix, characteristic of class A GPCRs, is shown in a blue box. In Ballesteros-Weinstein labelling (Ballesteros and Weinstein, 1995), this residue is x.50 (where x is the number of the TM domain). Asparagine mediated glycosylation sites are shown in black; potential cysteine disulphide bridges are shown in grey; and palmitoylation sites are shown in red.

1.4.3 Physiological roles of FFA1 and GPR120

The following section will deal with the physiology of FFA1 and GPR120 and their potential roles as nutrient sensors.

1.4.3.1 Insulin secretion and pancreatic β cell function

Most of the initial work on FFA1 focused on its high levels of expression in pancreatic β cells, which can be further increased (by FFA1 gene transcription) under conditions of high glucose (Kebede et al., 2012). In pancreatic β cells, FFA1 rapidly potentiates GSIS in the presence of FFAs. FFA1 mediates these acute affects of FFAs, by increasing intracellular calcium signalling, to increase insulin secretion (Itoh et al., 2003; Matsuda-Nagasumi et al., 2013). FFA1 has also been implicated in mediating the chronic effects of fatty acids that can lead to lipotoxicity (Steneberg et al., 2005); however, these studies on FFA1 and lipotoxicity have been controversial. Two studies concluded that FFA1 was not responsible for the chronic effects that lead to lipotoxicity in β cells (Latour et al., 2007; Tan et al., 2008).

In fact, lipotoxicity could simply be due to excess β oxidation in the mitochondria. Chronic excess fatty acids can lead to defects in this process in the mitochondria, leading to β cell failure (Joseph et al., 2004; Lu et al., 2010). Thus, FFA1 knockout mice have shown impaired GSIS in β cells (Alquier et al., 2009), but this knock out has not been shown to prevent the development of insulin resistance in other cell types (Kebede et al., 2008; Lan et al., 2008), or glucose intolerance, even on a high fat diet or diabetes background (Matsuda-Nagasumi et al., 2013). Additionally, the FFA1 knock out animals did not

display altered β cell architecture (Matsuda-Nagasumi et al., 2013). Also, in one study, transgenic over-expression of FFA1 actually led to improved glucose tolerance and increased insulin secretion (Nagasumi et al., 2009), suggesting that FFA1 activity may even have a positive effect in the long term.

These sets of conflicting studies led to a long debate on whether an agonist (Nagasumi et al., 2009) or antagonist (Steneberg et al., 2005; Vettor et al., 2008) would be best as a potential treatment for type II diabetes. The published findings of agonist TAK-875 (Sasaki et al., 2011) concluded that FFA1 does not mediate the chronic effects of FFAs that cause lipotoxicity (Tsujihata et al., 2011), with clinical trials showing that in terms of treating diabetic patients at least (Kaku et al., 2013), FFA1 agonists are the way forward (Leifke et al., 2012). This does not rule out antagonists though, in perhaps playing a role in blocking the pancreatic effects of chronically elevated levels of FFAs, or perhaps for improving insulin secretion (Hu et al., 2009; Zhang et al., 2010b).

PPARγ is also found in pancreas, and like the fatty acid receptors is activated by fatty acids. Its activation results in the transcription of genes involved in insulin signalling, glucose and lipid homeostasis (Herzig et al., 2003). There is also evidence that PPARγ activation may increase the expression of FFA1 (Kim et al., 2013a), further suggesting an relevant role for FFA1 in fatty acid control in the pancreatic β cell.

There have also been suggestions of GPR120 expression in both the pancreatic β cells (Morgan and Dhayal, 2009) and the α cells, which release

glucagon. It was postulated that GPR120 in the α cell may play a role in FFA potentiation of glucagon release, as shown by the attenuation of glucagon release in GPR120 KO cells (CP Briscoe, Janssen Pharmaceuticals, personal communication).

As discussed below, increased incretin hormone levels mediated through GPR120 (and possibly FFA1) in gut endocrine cells has been shown to enhance GSIS and increase proliferation of pancreatic β cells (Tanaka et al., 2008b). Perhaps this increase in β cell number is in part due to GPR120 also having a role in the inhibition of fatty acid induced, but not glucose induced islet apoptosis (Katsuma et al., 2005; Taneera et al., 2012).

1.4.3.2 FFA1 and GPR120 in intestinal endocrine cells

FFA1 is also expressed by the K, L and I endocrine cells in the gut. The K cells are found in the duodenum and jejunum, and secrete glucose-dependent insulinotropic peptide (GIP) (Parker et al., 2009). Due to its action as a GI hormone that causes insulin release, GIP is called an incretin (Thorens, 1995). K cells have been found to release GIP following the activation of FFA1 (Luo et al., 2012). The L cells are found in the small intestine and colon (Reimann et al., 2008), and are associated with the release of GLP-1 and peptide YY (PYY). GLP-1 is also an incretin (Thorens, 1995). FFA1 activation was also found to mediate the secretion of GLP-1 (Habib et al., 2013; Li et al., 2013; Luo et al., 2012; Xiong et al., 2013). Additionally, the I cells are found in the duodenum and small intestine, and secrete CCK. These cells have also been found to express FFA1 (Sykaras et al., 2012), whose activation has also shown to cause

CCK release (Liou et al., 2011). This involvement and action of FFA1 is of interest because all incretins (CCK, GIP, GLP-1 and PYY) increase insulin secretion from β cells (Edfalk et al., 2008; Luo et al., 2012), as well as playing a role in promoting satiety (Naslund et al., 1998).

However, assignment of a specific role of FFA1 in intestinal endocrine secretion is complicated by the fact that GPR120 is also predominantly expressed in the gut endocrine cells. GPR120 has also been found to be expressed in the same sets of K cells (Parker et al., 2009), I cells (Sykaras et al., 2012) and L cells (Habib et al., 2013) as FFA1. GPR120 mediates GLP-1 release (Hirasawa et al., 2005; Tanaka et al., 2008b), with the G protein alpha subunit gustducin implicated in the coupling mechanism between GPR120 and GLP-1 secretion (Li et al., 2013). Indeed, in studies using the intestinal endocrine cell line STC-1, GPR120 but not FFA1 siRNA mediated knockdown was capable of preventing FFA-stimulated incretin release (Hirasawa et al., 2005). In the I cells, GPR120 activation was found to cause CCK release (Tanaka et al., 2008a). Additionally, GPR120 has also been postulated to play a role in regulating the production of acylated-ghrelin in secretory cells of the stomach and small intestine, which is known as the only peripheral hormone to stimulate appetite (Janssen et al., 2012).

1.4.3.3 GPR120 In the adipocyte

GPR120 is also expressed in adipose tissue, and thought to have a role in adipogenesis, allowing adipocyte maturation and differentiation (Gotoh et al., 2007). GPR120 has also been shown to increase glucose uptake though

intracellular calcium signalling (Oh da et al., 2010) and also play a role in regulating glucose metabolism in these cells (Liu et al., 2012a).

1.4.3.4 Other sites of interest

GPR120 is expressed in the lingual cells on the tongue, which in conjunction with expression in the gut, gives the picture of GPR120 being a dietary lipid sensor (Matsumura et al., 2007). Additionally, GPR120 is expressed in macrophages and has been shown to have an anti-inflammatory role (Oh da et al., 2010). There is also evidence for an anti-inflammatory role for FFA1 (Fujita et al., 2011).

Both FFA1 and GPR120 have found to be expressed in bone, with GPR120 being found in osteoblasts and FFA1 in osteoclasts. It was found that long chain fatty acids inhibit osteoclastogenesis and stimulate osteoblast function, contributing to a positive effect upon bone density (Cornish et al., 2008). This has been corroborated by more recent work which also showed that the activation of FFA1 was found to protect against bone loss by preventing the differentiation of osteoclasts (Wauquier et al., 2013). Interestingly though, the activation of FFA1 by TZD treatment has been shown to increase the incidence of bone fractures (Mieczkowska et al., 2012).

FFA1 is substantially expressed in brain tissue (Briscoe et al., 2003), but its functions remain largely unclear. One group found FFA1 to play a role in antinociception (Nakamoto et al., 2012). Another group postulated that FFA1 may have a role in PUFAs, such as DHA, being neuroprotective (Boneva et al., 2011).

1.4.4 FFA1 and GPR120 as targets for diabetes and obesity

1.4.4.1 Type II diabetes

The world-wide prevalence of type II diabetes is predicted to increase from approximately 171 million in 2000 to 366 million in 2030 (Wild et al., 2004). Diabetes can be classified as type I or type II. Type I typically presents in the young (<20 years), is characterised by the autoimmune destruction of pancreatic β cells which causes a lack of insulin production and secretion, and is treated by exogenous insulin. Type II typically presents in the older population, >50 years. The root cause is thought to be hyperglycaemia, which leads to an increase in insulin secretion to counteract this, which also gives rise to hyperinsulinaemia. Over time, a lack of insulin sensitivity develops within target tissues such as the liver, muscle and adipose tissue, which results in further hyperinsulinaemia to compensate for the lack of action. Eventually, this causes β cell death, leading to a lack of insulin production (Prentki and Nolan, 2006). Lipotoxicity can therefore be seen as the detrimental effects upon the function of pancreatic β cells caused by sustained elevation of glucose and fatty acids (Poitout et al., 2009). Combined prolonged elevated fatty acids and glucose levels have been linked with inhibition of insulin biosynthesis (Harmon et al., 2001) and inhibition of GSIS (Briaud et al., 2002) and increased β cell apoptosis (El-Assaad et al., 2003), also potentially leading to type II diabetes.

There are other short and long term effects of uncontrolled hyperglycaemia, both due to an increase in glycosylation products such as glycosylated

haemoglobin (Ramasamy et al., 2011). The shorter term effects appear to be in the macrovascular vessels, causing atherosclerosis (Madonna and De Caterina, 2011; Wang et al., 2009). The longer term effects of hyperglycaemia involve the microvascular system, such as capillaries and can result in retinopathy, nephropathy and neuropathy. (Campos, 2012). Type II diabetes can be treated with diet, exercise and/or drugs, which will now be discussed prior to considering approaches through targeting FFA1 and/or GPR120.

1.4.4.1.1 Treatments for type II diabetes

1.4.4.1.1.1 Diet/exercise

Both weight loss (or more specifically, the loss of adipose tissue) using a calorie controlled diet especially by avoiding sugar rich foods to prevent spikes in plasma glucose (Albu et al., 2010), and exercise (De Feyter et al., 2007) can improve β cell function and improve fasting glucose levels and insulin sensitivity.

1.4.4.1.1.2 Insulin and sulphonylureas

Traditionally, both sulphonylureas and insulin have been used to treat type II diabetes. Injection of exogenous insulin, is used to maintain normal glycaemia in type II diabetics (Mudaliar and Edelman, 2001), but can lead to either hypo- or hyperglycaemia (Kourtoglou, 2011). Sulphonylureas are sometimes used in conjunction with insulin therapeutically (Kabadi and Kabadi, 2003). Sulphonylureas stimulate insulin release from the β cells, by binding to and inhibiting K_{ATP} channels, causing depolarisation of the plasma membrane,

activating Ca^{2+} channels and thus stimulating insulin release (Remedi and Nichols, 2008). Unfortunately, two major side effects with both insulin and sulphonylureas are hypoglycaemia and weight gain (Ahren, 2013).

1.4.4.1.1.3 Metformin

Another drug is the oral biguanide, metformin. It suppresses glucose production in the liver, has a low risk of hypoglycaemia (Hundal et al., 2000) and also improves insulin sensitivity (Collier et al., 2006). It is thought to be superior to other antidiabetic drugs due to a decrease in cardiovascular complications (Holman et al., 2008), but it does have GI side effects (Bolen et al., 2007).

1.4.4.1.1.4 Thiazolidinediones

TZDs were another class of drugs used in the treatment of type II diabetes, and are PPARγ agonists that improve insulin sensitivity in the muscle, whilst causing a decrease in plasma levels of glucose, lipids and insulin (Lehmann et al., 1995). TZDs were prescribed for treatment of type II diabetes, but were later withdrawn due to safety concerns. Troglitazone was the first to be withdrawn in 2000, after being shown to cause fatal hepatoxicity (Saha et al., 2010). Next, a large study showed rosiglitazone to significantly increase the risk of myocardial infarction (Nissen and Wolski, 2007), and was followed by its withdrawal from Europe and its restriction in the US in 2010 (Pouwels and van Grootheest, 2012). Studies on pioglitazone have shown it to decrease the risk of cardiovascular complications (Dormandy et al., 2005), but more recent work has shown it to increase the risk of bladder cancer (Sato et al., 2011). As

discussed in chapters 3 and 4, TZDs are now known to have additional mechanisms of action including binding and activation of FFA1 receptors (Kotarsky et al., 2003; Smith et al., 2009).

1.4.4.1.1.5 GLP-1

GLP-1 activates a class B GPCR from the secretin-like family, GLP-1R, whose activation enhances GSIS (Naslund et al., 1998). GLP-1 administration has been shown to enhance β cell proliferation, cause an increase in insulin secretion and enhance glucose tolerance (Perfetti et al., 2000), decrease glucagon levels (Buse et al., 2009) and inhibit food intake both in rats (Turton et al., 1996) and humans (Flint et al., 1998). In man, GLP-1 suppresses appetite and promotes satiety (Toft-Nielsen et al., 1999), and leads to weight loss (Vilsboll et al., 2012). GLP-1 analogues, exendin-4 (Egan et al., 2002) and Liraglutide (Buse et al., 2009) have been investigated for their potential use in the treatment of type II diabetes, but have been found to have the side effect of nausea (Sun et al., 2012). Unfortunately, from the point of view of drug development, GLP-1 itself has a short half-life in vivo, but modifications can be made to make the peptides more resistant to degradation (Buse et al., 2009). In addition, the degradative enzyme dipeptidyl peptidase (DPP)-4 can be targeted by inhibitors to prevent the breakdown of endogenous GLP-1, and this also has the positive effect of a decreased incidence of nausea (Scheen, 2013).

1.4.5 Evaluation of FFA1 and GPR120 as therapeutic targets

FFA1 and GPR120 are seen as therapeutic targets for type II diabetes. This short section will quickly summarise what is already known about the potential drugs for these receptors, and whether from a drug discovery perspective, they would work as a pharmaceutical treatment for type II diabetes.

FFA1 has been shown to potentiate GSIS in the presence of FFAs, from the pancreatic β cells (Stoddart et al., 2008), and the majority of the evidence presented above suggest that FFA1 does not mediate any lipotoxic effects long term (section 1.4.3.1), making it a good target. A range of FFA1 agonists have been synthesised (which will be covered in chapter 4). These have also been optimised for their pharmacokinetic profiles, as well receptor agonist properties.

The most prominent example of an FFA1 agonist is TAK-875. It has been shown in clinical trials to be successful at improving the glyceamic control in type II diabetic patients (Kaku et al., 2013).

Another example is TUG 424, which had nanomolar potency in increasing GSIS (Christiansen et al., 2008). Further optimisation of this compound has lead to complete bioavailability and low micromolar efficacy in improving glucose tolerance in mice (Christiansen et al., 2013).

Finally, there are the Amgen compounds, including the partial agonist AMG-837, which had a good pharmacokinetic profile as well as evidence of it being

a glucose-dependent insulin secretagogue (Houze et al., 2012). Another duo of full agonists from the same group are AM-1638 and AM-6226, whom have been shown to promote insulin secretion, but also act upon the enteroendocrine system to elicit GLP-1 and GIP secretion (Luo et al., 2012). In fact, this group suggested combination therapy of both the partial and full agonists to engage both the satiety effects from activating the enteroendocrine cells, and also the increase in insulin secretion from the β cell in the treatment of type II diabetes.

There is also evidence that GPR120 agonists could be a target for type II diabetes treatments, because the activation of GPR120 has been shown to stimulate incretin release, such as GLP-1 (Hirasawa et al., 2005) and CCK (Tanaka et al., 2008a). Additionally, GPR120 has been shown to exert anti-inflammatory actions, which would counter the "metabolic inflammation" that also contributes to type II diabetes (Oh et al., 2010).

1.4.5.1 Obesity

There is an increasing prevalence in obesity in the Western world (Ogden et al., 2006; Rennie and Jebb, 2005). One estimate puts the worldwide rate at over 1.5 billion individuals being overweight or obese (Nguyen and Lau, 2012; Simpson et al., 2009). In the UK and US, being overweight is classified as having a BMI 25 – 30, whilst being obese is to have a of BMI 30+. BMI is a simple tool to measure weight, where body mass index equals mass (kg) divided by height $(m)^2$, but BMI classifications may actually underestimate obesity (Shah and Braverman, 2012). Obesity predisposes to other co-

morbidities such as hypertension, cardiovascular diseases (Nguyen and Lau, 2012), type II diabetes (Wild et al., 2004) and cancer (Schottenfeld et al., 2013).

Weight gain occurs with an energy imbalance, when food intake is greater than energy expenditure (due to either exercise or basal metabolism) (Redinger, 2009). Less simple to explain is the complex interplay of appetite and "reward" signalling in the brain in relation to appetite. Simplistically, the gut brain axis of control of food intake is as follows: a decrease in food intake leads to an increase in circulating levels of ghrelin released from the stomach, which also causes release of orexigenic neuropeptide Y (NPY) from hypothalamic arcuate neurones. Via its receptors in the hypothalamus, NPY acts to inhibit POMC (pro-opiomelanocortin) and CART (cocaine and amphetamine related transcript) satiety neurones and causes an increase in appetite. Conversely, food intake causes release of GLP-1, CCK and PYY from the gut, which activate their respective receptors in the hypothalamus, inhibit NPY neurones, and stimulate POMC/CART neurones to promote satiety (Redinger, 2009; Simpson et al., 2009). Equally leptin (released from adipose tissue) (Feng et al., 2012), and insulin (from the pancreas) (Shiraishi et al., 2011) are negative regulators of the hypothalamic appetite circuits. Hypothalamic food intake is also modulated by other central pathways, for example those recognising reward, and this may involve other mediators such as endocannabinoids (Gardner and Vorel, 1998). Endocannabinoids are also an orexigenic signal via their activation of CB1 receptors, to stimulate appetite (Pagotto et al., 2006).

1.4.5.2 Current therapeutic strategies

1.4.5.2.1 Lifestyle interventions

The least aggressive treatment for obesity is to undertake a calorie controlled diet in conjunction with exercise, which along with weight loss has been shown to improve other factors such as cardiovascular risk (Unick et al., 2013).

1.4.5.2.2 Bariatric surgery

Currently, the only effective treatment for long term weight loss for the morbidly obese (defined as BMI >40) is bariatric surgery, which not only decreases body weight (Borg et al., 2006), but has also been shown to improve type II diabetes (Pournaras et al., 2012). It has been suggested that bariatric surgery is particularly successful because it alters the secretion of gut hormones (Pournaras et al., 2012). A challenge now is to emulate this pharmacologically. One gut hormone of interest is PYY, which is released from the L endocrine cells and has been shown to reduce food intake and promote satiety (Stanley et al., 2004) by acting on the hypothalamus (Zhang et al., 2011a). One study on PYY found that intravenous PYY caused an equivalent satiety in both obese and lean subjects, therefore it was suggested that obesity is not associated with a resistance to PYY, but rather perhaps there is a lower postprandial release of PYY or some other sort of deficiency in circulating PYY (Batterham et al., 2003), but these results could not be replicated by other groups (Boggiano et al., 2005).

Also of interest, is the combination of hormones to emulate the post prandial state, for example when PYY_{3-36} is combined with another gut hormone such as oxyntomodulin (also a GLP-1 homologue and agonist) they are additive as anorectic signals and require lower doses, therefore avoiding side effects such as nausea (Field et al., 2010). This strengthens the argument that the combination of both GLP-1 and Y2 agonists may be an attractive target for obesity drugs (Neary et al., 2005; Talsania et al., 2005).

1.4.5.2.3 Current drugs and potential FFA receptor agonists as anti-obesity agents

Two obesity medications have been withdrawn due to deleterious side effects. Rimonabant is a CB1 antagonist, which blocked orexigenic signalling, but it was associated with increased risk of depression and suicide (Despres et al., 2005). Sibutramine is a 5-HT uptake inhibitor, which decreased food intake (Heal et al., 1998), but had cardiovascular side effects (James et al., 2010; Rucker et al., 2007). The only drug currently still on the market is orlistat, a pancreatic lipase inhibitor. It prevents the breakdown of ingested fat and its absorption from the gut, but has the unpleasant side effect of steatorrhea (Filippatos et al., 2008).

The fact that only one drug is left on the market shows the clinical need for new drugs at new targets. GPR120 is a good target for novel anti-obesity therapies. Its activation causes incretin release, which by their nature confer satiety signals, and as discussed above have beneficial actions on insulin secretion that reduce the risk of associated type II diabetes. Additionally, due

to its lumenal localisation on the intestinal endocrine cells, any drugs targeting GPR120 do not require systemic absorption. Also, GPR120 has also been shown to elicit anti-inflammatory effects (Oh da et al., 2010), which would also be advantageous for obese patients as they often have systemic low grade inflammation, termed “meta-inflammation” (Talukdar et al., 2011). Many of these beneficial advantages are in principle also shared by FFA1 agonists, as this receptor is also found on similar populations of intestinal endocrine cells; however GPR120 has received most attention to date in this respect, because of the early evidence that GPR120, rather than FFA1 signalling appears most relevant for stimulating incretin release from L cells (Hirasawa et al., 2005).

1.5 The general molecular pharmacology of GPCRs

In this section, the overall common themes in GPCR ligand binding, signalling and regulation are discussed. More detailed information on the ligand binding and activation of FFA1 and GPR120 receptors will be covered in Chapters 3 and 4.

1.5.1 Structure and activation of class A GPCRs

Although GPCRs can be split into 5 groups, they still all share the common feature of a structure that traverses the plasma membrane with seven helical domains (e.g. Figure 1.2), forming a predicted serpentine structure which was then confirmed by their crystallisation. The first GPCR to be crystallised was rhodopsin, which is comprised of the protein opsin covalently bound to a vitamin A derivative, 11-*cis*-retinal that acts as an inverse agonist. Once

activated by photons, this ligand becomes all *trans* and behaves as an agonist to alter receptor conformation, allowing vision (Palczewski et al., 2000). This initially gave a template upon which to propose structures for other GPCRs. The β_2 adrenoceptor (β_2AR) was crystallised next in the presence of partial inverse agonist carazolol (Cherezov et al., 2007; Rosenbaum et al., 2007). In the following six years, a rapid expansion has occurred and 18 GPCRs now have an x-ray structure reported for them (Venkatakrishnan et al., 2013).

These have shown that all GPCRs can be split into 3 segments: the extracellular domain which modulates ligand access; the TM helical bundle that forms the core of the GPCR, and allows for conformational change to be transmitted from the agonist binding pocket to the intracellular face; and the intracellular face which interacts with effector signalling proteins.

1.5.1.1 Common themes in ligand binding

These structures have uncovered some common themes of ligand binding within the receptors, such as the involvement of ECL2 in controlling ligand access and the formation of a transmembrane binding pocket for small molecule ligands.

1.5.1.1.1 Extracellular loop 2

From comparison of the current x-ray structures, there appears to be 2 different types of extracellular domain, defined principally by ECL2. One type allows for water-accessible, downwards ligand access and examples of these domains are quite variable; whilst the other type prevents access to the

binding pocket, and these receptors have hydrophobic ligands, thought to bind the receptor transversely through the plasma membrane.

The receptors that allow for downwards access appear to have an ECL2 that contains secondary structure composed of alpha helices, such as the β adrenoceptors and adenosine receptors. The β_2AR has a fairly large, solvent exposed ECL2 that holds itself out of the binding pocket, in part by disulphide bonds, for example one disulphide bridge links ECL2 to TM 3, constraining the structure. This allows the small ligands access to the binding site deep within the TM helices (Cherezov et al., 2007). Similar to the β_2AR, the β_1 subtype also contains alpha helical structure within ECL2. In this case, ECL2 is thought to contribute to the binding pocket and helps to define what ligands bind with high affinity. Despite very similar residues within the TM binding pocket, the amino acid sequence of β_1 receptors differs markedly from β_2 in the ECL2 region, which alters the charge distribution and shape of the entrance to the binding pocket. This may explain some of the differences in ligand specificity between the two (Warne et al., 2008). The crystal structure of A_{2A} adenosine receptor showed that its ECL2 was more disordered than β_2, with no elements of secondary structure. There was however, a network of disulphide bonds that hold ECL2 in a position that allowed the ligand binding pocket to be readily accessible to solvent, and presumably also for small diffusible ligands such as adenosine (Jaakola et al., 2008).

In the muscarinic receptor class, ECL2 also appears to be key in regulating ligand entry into the binding pocket. In the x-ray structure of the M_3 receptor

it was found that Leu225 in ECL2 creates a pocket that does not exist in M_2 (Leu225 substituted with Phe181) which is thought to contribute to the altered binding of the M_3 selective antagonist tiotropium (Kruse et al., 2012). Other experimental approaches have also shown the importance of ECL2 in dictating ligand binding in other GPCRs (Avlani et al., 2007; Shi and Javitch, 2004), and as discussed in Chapter 4, there is evidence that it regulates ligand binding and activation of FFA1.

Interestingly, ECL2 structures in rhodopsin (with a covalently bound ligand), and the S1P receptor (with a hydrophobic ligand) are substantially different. The ECL2 of rhodopsin occludes the binding pocket by forming a 4 strand β sheet structure with the receptor amino terminus, holding 11-*cis*-retinal within the TM domains. This structure is probably due to the fact that the ligand does not have to diffuse into the binding pocket (Palczewski et al., 2000). The S1PR also has a binding pocket occluded by ECL2 and the amino terminus (described in more detail in Chapter 4). This is predicted to result in its hydrophobic ligands activating laterally from within the lipid bilayer (Hanson et al., 2012).

1.5.1.1.2 Binding pocket

From the class A GPCR structures so far, a "ligand binding cradle" has been postulated (Venkatakrishnan et al., 2013). This is formed by interactions with diverse ligands mediated at residues in similar positions within TM 3 (e.g. 3.32, 3.36), 6 (e.g. 6.48, 6.51) and 7 (e.g. 7.39; see Figure 1.2 for information on Ballesteros Weinstein numbering). While some of these residues are highly

conserved (e.g. Trp 6.48 is part of the toggle switch activation mechanism, see section 1.5.1.3.2 below), the amino acid identities at others can be variable. Although this suggests a consensus GPCR scaffold structure for recognising ligands, naturally all binding pockets vary slightly depending upon ligand (Venkatakrishnan et al., 2013). In the x-ray structure of β_2AR, the cleft formed in the binding site carries an overall negative charge (Cherezov et al., 2007), centred around Asp 3.32, which makes contact with the positive amine of the agonists (Strader et al., 1988).

The opioid receptor family, with larger endogenous peptide ligands than amine receptors, consists of δ, μ and κ subtypes. Opioid receptors were theorised to have "message-address" pharmacology, where one peptide agonist can contain two discrete parts: message (efficacy: ability to activate the receptor by changing its conformation), thought to be mediated by the morphinan group found in opioid agonists (Zhang et al., 2011b); whilst the "address" part confers selectivity between the three subtypes.

The crystal structure of the μ opioid receptor showed the antagonist morphinan in the binding pocket, interacting with residues also found in the other opioid subtypes (Manglik et al., 2012). The δ opioid receptor was crystallised with selective antagonist naltrindole, and binds in a deep but easily solvent-accessible pocket. Selectivity at this receptor is mediated by the indole group of natrindole interacting with Leu300 found in the upper binding pocket. In contrast, residues at this position in the other receptor subtypes prevent natrindole binding (Granier et al., 2012). A similar story is highlighted

by the structure of the κ opioid receptor. The basis of its selectivity for the antagonist JDTic is again in the upper part of pocket, mediated by Glu297 (Wu et al., 2012).

1.5.1.1.3 Differences in class A GPCR x-ray structures

While there are evidently conserved elements in the x-ray structures so far, the individual nature of many GPCRs is illustrated by the structure of the chemokine receptor CXCR4, which shows multiple differences to the structures of the β_2AR and the A_{2A} adenosine receptor. For example, when compared to these receptors, CXCR4 contains a tighter turn in TM 2, adapting the helix to allow conserved residues to face the binding pocket (Wu et al., 2010). Also, CXCR4 contains only a partial helix 8, important for G protein activation (Wu et al., 2010). This illustrates some of the potential limitations when modelling receptor sequences, on even closely related GPCR structures (see also Chapter 4).

1.5.1.1.4 Helical bundle

Comparison of all known x-ray structures demonstrate that the 7TM helical domains have structural similarity, forming a common core (Venkatakrishnan et al., 2013). All seven transmembrane helices form a circular arrangement with TM helices 1-4 forming a central, stable core with TM 3 tilted across the centre of this core whilst helices 5-7 interact with the core but are much less densely packed (Patel et al., 2005).

1.5.1.2 The role of "class A" conserved residues and motifs in the inactive state

GPCRs are thought to be constrained in the inactive state through a variety of non-covalent interactions, including those mediated by conserved class A motifs identified in part by the core amino acids in Figure 1.2. Interactions between the central core of TM 1-4 and TM 5-7 include two conserved class A motifs.

1.5.1.2.1 TM 3: DRY motif

Firstly, the Glu/Asp-Arg-Tyr (E/DRY) motif is found at the bottom of TM 3 centred on Arg 3.50 (Figure 1.2). This forms a stabilising ionic salt bridge within itself between the Asp/Glu and Arg, but Arg also constrains the receptor in an inactive conformation by interacting with residues found at the bottom of TM 6, which in rhodopsin are Asp and Thr (Palczewski et al., 2000; Scheerer et al., 2008). The role of the DRY motif has been extensively studied by mutagenesis in GPCRs, and arguments have been made for two groups defined by its different effects on receptor activation (Rovati et al., 2007).

In the first group the DRY motif holds the receptor in the inactive state, and mutations cause constitutive receptor activation in the absence of agonist (Scheer et al., 2000). One example of this group is of the β_2AR, in which an ionic lock is proposed between the Arg of the DRY and a Glu found at the bottom of TM 6 (Ballesteros et al., 2001). However, this interaction was not present in the inactive crystal structure (Cherezov et al., 2007). This may be due to the methods employed to crystallise receptors, for example large

protein modifications to the receptor or the particular conformation adopted using the particular ligands employed for crystallisation.

The second group are thought to be resistant to induced constitutive activity following mutation, and instead the DRY motif appears to play more of a role in interacting with and activating the G protein (Rovati et al., 2007). For example, in the human histamine H4 receptor the DRY "lock" partner residue at the bottom of TM 6 is missing (an uncharged Ala). Whilst it was postulated that this may be why the H4 receptor has a high constitutive activity, the inactive receptor was not stabilised when engineered to contain a negative amino acid at the key TM6 position; in fact this substitution also prevented G protein activation (Schneider et al., 2010).

1.5.1.2.2 TM VII: NPxxY motif

Another stabilising interaction that holds the receptor in an inactive state is Asn-Pro-X-X-Tyr (NPxxY) motif present in TM 7 (centred on Pro7.50), which forms a network of stabilising interactions with residues in TM 2 (Balaraman et al., 2010) and helix 8 (Park et al., 2008). The Tyr in the NPxxY motif interacts with a conserved Phe found in helix 8 (Park et al., 2008). Meanwhile, in the β_1AR, mutation at Phe 7.48 led to an alteration of the interaction between NPxxY and TM 2 and helix 8. This mutant had lower constitutive activity, though to be due to a stabilisation of the inactive state (Balaraman et al., 2010). Also, in the inactive state, the NPxxY motif interacts with Trp 6.48 in the CWxP motif (including Pro 6.50) in TM 6. (Bhattacharya et al., 2008b).

1.5.1.3 Structural changes in GPCR activation that transduce the signal to the intracellular face

GPCR activation requires structural change between inactive and active conformations. Agonists stabilise an active receptor conformation, whilst inverse agonist ligands stabilise the inactive receptor state (thereby reducing its constitutive activation, if present). Early studies supported this inverse structural relationship between agonist activation and inverse agonist effects. For example, a fluorescence based assay used purified β_2AR labelled at cysteine residues using a compound sensitive to the polarity of its environment (i.e. the fluorescence increased when the polarity of the environment decreased). This study showed that agonist binding caused an agonist specific, dose-dependent decrease in fluorescence (i.e. fluorophore is moved to a more hydrophobic environment in the centre of the receptor protein core). Meanwhile, inverse agonists produced a small increase in fluorescence, suggesting that receptor activation and inactivation are elicited by the same but opposite changes in receptor conformation (Gether et al., 1995). This theory has been backed up by later studies using fluorescence resonance energy transfer (FRET) (Zurn et al., 2009).

During activation, structural receptor interactions between key residues are modulated and changed, probably through a simultaneous whole receptor rearrangement, rather than a step by step rearrangement.

1.5.1.3.1 DRY motif

Following activation, the Asp or the DRY lock becomes protonated and the Arg no longer forms a salt bridge with negative residues found at the bottom of TM 6, (Farrens et al., 1996), instead interacting with TM 5 Tyr, moving TM 3 and 5 relative to each other (Patel et al., 2005; Scheerer et al., 2008), but these interactions are not present in the crystal structures (Rasmussen et al., 2011a; Rasmussen et al., 2011b).

1.5.1.3.2 CWxP molecular switch

The breaking of the ionic lock also causes TM 3 and TM 6 to move apart (Rasmussen et al., 1999). The centre of this change is the TM 6 CWxP "toggle switch". The Pro6.50 bend in TM 6 is increased such that the extracellular end of this helix does not move, but the intracellular end moves outward relative to TM 3 (Bhattacharya et al., 2008b). It is thought that when agonists bind to β_2AR, they interact with the Trp contained in the CWxP motif, causing this molecular switch to occur (Bhattacharya et al., 2008a). Activation of the CWxP molecular switch on TM 6 also leads to its movement towards TM 5 and a tighter interaction with the NPxxY motif on TM 7 (this movement is covered in more depth in section 1.5.1.3.3) (Liu et al., 2004; Rasmussen et al., 2011a).

1.5.1.3.3 Change in TM 6 due to Pro kink

This "see-saw" motion around the proline kink (Altenbach et al., 2008) is therefore also part of the "toggle-switch model" (Schwartz et al., 2006). In addition, TM 6 has been shown undergo a twisting motion clockwise away from the TM 3 DRY motif, out of the receptor core upon activation (Jensen et

al., 2001), and towards TM 5 in both β_2AR (Ghanouni et al., 2001) and rhodopsin (Dunham and Farrens, 1999). TM 5 and 6 rearrange their side chains to stabilise this conformational change (Patel et al., 2005) by aromatic stacking interactions forming a lock between Phe in TM 5 and Trp in the CWxP motif of TM 6 (Holst et al., 2010).

Cross-linking studies on TM 6 have shown its movement as important in receptor activation not only for rhodopsin (Cai et al., 1999; Farrens et al., 1996) and β_2AR (Bhattacharya et al., 2008a), but even for a family B GPCR, the parathyroid hormone receptor (Sheikh et al., 1999), which is surprising because class B GPCRs do not contain the same conserved residues as class A. This shows that a global model for receptor activation may be a common feature, evolutionarily shared for all GPCRs, not just specific for family A receptors.

1.5.1.3.4 TM 7 (7.50): another Pro rearrangement

The see-saw action of TM 6, and TM 7 which also contains a conserved Pro residue, causes an inwards movement of the top portions of the TM helices, towards TM 3. This closes the entrance to the binding site in the structures of both the A_{2A} and β_2AR (Cherezov et al., 2007; Jaakola et al., 2008; Rosenbaum et al., 2007), and opens up the intracellular face for effector proteins to bind.

1.5.1.3.5 Movement of NPxxY from helix 8 to TM 6

This tighter interaction in the extracellular portion of the receptor is probably due to a breaking of the interaction between NPxxY and helix 8. The Tyr of

NPxxY forms a new interaction with the hydrophobic patch found on the intracellular portion of TM 6 (Fritze et al., 2003; Park et al., 2008).

1.5.1.3.6 Other conserved residues

There are some other highly conserved residues among class A GPCRs (Figure 1.2), which may not be involved in activation, but may still play a role in maintaining the conformation of the receptor.

1.5.1.3.6.1 TM 1: Asn 1.50

Although generally speaking TM 1 is not involved in receptor activation, the highly conserved Asn 1.50 has been shown to be key in mediating in the interaction between TM 1, TM 2 and TM 7 in a non class A GPCR (Singh et al., 2011).

1.5.1.3.6.2 TM 2: Asp 2.50

This highly conserved residue is thought to interact with a sodium ion in a water cluster, which stabilised the A_{2A} receptor (Liu et al., 2012b). In many receptors, this residue is thought to be responsible for sensitivity of agonist binding and G protein activation to the sodium ion concentration (Costa et al., 1990).

1.5.1.3.6.3 TM 5: Pro 5.50

The highly conserved proline in TM 5 plays a similar role to the proline in TM 6 in kinking the transmembrane helix, but does not undergo such a significant movement upon receptor activation (Bhattacharya et al., 2008b; Deupi, 2012).

The rearrangements discussed above cause concomitant movements in ICL2, ICL3 and the carboxyl tail, allowing effectors such as β-arrestins (Marion et al., 2006) and G proteins to bind in a pocket formed by TM 3, 6 and 7 on the intracellular side of the receptor (Gerber et al., 2001; Nygaard et al., 2009). The β_2AR x-ray structure showed the cytoplasmic face of the receptor to carry a positive charge overall, which could also be involved in G protein binding and activation (Cherezov et al., 2007; Lebon et al., 2011).

1.6 Signalling & Trafficking

1.6.1 G proteins

Next, the principal GPCR effector protein, the G protein, will be discussed.

1.6.1.1 Activation of the G protein and the G protein cycle

The conformational changes elicited by agonist binding result in classical signal transduction, via coupling with heterotrimeric guanine nucleotide-binding proteins (G proteins), for which GPCRs are named. The G protein heterotrimer is made up of an α subunit (16 encoding genes, although when including splice variants, over 20 Gα protein subunits are expressed; Table 1.1) bound to guanosine diphosphate (GDP); a β subunit (5 genes); and a γ subunit (12 genes) (Simon et al., 1991).

Main class	Effector	Signalling outcome	Types
Gs	Stimulation of adenylyl cyclase	↑ cAMP	αs, αolf
Gi/o	Inhibition of adenylyl cyclase	↓ cAMP	αi1, αi2, αi3, αoa, αgust, αz
	Activation of phospholipase Cβ	↑ Calcium	
Gq/11	Activation of phospholipase Cβ, causes cleavage of PIP_2 to release IP_3 and DAG	↑ Calcium from intracellular stores (IP_3) and PKC (DAG) activation	αq, α11, α14, α15
G12/13	Activation of RhoGEF, leading to activation of small monomeric GTPase RhoA	↑ MAPK, cytoskeletal rearrangement	α12, α13
Transducins	Activation of cGMP phosphodiesterase	↓ cGMP	αt1, αt2

Table 1.1 The main classes of Gα.

The types of Gα, the effectors and signalling associated with them. cAMP, cyclic adenosine monophosphate; PIP_2, phosphatidylinositol 4,5-bisphosphate; IP_3, inositol 1,4,5-trisphosphate; DAG, diacyl glycerol; MAPK, mitogen activated protein kinase; RhoGEF, Rho guanine nucleotide exchange factor.

There are two models to how G proteins associate with the receptor; pre-coupling and collisional. BRET studies have shown evidence for the pre-coupling model (Gales et al., 2006), where the G protein and receptor are pre-assembled in an inactive form that is only activated once the ligand has bound to the receptor (Hu et al., 2010; Qin et al., 2011). On the other hand, free collision coupling states that the G protein:receptor complex is only formed after a ligand has bound to the receptor. Evidence for this collisional model has been provided using FRET studies (Hein et al., 2005).

1.6.1.2 G protein cycle

Once activated, the receptor acts as a guanine nucleotide exchange factor (GEF) upon the G protein. Receptor and G protein coupling causes GDP to be released, and guanosine triphosphate (GTP) to become bound to the Gα subunit. This activates the G protein, as the presence of the γ phosphate elicits conformational changes within the G protein in the 3 flexible loops named switches I, II and III (Lambright et al., 1994), causing Gα to dissociate from both the GPCR and the βγ subunit, and to activate effector proteins and secondary messengers.

G protein activity is regulated by Gα GTPase activity; the hydrolysis of bound GTP to GDP allows heterotrimer reformation. GTPase activating proteins, such as regulators of G protein signalling (RGS) proteins hasten this intrinsic GTPase activity (Oldham and Hamm, 2008).

1.6.1.3 Ternary complex

In pharmacological terms, GPCR activation of the G protein (or other effectors) is most commonly described by the ternary complex model which considers agonist (A), receptor (R), and G protein (G). When a receptor is activated by an agonist, it forms a low affinity AR complex (agonist:receptor), which then causes the receptor to couple with a G protein, thus forming a high affinity ARG ternary complex (ligand:receptor:G protein). Therefore, it was postulated that ligands are agonists because their binding selectively promotes and stabilises this high affinity state, leading to the activation of effector proteins which causes the cellular response. This model also allows for the formation of the RG complex spontaneously (generating constitutive activity or agonist-independent receptor activity as previously described, for example for the GPCR DRY motif mutations in section 1.5.1.2.1). Neutral antagonists can bind to either form equally (as these do not stabilise the ternary complex, but prevent agonist binding). This model describes interactions solely based on ligand affinity (ability to bind the receptor), assuming that intrinsic efficacy (ability to activate the receptor once bound) can be treated as a separate independent parameter (De Lean et al., 1980; Stephenson, 1956).

This theory was then embellished into the extended ternary complex model. This stated that the receptor can also exist in two forms: R and R*, where R* is the activated receptor. In this model, agonists stabilise the activated receptor, and only the activated receptor R* can interact with G proteins, therefore

AR*G is the only active state. Constitutive activity is represented by receptors adopting R* spontaneously. This allows for the description of inverse agonist activity, because unlike neutral antagonists, inverse agonists bind to the R state preferentially, thus decreasing constitutive activity (Samama et al., 1993).

1.6.1.4 G protein structure

The Gα subunit has a conserved protein fold of a GTPase domain (made up of 5 helices plus a 6 stranded beta sheet), which is highly conserved throughout all GTPases, and a helical domain that is specific to Gα proteins (6 alpha helices), with the nucleotide binding site located at the interface between the two domains (Noel et al., 1993).

The structure of the β subunit is of a seven pronged β propeller that contains seven WD-40 motif repeats (Wall et al., 1995). The amino terminal helix of the β subunit interacts with the γ subunit, by forming a parallel coiled-coil interface through hydrophobic interactions with the amino terminal helix also present on the γ subunit (Sondek et al., 1996). Gγ subtypes contain a CAAX motif in the carboxyl terminus that allows for prenylation, a post translational modification that causes addition of an unsaturated lipid moiety to the subunit. This modification targets the βγ subunit to the cell membrane (Simonds et al., 1991) and stabilises interactions with the Gα subunit, receptor and effector molecules (Gautam et al., 1998). This βγ subunit is functional and also capable of signalling (Khan et al., 2013); for example, the galanin 1 receptor signals though Gαi, liberating Gβγ which causes mitogen activated

protein kinase (MAPK) activation (Wang et al., 1998). There is also evidence for Gβγ activating src activity, also feeding into the MAPK pathway, causing a myriad of cellular responses such as the rearrangement of the cytoskeleton, vesicular trafficking, proliferation and survival (Luttrell and Luttrell, 2004).

Gα also forms an interaction with Gβ in the region of switch I and II of Gα, and it is rearrangement of this area following GTP binding that causes Gβγ to dissociate from Gα (Lambright et al., 1996; Wall et al., 1995). There is also an interaction between the amino terminus of Gα and the propeller region of Gβ, but there appear to be no direct interactions between Gα and Gγ (Lambright et al., 1996). Interestingly though, more recent studies using FRET (Lohse et al., 2012) have shown evidence that Gα and βγ do not always dissociate following activation, as previously thought (Bunemann et al., 2003). This has been further backed up with studies on G proteins of the Gi family that showed that the constituents of Gi G proteins instead undergo a rearrangement, rather than dissociation (Frank et al., 2005).

G proteins have been shown to form an interaction with the GPCR between both the amino and carboxyl termini of Gα, and ICL3 in the receptor (Cai et al., 2001; Itoh et al., 2001). There is also evidence for interactions between helix 8 of the GPCR and the G protein (Qin et al., 2011),and that Gα interacts with a interface found at TM 5 and TM 6 (Hu et al., 2010). There is also now a crystal structure of β_2AR in complex with a Gαs protein. This showed extensive contacts between the ICL2, TM 5 and TM 6 of the receptor and the junction of

the amino tail and β strand 1, helix 4, helix 5, and β strand 3 of the Gαs protein (Rasmussen et al., 2011b).

1.6.1.5 G protein coupling selectivity

It is thought that there are molecular determinants present on receptors that account for the differential G protein coupling exhibited. The muscarinic receptors lend themselves well to the study of this, because there are 5 receptor subtypes that fall into two groups in terms of their G protein coupling. M_1, M_3 and M_5 couple to Gq, where as M_2 and M_4 couple to Gi (Caulfield and Birdsall, 1998).

A predominant thought is that hydrophobic residues at the juxtamembrane amino and carboxyl ends of ICL3 are important in forming a surface for determining the selectivity of G protein coupling (Moro et al., 1994). This region was found to be crucial for coupling in M_5 (Burstein et al., 1995) and the carboxyl end of TM 5 contains the VTIL motif for Gi coupling to M_2 and M_4 (Kostenis et al., 1997), which is completely different in the Gq coupled muscarinic receptors: AALS (Liu et al., 1995). Later work has suggested that ICL3 of M_3 is not necessary for precoupling with Gq. Instead, helix 8 of M_3 partially mediates its coupling with Gq (Qin et al., 2011). Mutational analysis of the region at the amino terminus of ICL3 found that Tyr254, which is present only in the Gq coupled muscarinic receptors and is replaced by serine in M_2 and M_4 subtypes, is at least partially responsible for G protein coupling with Gq and the activation of the phosphatidylinositol pathway (Bluml et al., 1994). This Tyr254 was been implicated in Gq coupling in conjunction with the

SRRR motif in ICL2 (Ser168, Arg171, Arg176, Arg183) with Arg176 being of particular importance. This residue is replaced with Pro in M_2 and M_4 and is thought to considerably alter protein secondary structure (Blin et al., 1995). Further work on ICL2 suggested that whilst ICL2 is generally relevant for G protein coupling (Hu et al., 2010), selectivity is governed by other sites (Moro et al., 1993a).

More recent work has further shown the importance of the position of the cytoplasmic end of TM 5 and 6 in determining G protein selectivity (Rasmussen et al., 2011b). The position of TM 5 appears to be M_2-like in all known Gi/o coupled receptor structures; they have an increased TM 5 to TM 6 distance, where as Gq receptors have a decreased TM 5 to 6 distance, resulting in a different conformation of ICL3 (Hu et al., 2010; Kruse et al., 2012). Helix 8 also appears to be a key interface between receptor and G protein (Hu et al., 2010; Qin et al., 2011). Additionally, the carboxyl tail of the Gα also governs selectivity (Rasmussen et al., 2011b), for example switching the terminal 5 amino acids (Gqi5 chimera) can direct receptor coupling from Gq to Gi (Hamm, 1998).

1.6.1.6 Downstream G protein signalling pathways

Both Gαs and Gαi act to regulate the activity of cAMP. Gαs stimulates adenylyl cyclase (an enzyme that converts ATP to cAMP; of which there are 9 isoforms (Simonds, 1999)), thus causing cAMP production and activating protein kinase A (PKA); whilst Gαi inhibits adenylyl cyclase and inhibits cAMP production (Table 1.1). This process is under regulation from a negative feedback loop:

once activated by an increase in cAMP levels, PKA can activate some phosphodiesterases (PDE) isoforms which break down cAMP. Then, once cAMP levels decrease, so do activated PKA levels. In addition to the Gα subunit, the Gβγ subunit has also been demonstrated to also regulate cAMP generation, depending on which isoform of adenylyl cyclase is present. For example, Gβγ can inhibit adenylyl cyclase 1, stimulate the enzyme activity of adenylyl cyclase 2 or have no effect upon adenylyl cyclase 3 (Simonds, 1999).

Meanwhile, the stimulation of Gαq/11 activates phospholipase C (PLC) β, which cleaves membrane bound phosphatidylinositol 4,5-bisphosphate (PIP_2) into inositol 1,4,5-trisphosphate (IP_3) and diacylglycerol (DAG). IP_3 diffuses through the cytosol to bind to IP_3 receptors present on the surface of the endoplasmic reticulum to elicit calcium release from intracellular stores. Meanwhile, DAG remains membrane localised, and in combination with the increase in intracellular calcium, activates protein kinase C (PKC). This process is also regulated through PKC, which becomes recruited to the cell membrane and can negatively regulate PLC activity. Additionally, DAG kinases phosphorylate DAG and thus prevent further signalling to PKC (Litosch, 2012). The IP_3 receptor on the endoplasmic reticulum can also be inactivated by phosphorylation with many kinases, including PKC to form another negative feedback loop (Vanderheyden et al., 2009).

1.6.2 β-arrestin

The next effector protein to be discussed will be β-arrestin. β-arrestins were historically known for switching GPCR G protein signalling “off”, a process

known as desensitisation when it occurs rapidly (minutes). However, they are now appreciated to have much more diverse functions, and also mediate their own signalling pathways.

1.6.2.1 Desensitisation

One mechanism of GPCR desensitisation involves the activated receptor becoming phosphorylated by GPCR related kinases (GRKs), leading to β-arrestin binding (Gurevich and Gurevich, 2006). β-arrestin is recruited to the plasma membrane from the cytosol, and β-arrestin binding desensitises the receptor (Barak et al., 1997; Krilov et al., 2011; Moro et al., 1993b; Wu et al., 1997), by physically uncoupling the receptor from its cognate G protein and associated signalling pathways (Kong et al., 1994).

Key to desensitisation are arrestins, of which there are 4 isoforms. Two are expressed only in the eye; arrestin-1 in the rods and arrestin-4 in the cones. The other two are the widely expressed non-visual arrestins, isoforms β-arrestin1 and β-arrestin2 (also known as arrestin-2 and arrestin-3 respectively) (Attramadal et al., 1992; Lohse et al., 1990). It is thought that β-arrestin contains two molecular sensors: one which detects the activated receptor conformation, and the other which can detect whether the receptor is phosphorylated. Therefore, for high affinity β-arrestin binding, the receptor must be both activated and phosphorylated (Gurevich and Gurevich, 2006).

The GRKs carry out rapid (on the time scale of seconds) agonist dependent phosphorylation (Kim et al., 1993). GRKs require agonist occupancy of the receptor for phosphorylation to occur, and this is an example of homologous

desensitisation. This is in contrast to heterologous desensitisation, which occurs in the absence of β-arrestin, and is mediated by protein kinases such as PKA and PKC. These protein kinases phosphorylate key motifs in receptor ICLs and carboxyl tail, which prevent G protein coupling, and can desensitise receptors in the absence of agonist (Montiel et al., 2004).

There are 7 subtypes of GRKs. There is the visual system based rhodopsin kinase family, that is comprised of GRK1 which is expressed in rhodopsin (Orban et al., 2012); and GRK7, which is specific for cone opsin (Chen et al., 2001). GRK2 and 3 (also called β adrenoceptor kinase 1 and 2 respectively) were historically associated with β-arrestin, due to their discovery in relation to "arresting" the function of β_2AR (Ferguson et al., 1995; Freedman et al., 1995; Richardson et al., 1993). Meanwhile, GRK4, 5 and 6 form the GRK family (Penela et al., 2003).

GRK1, 4, 5, 6 and 7 undergo a lipid post translational modification that targets them to the plasma membrane (Pitcher et al., 1998). GRK2 and 3 do not have this, and have a widespread cytosolic localisation (Penn et al., 2000). These isoforms are instead recruited to the plasma membrane by Gβγ following receptor activation (Li et al., 2003). GRKs are thought to predominantly phosphorylate serine and threonine residues present on ICL3 and the carboxyl tail (Appleyard et al., 1999), and following this receptor phosphorylation, β-arrestin can bind to agonist-activated receptors (Gurevich et al., 2012).

β-arrestin binding to the receptor is thought to occur through motifs found in ICL2, such as the DRYxx**V**/**I**xxPL motif. The DRY motif, at the bottom of TM 3, is

known for its role in receptor activation (section 1.5.1.2.1). Structures of GPCRs have shown the opioid, muscarinic and aminergic receptors to contain a salt bridge between ICL2 and the DRY motif, perhaps this holds ICL2 in the correct conformation (Venkatakrishnan et al., 2013). Also, mutation of one of the salt bridge partners, ICL2 Tyr3.60 in β_2AR also led to inhibition of tyrosine phosphorylation, and caused hypersensitivity of this receptor to agonists (Valiquette et al., 1995), which could be due to a lack of desensitisation. The conserved proline residue within this ICL2 helix motif (Pro 3.57) is also seen as important for β-arrestin binding, because its removal decreases β-arrestin binding and ability to undergo endocytosis (see 1.6.2.2 below), whilst its addition to receptors that otherwise lack the proline improves these functions (Marion et al., 2006). The central residue of this motif (at position 3.56) is also highly conserved as a hydrophobic residue. In this position in the M_1 is Leu131, Phe139 in the β_2AR (Moro et al., 1994) and Leu147 in the gonadotropin-releasing hormone receptor (Arora et al., 1995). Mutations throughout it have been shown to disrupt G protein coupling and arrestin-mediated internalisation (Moro et al., 1994).

1.6.2.2 Role of arrestins in receptor internalisation

Once β-arrestin is bound to the receptor, it also acts as a scaffold, interacting with clathrin (Kang et al., 2009), adaptor protein (AP)-2 (Goodman et al., 1996) and dynamin to facilitate receptor internalisation, via clathrin coated vesicles (Kang et al., 2009; Tsuga et al., 1994). β-arrestin is known to interact with clathrin through the LIEFE (on β-arrestin2) or LIELD (on β-arrestin1)

binding domain (Kim and Benovic, 2002; Krupnick et al., 1997). β_2AR requires β-arrestin2 to internalise via clathrin coated pits (Kang et al., 2009). β-arrestin also interacts with AP-2, a clathrin adaptor protein (Goodman et al., 1996), to form a complex with the receptor and β-arrestin (Laporte et al., 1999) through a domain found in the carboxyl tail of β-arrestin2 (DeFea, 2011; Laporte et al., 2000). β_2AR internalisation also requires the phosphorylation of dynamin by Src; additionally Src is also activated by arrestin (Ahn et al., 1999) in conjunction with Gβγ (Luttrell et al., 1999). Dynamin isoforms are small monomeric G proteins involved in the pinching of endocytic vesicles from the plasma membrane (Hinshaw and Schmid, 1995; Takei et al., 1995). Studies using a dominant negative form of dynamin, dynamin K44A, have supported a crucial role for dynamin in clathrin-mediated endocytosis (Damke et al., 1994; Gagnon et al., 1998; Zhang et al., 1996). Conversely, some other GPCRs, such as the angiotensin II type 1A receptor ($AT_{1A}R$) have been found to not require dynamin or β-arrestin to internalise (Zhang et al., 1996). Additionally, removal of the carboxyl tail from the A_2B adenosine receptor altered its internalisation phenotype, to one that still relied upon dynamin, but was also both clathrin and β-arrestin-independent (Mundell et al., 2010).

1.6.2.3 Receptor trafficking and sorting pathways

Once internalised, the receptor traffics into the early endosomes (Iwata et al., 1999; Moore et al., 1995). Here, the receptor becomes dephosphorylated by protein phosphatase 2A (PP2A) (Pitcher et al., 1995) and can be recycled back to the plasma membrane, termed receptor resensitisation (Pippig et al.,

1995). Alternatively, the receptors may be sorted to lysosomal compartments, contributing to a longer term decrease in cell surface expression ("downregulation"), and long term tolerance to agonist stimulation. The rate of trafficking and which pathway (recycling or degradation) the receptor follows is determined by many factors, some of which will be covered now.

The entry into a specific intracellular trafficking pathway can be influenced by whether its internalisation is GRK and β-arrestin dependent or independent (e.g. requiring PKC instead), and which types of clathrin-coated pits are engaged. For example, P_2Y_{12} purine receptors have been found to internalise in a β-arrestin dependent way and via a CCP-1 class pit. Meanwhile P_2Y_1 receptors internalised independently of β-arrestin and entered a CCP-2 class pit. It is thought that this difference influences trafficking, i.e. CCP-1 class receptors such as P_2Y_{12} and β_2AR rapidly recycle back to the surface, whilst the CCP-2 pit receptor, P_2Y_1 receptors undergo further sorting (Mundell et al., 2006). Also thought to influence these distinct profiles, is sorting nexin 1 (SNX1), a protein known for directing receptors towards endosomal retention. The fact that P_2Y_1 receptors undergo slow recycling seems to be mediated by SNX1, because once SNX1 function is inhibited, P_2Y_1 receptors then undergo faster recycling (Nisar et al., 2010).

Different categories of receptor trafficking behaviour can be described dependent on the stability and nature of interactions with arrestins. Class A GPCRs (e.g. β_2AR, endothelin A, dopamine D_1) preferentially bind β-arrestin2, then dissociate rapidly from β-arrestin2 (because receptor:β-arrestin2

interactions are transient) and recycle. In contrast, class B GPCRs (e.g. the vasopressin V_2 receptor, $AT_{1A}R$) bind both β-arrestins with similar affinity and in a sustained manner, and most have slower rates of recycling, with increased targeting to the degradative pathway. The switching of carboxyl tails of the β_2AR and V_2 receptor switched phenotype accordingly, showing that carboxyl tail plays a key role for these receptors in controlling interactions between the receptor and β-arrestin (Oakley et al., 2000). Comparison of the carboxyl tails of these two groups of receptors found that the rapid recycling receptors lack multiple clustered phosphorylation sites, whilst the slower recycling receptors contain highly conserved clusters of GRK-phosphorylated Ser or Thr residues. Therefore, the presence of these residues appears to strengthen β-arrestin interactions and affect receptor dephosphorylation, which then influences the rate of recycling. β-arrestin dissociates from the β_2AR near the plasma membrane, and because β-arrestin is not present on the receptor in the endocytic vesicles, then the receptor can be rapidly dephosphorylated and recycle. The same is true of the dopamine D_1 receptor and endothelin type A receptor (Zhang et al., 1999). Conversely, the V_2R remains bound to β-arrestin into endocytic vesicles, which is thought to prevent receptor dephosphorylation (Oakley et al., 1999). This was also found for the neurotensin receptor 1 and $AT_{1A}R$ (Zhang et al., 1999).

A number of GPCRs contain PDZ (**P**ostsynaptic density 95/**D**isc large/**Z**onula occludens-1 homology) binding domains at their carboxyl terminus (in the β_2AR the amino acid sequence is DSLL), a further recycling determinant key for the sorting of internalised receptors. The PDZ binding is responsible for

interacting with the PDZ domain present on scaffold proteins such as EBP50 (ezrin-binding protein, also known as NHERF1,Na^+-H^+ exchange regulatory factor 1). This appears to facilitate further interactions with the actin cytoskeleton and facilitates β_2AR recycling. In the β_2AR, Ser411, found within this binding domain, becomes phosphorylated by GRK5, but not by GRK2. GRK2 appears to play no role in β_2AR recycling, because even over-expression of GKR2 had no effect, suggesting GRK-specific roles in receptor trafficking. Phosphorylation of Ser411 by GRK5 on the other hand, recreated in the S411D mutant (phospho-dominant), prevented EBP50 from binding the β_2AR, and thus inhibited its recycling (Cao et al., 1999). Additionally, the removal of this region in the A_2B adenosine receptor switched its phenotype, and inhibited recycling (Mundell et al., 2010).

Receptors can also enter the degradation pathway, which targets receptors to the lysosomes, causing long term down-regulation, for example the δ opioid receptor (Marchese et al., 2003; Tsao and von Zastrow, 2000). For several GPCRs, ubiquitination has been found to have a role in targeting the receptor protein to the lysosomes for degradation, mediated by E3 ligases, a family of enzymes which covalently attach ubiquitin to the receptor (Shenoy et al., 2001; Shenoy et al., 2009). Interestingly, ubiquitination has also been found to play a role in regulating the internalisation and trafficking of GPCRs (Canals et al., 2012; Wolfe et al., 2007). Similarly, receptors also contain more motifs in their carboxyl terminus which regulate the binding of sorting proteins (Castro-Fernandez and Conn, 2002), such as the GPCR sorting associated protein

(Thompson and Whistler, 2011), and SNX1 (Kurten et al., 1996), both of which are implicated in lysosomal targeting (Gullapalli et al., 2006).

Thus, a combination of β-arrestin regulation, receptor phosphorylation or ubiquitination, and other scaffold proteins such as those discussed above, all have the capacity to influence receptor trafficking and the ultimate destination to recycling or degradative pathways.

1.6.3 β-arrestin dependent signalling

Increasing evidence suggests that GPCRs can undergo β-arrestin mediated signalling. This is thought to be due to the fact that when β-arrestin binds to the activated receptor, it can also act as a scaffold for other proteins, for example for both clathrin and AP-2, which are required for endocytosis (section 1.6.2.2), or for both src and extracellular signal-related protein kinase (ERK)1/2, signalling pathways (Shenoy and Lefkowitz, 2003). This gave rise to a theory that, as well as the original ternary complex of agonist, receptor and G protein, it is also possible to postulate that an alternative ternary complex of agonist, receptor and β-arrestin may also exist, and can elicit signalling, such as ERK activation.

1.6.3.1 The ERK signalling cascade

The ERK pathway (classically also known as the MAPK pathway; originally associated with tyrosine kinase linked receptors), can be activated by GPCRs in a β-arrestin or G protein dependent manner. β-arrestin mediated ERK signalling has been found to be slower, but longer lasting than G protein mediated ERK signalling, and was localised to the endosomes in the cytosol

(Ahn et al., 2004). This is in contrast to the G protein mediated ERK signalling which has been found to be rapid but transient, and resulted in activated ERK being translocated to the nucleus (Ahn et al., 2004). In vascular smooth muscle cells, β-arrestin activation of ERK requires PKCζ, and both the G protein and β arrestin pathway appear to regulate proliferation independently of each other (Kim et al., 2009).

β-arrestin activation of ERK and related pathways such as c-Jun N-terminal kinase (JNK) is via activation of the MAPK cascade of phosphorylation. The activation of MAPKKKs (e.g. Raf-1 for ERK), leads to the phosphorylation of MAPKKs, which in turn phosphorylate MAP kinases, such as JNK, ERK and p38. pJNK and pERK become stabilised in the endosomes, or translocate to the nucleus. Here, they mediate the phosphorylation and transcription of genes involved in differentiation and proliferation (Morrison and Davis, 2003). An example of this is in the mesenchymal stem cells: prostaglandin E2 mediated activation of β-arrestin and subsequent activation of JNK leads to both cellular migration through the reorganisation of the cytoskeleton (Xiao et al., 2010) and proliferation (Yun et al., 2011). Additional examples of receptors that undergo β-arrestin mediated ERK signalling include β_2AR (Luttrell et al., 1999), protease activated receptor (PAR)2 (DeFea et al., 2000) and CXCR7 (Canals et al., 2012). There is also evidence for ERK recruitment and signalling continuing once the “desensitised” receptor:β-arrestin complex has entered the endosomes (Zimmerman et al., 2011).

1.6.3.2 Src scaffolding

β-arrestin can also activate ERK, via scaffolding with Src (Charest et al., 2007; Luttrell et al., 1999; Luttrell et al., 2001); for example src regulates the Rb-Raf1 pathway, which causes cell proliferation, thought to be the GPCR pathway through which nicotine is mitogenic and carcinogenic (Dasgupta et al., 2006). This receptor:β-arrestin:Src interaction can also influence internalisation (Miller et al., 2000). Src also activates JNK (Kraus et al., 2003) in a β-arrestin dependent manner (McDonald et al., 2000), and also in a β-arrestin dependent manner to mediate ghrelin receptor activation of Akt (Lodeiro et al., 2009).

1.6.3.3 Akt and PP2A

β-arrestin can also form a signalling scaffold with Akt (also known as protein kinase B) and PP2A. Akt plays a role in the P13K > Akt > mammalian target of rapamycin (mTOR) signalling pathway that is involved in mediating apoptosis, cell proliferation and migration (Morgensztern and McLeod, 2005). Meanwhile, the activity of PP2A can inhibit Akt signalling (Pandey et al., 2013). Therefore, it was interesting that dopamine receptor activation led to a reduction in Akt activity in a β-arrestin dependent way. This was found to be due the fact that β-arrestin interacts with both Akt and PP2A, bringing them both together in a signalling scaffold. Altogether, the dysregulation of this complex, and its consequent effects on synaptic transmission, could be involved in dopamine-related disorders such as schizophrenia (Beaulieu et al., 2005).

1.6.3.4 Phosphodiesterases

The activation of β_2AR can also result in the formation of another signalling complex, mediated by β-arrestin. In this example, the signalling complex is completed by a PDE4D, which causes the degradation of cAMP. The formation of this signalling complex is thought to play a role in the regulation of β_2AR cAMP dependent signalling. More complex consequences can also arise via alterations in PKA regulation of the β_2AR, which can modify its G protein coupling from Gs to Gi, and also affect downstream ERK signalling in cardiomyocytes (Baillie et al., 2003).

1.6.4 Biased signalling

The realisation that GPCRs can couple to multiple signalling pathways has given rise to the concept of biased signalling, in which receptor may show a preference for signalling through a particular effector (e.g. G protein or β-arrestin) dependent upon which ligand is bound. This is thought to be due to a multi state model of activation, whereby different ligands may stabilise different conformations of the receptor which then differentially activate different signalling molecules (Azzi et al., 2003). For example, one ligand could stabilise the receptor in a conformation that uncovers certain cytoplasmic loops that allow for G protein coupling and the subsequent signalling through that pathway, whereas another ligand could stabilise the receptor in a different conformation that uncovers β-arrestin binding sites, giving the basis for ligand bias (Kenakin, 2001). The β-blocker propranolol was an early example of a ligand with signalling bias. At β_2AR it was found to be an inverse

agonist on the Gs coupled pathway of adenylyl cyclase, which led to a decrease in cAMP production, whilst it was an agonist on the MAPK pathway and activated ERK1/2 through a G protein independent pathway (Azzi et al., 2003; Baker et al., 2003).

This has also been observed in the M_3 receptor, where in response to different ligands the receptor was shown to undergo different patterns of phosphorylation, which then led to different signalling outcomes. Thus, a phosphorylation "bar code", in addition to ligand specific receptor conformations, could also offer an explanation for biased signalling (Butcher et al., 2011).

In the δ opioid receptor, it has been found that the ligands DPDPE and SNC-80 elicit different recycling profiles by causing distinct receptor conformations, altering their interactions with β-arrestin. This work also showed that although the δ opioid receptor is characterised as being a typical degradation pathway receptor, it can also undergo agonist-specific recycling, giving an example of ligand directed receptor regulation (Audet et al., 2012).

1.6.5 The role of GPCR dimerisation

Another emerging phenomenon that has been shown to regulate GPCR function is the potential formation of receptor oligomers (the simplest case being a dimer). The arguments and experimental evidence both for and against GPCRs undergoing dimerisation will now be presented.

1.6.5.1 Evidence for GPCRs as monomeric receptors

The question of whether class A GPCRs form dimers is controversial (Chabre and le Maire, 2005). Some argue that GPCRs exist as monomers, and that the formation of dimers *in vitro* is an artefact, due to co-operativity between over-expressed receptors in an artificial environment (the recombinant system), a situation that may not occur *in vivo* (Chabre et al., 2009). There is some evidence for the existence of monomers using artificial systems, and that these monomers could be functional at all levels of receptor activation.

Firstly, the μ opioid receptor was reconstituted into high density lipoprotein (HDL) discs, and using single-molecular imaging was found to be monomeric and capable of binding the agonist dermorphin (Kuszak et al., 2009). FRET was utilised in the study of β_2AR (Whorton et al., 2007), and rhodopsin (Ernst et al., 2007), which were found to be able to dock with the relevant G proteins, Gs and transducin respectively, as monomers. Rhodopsin was also reconstituted into HDL discs, determined to be a monomer using a size exclusion column, and was shown to efficiently activate transducin (Whorton et al., 2008). Rhodopsin monomers in nanodiscs were found to activate the signalling proteins transducin (Bayburt et al., 2007), rhodopsin GRK1 and arrestin1 (Bayburt et al., 2011). Additionally, the crystal structure of Gs bound to β_2AR was shown to be in monomeric form (Rasmussen et al., 2011b).

1.6.5.2 Evidence for GPCR homodimers

Despite the ability of GPCRs to activate their effectors as monomers, many studies, using various techniques have shown evidence for a multitude of

class A GPCRs forming dimers (reviewed in (Milligan, 2009)), from which some examples are discussed below.

1.6.5.2.1 Functional "mutant rescue" studies

There is evidence for receptor dimers in both recombinant systems and native cells. Early work on chimeric receptors found that both the α2 adrenergic and β_2AR (Kobilka et al., 1988), and the M_3 muscarinic and α adrenergic receptors could be split into two halves, i.e. TM 1-4 and TM 5-7, which could then interact when co-expressed undergo complementation to restore receptor function (Maggio et al., 1993). Also, in another study, mutants of the type 1 angiotensin receptor were created. One mutant was deficient in binding ligand, whilst another could no longer couple to G protein. Co-expression of the two restored function, thought to be mediated through transcomplementation (Monnot et al., 1996). This gave the first glimpse at the existence of GPCR dimers, but did not exclude the possibility that one functional monomer unit was generated by "swapping" the relevant TM domains, though this possibility is perhaps less likely from the recent crystal structures.

Recently, functional co-operativity between binding and signalling receptor mutants has also been demonstrated *in vivo*. A study on the luteinizing hormone (LH) receptor using transgenic mice found that the co-expression of a binding mutant with a signalling mutant led to co-operation between the mutants. Intermolecular functional complementation between the two was

observed to restore the normal action of LH, which the authors postulated was due to dimer formation between the mutants (Rivero-Muller et al., 2010).

Additionally, various types of microscopy have also been utilised to determine dimerisation, which will now be covered.

1.6.5.2.2 Dimers indicated by FRET and BRET

These approaches use measurement of the energy transfer between a donor (fluorescence or luminescence) and acceptor label to indicate close proximity (< 10 nm) of the tagged proteins. They have been very widely used to demonstrate the presence of GPCR oligomers (for a review see (Milligan and Bouvier, 2005)). The principle of FRET is of energy transfer between two chromophores fused to the proteins of interest. The donor chromophore, typically CFP, is laser excited, and if it is within ~100 Å of its FRET partner, typically YFP, it transfers energy to the acceptor (Milligan and Bouvier, 2005). This technique was used to determine that the serotonin 5-hydroxytryptamine2c receptor expressed on HEK293 (human embryonic kidney) cells undergoes homodimerisation on the plasma membrane, and this was also backed up biochemically using co-immunoprecipitation and Western blotting (Herrick-Davis et al., 2004). Moreover, the application of time resolved (TR)-FRET in native tissues using fluorescent ligands demonstrated the presence of endogenous oxytocin receptor higher order oligomers in the mammary gland (Albizu et al., 2010). TR-FRET was also used in the detection of $GABA_B$ receptor tetramers in the plasma membrane of brain tissue (Comps-Agrar et al., 2011). One limitation of FRET is that it requires a laser as the

input to activate the first FRET partner, which can cause background or photobleaching. To counteract this, bioluminescence resonance energy transfer (BRET) was developed, which requires no laser input, because it uses *Renilla* luciferase and a chemical substrate to activate the donor luminescent partner.

Use of BRET for example (Gales et al., 2005), demonstrated that CXCR4 undergoes constitutive oligomerisation, which was again backed up biochemically using co-immunoprecipitation (Babcock et al., 2003), and later by the presence of a dimer structure in the x-ray crystals of CXCR4 (Wu et al., 2010). However, there is some controversy to the BRET technique, in whether receptor over-expression can produce artefacts (James et al., 2006).

1.6.5.2.3 Other microscopy

Atomic force microscopy was used on native rod membranes and discovered that rhodopsin existed in "arrays" of dimers (Fotiadis et al., 2003). Finally, two microscopic techniques were employed to undergo single cell imaging. Firstly, total internal reflection fluorescence microscopy was used to image a fluorescent M_1 antagonist bound to its receptor, which suggested that ~30 % of the antagonist-occupied M_1 muscarinic receptors were in dimeric form at any one time (Hern et al., 2010). Fluorescence recovery after photobleaching (FRAP) has also been utilised to determine that β_1AR undergoes transient dimerisation, whilst β_2AR was found to form sustained dimeric formation (Dorsch et al., 2009). Additionally, the utilisation of other techniques to measure dimerisation such as FCS and PCH will be discussed in chapter 5.

1.6.5.2.4 Structural information about GPCR dimer interfaces

The x-ray structure of the μ opioid receptor crystallised with the antagonist morphinan, showed evidence of higher order oligomer organisation, with interactions between TM 1, TM 2 and helix 8 (Manglik et al., 2012), as did the κ opioid receptor structure, bound to selective antagonist JDTic (Wu et al., 2012). This interaction has been seen in other x-ray crystal structures of opsin (Park et al., 2008), rhodopsin (Salom et al., 2006) and β_2AR (Cherezov et al., 2007) and β_1AR (Huang et al., 2013).

The x-ray structure of CXCR4, which is involved in the regulation of leukocyte migration, was revealed to be in a dimer formation, interacting on the extracellular side through TM 5 and 6 (Wu et al., 2010), as also seen in the μ opioid receptor, where TM 5 and TM 6 of each protomer interacted through a four helix bundle motif (Manglik et al., 2012). Interactions between TM 5 have also been seen in the M_3 muscarinic receptor (Hu et al., 2012). Meanwhile, on the intracellular side CXCR4 interacts through TM 2 and 4 with ICL2 (Wu et al., 2010).

This was similar to the second interface seen in the β_1AR dimer, mediated through TM 4, TM 5 and ICL2, but that only the other form of dimer (TM 1, 2 and 8) could interact with the G protein (Huang et al., 2013). The δ opioid dimer has also been suggested to have an interface through TM 4 and 5 (Johnston et al., 2011), but its x-ray structure showed no clear dimerisation (Granier et al., 2012).

1.6.5.3 GPCR heterodimers

The strongest evidence for GPCR dimerisation originates from the class C receptor family. Indeed, the $GABA_B$ receptor requires hetero-dimerisation between 2 subunits for plasma membrane expression and function. Both the $GABA_{B1}$ and $GABA_{B2}$ subunits must be present in dimer formation for the $GABA_B$ receptor to be fully functional (White et al., 1998). This is because both subunits are required for the trafficking of the dimer to the cell surface, as they interact directly through coiled coil α helices present in their intracellular tails (Kammerer et al., 1999; Kuner et al., 1999). This causes the $GABA_{B2}$ subunit to cover an endoplasmic reticulum retention signal of positively charged amino acids, RSRR, present on the carboxyl tail of the $GABA_{B1}$ subunit, which then allows the heterodimer to be cell surface expressed (Margeta-Mitrovic et al., 2000).

Studies have also shown that the $GABA_{B1}$ subunit must be present to allow agonist binding, whilst the $GABA_{B2}$ subunit couples to the G protein (Jones et al., 1998; Kaupmann et al., 1998). Further work showed more complexity in that allosteric modulation between both subunits also contributes to function. $GABA_{B2}$ increases the affinity of GABA for $GABA_{B1}$, whilst $GABA_{B1}$ improves coupling efficacy of $GABA_{B2}$ (Galvez et al., 2001; Mukherjee et al., 2006).

1.6.5.3.1 FRET and BRET approaches to detect heterodimers

The venus fly trap motif present in class C receptors also plays a significant role in $GABA_B$ heterodimerisation and the homodimerisation of metabotropic glutamate receptors, involving a disulphide bond between the motifs

(Rondard et al., 2008). In fact, the GABA receptors (but not glutamate receptor mGluR1 dimers), were found to form higher order tetramers, using a combination of labelled SNAP-tag and FLAG-tagged receptors and measuring their interactions using TR-FRET (Comps-Agrar et al., 2011; Maurel et al., 2008).

Both FRET and BRET have been used extensively to suggest class A GPCR heterodimer pairings (in the absence of the clear structural motifs present in class C receptors (Milligan and Bouvier, 2005)). For example, BRET was used to study the propensity of the opioid δ, μ and κ receptor subtypes to form heterodimers. It was found that all three subtypes were equally as likely to form heterodimers with each other, but they did not form dimers with the M_2 muscarinic receptor, suggesting that these dimer interactions are specific to opioid receptors (Wang et al., 2005). This complements biochemical studies done on this group of receptors. Both δ and κ (Jordan and Devi, 1999), and μ and δ (George et al., 2000) were found to form heterodimers using co-immunoprecipitation, whilst μ and κ were found to heterodimerise using crosslinking approaches (Chakrabarti et al., 2010).

1.6.5.3.2 Radioligand binding

Binding has also been used to examine GPCR heterodimerisation (Birdsall, 2010). One study used radioligand binding studies on the κ and δ opioid receptors. Selective ligands were used at the κ:δ heterodimers, and were found to have lower affinity than for the single subtype expressed alone Interestingly however, these ligands were found to bind co-operatively and

have synergistic responses in cells expressing both subtypes (Jordan and Devi, 1999).

1.6.5.3.3 The potential of dimers to influence the stoichiometry of ligand:receptor:effector interaction

One of the key unresolved questions about the functional role of GPCR dimers is the influence this process has on the stoichiometry between ligand, receptor and signalling effector molecules. Differences in receptor stoichiometry for different ligand and effector combinations for example, might lead to an explanation for biased signalling (section 1.6.4). Understanding the way in which dimers interact with effectors is also critical for explaining how heterodimers might couple to "new" signalling pathways not shared by the single receptor subtypes. Four models have been postulated for how this stoichiometry may form in the context of G proteins (Gurevich and Gurevich, 2008) which are detailed as follows:

A) one active receptor monomer: one G protein. As discussed above, various studies on rhodopsin, β_2AR and μ opioid receptors have found them to be fully functional as a monomer in activating one G protein. In these studies, the receptors were reconstituted into lipid discs of a defined diameter to only allow the incorporation of a monomer, (Bayburt et al., 2007; Ernst et al., 2007; Kuszak et al., 2009; Whorton et al., 2007; Whorton et al., 2008).

B) one active receptor in a dimer: one G protein

Some class C receptor studies, for example using mutated protomers of the class C mGlu receptors, have suggested that a dimer activates a single G protein (Baneres and Parello, 2003; Hlavackova et al., 2005).

Studies have also been carried out on class A receptors. The CXCR4 receptor for example, forms heterodimers with CCR2, and experiments using BRET found that these dimers are responsive to the agonists for both receptors, but only one receptor undergoing activation is required for a response from both protomers (Percherancier et al., 2005). Another class A receptor, rhodopsin, was reconstituted as dimers in nanodiscs, and it was found that, due to steric hindrance, only one rhodopsin moiety in the dimer was able to couple with transducin (Bayburt et al., 2007); this also reflects the inhibitory action of NTS1 dimers on G protein activation (White et al., 2007).

Additionally, work on a fluorescently labelled class A leukotriene B_4 receptor showed it to be activated when only one protomer was activated by ligand, leading to asymmetric activation of the G protein (Damian et al., 2006). Similarly, using a luminescence assay, a dopamine D_2:D_4 heterodimer was found to undergo asymmetrical activation of one G protein (Han et al., 2009).

C) two active receptors in a dimer: two G proteins (i.e. each receptor in the dimer activates its respective G protein)

This setup is thought to be less likely. In the study on purified neurotensin NTS1 receptors, it was possible for two receptors to activate two G proteins,

but there is negative co-operativity between the two G protein binding sites on the two NTS1 protomers, resulting in reduced G protein coupling compared to in a monomer (White et al., 2007).

D) two active receptors in a dimer: one G protein

Using FRET, it was found that the 5-HT_{2C} heterodimer could bind two molecules of ligand, which together only activated one G protein (Herrick-Davis et al., 2005).

1.6.5.3.4 β-arrestin as an alternative coupling protein

A final point to consider is β-arrestin as an alternative effector protein. It has been suggested (on the basis of modelling inactive structures) that 2 rhodopsins might interact with one β-arrestin molecule (Fotiadis et al., 2003). There is also some evidence for hetero-dimerisation modulating β-arrestin dependent internalisation (see section 1.6.5.4.3). Conversely, receptors can also internalise as monomers (Gurevich and Gurevich, 2008), and in rods, the ratio of rhodopsin:β-arrestin has been reported to be 1:1 (Hanson et al., 2007).

1.6.5.4 The potential for GPCR dimerisation to lead to altered signalling

The formation of a receptor dimer may have different signalling characteristics to a monomer, perhaps by modulating the response, changing it entirely, or creating a novel response (Rozenfeld and Devi, 2011).

1.6.5.4.1 Novel signalling pathways and pharmacology for GPCR heterodimers

An interesting example of this was found by the co-activation of both Gs coupled D_1 and Gi coupled D_2 dopamine receptors, which was found to give a novel Gq mediated calcium signalling response. This response was not mediated by either receptor alone, giving evidence of dimerisation being responsible for a completely novel signal (Lee et al., 2004).

The μ:δ opioid heterodimer had novel signalling responses as a dimer, because although both subtypes are Gi coupled, these responses were no longer sensitive to the Gi inhibitor *Pertussis* toxin (PTx). Dimers also had altered pharmacology in response to the selective agonists of DAMGO at μ, and DPDPE for δ (George et al., 2000).

Equally, heterodimers may generate entirely novel pharmacology for ligands. For example, a ligand that specifically activates κ:δ opioid heterodimers, but not homodimers has been identified, suggesting that the heterodimers form a novel binding site. This demonstrated the relevance of targeting opioid heterodimers in *vivo*, and that these could be a druggable target for analgesia (Waldhoer et al., 2005).

1.6.5.4.2 Modulating the overall level of response

As discussed in 1.6.5.4, different stoichiometries of ligand:receptor:effector interaction have potential to produce different levels of associated coupling. While for many dimeric receptors, asymmetric activation of the G protein has been proposed (option B, section 1.6.5.4), there are exceptions that suggest

dimers could increase coupling. For example a study of the serotonin 5-HT_4 receptor showed that activation of both protomers in the dimer was required for full activation of signalling, which is in direct opposition to the findings that the NTS1 protomers exerted negative co-operation upon each other in a dimer with respect to their ability to elicit G protein coupling (White et al., 2007). This was thought to result from co-operativity between the two promoters which doubled the level of G protein activation, measured using GTPγS incorporation. The authors postulated that this may give rise to graduated levels of response depending on the activation of one or both protomers (Pellissier et al., 2011). A similar finding was also shown for the mGlu1 receptor. When agonist bound to one protomer, the receptor was partially activated; but for full activation agonist needed to bind both protomers in the dimer (Kniazeff et al., 2004). Another example is how heterodimerisation appeared to modulate signalling by the opioid receptor family. A switch from β-arrestin mediated ERK signalling in μ:δ opioid receptor co-expressing cells to non β-arrestin mediated ERK activation was observed when cells were co-treated with both μ and δ ligands (Rozenfeld and Devi, 2007).

1.6.5.4.3 Modulating intracellular trafficking

Perhaps related to the change in arrestin recruitment patterns, μ:δ opioid receptor heterodimers also show differential intracellular trafficking compared to either subtype expressed alone. The agonist etorphine, which induces internalisation of the δ opioid receptor, did not cause internalisation

of the heterodimer (George et al., 2000). Also, the presence of the κ opioid receptor in a co-expressed population prevented internalisation in response to opioid agonists when expressed with the δ opioid receptor (Jordan and Devi, 1999), or in response to adrenergic agonists when expressed with the β_2AR. Conversely, when β_2AR was co-expressed with the δ opioid receptor, the heterodimer readily internalised in response to both types of agonists (Jordan et al., 2001).

1.7 Aims and objectives of the thesis

This introduction has demonstrated that whilst obesity and type II diabetes are growing health concerns in the world, there is an enduring need for new pharmacological tools to clinically deal with both morbidities. Of a range of novel therapeutic targets, the FFA nutrient sensing GPCRs FFA1 and GPR120 have been identified as being of particular interest, because of their localisation on gut and pancreatic endocrine cells, and their potential to stimulate insulin and satiety hormone secretion. The understanding of the pharmacology and signalling exhibited by these receptors is still at a relatively early stage. The aims and objectives of this thesis could be seen as follows. Firstly, following the de-orphanisation of GPR120, no full comparison of its signalling and regulatory pathways has been carried out, particularly in the context of the two splice variant isoforms. To address this, these pathways will be investigated, to ascertain if there are any pharmacologically relevant isoform specific differences (chapter 3). This characterisation will be achieved using an array of both high content screening and confocal imaging

techniques in conjunction with functional assays. Additionally, constrained GPR120 and FFA1 dimers will be generated using the technique of bimolecular fluorescence complementation to investigate the possibility of novel ”dimer” pharmacology. Following on from this, there is published mutagenesis information defining the FFA1 binding site but not for GPR120. Therefore, if drugs are to be designed to selectively target GPR120 over FFA1 (or vice versa), more detailed knowledge of the GPR120 binding site is required, which is addressed in chapter 4. Site-directed mutagenesis, led by molecular modelling from colleagues at AstraZeneca, will be used to define the way different endogenous and synthetic agonists bind GPR120.

There is also another issue for drug discovery at these receptors. There is a lack of high affinity selective radiolabelled ligands for traditional binding assays. These types of assay are key for deriving essential data (affinity estimates) about potential drug candidates. Therefore, a fluorescent agonist will be generated and characterised with the aim of replicating these binding assays to determine ligand affinity, for example at FFA1. Fluorescence correlation spectroscopy studies will also be undertaken to characterise the diffusion and stoichiometry of FFA1 receptors, and to demonstrate the ability to measure ligand binding at the single cell level (chapter 5).

Chapter Two: Materials and Methods

2.1 Materials

pcDNA4/TO and pcDNA3.1zeo DNA vectors, HEK293T/TR cells, lipofectamine, Optimem, selection antibiotics, Fluo4AM, Pluronic® F-127, LysoTracker® red and transferrin conjugated to AlexaFluor(AF)-633 were from Invitrogen, Paisley, UK.

Restriction enzymes, fast shrimp alkaline phosphatase and pJET cloning kit were from Fermentas, St. Leon-Rot, Germany.

All other chemicals and reagents were purchased from Sigma Aldrich, Poole, UK unless otherwise stated.

2.2 Methods

2.2.1 Molecular Biology

All molecular biology procedures that follow were a modified version of those found in “Molecular Cloning” by Sambrook and Russell (Sambrook and Russell, 2001).

2.2.1.1 Analysis of DNA products

To analyse a DNA product, it had to be excised from the vector in which it was contained by performing a restriction digest. This digest product was then run on an agarose electrophoresis gel to determine its size. If the band was of the correct size, this band would be excised to liberate the DNA. This protocol will be covered in the next 3 sections.

2.2.1.1.1 Restriction digestion

The choice of enzymes for performing a restriction digest was key, because they must only cut in the one place required. Also, it was seen as preferential to use 2 different enzymes, one at either end of the insert, where the purpose was to ligate an “insert” DNA (e.g. for the receptor) into a different plasmid vector. This ensured that the insert could only go into the plasmid in the correct orientation. Additionally, the enzymes chosen also produced “sticky” ends that overhang, again to ensure the correct orientation of insert in the vector (the exception to this is pJET ligation, in which blunt ended PCR products were used, covered in section 2.2.1.7.3).

To perform a restriction digest, a reaction mixture of 20 µl in total was prepared in a sterile 0.5 ml tube, and consisted of 2 µg of DNA, 1 µl (1 unit; 1 unit is defined as the amount of enzyme required to incorporate 10 nmoles of dNTPs into acid insoluble form in 30 min at 72^{o}C) per restriction enzyme (Fast Digest, from Fermentas) with 2 µl of 10x Fast Digest buffer (supplied with enzyme). This underwent a 1 hr incubation at 37^{o}C, then a 20 min incubation at 65^{o}C, with an additional enzyme heat inactivation step of 5 min at 80^{o}C.

2.2.1.1.2 Gel electrophoresis

Following restriction enzyme digestion, gel electrophoresis was utilised to separate the DNA fragments produced (e.g. insert and plasmid vector). The principle behind this is that the negatively charged DNA migrates via the gel pores towards the positive electrode in a size dependent manner, i.e. the smaller DNA products migrate faster than the larger DNA products.

This was done by preparing an agarose gel that consisted of agarose (1 % w/v) dissolved in TBE buffer (89 mM Tris HCl, 89 mM Boric acid, 2 mM EDTA (ethylenediaminetetraacetic acid), pH 7.6) using a microwave. After allowing the mixture to cool slightly, ethidium bromide (0.1 µg ml^{-1}) was added, because this is an agent that intercalates into DNA, which allowed for the visualisation of the DNA under ultra violet light. This was then poured into a tray and a comb was added. Once set, this was placed into an electrophoresis tank and covered completely with TBE buffer. DNA samples were mixed with a blue loading buffer (0.25 % w/v bromophenol blue, 50 % v/v glycerol in TBE) and loaded into the wells created by the comb. A molecular weight marker

was also added to a well (BenchTop 1 kb DNA ladder, Promega). The gel was then run at 80 V until sufficient separation has been achieved based on dye migration. DNA was visualised on a Syngene GVS-30 transilluminator, which allowed the size of the DNA sample to estimated by comparison to the molecular weight marker (an example gel is shown in Figure 2.1).

2.2.1.1.3 Gel extraction

The DNA was then purified using a Gel Purification Kit (Sigma) to manufacturer's instructions. This kit used a silica gel-based method of DNA purification using column chromatography. Firstly, the gel was weighed in an Eppendorf and 3 gel volumes of gel solubilisation solution were added (i.e. for 100 mg of gel, 300 µl of solution was added) and incubated for 10 min at 60^{o}C, with occasional vortexing to help solubilisation. This solution contained a chaotropic salt, which removed the water molecules that surrounded the DNA phosphate backbone. This resulted in these phosphates being able to bind onto the silica in the columns. One gel volume of isopropanol was added to the solubilised gel solution (this both enhanced specific binding and reduced non-specific binding to the silica), and the binding column was prepared with column preparation solution, prior to the addition of the solubilised gel solution to the binding column. This addition resulted in the DNA becoming bound to the silica filter. An ethanol based wash solution was used to remove contaminants, but does not affect the DNA binding. The DNA was then eluted in 50 µl dH_20, resulting in rehydration of the DNA which then allows the DNA to become unbound from the silica in the column.

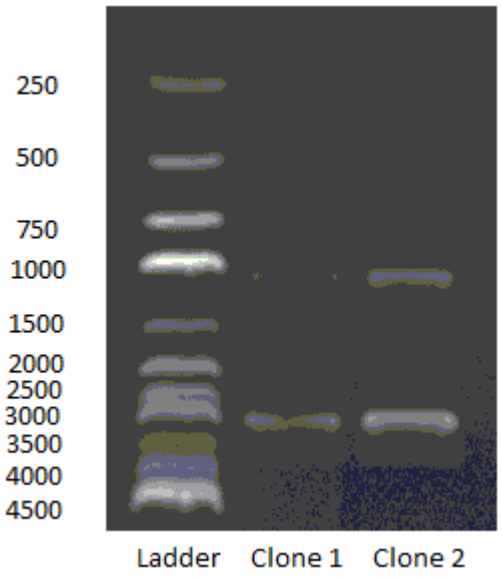

Figure 2.1 A representative agarose gel.
Clone 1 (middle lane) and 2 (right lane) have been digested with BamHI and XhoI, and for clone 2, this liberated the insert, SNAP-GPR120S-Δ346 of the correct size (1041 bp) from the pJET cloning vector (2974 bp), with a DNA ladder in the left lane.

2.2.1.2 Transformation of DNA into chemically competent cells

Next to be described is the protocol by which DNA was transferred into chemically competent cells, which allowed for further downstream applications such as mini prep DNA purification.

2.2.1.2.1 Preparation of competent cells

There are a few strains of *E.coli* suitable for making chemically competent cells, including XL-1. These cells contain mutations to make them more suitable for DNA transformation. For example, XL-1 cells contain a *hsd*R17 mutation which knocks out the *Eco*K I methylase, preventing the cells from cleaving plasmid DNA by the *Eco*K endonuclease enzymes; they lack both *endA* nuclease, which improves the quality of DNA purified using the miniprep protocol and *recA* recombinase which improves the stability of inserts; and they also contain a gene for tetracycline resistance.

Prior to transformation, agar plates were produced. Luria Bertani (LB) agar was made using 35 g of commercially available powder (containing 1 % peptone, 0.5 % yeast extract and 1 % NaCl), made up to 1 L using deionised water. This was sterilised by autoclaving, and when it had cooled to 55^{o}C, tetracycline was added at 10 µg ml^{-1}. The mixture was then poured into Petri dishes, any bubbles were removed and the dishes allowed to set.

To generate chemically competent cells, XL-1 strain *E.coli* cells were then streaked out onto an LB agar plate. Streaking involves using sterile apparatus such as an inoculation loop to introduce progressively fewer bacterial cells to the agar, until single colonies are able to grow. This plate was incubated

overnight at 37^{o}C. The next day, one colony was picked using a sterile pipette tip and grown overnight in 5 ml LB broth at 37^{o}C. On the third day, this 5 ml was added to 20 ml 2YT (2x yeast and tryptone; 1.6 % peptone, 1 % yeast extract and 0.5 % NaCl) media, and agitated at 250 rpm until the cells had grown to a density of OD_{600} = 0.2 – 0.8 (this corresponds roughly to the mid-log phase of bacterial growth). When at the correct density, this was then poured into 1 L flask containing 80 ml 2YT medium plus 10 µg ml^{-1} tetracycline, and was agitated again until OD_{600} = 0.5 – 0.9. This was then further diluted to 250 ml using 2YT medium, and again agitated until OD_{600} = 0.6. This was then rapidly cooled in ice water with gentle shaking. The pellet was collected by centrifugation for 15 min at 4,000 rpm at 4^{o}C. The pellet was resuspended in 50 ml TfB I (30 mM potassium acetate, 50 mM $MnCl_2$, 64 mM KCl, 10 mM $CaCl_2$, 15 % glycerol at pH 5.8) with gentle shaking on ice. The pellet was again collected by centrifugation for 8 min at 4,000 rpm at 4^{o}C, then the supernatant was poured off. The pellet was resuspended in 10 ml cold TfB II (10 mM 3-(N-morpholino)propanesulphonic acid [MOPS], 1 mM KCl, 75 mM $CaCl_2$, 15 % glycerol, pH 7.0) with gentle shaking on ice. 400 µl were aliquoted into pre-chilled microfuge tubes, snap frozen in liquid nitrogen and stored as competent cell aliquots at -80^{o}C until required for use.

2.2.1.2.2 Transformation

The appropriate number of aliquots of cells were thawed on ice, and then aliquoted into chilled Eppendorf tubes, 100 µl per tube for each transformation reaction. 1.5 µl of β-mercaptoethanol was added (1.4 M in

H_20), which is a reducing agent used to break disulphide bonds and inactivate surface nucleases, increasing efficiency of transformation of DNA across the cell wall (Brzobohaty and Kovac, 1986). The cells were swirled to mix and incubated for 10 min on ice, swirling every 2 min. 10 ng circular plasmid DNA, or 5 µl of a ligation reaction was added and swirled. This was incubated on ice for 30 min. Then, it was heatshocked for 45 s at 42^{o}C (this temperature and time period are crucial for maximum efficiency of transformation). The tubes were returned to ice for 2 min, then 400 µl LB was added and incubated for 1 hr at 37^{o}C, shaking at 250 rpm. 200 µl was plated onto LB agar plates containing the correct plasmid selection antibiotic (e.g. 75 µg ml^{-1} ampicillin or 30 µg ml^{-1} kanamycin), and grown overnight at 37^{o}C. The next day, a minimum of two colonies were picked and placed in a 20 ml tube containing 5 ml LB broth and 75 µg ml^{-1} ampicillin, and grown overnight at 37^{o}C with shaking (250 rpm).

2.2.1.3 Small scale (miniprep) isolation and purification of cDNA

The next day, this was screened using the GenElute Plasmid Miniprep Kit (Sigma-Aldrich). This procedure purified the DNA using a silica binding-spin column format of the alkaline-SDS lysis procedure and was performed according to the manufacturer's instructions. A brief overview is as follows: first, 3 ml of the overnight culture was pelleted by centrifugation for 5 min at 5,000 rpm. This pellet was resuspended in resuspension buffer, which was a hyperosmotic sucrose solution containing RNase that degraded any RNA that may be present.

Then, an alkaline-detergent solution (NaOH/SDS) lysed the cells. It does this by the SDS degrading the cell walls, whilst the alkaline pH irreversibly denatured the chromosomal DNA, but not plasmid DNA. This occurs because the alkaline pH disrupts DNA base pairing, but due to the supercoiled structure of the plasmid DNA, it is not irreversibly affected. However, the chromosomal DNA, along with proteins and lipids, become coated with dodecyl sulphate.

Once this solution was neutralised with potassium acetate, the chromosomal DNA, proteins and lipids undergo precipitation into an insoluble cluster, due to the replacement of Na^+ with K^+ (Ish-Horowicz and Burke, 1981), which left the plasmid DNA intact in the supernatant. This step also added the chaotropic binding salts, which enabled the plasmid DNA to become bound to silica. This solution was then pelleted by centrifugation for 10 min at 13,000 rpm to remove the contaminants and prepare the plasmid DNA-containing lysate.

The binding column was placed into a microcentrifuge tube and column preparation solution was added and centrifuged. This maximised the DNA binding to the membrane in the column. The lysate was transferred to the column, and centrifuged, resulting in binding the DNA to the silica filter.

Next, the filter was washed with a wash solution containing solvent (80 % ethanol) which removes residual salts and other contaminants from the DNA, and was then re-spun without additional wash solution to remove excess ethanol. This then allowed the DNA to be eluted in 100 µl water or Tris-EDTA

(TE, 10 mM Tris HCl, 0.1 mM EDTA; pH 8.0) (Birnboim and Doly, 1979; Vogelstein and Gillespie, 1979).

2.2.1.4 Generating tagged receptors from pre-existing constructs

Human GPR120S (GenBank accession number BC101175) and GPR120L (NM_181745) cDNAs were supplied by AstraZeneca, Alderley Park, Cheshire, UK; and human FFA1 (NM_005303) cDNA was supplied by Prof T Schwartz, University of Copenhagen, Denmark. These cDNAs were inserted into three different expression vectors (Table 2.1).

These vectors had the following main features (see also plasmid maps Figure 2.3, 2.4 and 2.5): a human cytomegalovirus (CMV) promoter, which allows for high level expression and provides a binding site for sequencing. In pcDNA4T/O, this promoter also includes the tetracycline repressor protein site for tetracycline regulated expression in mammalian cells. There is also a polyadenylation signal derived from bovine growth hormone mRNA (BGH) designed for mRNA stability, which again provides a primer binding site for sequencing. The vector also provides other sites for sequencing primers to bind. In pcDNA4T/O, these are CMV F and BGH Rev; in p3.1 zeo they are T7 and BGH Rev; and in pCMV FLAG these are T3 and T7. The vectors also contain sites of antibiotic resistance for both selection in transfected mammalian cell lines and transformed bacterial cells, see table 2.1 for specific details. All vectors also contain a multiple cloning site (MCS) that contains several restriction enzyme sites to insert genes of interest into the vector.

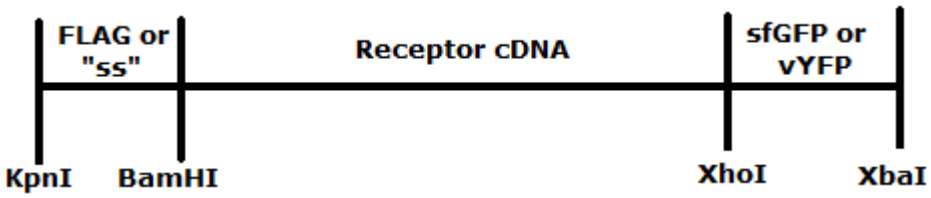

Figure 2.2 Map of restriction enzymes typically used in generating FFA receptor constructs.

Positions of KpnI, BamHI, XhoI and XbaI restriction sites used to generate receptor constructs in a vector, and positions of FLAG epitope, signal-sequence SNAP-tag (“ss”), receptor cDNA and sfGFP or vYFP if applicable.

Inserted FFA receptor cDNA sequences (Figure 2.2) lacked the start Met codon and included a stop codon unless stated otherwise. Additionally, some constructs were also modified to include the insertion of a Kozak site for translation initiation (GCCACC) followed by appropriate coding sequences between KpnI (5') and BamHI (3') to generate receptors tagged at the N terminus, with either the FLAG epitope tag (MDYKDDDDK) or a $5HT_3$ receptor derived signal sequence (MRLCIPQVLLALFLSMLTGPGEGSRK) joined to the SNAP-tag (181 amino acids), which allowed for fluorescent labelling (Keppler et al., 2003).

Some cDNA sequences also had the 3' stop codon removed to allow the addition of a fluorescent protein between XhoI (5') and XbaI (3'), using an LE linker. The fluorescent proteins used were green fluorescent protein (GFP) containing superfolder mutations S30R, F99S, N105T, M153T and V163A (Pedelacq et al., 2006), venus yellow fluorescent protein (vYFP) (Nagai et al., 2002), or YFP BiFC fragments 2-172 (vYN) or 155-238 vYC; these residue numbers correspond to the native GFP sequence (Kilpatrick et al., 2012)

A full table of vectors and their receptors follows (Table 2.1).

Vectors	Receptor insert	Bacterial resistance	Mammalian resistance	Tags	Tetracycline inducible?	Made in current project	Experimental use	Plasmid map
pcDNA4/TO	SNAP-GPR120S-GFP	Ampicillin	Zeocin	SNAP	Yes	Y	Multiple	Figure 2.3
	SNAP-GPR120L					Y		
	SNAP-GPR120S					Y		
	Includes all mutants:							
	SNAP-GPR120S R99A					Y		
	SNAP-GPR120S R178A					Y		
	SNAP-GPR120S N215A					Y		
	SNAP-GPR120S W277A					Y		
	SNAP-GPR120S W277F					Y		
	SNAP-GPR120S F311A					Y		
	SNAP-GPR120S Δ346					Y		
	SNAP-FFA1-GFP					Y		
	SNAP-FFA1					Y		
	Includes mutant:							
	SNAP-FFA1 R258A					N		
pCMV FLAG	FLAG-GPR120S-vYC	Kanamycin	Neomycin (G418)	FLAG	No	N	β-arrestin association	Figure 2.4
	FLAG-GPR120L-vYC						Constrained dimers	
	FLAG-FFA1-vYC							
p3.1 zeo+	SNAP-GPR120S-vYNL	Ampicillin	Zeocin	SNAP	No	Y	Constrained dimers	Figure 2.5

Table 2.1 Table of tagged receptor constructs.

This table shows which receptor cDNAs were inserted into which vector. It also details the major features of these vectors.

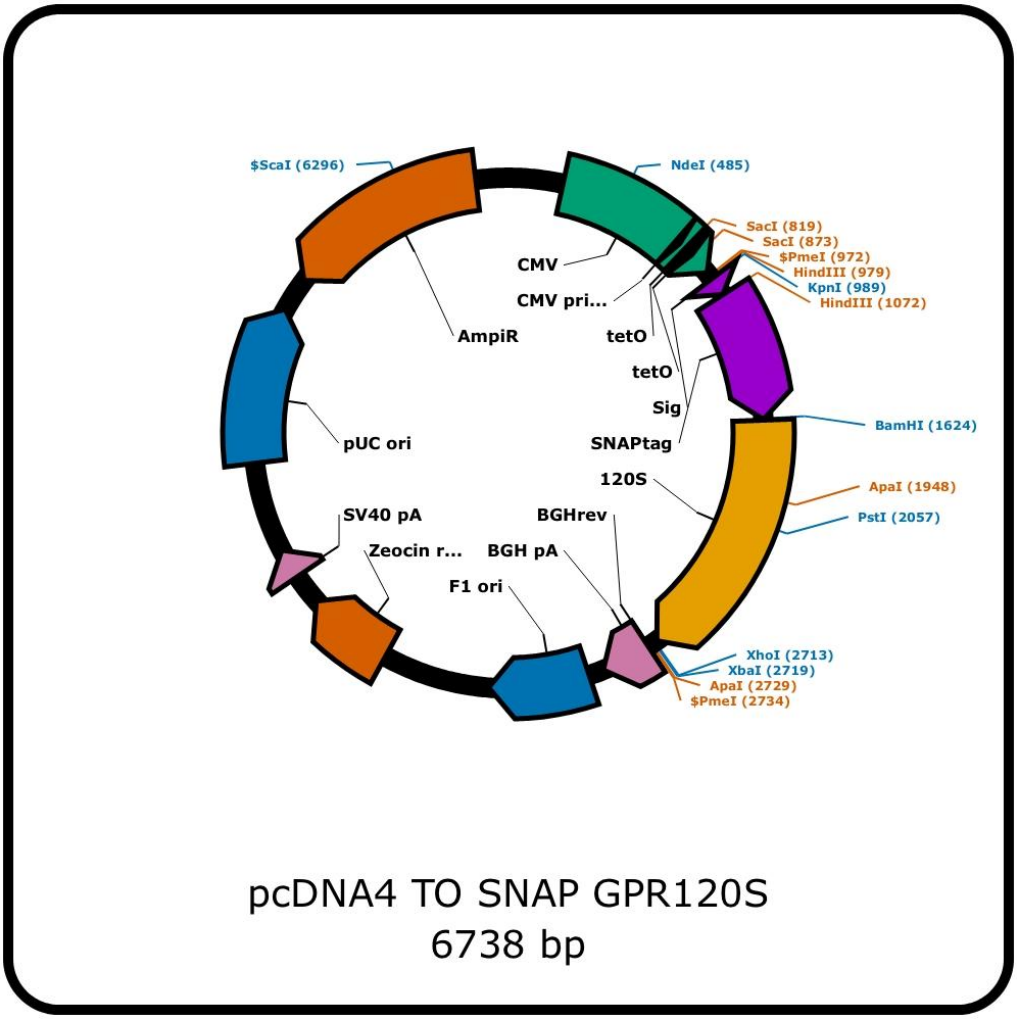

Figure 2.3 Vector map of pcDNA4T/O.

SNAP-GPR120S was placed into the pcDNA4T/O vector and contained the following features: enzyme that only cut once in the vector (blue); enzymes that cut twice in the vector (orange); the tet repressor operon binding site (TetO); bacterial origin of replication (ori); the polyadenylation sequence (pA); the signal sequence (sig); and the sites of antibiotic resistance (zeocinR; ampiR).

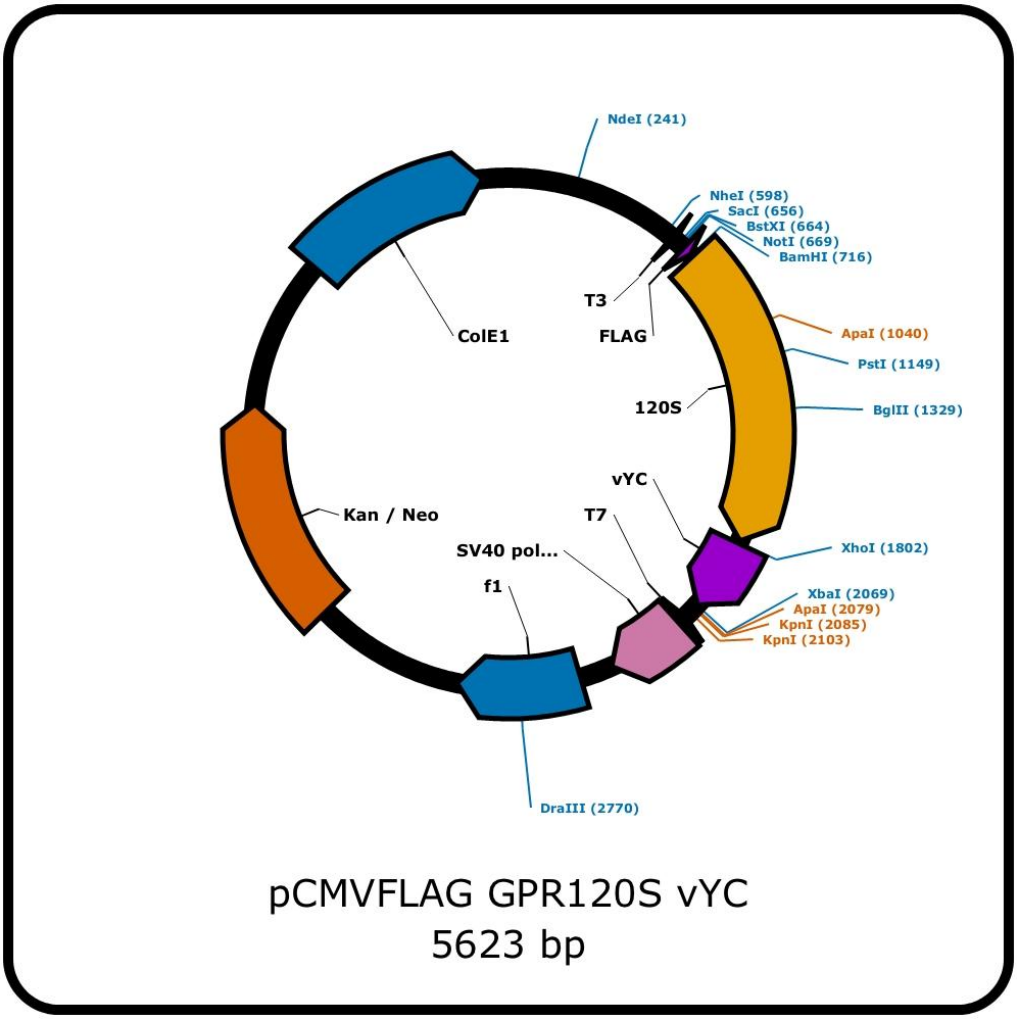

Figure 2.4 Vector map of pCMV FLAG.

GPR120S-vYC was placed into the pCMV FLAG vector and contained these features (see Figure 2.3 legend for more details on abbreviations). The pCMV FLAG vector was from Stratagene, Agilent (Cheshire, UK).

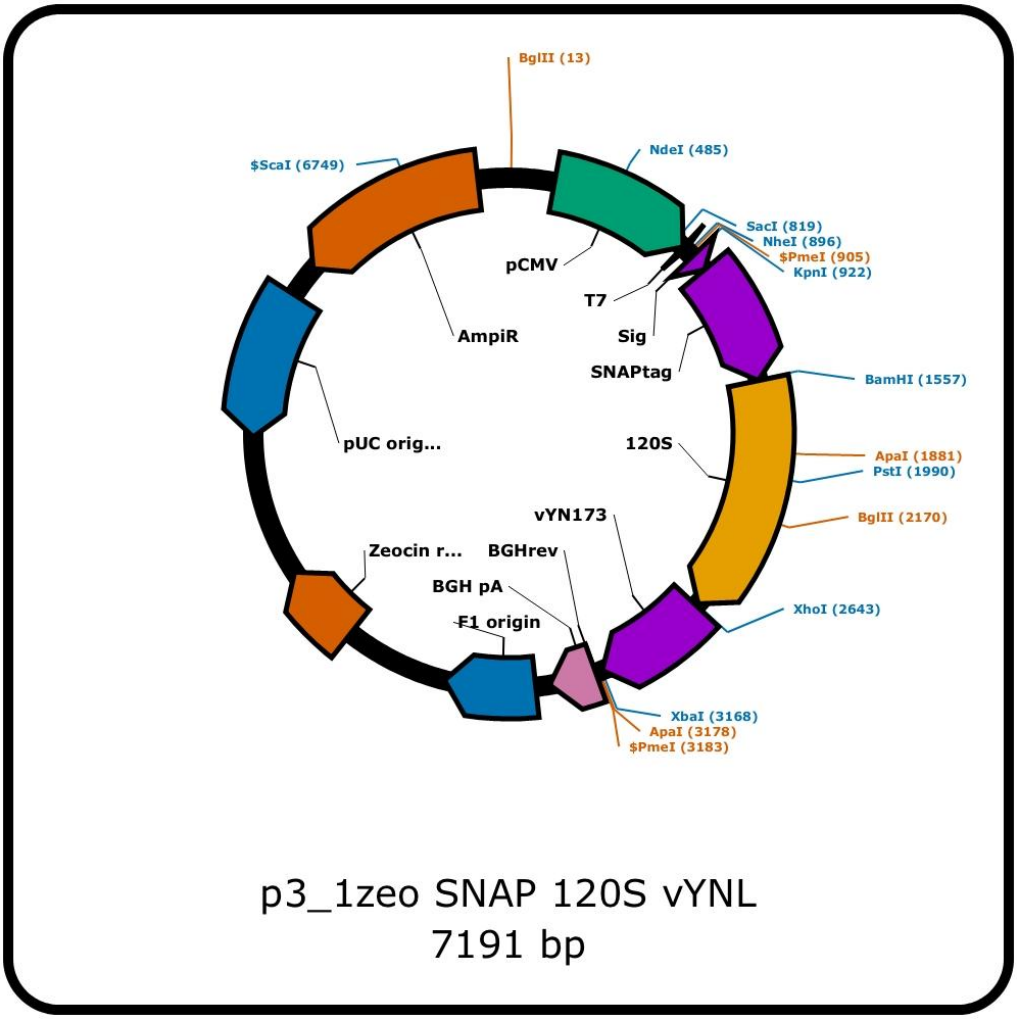

Figure 2.5 Vector map of p3.1 *zeo.*

SNAP-GPR120S-vYNL was placed into the pcDNA 3.1 zeocin (+) (p3.1) vector and contained these features (see Figure 2.3 legend for more details on abbreviations); additionally, the + refers to the orientation of the multiple cloning sequence.

These receptor cDNAs were inserted into pre-existing plasmid vectors between restriction sites BamHI (5') and XhoI (3'; Figure 2.2) using the following protocol.

2.2.1.4.1 Preparation of "insert" cDNA

The "insert" was defined as the receptor cDNA. This was prepared by restriction digestion, isolated by electrophoresis on an agarose gel, visualised using UV light, cut out and purified (see section 2.2.1.1).

2.2.1.4.2 Preparation of "vector" cDNA

The "vector" was defined as the plasmid. The vector underwent shrimp alkaline phosphatase (SAP) treatment (2 µl (2U) SAP buffer (supplied with enzyme; 100 mM Tris-HCl, 50 mM $MgCl_2$, 1 M KCl, 0.2 % Triton X-100, 1 mg ml^{-1} BSA; pH 8.0) and 2 µl SAP) for 1.5 hr at 37^{o}C, followed by 20 min at 75^{o}C to heat inactivate the enzyme. This step was to dephosphorylate the 5' end of the DNA, to prevent self re-ligation. The vector was then purified using a PCR Clean-Up Kit (Sigma), to remove contaminants using a silica binding format as before, to manufacturer's instructions except that the DNA was eluted into 40 µl dH_2O.

2.2.1.4.3 Ligations

The insert and vector were ligated together overnight, in a 3:1 insert:vector ratio, where DNA amounts were initially calculated using the equation as follows, assuming 80 % yield from the gel purification kit (insert) or PCR clean up kit (vector) and starting from 2 µg DNA:

In the 3:1 molar ratio, 50 ng of vector DNA was optimal for ligation (to produce single circular plasmids rather than long concatenated products. To determine the correct amount of insert DNA to be used for the molar ratio, assuming x moles of vector in 50 ng, the following equation was used, then multiplied by 3:

The volume of insert and vector added was then calculated. Positive and negative ligations were set up in Eppendorf tubes: 50 ng vector and 3 times the molar ratio of insert (as above, or none for a negative control), 1 µl ligase buffer (provided with enzyme) and 1 µl (3U) T4 DNA ligase in a total volume of 10 µl with dH_2O, and were incubated for 16 hr at 16^oC.

5 µl of this ligation reaction was transformed into XL-1 cells, grown into miniprep cultures and screened for inserts by the appropriate restriction digests (see section 2.2.1.2).

2.2.1.5 Large scale (maxiprep) isolation and purification of DNA

If the miniprep screening yielded the correct results, the cDNA required for cellular transfection was cultured on a larger scale using the maxiprep kit (Sigma-Aldrich) to manufacturer's instructions.

To do this, a “starter” culture was started in the morning, consisting of 20 µl of the cells from the respective miniprep placed in a 20 ml tube containing 5 ml LB with 75 µg ml^{-1} ampicillin and incubated for 6 hr at 37^{o}C, with 250 rpm. After 6 hr, this starter culture was added to 120 ml sterile LB containing 75 µg ml^{-1} ampicillin, in a 500 ml conical flask, and left to incubate overnight at 37^{o}C, 250 rpm.

The next day, the overnight culture was pelleted by centrifugation for 15 min at 4,000 rpm. This pellet was resuspended in resuspension buffer, which was a hyperosmotic sucrose solution containing RNase that degraded any RNA that may be present.

Then, an alkaline-detergent solution (NaOH/SDS) was added, and underwent immediate inversion to lyse the cells. Again, the SDS degraded the cell walls, liberating cell contents, allowing the alkaline pH to irreversibly denature the chromosomal DNA, whilst leaving the plasmid DNA unaffected. The chromosomal DNA, along with proteins and lipids, become coated with dodecyl sulphate. This solution was allowed to sit for 3 -5 min, until clear and viscous. During this time a filter syringe is prepared, by removing the plunger and the barrel placed upright in a rack.

This solution was then neutralised with chilled neutralisation solution containing potassium acetate and gently inverted. The chromosomal DNA, proteins and lipids undergo precipitation into a white aggregate, due to the replacement of Na^{+} with K^{+} (Ish-Horowicz and Burke, 1981), which leaves the plasmid DNA intact in the supernatant.

A binding solution was then added, which contained the chaotropic binding salts that enabled the plasmid DNA to become bound to silica. This solution was then immediately poured into the barrel of the filter syringe, and allowed to sit for 5 min. During this step, the binding column was placed into a 50 ml collection tube, column preparation solution was added and centrifuged at 4,000 rpm for 2 min, which allows for maximum DNA binding to the membrane in the column.

Half of the cleared lysate was expelled from the syringe into the binding column, centrifuged at 4,000 rpm for 2 min and the eluate discarded. The remaining lysate was also centrifuged in the same way, resulting in the DNA becoming bound to the membrane.

Next, the filter was washed with two wash solutions, the first at 4,000 rpm for 2 min; then the second wash solution containing solvent (80 % ethanol) which removes residual salts and other contaminants from the DNA by centrifugation at 4,000 rpm for 5 min.

The binding column was then moved to a clean 50 ml collection tube, 3 ml of elution solution is added, and centrifuged at 4,000 rpm for 5 min. This eluate then underwent a further ethanol precipitation treatment to further concentrate and purify the DNA.

The ethanol precipitation was as follows: 3 M sodium acetate (pH 5.0) was added in a 1:10 ratio (300 µl, resulting in a final concentration of 0.3 M) to the 3 ml DNA eluate and 2.2 volumes of chilled 100 % ethanol (7.2 ml) was also added. Ethanol displaced the less polar water molecules that surrounded the

DNA phosphates, which then allowed the Na^+ ions from the sodium acetate to bind to the DNA phosphates instead. This reduced the repulsive charges between DNA and caused the DNA to undergo precipitation. This was then centrifuged at 4,000 rpm for 30 min, which produced a DNA pellet.

1 ml of chilled 70 % ethanol was then added, and the sample re-centrifuged for 10 min at 4,000 rpm, to remove salt contaminants. The supernatant was then poured off and the DNA pellet was left to air-dry for approximately 15 min. After this, the pellet was resuspended in TE buffer (10 mM Tris-HCl, 1 mM EDTA; pH 7.5), typically 200 µl. The purity and concentration was then estimated using a spectrophotometer (BioPhotometer, Eppendorf). The concentration was measured at A_{260}, as absorption for double stranded DNA is greatest at 260 nm; the conversion factor is based on A_{260} of 1, representing 50 µg ml^{-1} double stranded DNA. Additionally, proteins absorb at 280 nm, therefore the ratio $A_{260/280}$ is used to indicate purity of the sample. An absorption ratio between 1.7 and 1.9 indicates relatively pure double stranded DNA, because < 1.7 indicated protein contamination, whilst > 1.9 indicated RNA contamination.

2.2.1.6 Site-directed PCR mutagenesis of GPR120S point mutants

Point mutations were introduced into the target GPR120S cDNA sequence using site-directed PCR mutagenesis (QuikChange). This method used Accuzyme, a 5’ – 3’ DNA polymerase with a 3’ – 5’ proofreading exonuclease activity, that produces blunt ended products. It is advantageous to use it in this protocol because it amplifies long DNA fragments, such as the entire

plasmid DNA that requires amplification (~7 – 8 kbp), with minimal errors. This protocol also requires DpnI. DpnI is a restriction enzyme that cleaves methylated DNA; therefore it digests any remaining methylated "parental" DNA, leaving only the non-methylated amplified DNA which contains the mutation.

2.2.1.6.1 Primer design

The design of PCR primers for point mutations, involved taking the cDNA sequence and identifying the codon for the amino acid required for mutation (mutation highlighted in yellow; Figure 2.6). The sequence either side of this codon is duplicated, approximately 12-15 bases either side; long enough to minimise primer mishybridisation to other parts of the DNA template. For the forward primer, the sequence is complementary to the cDNA (except for the mutation). When choosing which amino acid codon to mutate to, some amino acids have degenerate codes, so it was best to mutate to a codon that is used most frequently in man (human embryonic kidney cell hosts) to comply with codon usage bias and avoid undue influences on protein expression. The reverse primer is the reverse complement of the forward primer sequence. Primers were also designed to have at least 40 % GC content, and the primers ended where possible with a GC "clamp", as the 3 hydrogen bonds present "clamp" the ends, which helps with annealing. All the PCR primers used are indicated in Table 2.2; primers were purchased from Eurogentec (Southampton, UK).

```
GPR120S:
 307-V  A  F  T  F  A  N  S  A-315
918-ggtggccttcacatttgctaattcagccc-947

GPR120S F311A:
 307-V  A  F  T  A  A  N  S  A-315
918-ggtggccttcacagccgctaattcagccc-947

Forward primer:
 5'-ggtggccttcacagccgctaattcagccc-3'

Reverse primer:
 5'-gggctgaattagcggctgtgaaggccacc3'
```

Figure 2.6 Example of point mutation PCR primer design for GPR120 F311A. The top line shows the numbered native GPR120S amino acid sequence, with the residue and its corresponding codon in the numbered nucleotide sequence to be mutated highlighted. The second line shows the proposed mutation highlighted. The third line shows the sequence for the forward primer (sense; which is identical to the sequence), whilst the fourth line shows the sequence for the reverse primer (antisense; the reverse complement).

Mutant	Forwards Primer (5'-3')	Reverse Primer (5'-3')	T_m (°C)	% GC	Length
SNAP-GPR120S R99A	accacgaccggcaccggacctgactccggacc	ggtccggagtcaggtccggtgccggtcgtggt	85	72	32
SNAP-GPR120S R178A	gcctctctgcgtcttcttcgcagtcgtcccgcaacggc	gccgttgcgggacgactgcgaagaagacgcagagaggc	87	66	38
SNAP-GPR120S N215A	ggatgtctcttttgttactttggccttcttggtgccagg	cctggcaccaagaaggccaaagtaacaaaagagacatcc	78	49	39
SNAP-GPR120S W277A	ccttcttcatcatggctagccccatcatcatcacc	ggtgatgatgatggggctagccatgatgaagaagg	77	51	35
SNAP-GPR120S W277F	ccttcttcatcatgttcagccccatcatcatcacc	ggtgatgatgatggggctgaacatgatgaagaagg	77	49	35
SNAP-GPR120S F311A	ggtggccttcacagccgctaattcagccc	gggctgaattagcggctgtgaaggccacc	77	62	29
SNAP-GPR120S Δ346	gcaaggatcctcccctgaatgcgcgcgg		82	68	28
		gcttctcgagctataaaatggctccctttttctgg	73	47	34

Table 2.2 PCR primers used for point mutagenesis and GPR120S truncation.

This table contains the PCR primers used to generate all the GPR120S mutants. The mutation is indicated in red. Also included are the melting temperatures (T_m), % GC and length of primer.

2.2.1.6.2 PCR reaction protocol for site-directed mutagenesis

The PCR reaction was set up in a 50 µl reaction volume within 200 µl PCR tubes. It was comprised of 5 µl 10x AccuBuffer reaction buffer (60 mM Tris-HCl, 6 mM $(NH_4)_2SO_4$, 10 mM KCl, 2 mM $MgSO_4$, pH 8.3), 25 ng of template pcDNA, 200 µM dNTPs, 125 ng of forward and reverse primers and 2.5 units of Accuzyme (from Bioline, London, UK), in double distilled water (ddH_2O). This reaction mixture was set up in the PCR tubes, omitting Accuzyme. The PCR tubes were then placed in the thermocycler block (Mastercycler gradient, Eppendorf, UK), and reactions underwent the initial denaturation step of 30 sec at 90^{o}C. At this point, the thermocycler block cooled, typically to 60^{o}C for mutagenesis (can be varied depending on the annealing temperature of the primers; see table 2.2), at which point Accuzyme was added to the PCR tubes. This was hot start PCR, which aimed to prevent any non-specific DNA amplification by the polymerase that could occur at lower temperatures. At this point the thermocycler then went through 18 cycles of denaturation (30 s at 90^{o}C), annealing (1 min at 55^{o}C) and extension (10 min at 68^{o}C, which corresponds to approximately 1.5 min per kbp). Once these cycles had completed, the tubes were cooled to, and held at 4^{o}C.

Following PCR, the samples underwent DpnI treatment for 2 hr at 37^{o}C to digest template DNA. They were then transformed into XL-1 cells (section 2.2.1.2), DNA was isolated using a miniprep (section 2.2.1.3), and screened using restriction digestion enzymes (section 2.2.1.1.1) and sequenced (Section 2.2.1.8).

If the sequence was correct the DNA was ligated into a fresh vector plasmid, to ensure that no unwanted mutations are carried over into the DNA used for transfections. DNA was again transformed into XL-1 cells (section 2.2.1.2), then the cDNA was cultured on a larger scale using the maxiprep protocol (section 2.2.1.5).

2.2.1.7 Generation of the carboxyl tail-truncated GPR120S receptor using PCR

2.2.1.7.1 Primer design

When SNAP-GPR120S Δ346 (numbered because GPR120S was truncated at residue 346) was made, it followed a different protocol. This is because the entire receptor cDNA was amplified from residue 2 to residue 346 using a PCR approach. After identifying the residue at which to prematurely truncate the protein, the reverse primer was designed to introduce a stop codon, plus the code for a desired restriction enzyme site (XhoI). The forward primer consisted of a restriction enzyme site of choice (BamH1), followed by the sequence for the receptor, starting at residue 2 because the start codon has been removed (mutation highlighted in yellow; Figure 2.7; Table 2.2).

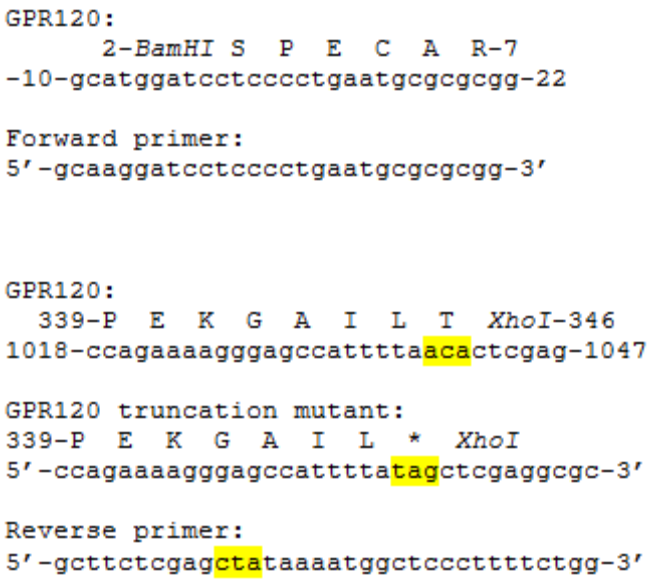

Figure 2.7 Example of a truncation mutation PCR primer design for GPR120Δ346 mutant.

The top section shows the primer design for the forwards primer, with the top line being the WT sequence, and the second line shows the primer sequence. The second section shows the primer design for the reverse primer, with the top line again being the numbered amino acid GPR120 sequence; the second line shows the site for the introduction of the stop codon, with the nucleotide sequence number for GPR120; and the third line shows the sequence for the reverse primer (the reverse complement).

2.2.1.7.2 PCR reaction protocol

The carboxyl tail truncated GPR120S receptor was generated using a slightly different protocol and a different enzyme, PWO (Roche, Burgess Hill, UK). PWO is a 5' – 3' DNA polymerase, with 3' – 5' exonuclease proofreading activity, which produces blunt ended products. The reaction mixture comprised of 5 µl 10x PWO buffer (10 mM Tris-HCl, 25 mM KCl, 5 mM $(NH_4)_2SO_4$, 2 mM $MgSO_4$, pH 8.9), 25 ng template DNA, 200 µM dNTPs, 600 nM of both forward and reverse primers and 0.5 µl (2.5 U) Pwo enzyme, made up to a total reaction volume of 50 µl. The protocol then followed the same thermocycler protocol as for Accuzyme, with a slight modification to the extension step (since the receptor fragment amplified is smaller, 1.2 kbp). The first 10 cycles had an extension step of 1 min 15 s, then for the next 15 extension steps, 5 s was added to this extension period each cycle. Following PCR, the DNA was ran on a gel; and if correct, excised and purified (section 2.2.1.1).

2.2.1.7.3 Ligation of the mutant into the pJET vector

The truncated receptor PCR cDNA was then cloned into the pJET vector (CloneJET PCR cloning kit, Fermentas). A feature of this vector is that the successful blunt end ligation of the receptor DNA insert interrupts the expression of a lethal restriction endonuclease enzyme (eco47/R), therefore only bacterial clones that contain the DNA insert grow. The ligation reaction was 10 µl 2x pJET reaction buffer (provided with enzyme), 1 µl purified PCR product, 1 µl (50 ng) pJET vector, 1 µl (5U) T4 DNA ligase, made up to a total

volume of 20 µl with nuclease free water. This ligation reaction was incubated for 30 min at 22^{o}C. This was then transformed into XL-1 cells (section 2.2.1.2), DNA was isolated using a miniprep (section 2.2.1.3), and screened using restriction digestion enzymes (section 2.2.1.1.1) and sequenced (section 2.2.1.8). If the sequence was correct, then the cDNA was cultured on a larger scale using the maxiprep protocol (section 2.2.1.5).

2.2.1.8 Sequencing

Receptor cDNA sequences were confirmed by sending the vectors to the School of Biomedical Sciences sequencing facility, using appropriate forward and reverse primers (primers chosen were dependent upon which vector cDNA had been inserted into, see Table 2.1). A sample of a sequence chromatogram loaded using Chromas 2 shows the correct codon mutation was present for F311A (Figure 2.8).

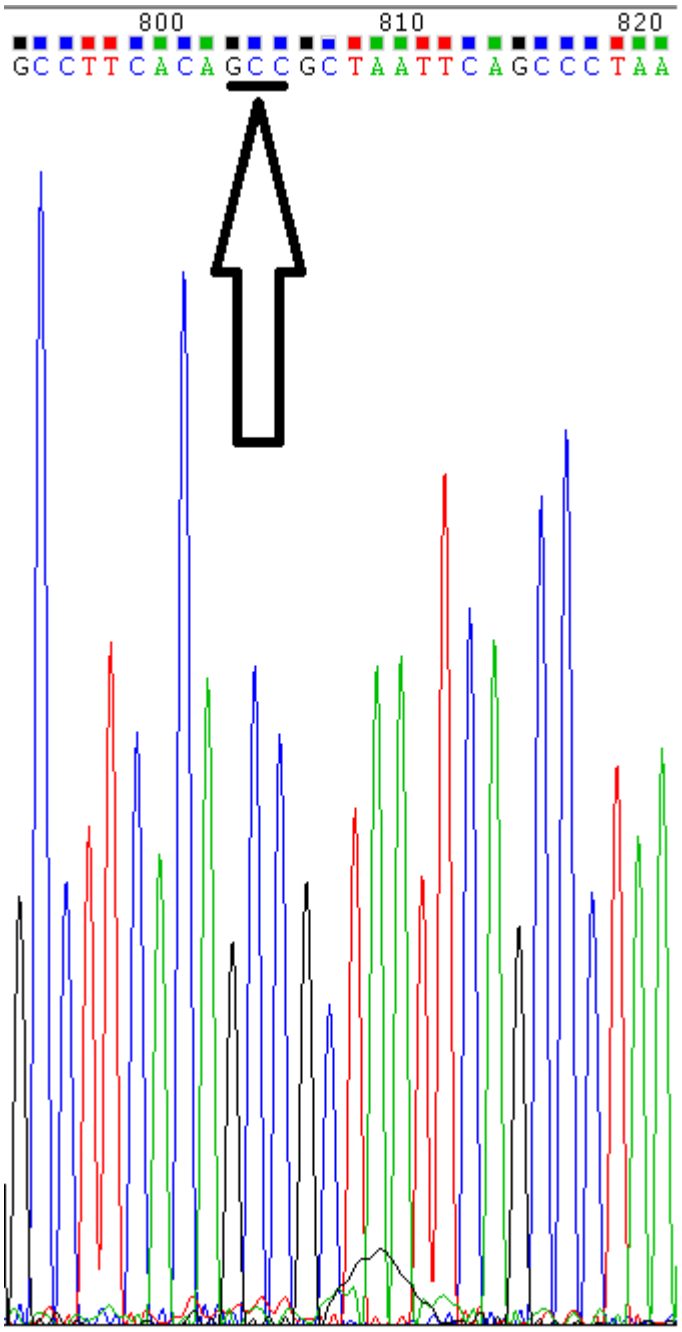

Figure 2.8 A sequence chromatogram showing the position of the SNAP-GPR120S F311A mutant.

The chromatogram was generated using Chromas 2. The arrow shows the position of the altered nucleotide codon that resulted in the Phe (TTT) to Ala (GCC) substitution at position 311.

2.2.2 Cell Culture

In this section the methods of generating and maintaining mammalian cell lines, using human embryonic kidney (HEK293) cells expressing the receptor of interest will be covered.

2.2.2.1 Standard cell line maintenance

2.2.2.1.1 Cell lines and passaging

The HEK293TR inducible cell lines were used for the majority of the experiments. The receptor sequences were placed between BamHI and XhoI in the pcDNA4T/O vector, downstream of the signal-SNAPtag sequence or FLAG epitope.

The cell line used for bimolecular fluorescence complementation (BiFC) studies of receptor:β-arrestin association were dual transfects. They were dually transfected with β-arrestin2 fused to vYFP fragment 2-172 (vYN) and FLAG-tagged receptor cDNAs lacking the STOP codon in pCMV FLAG with the vYFP fragment 155 – 238 (vYC; these residue numbers correspond to the native GFP sequence) inserted between XhoI and XbaI using the LRPLE linker, generating FLAG receptor-vYC fusion (Kilpatrick et al., 2012).

The cell lines used for BiFC studies of constrained dimers were also dual transfects. Receptor-vYNL cDNA was also generated as above (section 2.2.1.4.1-3), but was instead placed within the p3.1 zeo+ vector and cotransfected with pCMV FLAG receptor vYC (Kilpatrick et al., 2010).

Most transfected cell lines were stable mixed populations, and were kept in Dulbecco's modified Eagle's medium (DMEM) with 10 % foetal bovine serum (FBS), the appropriate concentration of the antibiotics needed for that particular cell line (see Table 2.3) and grown in a T75 flask at 37^{o}C and 95 % O_2/5 % CO_2 in a humidified incubator. The antibiotics used were blasticidin, zeocin and G418. Blasticidin prevents protein synthesis by causing premature translation termination by interfering with peptide transfer (Izumi et al., 1991; Kimura et al., 1994). G418 (neomycin) also interferes with protein synthesis, but by blocking ribosomal functions (Southern and Berg, 1982), whilst zeocin intercalates into DNA, causing strand cleavage (Mulsant et al., 1988).

Cells were passaged by washing with PBS to remove residual FBS that would deactivate trypsin, followed by treatment with 1 ml trypsin at 37^{o}C (0.25 % w/v in Versene; Lonza Wokingham Ltd (Wokingham, UK) to detach cells from the flask. The flask was then washed with 10 ml DMEM to wash the cells off the flask surface. This was then transferred into a 20 ml tube and centrifuged for 5 min at 1,000 rpm, and resuspended in an appropriate volume of DMEM. If cells were being split for experiments, this typically occurred two days prior to experimentation for tetracycline inducible lines. The cells were counted under a light microscope using a haemocytometer. 100 µl of cell suspension was loaded and the number of cells within two 1 mm^2 areas (each 0.1 µl volume) were counted. This number was divided by 2 and multiplied by 10,000 to get an average number of cells per ml. The cells were then resuspended in DMEM to give the required cell density, and were seeded into an appropriate plate that had been poly-D-lysine coated (10 µg ml^{-1} made up

	Antibiotic resistance				
Parent cell line	**Cell line**	**Concentration**	**Receptor plasmid**	**Concentration**	**Experiments**
HEK293TR	Blasticidin (tetracycline repressor protein)	5 μg ml^{-1}	Zeocin	20 μg ml^{-1}	Most
HEK293T	Zeocin (βarrestin2-vYNL)	5 μg ml^{-1}	Neomycin (G418)	0.2 mg ml^{-1}	BiFC β-arrestin association
HEK293T	Zeocin (SNAP-GPR120S vYNL)	5 μg ml^{-1}	Neomycin (G418)	5 μg ml^{-1}	BiFC constrained dimers

Table 2.3 A summary of the use of antibiotics in routine cell culture.

A table showing the antibiotics used in routine cell culture, and what they select for (parent cell line plasmids for tetracycline repressor protein, arrestin and receptor BiFC partners; versus introduced receptor vector) and at what concentration they were used at.

in HBSS, 100 µl was pipetted into each well and incubated at room temperature for 30 min; then aspirated and the wells washed with media). The next day, 18 hr prior to experiment, the medium was replaced with DMEM containing 1 µg ml^{-1} tetracycline.

2.2.2.1.2 Tetracycline induction of receptor expression

The promoter of pcDNA4T/O allowed for tetracycline regulation of receptor expression because it contained two tetracycline operon sites ($TetO_2$), that the repressor protein co-expressed in HEK293TR cells bind to (Figure 2.3). Following tetracycline treatment (1 µg ml^{-1}, 18-21 hr), a de-repression mechanism occurs, by which the tetracycline binds to the repressor protein, dissociating it from the $TetO_2$ sites, and allowing receptor expression (Yao et al., 1998).

2.2.2.1.3 Freezing

Routinely, cells were frozen down for long term storage. This followed the above protocol (section 2.2.2.1.1), but instead of resuspension in DMEM, cells from a T75 flask were instead resuspended in 3 ml freezing solution (10 % v/v DMSO in FBS) and placed into cryovials in 1 ml aliquots. These aliquots were initially placed in a freezing container at -80^{o}C (the container was filled with isopropanol to allow a gradual temperature decrease), and at least 24 hr later moved to liquid nitrogen for long term storage at -190^{o}C.

2.2.2.1.4 Defrosting

Aliquots were allowed to defrost naturally at room temperature. They were then transferred to a 20 ml universal tube with 9 ml DMEM and centrifuged for 5 min at 1,000 rpm. They were then resuspended in an appropriate volume of DMEM and allowed to grow overnight in a T75 flask at 37^{O}C and 95 % O_2/5 % CO_2 in a humidified incubator. The next day, the cells were passaged again (section 2.2.2.1.1), but this time were grown in a T75 in the presence of the appropriate antibiotics.

2.2.2.2 Transfections

Stable transfections to generate mixed populations were performed using the appropriate cell line (typically HEK293TR cells) using lipofectamine in Optimem (Invitrogen). Per flask (T25) of 90 % confluent cells, a reaction mixture of 2 µg DNA (in 200 µl Optimem) to 18 µl lipofectamine (1:9 ratio; also in 200 µl Optimem) was prepared, then combined to make a total volume of 400 µl in a 30 ml tube. This was left at room temperature for 45 min, whilst 1.2 ml optimem was added to replace the medium in the flask of HEK293 cells and also left for 45 min at 37^{O}C. A further 800 µl Optimem was added to the DNA-lipofectamine reaction mix, which was added to the cells and left for 24 hr at 37^{O}C. The next day, the cells were passaged as per standard protocol (section 2.2.2.1.1), with the addition of antibiotics for selection (Table 2.3).

2.2.2.3 Dilution cloning

Dilution cloning was used to generate a clonal SNAP-GPR120S-vYNL modified cell line for creating a dual transfect cell line for BiFC dimer experiments

(Chapter 3). Following the establishment of a mixed population by stable transfection (section 2.2.2.2), cell density in a 5 ml resuspension (after trypsinisation; in section 2.2.2.1.1) was calculated using a haemocytometer. This suspension was turned into serial dilutions that resulted in ~100 cells per 10 ml, and this solution was plated out, 200 µl per well onto a 96 well plate, resulting in 1 to 2 cells per well. Seven days later, this plate was screened, and wells with no colonies or multiple colonies were discarded. During this dilution phase, cells were selected for using the appropriate antibiotics (Table 2.3). The SNAP-GPR120S-vYNL clonal cell lines were then screened for expression using SNAP-tag fluorophore labelling and imaging on the IX Ultra plate-reader, prior to expansion. The vYC (Table 2.3) constructs were then co-transfected into this cell line as a mixed population.

2.2.3 Cell signalling assays

2.2.3.1 Ligand preparation

FFAs were stored at 100 mM in DMSO, whilst 10 mM stocks were made of GW9508 (from Tocris Bioscience, Bristol, UK), thiazolidinediones (from Cayman Chemical, Tallinn, Estonia), and GW1100 and Metabolex compound 36 (Met36; from AstraZeneca, Alderley Park, UK). These were stored as aliquots at -20^{o}C until required, when they were defrosted on the day of the experiment. From this, FFAs were made into 1.8 mM DMSO stock solutions; whilst synthetic ligands were simply defrosted, and both underwent serial dilution, typically to 6x or 10x the required final assay concentration in HBSS,

containing 0.02 % bovine serum albumin (BSA, unless otherwise stated) to aid in solubilisation.

2.2.3.2 Calcium mobilisation assay

FFA1 or GPR120 receptor cell lines were seeded at 20,000 cells per well in poly-D-lysine coated 96 well clear-bottomed black-sided plates (Costar 3904, from Corning Life Sciences (Corning, NY)). The next day, tetracycline was added (section 2.2.2.1.2). In the inhibitor studies 100 nM PTx (from Calbiochem, La Jolla, CA) was also added at this stage, for 18 hr at 37^{o}C. The next day, plates were incubated with DMEM/10 % FBS, 2.5 mM probenecid, 1.5 µM Fluo4AM and 0.023 % pluronic acid for 45 min at 37^{o}C. Fluo4 is a calcium sensor, which undergoes increased fluorescence in the presence of calcium ions. Its excitation and emission spectral peaks are 494 nm and 506 nm respectively. A cleavable ester (AM) form of Fluo4 was used, as this provided initial cell permeability. Probenecid was used to prevent the export of cleaved, negatively charged Fluo4, by its blocking action upon organic anion transporters. Pluronic acid was also used, because it is a non-ionic surfactant that facilitated the solubility of Fluo4 in aqueous solution. Cells were washed once and then incubated in HEPES buffered saline solution (HBSS; 25 mM HEPES, 140 mM NaCl, 5 mM KCl, 1 mM $MgSO_4$, 2 mM sodium pyruvate and 1.3 mM $CaCl_2$) with 2.5 mM probenecid and 0.02 % fatty acid free BSA (unless otherwise stated) for 20 min at 37^{o}C. In antagonist assays, antagonist, or in inhibitor studies, 50 µM 2-aminoethoxydiphenyl borate (2-APB) (from Tocris Bioscience, Bristol, UK), was present in the HBSS added at this step. Plates

were then loaded onto the FlexStation I or FlexStation III (Molecular Devices, Sunnyvale, CA, USA) and fluorescence (settings for excitation 485 nm, emission 520 nm; cut-off 515 nm) was measured every 1.52 s for 165 s after agonist (in HBSS/BSA) addition from a compound plate at 15 s (May et al., 2010).

2.2.3.3 Dynamic mass redistribution

SNAP-GPR120S, SNAP-GPR120L or HEK293TRs were seeded at 15,000 cells per well on fibronectin coated 384 well clear-bottomed black-sided plates (Corning 5042, from Corning Life Sciences (Corning, NY), one day prior to experiments in medium containing tetracycline (section 2.2.2.1.2); this medium also contained 100 nM PTx in the inhibitor studies. 2 hr prior to experiment, plates underwent a 5 wash buffer exchange (HBSS/0.02 % BSA) and were left to equilibrate (2 hr at 26^{o}C) in the Corning Epic Biosensor (Corning Life Sciences, Corning, NY), which is a label free system that measures dynamic mass redistribution (DMR); a measure of whole cell response in real time (Schroder et al., 2010). DMR has been postulated to be a mechanism for identifying which G protein is coupled to the receptor because each G protein gives a unique response signature. Responses due to Gi showed a steep positive increase, followed by a gradual decrease, in contrast to Gq which gave a gradual positive increase. G12/13 gave a sharp increase, followed by a slight dip, and then another gradual increase, but G12/13 was measured in HEK cells, whereas the others were in CHO cells (Figure 2.9). A difficulty in this assay is that the signature response for Gs varies depending

on the cell background. In CHO cells, Gs responses were a steep negative decrease followed by a plateau, whilst in HEK cells Gs gave a positive inflection (Schroder et al., 2010).

If 2-APB was used, this was added 1 hr post buffer exchange, and plates were left to equilibrate for 1 hr. Agonists were made on a DMSO stock plate at [1000x], which were then transferred into a [5x] compound plate. Agonists were added in quadruplicate (0.1 % final DMSO concentration) and readings were taken every 40 s for 50 min. 100 µM ATP was used as a positive control to stimulate endogenous P2Y receptors, and data were normalised to this response.

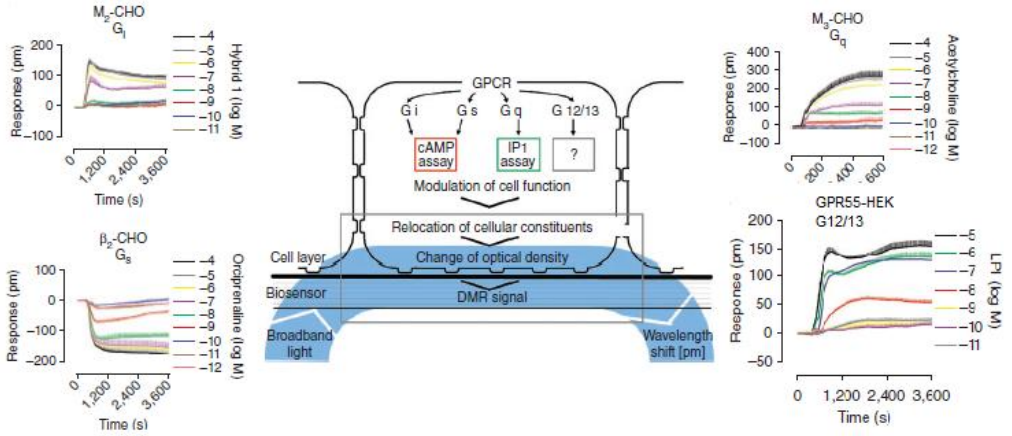

Figure 2.9 Diagram showing the principle of DMR.

The GPCR is activated, coupling to a G protein and eliciting cellular effects, causing the movement of cellular constituents. This movement is measured by a wavelength shift in the broadband light that is shone into the layer of adherent cells on the plate. Image adapted from Schroder et al., 2010.

2.2.4 Automated imaging of receptor internalisation

2.2.4.1 FFA receptor visualisation

FFA1 or GPR120 receptors were visualised directly through fluorescent protein carboxyl terminal fusions, or more commonly using the SNAP-tag system (SNAP-surface reagents were from New England Biolabs, Hitchin, UK; Figure 2.10). As described above, the receptor cDNA was cloned directly downstream of the SNAP-tag and fusion proteins expressed in tetracycline inducible HEK293 cells. The SNAP-tag is a 20 kDa mutant of a DNA repair protein, an alkyl guanine-DNA transferase. This reacts covalently with fluorescent benzyl-guanine (BG), leading to irreversible labelling of the SNAP-tag with a fluorescent probe and enabling receptor visualization. The advantages of this system are that one cell line can be labelled with a variety of different wavelength fluorophores, and also that SNAP-surface label variants are membrane impermeant, so that only receptors that have reached the cell surface are labelled, and not nascent polypeptides in the endoplasmic reticulum or Golgi apparatus.

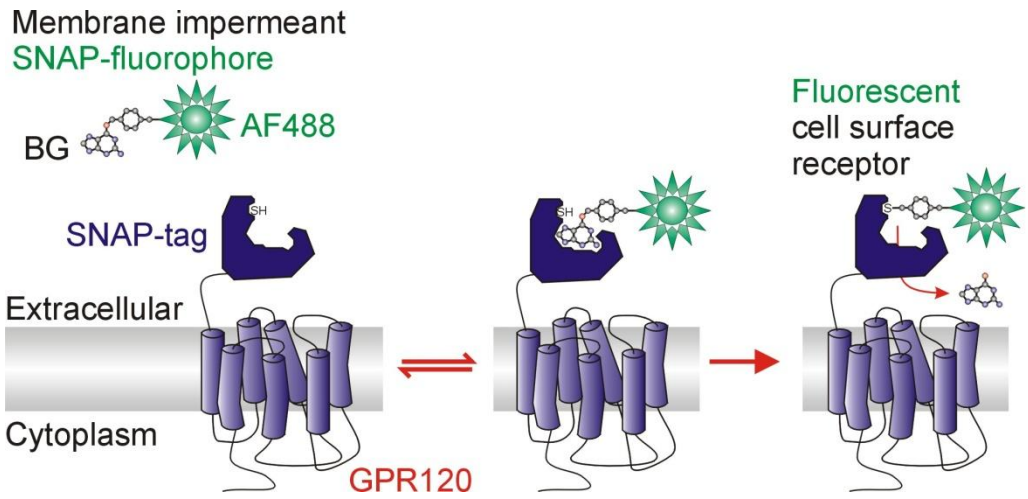

Figure 2.10 A schematic of the SNAP-tag receptor system.
The first panel shows the modified receptor containing the SNAP-tag protein fused to the amino terminus. The second and third panels depict the reaction of the benzyl-guanine label (SNAP-surface fluorophore) undergoing the specific reaction which results in the receptor becoming fluorescently labelled.

2.2.4.2 Internalisation assay using an automated confocal platereader

SNAP-FFA1 or GPR120 receptors were seeded at 20,000 cells per well in poly-D-lysine coated 96 well clear-bottomed black-sided plates (Greiner 655090; from Greiner Bio-One, Stonehouse, UK). The next day, tetracycline was added (section 2.2.2.1.2). Then, the next day, the day of the experiment, plates were incubated with DMEM/10 % FBS containing 0.1 μM SNAP-surface AlexaFluor(AF)-488 (unless otherwise stated) for 30 min at 37^{o}C. Cells were washed once with and then incubated in HBSS. Vehicle or agonist (in HBSS/0.02 % fatty acid free BSA unless otherwise stated) were added in triplicate wells and incubated for the indicated times at 37^{o}C. Following this, cells were rinsed twice with PBS, then fixed in 3 % paraformaldehyde (PFA) in PBS for 10 min at room temperature, followed by another two 5 min washes with PBS, then treatment with nuclear stain H33342 (2 μg ml^{-1} in PBS), followed by two more washes in PBS, all at room temperature. Plates were then imaged on the IX Ultra confocal plate reader (Molecular Devices), with four central sites being imaged per well, using a Plan Fluor 40x NA0.6 (numerical aperture; signifies the objective's acceptance cone, the range of angles over which light can be accepted into the lens i.e. its light gathering power) extra long working distance air objective and 405 nm (H33342; cell nuclei) or 488 nm (SNAP-surface AF-488; receptor) laser excitation. The laser power, gain and offset settings were set relative to positive and negative controls on the plate. Initially, cells were also imaged live on the widefield IX Micro plate reader (Molecular Devices) using the same protocol, to optimise the concentrations of SNAP-surface fluorophore used.

2.2.4.3 Receptor Recycling

The same protocol as for internalisation (section 2.2.3.3.2) was followed, except that additional wash steps were included. SNAP-GPR120 expressing cells were treated as before for 30 min at 37^{o}C with agonist, then cells were washed with HBSS/0.1 % BSA (the higher BSA concentration used to more effectively remove receptor bound FFA) and incubated for 5–60 min at 37^{o}C. The cells were then washed and fixed as above (section 2.2.4.2).

2.2.5 Bimolecular fluorescence complementation

BiFC is a technique based around the formation of a functional, fluorescent protein, which in this study was venus yellow fluorescent protein (vYFP). This variant of YFP contains mutations F64L, M153T, V163A and S175G (Nagai et al., 2002). F64L accelerates oxidation of the chromophore, which is the rate-limiting step of fluorophore maturation, whilst the other mutations facilitate the vYFP to fold correctly into its beta-barrel structure (Nagai et al., 2002). This vYFP is split into 2 non-fluorescent fragments, which are fused to the proteins of interest, e.g. receptor-vYC (155-238) and β-arrestin2-vYNL (2-172) (Kilpatrick et al., 2010; MacDonald et al., 2006). During the course of the assay, the tagged proteins interact, allowing the fragments to associate and refold. Then, the chromophore matures, giving out YFP fluorescence and allowing visualisation of protein complex (Figure 2.11 (Hu et al., 2002; Kerppola, 2008)).

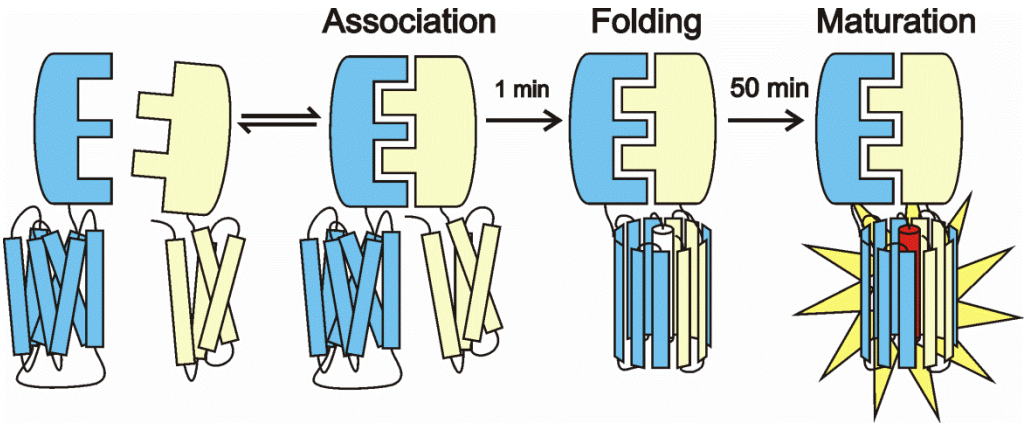

Figure 2.11 Diagram showing principle of BiFC.
Two proteins of interest are genetically engineered with two fragments of vYFP. Following protein interaction, these fragments undergo association and refold, generating fluorescence.

2.2.5.1 Measuring receptor association with β-arrestin using BiFC

Figure 2.12 shows the theory behind using BiFC to measure the receptor associating with β-arrestin2. Cells dually expressing FLAG-GPR120-vYc and β-arrestin2-vYN were seeded at 20,000 cells per well on poly-D-lysine coated 96 well clear-bottomed black-sided plates (Greiner 655090) one day prior to experiment. Cells were washed once with and incubated in HBSS/0.02 % BSA for 30 min at 37^{o}C. Agonist in HBSS/0.02 % BSA was added in triplicate and incubated, 30 min at 37^{o}C (unless otherwise stated). Cells were washed, fixed and imaged as for internalisation (Kilpatrick et al., 2010).

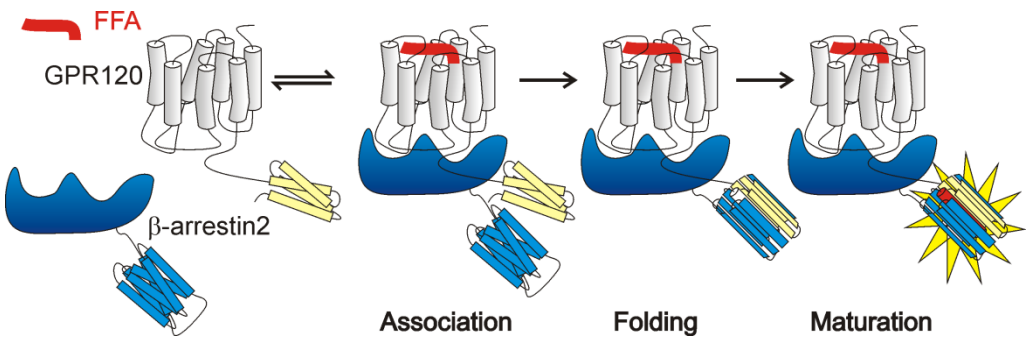

Figure 2.12 Diagram showing principle of BiFC used to study the interaction between receptor and β-arrestin2.

In this application of BiFC, split vYFP fragments are attached to the receptor carboxyl tail and β-arrestin2 to measure their interaction.

2.2.5.2 Constraining receptor dimers using BiFC

BiFC between two different receptor constructs allows a unique measurement of BiFC dimer internalisation, because it allows two series of images to be taken concurrently. These two sets are of the SNAP-surface BG-647 fluorophore labelling the SNAP-GPR120S-vYNL population, whilst the recombined vYFP fluorescence (measuring the BiFC dimer with the second expressed receptor-vYC construct) can also be simultaneously imaged using the 488 nm channel (Figure 2.13).

Cells dually expressing SNAP-GPR120S-vYNL and FLAG-tagged FFA1-vYC, GPR120S-vYC or GPR120L-vYC were seeded at 20,000 cells per well on poly-D-lysine coated 96 well clear-bottomed black-sided plates (Greiner 655090) one day prior to experiment (because these receptor cDNAs were not in a plasmid containing the tetracycline promoter). Cells were washed once with and incubated in HBSS/0.02 % BSA, 30 min at 37^{o}C. Agonist in HBSS / 0.02 % BSA was added in triplicate wells and incubated, 30 min at 37^{o}C (unless otherwise stated). Cells were washed, fixed and imaged as for internalisation (Kilpatrick et al., 2010).

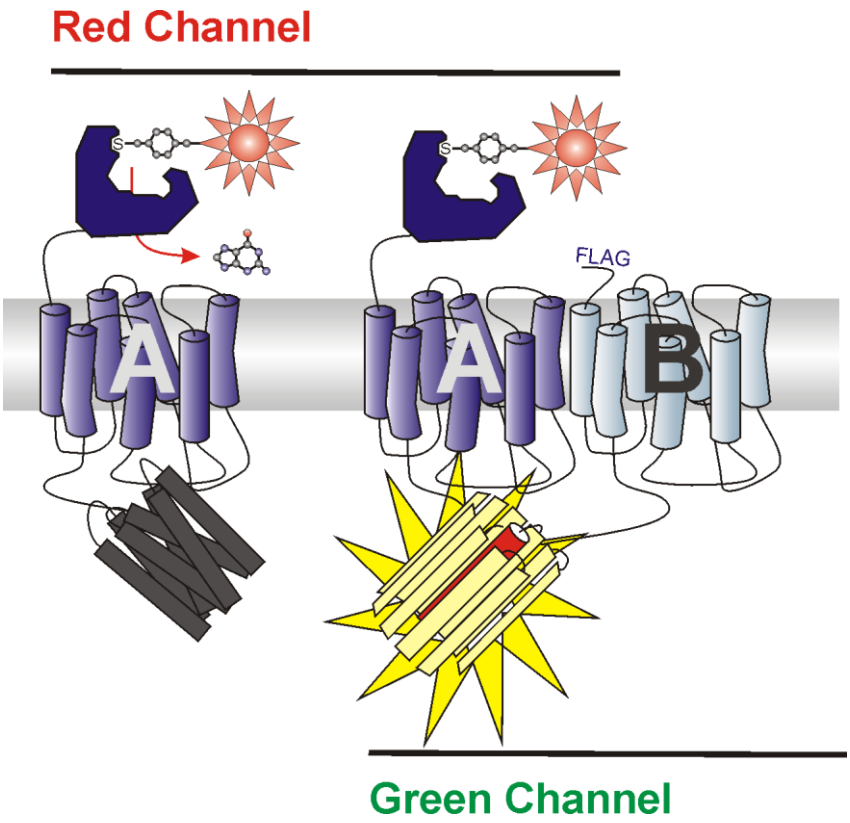

Figure 2.13 Diagram showing principle of BiFC used to study the interaction between two fatty acid receptor protomers.

In this application of BiFC, vYFP is split between the two fatty acid receptor constructs in question to measure the behaviour of the A-B receptor dimer in internalisation assays. This also allowed SNAP-surface measurements (of population A) in conjunction with vYFP (A-B) measurements.

2.2.6 Fluorescent ligand binding assay

HEK293TR FLAG-FFA1 cells were seeded at 10,000 cells per well on poly-D-lysine coated 96 well clear-bottomed black-sided plates (Greiner 655090). On the day of the experiment, medium was replaced with HBSS (in the absence of BSA) and left to incubate at 37^{o}C for 30 min. Competing ligands in the range of 0.01 nM to 300 μM were added and left to incubate for 5 min at 37^{o}C (unless otherwise stated), followed by treatment with 100 nM 40Ag-Cy5 (synthesised by CellAura Technologies, Nottingham, UK) for 30 min at 37^{o}C (unless otherwise stated). The plate was then imaged live immediately on the IX Ultra, 2 sites per well, using 633 nm laser excitation (Stoddart et al., 2012).

2.2.7 Confocal imaging

2.2.7.1 Colocalisation of internalised receptors with intracellular markers

HEK293TR SNAP-GPR120S or SNAP-GPR120L cells were seeded on poly-D-lysine coated 8-well clear plates (Nunc Lab-Tek, from Thermo Fisher Scientific, UK) at 20,000 cells per well. The next day, 1 μg ml^{-1} tetracycline was added (section 2.2.2.1.2). Then the next day, live cells were labelled with 0.5 μM SNAP-surface AF-488 as previously described (section 2.2.4.1), followed by treatment with vehicle or 300 μM oleic acid in HBSS/0.1 % FFA free BSA (60 min at 37^{o}C), with the HBSS also containing either 10 nM lysotracker red (Invitrogen; 60 min at 37^{o}C); or 5 μg ml^{-1} transferrin AF-633 (Invitrogen) added 15 min prior to imaging. Live cell images were taken, following 60 min treatment at 37^{o}C with vehicle or 300 μM oleic acid, using a Zeiss LSM (laser scanning microscope) 510 (Carl Zeiss, Ltd., Welwyn, UK) using a 63x Plan-

Apochromat NA 1.4 oil objective with Ar 488 nm (SNAP-surface AF-488), HeNe 543 nm (lysotracker red) and HeNe 633 nm (transferrin) laser lines for excitation. Images were taken sequentially with band passes of 505-530 nm (BG-AF488), 560-615 nm (lysotracker red) and a long bandpass of 650 nm (transferrin). Pinhole diameter was set to 1 Airy unit for the longest wavelength, and microscope detector gain and amplifier offset were adjusted (consistently within data groups) to ensure images were not saturated.

2.2.8 Fluorescence correlation spectroscopy

Fluorescence correlation spectroscopy (FCS) is a technique that measures the diffusion of fluorescent molecules through a fixed confocal detection volume (approximately 0.25 μm^3, approximately corresponding to approximately 0.1 μm^2 of the illuminated plasma membrane), by recording the time dependent fluctuations in intensity that result from this mobility (see analysis section 2.2.9.5 and Chapter 5 for more background). This technique has been estimated to be sensitive enough to measure the behaviour of approximately 1 – 100 particles within the volume (Briddon et al., 2011).

2.2.8.1 Calibration

FCS was carried out on a Zeiss Confocor 2 fluorescence microscope with a c-Apochromat 40x NA1.2 water immersion objective lens. The system was first calibrated using Cy5 (used to calibrate the 633 nm beampath; diffusion coefficient, D = 3.16 $x10^{-10}$ m^2/s; Amersham Pharmacia Bioscience) to determine the size of the confocal volume. Cy5 was diluted from a 5 mM stock solution respectively, to 1 µM and 20 nM solutions in fluorescence free

water, and 200 µl of each solution was placed into separate wells of an 8 well plate. Immersion water was placed on the objective lens, then the 8 well plate was placed over the objective, centred on the well containing the 1 µM Cy5 solution. Next, the reflection beampath was used to first find the lower, then the upper surface of the 8 well plate, and once this was found, the focal volume was placed 200 µm above into the solution containing the Cy5.

Next the beampath was selected, for the correct combination of laser excitation, dichroic mirror and emission filter. The excitation light was then turned on and laser power adjusted until the count rate was 250-500 kHz at the detector. The correction collar on the objective was adjusted to achieve the maximal count rate, and the pinhole was set to 1 Airy unit. Following this, the position of the pinhole in both x and y axes were scanned and adjusted automatically by the machine to obtain the maximum count rate, and similar optimisation of the collimator position (z) was carried out Following this, the objective was moved to the 20 nM well and the laser power was adjusted to achieve a count rate 20 -100 kHz.

Cy5 calibration reads were then carried out, 3 x 15 s at 5, 4, 3, 2, and 1 % laser power. These autocorrelation curve data were then fitted to one component 3D diffusion model using the analysis software (Zeiss AIM, Jena, Germany), ensuring the fitted structural parameter (the ratio of the confocal volume height to waist radius) was between 5 and 8. The dwell time measured by these calibration reads, in conjunction with the known value for the Cy5 diffusion coefficient, allowed for the detection volume to be calculated. This

in turn allowed the calculation of diffusion co-efficients and concentrations from dwell times and particle measurements from fluorescent ligands and receptors in cell data (section 2.2.9.5) (Briddon et al., 2011).

2.2.8.2 Experiments

HEK293TR cells expressing SNAP-FFA1 receptors were seeded at 20,000 cells per well on poly-D-lysine coated 8 well clear plates (Nunc Lab-Tek,Thermo Fisher Scientific, UK). The next day, tetracycline was added (section 2.2.2.1.2). Then, the next day the cells were ready for FCS studies.

2.2.8.2.1 Receptor diffusion

To measure receptor diffusion, HEK293TR cells expressing SNAP-FFA1 receptors were labelled with SNAP-surface BG-647 (section 2.2.4.1) and left to equilibrate at 22^{o}C. The nucleus of the cell was found using live imaging from the Zeiss Axiocam HR camera. This allowed positioning in xy, followed by a confocal z scan (at low laser power to prevent bleaching), to be performed to determine the position of the upper membrane above the nucleus (corresponding to peak fluorescence intensity). The confocal volume was then placed at the z position defined by this peak. Data were routinely collected following a 15 s prebleach at 0.5 % laser power at 633 nm, and then 3 x 15 s reads at 0.7 % laser power at 633 nm, with emission collected by avalanche photodiodes using a 650 nm long pass filter.

2.2.8.2.2 Ligand binding

To measure ligand binding to FLAG-FFA1 receptors, HEK293TR cells expressing SNAP-FFA1 were labelled with SNAP-surface AF-488 and left to equilibrate at 22^{o}C. The nucleus of the cell was found using the SNAP-labelled receptors imaged from the Zeiss Axiocam HR camera, and the confocal volume was positioned using a z scan as before. However, in this case the confocal volume was placed at one 0.5 µm step above the upper membrane peak intensity.

Data were then collected using SNAP-FFA1 receptor expressing cells treated with fluorescent 40Ag-Cy5 (25–100 nM). Some experiments examined the effect of 1 µM GW1100, which was added 10 min prior to the addition of 100 nM 40Ag-Cy5 (5 min at 22^{o}C). Data were routinely collected following a 15 s prebleach at 0.5 % laser power at 633 nm, and then 3 x 15 s reads at 0.7 % laser power at 633 nm, with emitted photons collected by sensitive avalanche photodiodes through a 650 nm long pass filter.

2.2.9 Data analysis

2.2.9.1 Calcium mobilisation

Calcium signalling data were analysed by the peak agonist response (maximum–minimum) using an average of triplicate wells. Data were generally normalised as a percentage response to a positive agonist control (typically 300 µM oleic acid, unless stated otherwise). In some cases, to allow for comparison between cell lines, peak calcium data were analysed as fold over basal levels instead. In either case, experiments were pooled, and data expressed as mean ± S.E.M. to generate concentration response curves fitted

using nonlinear least-squares regression (Prism v5.02; GraphPad Software, Inc., San Diego, CA, USA). EC_{50} values were quoted (as –log EC_{50}; pEC_{50}) if a maximum agonist response could be defined.

The effects of antagonist in calcium signalling studies were further analysed, using the Gaddum equation:

The Gaddum equation links concentration ratio, CR, to antagonist concentration, [B] and allows K_B, the antagonist equilibrium dissociation constant to be calculated. A derivation results in the Schild analysis, giving the equation:

Log [CR-1] was plotted against log antagonist concentration (log [B]) on a Schild plot. This theoretically gives a straight line of slope 1 provided the experiment was under equilibrium conditions and the antagonist is both competitive and reversible, and the intercept gives –log K_B, called pA_2 when estimated by this method (Arunlakshana and Schild, 1959).

2.2.9.2 DMR

DMR data were analysed by the peak agonist response (maximum–minimum) using an average of quadruplicate wells. Data were normalised as a percentage response to a positive control (100 µM ATP). Experiments were pooled, and data expressed as mean ± S.E.M. to generate concentration

response curves fitted using nonlinear least-squares regression (Prism v5.02; GraphPad Software, Inc., San Diego, CA, USA). pEC_{50} values were quoted if a maximum agonist response could be defined.

2.2.9.3 Internalisation

2.2.9.3.1 Internalisation and BiFC

For quantitative analysis of internalisation and BiFC images (see Figures 3.15 and 3.13 respectively for examples), a granularity algorithm (MetaXpress 2.0, Molecular Devices) detected intracellular compartments as "granules" of specified diameter (typically 2-5 µm, unless stated otherwise) and set above a specified intensity threshold, which were set relative to negative (vehicle) and positive (300 µM oleic acid) controls present on the plate. Several parameters were given by this analysis, which were normalised to cell count (defined as cell nuclei stained by H33342), such as granule count, area and intensity per cell, all of which were averaged from triplicate wells (i.e. 12 sites per data point). All parameters produced similar results, and all figures presented were derived from measurements of average granule intensity per cell.

Experiments were pooled, and data expressed as mean ± S.E.M. to generate concentration response curves fitted using nonlinear least-squares regression (Prism v5.02; GraphPad Software, Inc., San Diego, CA, USA). pEC_{50} values were quoted if a maximum agonist response could be defined.

Time course data were analysed using single phase association kinetics, and a latency period where appropriate. This latency was to take into account that

FFA induced internalisation and β-arrestin recruitment showed a short delay (usually 2-5 min) between agonist addition and response.

2.2.9.3.2 Receptor expression

Comparisons of receptor expression were estimated by further analysis of control images acquired using identical settings, with reference cells expressing SNAP-GPR120S wild type on the same plate. SNAP-surface labelled receptors under vehicle conditions were analysed using the multiwavelength cell scoring algorithm (MetaXpress 2.0). This defined regions of the image covered by individual cells, on the basis of both the location of H33342 stained nuclei and the boundary of SNAP-surface labelled receptor staining. The mean pixel intensities within these regions (covering both plasma membrane and cytoplasm) were then averaged for all cells in each image. This measure of cellular fluorescence intensity was pooled between experiments (mean ± S.E.M.) and was used to indicate receptor expression levels.

2.2.9.4 Fluorescent ligand binding

Following acquisition of 40Ag-Cy5 binding images, a modified version of the granularity analysis was applied. The parameters of the granules were set to selectively record the fluorescent ligand bound to the cell expressed receptors ("white dots," granules 1-2 μm in diameter); with another set to exclude the larger, non-bound aggregates of ligand ("red dots", > 5 μm in diameter). Data were normalised, with no tet set as the negative control (0 %), and the totals were set as the positive control (100 %; Figure 2.14). Experiments were pooled, and data expressed as mean ± S.E.M. to generate inhibition curves

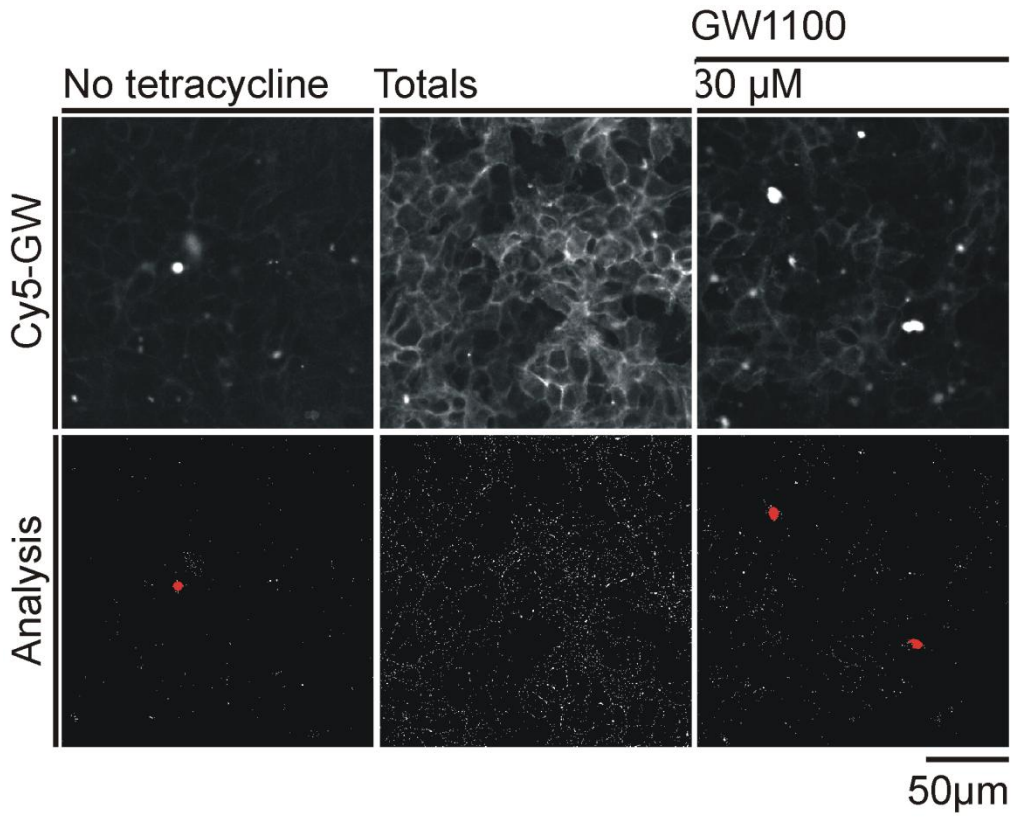

Figure 2.14 Representative images and quantitative analysis of 40Ag-Cy5 binding to FLAG-FFA1 receptors.

The top row shows representative images from the binding assay using 100 nM 40Ag-Cy5 throughout, whilst the bottom row shows the resulting analysis. The top (L-R) shows images of HEK293TR cells that did not undergo tetracycline induction of FLAG-FFA1 expression; cells that did not undergo competing ligand treatment (totals), then cells that were pretreated 30 µM GW1100; all underwent treatment with 40Ag-Cy5 for 30 min at 37^{o}C. The bottom row shows the granularity analysis, which measured the pit count on cell surface ("white dots," granules 1-2 µm in diameter) whilst excluding the larger aggregates ("red dots", > 5 µm in diameter).

fitted using nonlinear least-squares regression (Prism v5.02; GraphPad Software, Inc., San Diego, CA, USA), and IC_{50} values were calculated as appropriate.

Next, paired competition curves were carried out using the antagonist GW1100. This allowed for the estimation of the dissociation constant of 40Ag-Cy5. Two sets of displacements were carried out using 1 µM and 100 nM 40Ag-Cy5. This gave two pIC_{50} estimates, A and B, for GW1100, which allowed for the simultaneous solution of the Cheng-Prusoff equation (below) (Cheng and Prusoff, 1973). This resulted in an estimation of both the 40Ag-Cy5 (K_{FL}) dissociation constant and the GW1100 K_i.

pIC_{50} values from competition binding studies using other ligands were further analysed to derive affinity values (K_i) using the Cheng-Prusoff equation and the 40Ag-Cy5 concentration [FL] and dissociation constant (K_{FL}):

2.2.9.5 FCS

2.2.9.5.1 Autocorrelation analysis

In FCS, the confocal spot focuses on a small area of interest, such the plasma membrane (area 0.1–0.3 μm^2), defining a detection volume (~0.25fl), which is Gaussian in shape. Within this volume, fluctuations in fluorescent intensity are measured as fluorescently labelled receptors or ligand diffuse through (Figure 2.15). Autocorrelation analysis of these fluctuations gives quantitative data on the fluorescent particles present. This includes the average number of particles and their average dwell time, τD, which in conjunction with knowledge of the size of the confocal volume can then be used to calculate the particle concentration and diffusion co-efficients (D) of the fluorescent species respectively (Briddon and Hill, 2007).

Autocorrelation analysis does this by taking the size of a fluctuation (δI) from the average intensity at time T and comparing it with a subsequent fluctuation at time T+τ. Using the whole range of τ values gives G(τ), the autocorrelation function, which is normalised to the square of the mean intensity, <I>, resulting in an autocorrelation decay curve (see equation in Figure 2.16 C). The dwell time, τD, is derived from the halfway point of the G(τ) decay of the autocorrelation function, whilst the particle number, *N*, is derived from its inverse relationship to the amplitude of G_0 (Briddon and Hill, 2007).

In an actual experiment, calibration using a fluorophore with a known diffusion co-efficient, such as Cy5 (*D* 3.16 $x10^{-10}$ m^2 s^{-1}), allows the confocal volume and radius ($\omega_0 = (4D_{Cy5}\tau_D)^{1/2}$)to be calculated. In turn this allows the

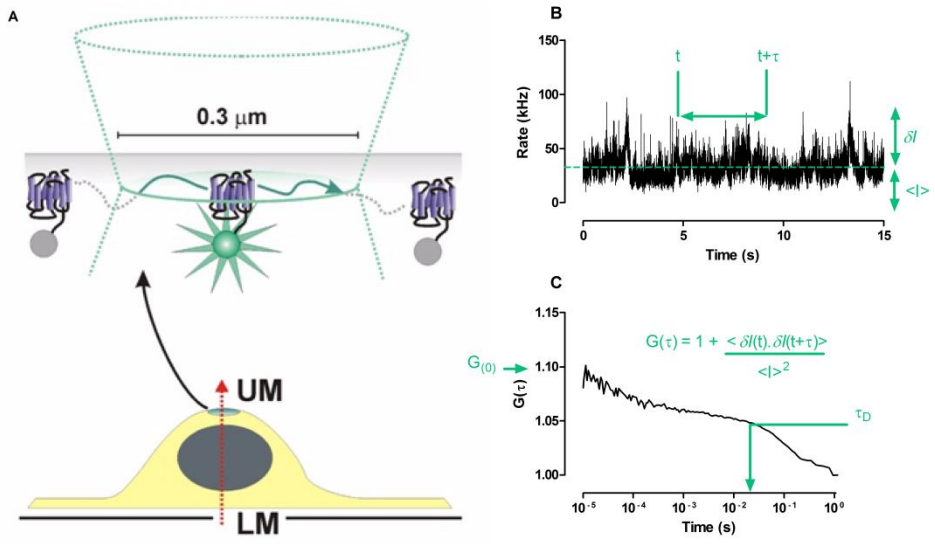

Figure 2.15 The principle of FCS.

As fluorescent molecules diffuse in and out of the confocal volume placed on the upper membrane of the cell (A), these fluorescent fluctuations are measured (B). These data are then fit to an autocorrelation analysis model (C).

diffusion co-efficient (D) of the labelled receptor or ligand to be calculated from individual τ_D values using $D=\omega^2_0/4\tau_D$; and the particle concentration (for the circular area on a 2D membrane) can be calculated using $N/(\pi\omega^2_0)$. These "normalised" values allow comparison between data sets.

Autocorrelation analysis can be fitted to different models (as follows overleaf). These models all incorporate a fast "blinking" component (< 10 μs) to account for the photophysics of the fluorescent molecule, a pre-exponential term which is not indicated in the following equations (Briddon and Hill, 2007; Briddon et al., 2011). The 1x3D model was used for the diffusion of the free ligand, because this incorporates movement in x, y and z dimensions. It was used to fit the data for the calibrations and free 40Ag-Cy5 in solution (other than definitions already given: m is the total number of components (here m=1), fi is the fractional contribution that component i makes to the curve while S is the structure parameter related to the shape of the confocal volume):

The 2D model was used for receptor-bound ligand or SNAP-labelled receptors, because this model only incorporates movement in x and y, and so was used to measure the diffusion of SNAP-FFA1 within the plasma membrane (here m=1 or 2 for 1/2 components):

For example, the 2x2D model gave two dwell times τ_{D1} and $\tau_{D2,}$ and their percentage contribution to the overall amplitude of the autocorrelation, $G_{(0)}$, which is expressed as τ_{D1} % and τ_{D2} % (related to fi). (Briddon et al., 2004). In the actual experimental data using fluorescent ligands, a combination of these models was required (1x3D + 1 or 2 2D components), with the 1x3D component used to account for ligand that was free in solution; whilst one or more 2D components were used to model ligand bound to FFA1.

2.2.9.5.2 PCH analysis

These raw measurements can also undergo an alternative statistical analysis (using Zeiss Zen 2000 software), known as the photon counting histogram (PCH) analysis (Chen et al., 1999). This analysis can provide a different calculation of the particle concentration, and also gives information on molecular brightness (ε), the brightness of each species. PCH is an amplitude rather than time dependent analysis. The fluorescence record is divided into bins of appropriate time, which should be lower than the FCS dwell times of the species of interest, but higher than those to be eliminated from the analysis. For example, the bin time in this study was 1 ms (to avoid contributions from the free diffusing ligand, and photophysics effects from the fluorophore). Throughout the record, the photon counts in each bin are calculated, and this generates a frequency histogram, with the number of photon counts *k* represented on the x axis, and the number of bins containing those counts *k* on the y axis. While this histogram might be expected to follow a Poisson distribution, the uneven illumination of the confocal volume (with

greatest excitation in the centre of the volume) generates deviations from the Poisson fit. PCH analysis measures this deviation from the ideal Poisson fit, and models it based on the number (N) and molecular brightness (ε) of one or more fluorescent species components.

The PCH calibration was fitted to the 1 component model. This gave a first order correction, which takes into account deviations from a Gaussian observation volume when using single photon (rather than multi-photon) excitation (Huang et al., 2004). This first order correction was then used in the analysis of the cell data, which was analysed using the 2 component PCH model, with the bin time of 1 ms.

2.2.9.6 Statistical significance

Statistical significance was determined as specified in figure legends, using GraphPad Prism. Typically, 2 way ANOVA (analysis of variance) with Bonferroni post-tests were used when comparing GPR120 isoform responses (Chapter 3); 1 way ANOVA was used when comparing the GPR120S mutants when studying the binding site (Chapter 4); and Kruskal-Wallis or Mann-Whitney test with Dunn's multiple comparison post-tests were used when analysing FCS data (Chapter 5). A Student's unpaired t test was used to test significance in all other situations, as stated.

Chapter Three: Signalling and trafficking characterisation of FFA1 and GPR120 isoforms

3.1 Introduction

3.1.1 Fatty acid receptor signalling pathways

Fatty acid receptors are G protein-coupled receptors, and therefore some of their effects are mediated through G proteins. FFA1 couples predominantly through the $G_{q/11}$ class of G proteins to elicit ERK activation (Seljeset and Siehler, 2012) and calcium signalling, leading to the potentiation of insulin secretion (Briscoe et al., 2003; Itoh et al., 2003), but it has also been found to couple partially through G_i to inhibit cAMP production (Schroder et al., 2010). Less is known about the specific coupling of GPR120, but it can stimulate calcium signalling, via $G_{q/11}$ (Oh da et al., 2010), and ERK activation which leads to GLP-1 secretion. GPR120 activation had no effect upon cAMP signalling (Hirasawa et al., 2005). Furthermore, there is evidence for FFA1 and GPR120 expression in the breast cancer cell line MCF-7, and treatment with oleic acid promoted ERK phosphorylation through Gi, leading to cell proliferation (Soto-Guzman et al., 2008).

In terms of non G protein mediated signalling, not much is known for GPR120. GPR120 has been shown to undergo internalisation (Fukunaga et al., 2006; Hirasawa et al., 2005), whereas there is no mention in the literature of this for FFA1. A recent investigation has suggested that GPR120 is capable of β-arrestin association using a DiscoverX complementation assay (Shimpukade et

al., 2012). Additionally, very little data exists directly comparing GPR120 isoforms, though it has previously been suggested that the longer form may be functionally impaired in initiating signalling cascades (Moore et al., 2009). It has also been found that the shorter form of the receptor is constitutively phosphorylated to a greater extent than the longer form (Burns and Moniri, 2010). Interestingly, one study found that GPR120 had cell specific signalling. It was found that in adipocytes the receptor signals through Gq for glucose uptake, whilst in macrophages, GPR120 was found to prevent insulin resistance through an inhibitory mechanism mediated by β-arrestin2 (Oh da et al., 2010). Perhaps this gives a hint to possible isoform specific functions, but there has been no published identification of corresponding isoform specific localisation in different cell types.

3.1.2 Potential fatty acid receptor dimerisation

FFA1 is known to be expressed in the β-cell (Briscoe et al., 2003), whilst the expression of GPR120 within this cell type is still up for debate (Morgan and Dhayal, 2009). Both receptors are also expressed in the colonic L cells (Katsuma et al., 2005). Interestingly, a link between the two systems has been show by an increase in incretin levels enhancing GSIS and increasing pancreatic β-cell proliferation (Tanaka et al., 2008b). As discussed in the introduction, GPR120 and FFA1 also have a similar range of endogenous ligands, in terms of size (medium to long chain) and both saturated and unsaturated fatty acids (Briscoe et al., 2003; Hirasawa et al., 2005). This

redundancy is intriguing, and perhaps it indicates the potential of these receptors to undergo homo- or heterodimerisation (section 3.2.6).

3.1.3 Novel techniques used in this study of fatty acid receptor signalling

3.1.3.1 DMR

This study utilised two novel methods: dynamic mass redistribution (DMR) and bimolecular complementation (BiFC). DMR was measured on the Corning Epic Biosensor and gave a measurement of the whole cell response in a label free system, by measuring the movement of cell constituents in the cell following receptor activation (the experimental technique can be found in section 2.2.3.2, whilst more detail on the theory can be found in section 2.2.3.3). One advantage of DMR was that it used label free technology, therefore cell lines do not have to be genetically modified either with a fluorescent moiety (e.g. GFP) or a genetic sequence that allows exogenous fluorescent labelling (e.g. SNAP-tag technology) (Schroder et al., 2010). Another advantage to DMR was the two types of high sensitivity; for example to determine endogenous receptor coupling at low receptor expression levels in native cells. It can also reveal subtleties in signalling pathways, for example how it uncovered novel pharmacology of FFA1. FFA1 was classified as coupling to $G_{q/11}$, but DMR found that FFA1 signals were only partially blocked using a G_q inhibitor (YM254890). The use of PTx demonstrated that FFA1 could also couple through Gi. In fact, only the use of both YM254890 and PTx inhibitors completely blocked FFA1 signalling. Also, when treated with either inhibitor,

the trace left was characteristic for the uninhibited G protein subtype in question (Schroder et al., 2010).

3.1.3.2 BiFC

BiFC is a technique based around the formation of a functional, fluorescent protein from non-fluorescent complementary fragment tags, allowing visualisation of the labelled protein-protein complex (covered in more detail in section 2.2.4). Here, BiFC was used in two ways. First the receptor:β-arrestin association assay (described in Kilpatrick et al., 2010) was adapted to study GPR120 arrestin recruitment. Secondly, BiFC was used to constrain FFA receptor homo- and hetero-dimers. The purpose of using BiFC to study the dimerisation of the fatty acid receptors is that it constrains the receptors in a known stoichiometry (Kilpatrick et al., 2012). Another advantage to the system is that it allows two simultaneous measurements to be made in receptor internalisation assays. The red channel allowed measurements of the overall SNAP-tagged GPR120 receptor-vYNL population, whilst the green channel measured recomplemented vYFP, and so the behaviour of the specific homo- or hetero-dimer held together by complementation.

3.1.4 Aims of this study

The primary aim of this study was the characterisation of the GPR120 isoforms to investigate the possibility of isoform specific signalling, because previously only their phosphorylation status had been determined (Burns and Moniri, 2010). This included using the novel DMR assay to compare results with the more traditional calcium signalling assay. Another non-standard

assay, BiFC was also employed to identify any novel interactions between the GPR120 isoforms and β-arrestin2, and if there were any isoform specific interactions, in conjunction with the receptor internalisation assay. Downstream intracellular trafficking of these receptors was then determined, and was important to study because the internalisation of these receptors had also not been studied before. Furthermore, BiFC was also used to identify GPR120 homo- and hetero-dimers and to investigate whether this altered their pharmacology.

3.2 Results

3.2.1 Cell surface expression & fluorescent labelling of receptors

Firstly, FFA1 or GPR120 receptor cDNAs were inserted into the expression vector, typically pcDNA 4T/O, between endonuclease enzyme restriction sites (section 2.2.1.4). The receptor was placed downstream of the SNAP-tag sequence which allowed for fluorescent labelling, and upstream of the GFP tag where applicable. These vectors were then transfected into HEK293TR cells (section 2.2.2.2), and receptor expression was under the control of a tetracycline inducible system (section 2.2.2.1.2).

These receptor cell lines were initially imaged on the IX Micro epifluorescence platereader to determine that the addition of the SNAP-tag did not affect receptor expression and that the receptor could be successfully labelled. Comparison of images from receptors that had been treated with vehicle (control conditions) and 300 μM oleic acid showed that the membrane impermeant SNAP-surface fluorophore only labelled plasma membrane expressed receptors, and that only once treated with oleic acid was the labelled receptor internalised, for example SNAP-GPR120S labelled with SNAP-surface AF-488 (Figure 3.1 B). Additionally, vehicle treated SNAP-FFA1-GFP was observed to be both present at the plasma membrane and in intracellular vesicles (Figure 3.2 A). However, the SNAP-labelled SNAP-FFA1-GFP population was predominantly plasma membrane localised (Figure 3.2 B). As the cell lines utilise a tetracycline inducible system to initiate receptor expression, it follows that in the absence of tetracycline pre-treatment, there

was no receptor expression. The no tetracycline controls thus show that the SNAP-surface label was specific for the receptor, as there was no labelling in the absence of receptor. This label specificity was also observed through comparison of images with GFP fluorescence, because the SNAP-surface labelled receptor images showed colocalisation with the images of receptor GFP fluorescence, for example when SNAP-GPR120S-GFP was labelled with SNAP-surface BG-546 (Figure 3.1 A).

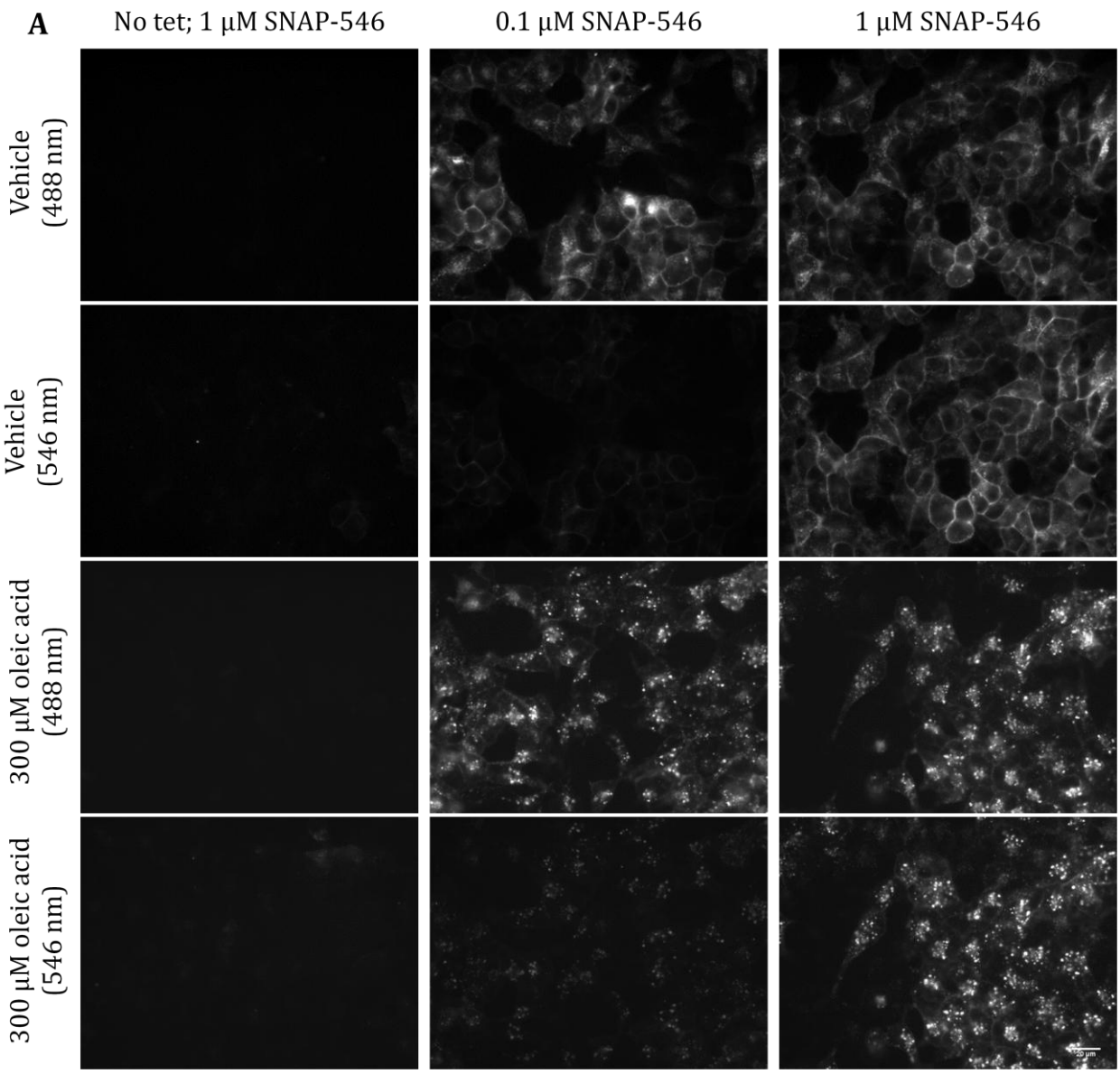
A
No tet; 1 μM SNAP-546
0.1 μM SNAP-546
1 μM SNAP-546
Vehicle (488 nm)
Vehicle (546 nm)
300 μM oleic acid (488 nm)
300 μM oleic acid (546 nm)

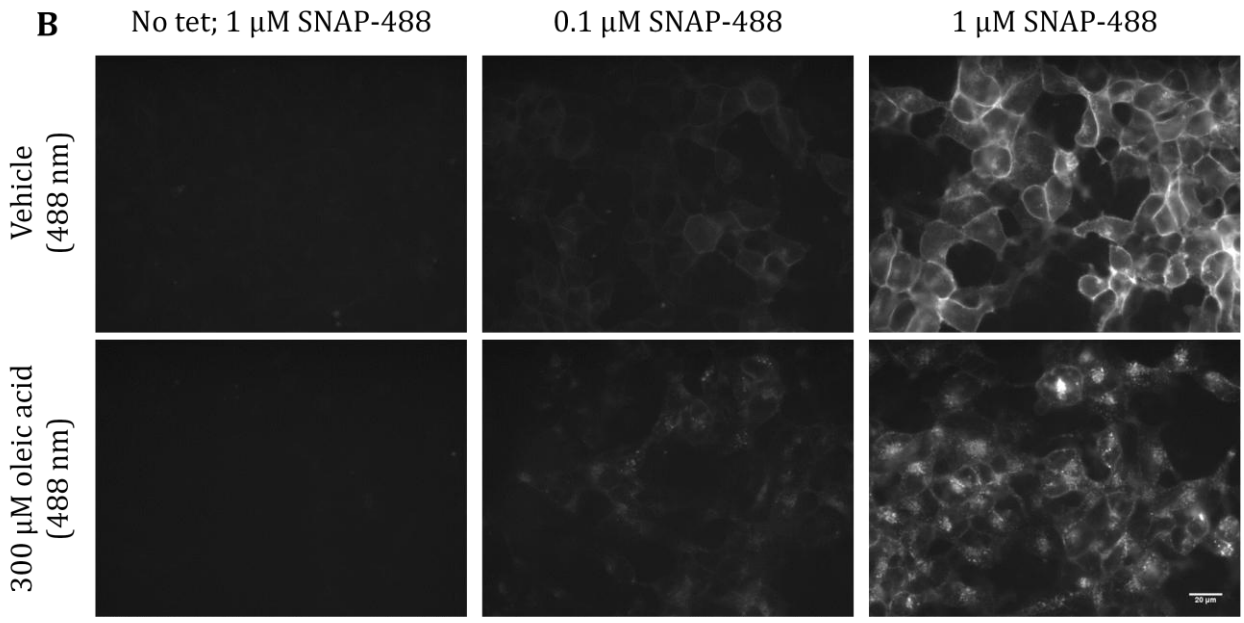

Figure 3.1 SNAP-surface BG-546 and SNAP-surface AF488 specifically label SNAP-GPR120S-GFP (A) and SNAP-GPR120S (B) respectively.

HEK293TR cells were stably transfected with SNAP-GPR120S-GFP (A) or SNAP-GPR120S (B). Receptor expression was induced by 18 hour treatment with tetracycline. Cells were then pre-treated with 0.1 µM or 1.0 µM SNAP-surface BG-546 (A) or SNAP-surface AF-488 (B), followed by treatment with vehicle or 300 µM oleic acid (30 min at 37^{o}C) and were imaged live on the IX Micro, using 546 nm (SNAP-surface BG-546) or 488 nm (GFP/SNAP-surface AF-488) excitation. Scale bar = 50 µm.

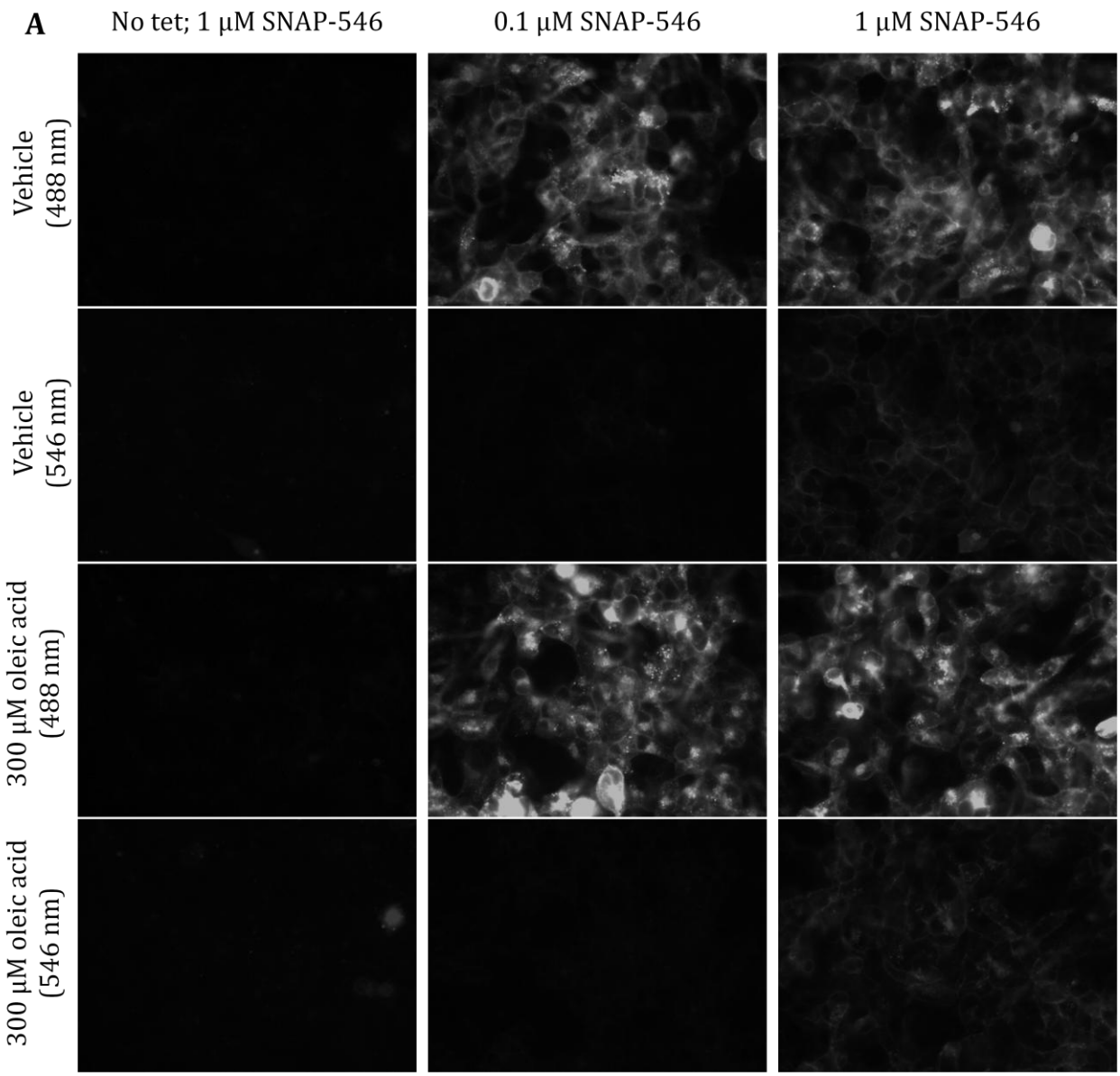
A
No tet; 1 μM SNAP-546
0.1 μM SNAP-546
1 μM SNAP-546
Vehicle (488 nm)
Vehicle (546 nm)
300 μM oleic acid (488 nm)
300 μM oleic acid (546 nm)

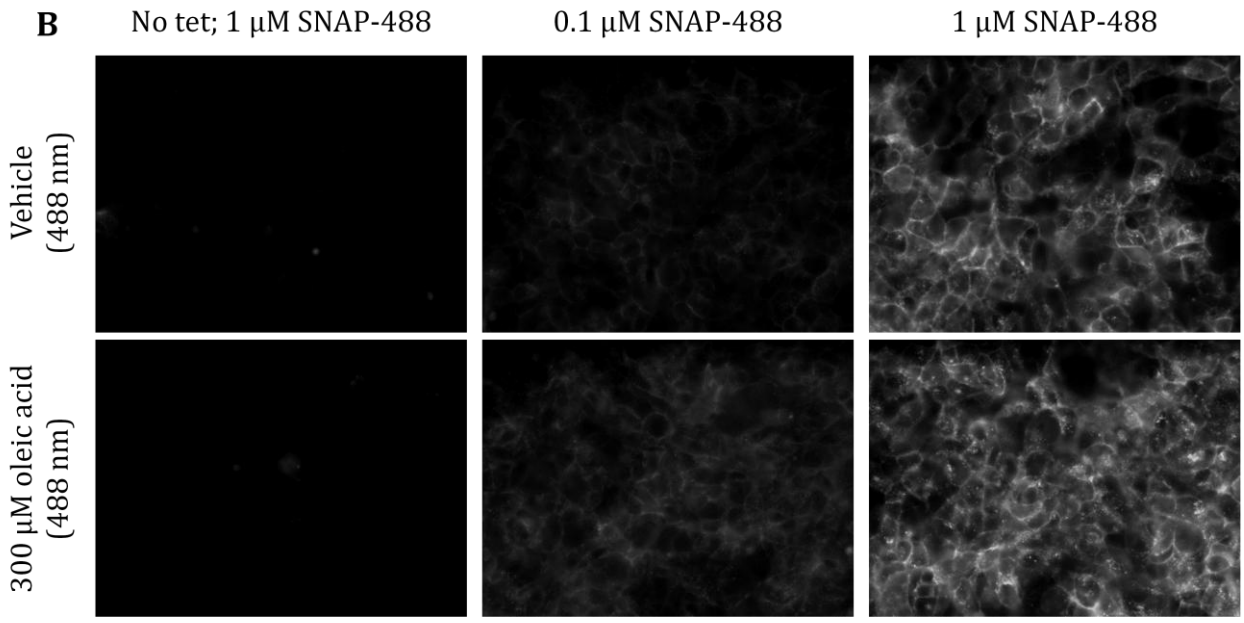

Figure 3.2 SNAP-surface BG-546 and SNAP-surface AF-488 specifically label SNAP-FFA1-GFP (A) and SNAP-FFA1 (B) respectively.

HEK293TR cells were stably transfected with SNAP-FFA1-GFP (A) or SNAP-FFA1 (B). Receptor expression was induced by 18 hour treatment with tetracycline. Cells were then pre-treated with 0.1 μM or 1.0 μM SNAP-surface BG-546 (A) or SNAP-surface AF-488 (B), followed by treatment with vehicle or 300 μM oleic acid (30 min at 37^{o}C) and were imaged live on the IX Micro, using 546 nm (SNAP-surface BG-546) or 488 nm (GFP/SNAP-surface AF-488) excitation. Scale bar = 50 μm.

3.2.2 G protein mediated calcium mobilisation

Firstly, expression levels of the two SNAP tagged GPR120 isoforms, expressed in separate stably transfected HEK293TR cell lines, were measured using quantitative imaging. Receptors were labelled with SNAP-surface AF-488 and treated with vehicle, then fixed, labelled with H33342 (a nuclear DNA stain) and imaged (section 2.2.3.4). Both SNAP-GPR120 isoforms showed similar plasma membrane localisation under unstimulated conditions (see Figure 3.15 for images). To these control images, a multiwavelength cell scoring algorithm (MetaXpress2) was applied. This defined regions of the image covered by individual cells, on the basis of both the location of H33342 stained nuclei and the boundary of SNAP-surface AF-488 labelled receptor staining. The mean pixel intensity within these regions (covering both plasma membrane and cytoplasm) was then averaged for all cells in each image. This measure of cellular fluorescence intensity was pooled between experiments (mean ± S.E.M.). Using this measure, expression of SNAP-GPR120L was quantified to be approximately 58 % of GPR120S (Student's t test, * $P < 0.05$; Figure 3.3).

Next, the effect of BSA concentration upon FFA1 and GPR120 stimulated calcium mobilisation (measured by Fluo4 fluorescence) was optimised for future experiments (section 2.2.3.2). There are multiple FFA binding sites found on albumin (Krenzel et al., 2013), which could be responsible for sequestering FFA (free fatty acids), and effectively causing a lower free concentration to be available to bind the receptor. A comparison of representative calcium time course traces show that ligands gave greater

absolute responses at SNAP-FFA1 compared to SNAP-GPR120S (Figure 3.4). The GW9508 peak response at SNAP-FFA1 was over twice the magnitude of that of SNAP-GPR120S, 23,621 ± 938 RFU for SNAP-FFA1, whilst at SNAP-GPR120S it was 11,090 ± 624 RFU (n= 3 – 5). These peak responses at 23 s were found to be significantly different, $P < 0.01$, using a Student's t test (Figure 3.4). For comparison between receptor cell lines, peak responses were normalised to a reference agonist, 300 µM oleic acid, and concentration response curves constructed to give potency values where a clear maximum response could be defined. This showed that ligands were also more potent at SNAP-FFA1 (Figure 3.6; Table 3.2) than at SNAP-GPR120S (Figure 3.5; Table 3.1). The difference in GW9508 pEC_{50} values for SNAP-GPR120S and SNAP-FFA1 were significantly different, $P < 0.001$ using a Student's t test (Table 3.3).

Altering BSA concentration from 0.02 % BSA (Figure 3.5 A; n = 5) to 0.1 % BSA (Figure 3.5 B; n = 3) did not affect the pEC_{50} of GW9508 at SNAP-GPR120S, but it did decrease the maximum response to 100 µM GW9508 (Table 3.1); this was not statistically significant when tested using a Student's t test. The potencies of oleic acid at SNAP-GPR120S and GW9508 at SNAP-FFA1 were significantly right-shifted by the increased BSA concentration (Table 3.1, Table 3.2); although clear pEC_{50}s could not be obtained, this was also evident for FFA1 responses to oleic acid and myristic acid.

From these results, 0.02 % BSA was chosen as the optimal assay concentration.

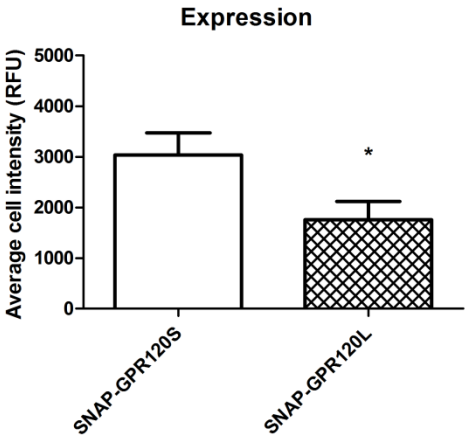

Figure 3.3 Relative expression levels of SNAP-GPR120S and SNAP-GPR120L.

Using images acquired on the IX Ultra of HEK293TRs stably transfected with SNAP-GPR120S and SNAP-GPR120L (see Figure 3.15) and labelled with 0.1 µM SNAP-surface AF-488, relative expression levels of each isoform could be determined. Statistical significance was determined using a Student's t test, * $P < 0.05$.

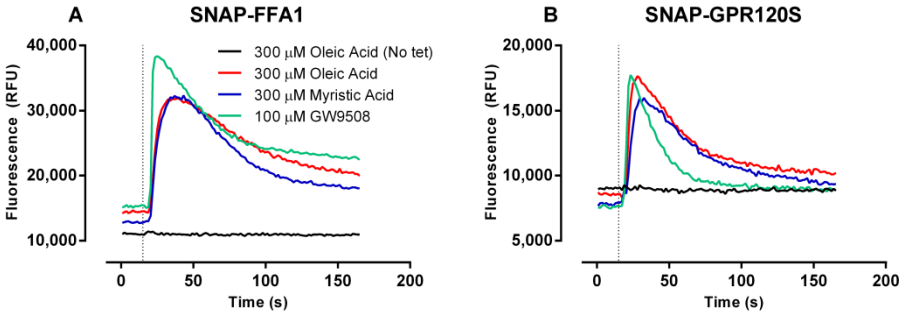

Figure 3.4 Time courses of calcium mobilisation following SNAP-FFA1 and SNAP-GPR120S activation by agonists.

The time courses of intracellular calcium mobilisation responses were measured by Fluo4 fluorescence in HEK293TR cells expressing SNAP-FFA1 (A) or SNAP-GPR120S (B) to 300 µM oleic acid and myristic acid, and 100 µM GW9508 at 0.02 % BSA. Dotted line represents time of agonist addition. Time courses shown are a representative trace of 5 individual experiments.

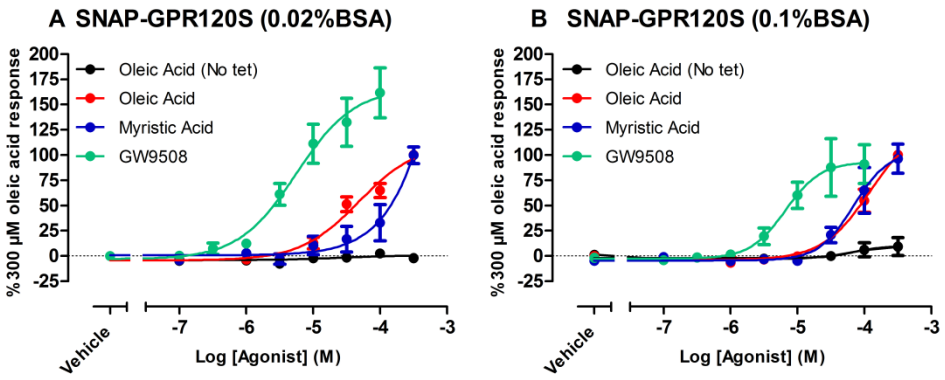

Figure 3.5 The effect of BSA concentration upon SNAP-GPR120S mediated calcium mobilisation in response to agonists.

The effect of 0.02 % (A) versus 0.1 % BSA (B) concentration upon oleic acid (with and without tetracycline (tet) induction of receptor expression), myristic acid and GW9508 in eliciting intracellular calcium mobilisation was measured in HEK293TR cells expressing SNAP-GPR120S. Data were normalised (%) to the 300 µM oleic acid response and pooled from 3 - 5 individual experiments, mean ± S.E.M.

	0.02% BSA		0.1% BSA	
Agonist	pEC_{50}	R_{max} (%)	pEC_{50}	R_{max} (%)
Oleic Acid	4.3 ± 0.1	100	3.9 ± 0.2 *	100
Myristic Acid	N.D.	100 ± 8	4.2 ± 0.1	97 ± 15
GW9508	5.3 ± 0.2	162 ± 25	5.2 ± 0.2	91 ± 19

Table 3.1 The effect of BSA concentration upon potency and maximal responses of agonists at SNAP-GPR120S as measured in the calcium mobilisation assay.

pEC_{50} and maximal responses of SNAP-GPR120S in response to OA, Myr and GW9508 at 0.02 % and 0.1 % BSA, were measured in HEK293TR cells expressing SNAP-GPR120S (see Figure 3.5). Myristic acid R_{max} values were determined from the maximal response at 300 µM. Oleic acid pEC_{50} values were found to be significantly different * $P < 0.05$ using Student's t test, whilst GW9508 maximal responses were not. Data were normalised (%) to the 300 µM oleic acid response and pooled from the minimum of 3 individual experiments, mean ± S.E.M. N.D. not determined.

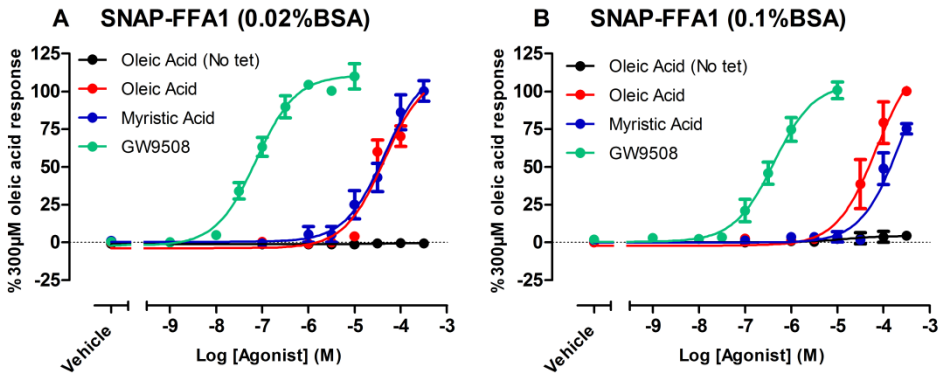

Figure 3.6 The effect of BSA concentration upon SNAP-FFA1 mediated calcium mobilisation.

The effect of 0.02 % (A) versus 0.1 % BSA (B) concentration upon oleic acid, myristic acid and GW9508 eliciting intracellular calcium mobilisation was measured in HEK293TR cells expressing SNAP-FFA1. The data were normalised (%) to the 300 µM oleic acid response and were pooled from a minimum of 5 individual experiments, mean ± S.E.M.

	0.02% BSA		0.1% BSA	
Agonist	pEC_{50}	R_{max} (%)	pEC_{50}	R_{max} (%)
Oleic Acid	N.D.	100	N.D.	100
Myristic Acid	N.D.	100 ± 7	N.D.	75 ± 3
GW9508	7.1 ± 0.1	110 ± 8	6.4 ± 0.1**	101 ± 6

Table 3.2 The effect of BSA concentration upon potency and maximal responses of agonists at SNAP-FFA1 as measured in the calcium mobilisation assay.

pEC_{50} and maximal responses of SNAP-FFA1 in response to oleic acid, myristic and GW9508 were measured in HEK293TR cells expressing SNAP-FFA1. Oleic acid and myristic acid R_{max} values were determined from the maximal response at 300 µM. GW9508 pEC50 values were found to be significantly different ** $P < 0.01$ using a Student's unpaired t test. Data were normalised (%) to the 300 µM oleic acid response and were pooled from a minimum of 5 individual experiments, mean ± S.E.M. N.D. not determined.

The SNAP-GPR120 cell lines were then tested in comparison to equivalent FLAG-tagged GPR120 (tagged at the amino terminus with the 8 residue epitope of DYKDDDDK) cell lines, to determine that the addition of the signal sequence SNAP-tag (209 residues) domain had not affected receptor function in eliciting calcium mobilisation responses to agonists.

Calcium mobilisation responses at FLAG-GPR120S (Figure 3.7 A; n = 4) and SNAP-GPR120S (Figure 3.7 C; n = 9) were measured in response to oleic acid, myristic acid and GW9508 (section 2.2.3.2). These responses were receptor specific because there were no responses in cells that had not undergone tetracycline induction of receptor expression. Agonist pEC_{50} values and maximal responses were similar in each cell line, indicating that the addition of the amino terminal SNAP-tag did not have a functional impact in this assay (Figure 3.7; Table 3.3). Interestingly, neither FLAG-GPR120L (Figure 3.7 B; n = 4) or SNAP-GPR120L (Figure 3.7 D; n = 3) gave calcium mobilisation responses following tetracycline induction of receptor expression.

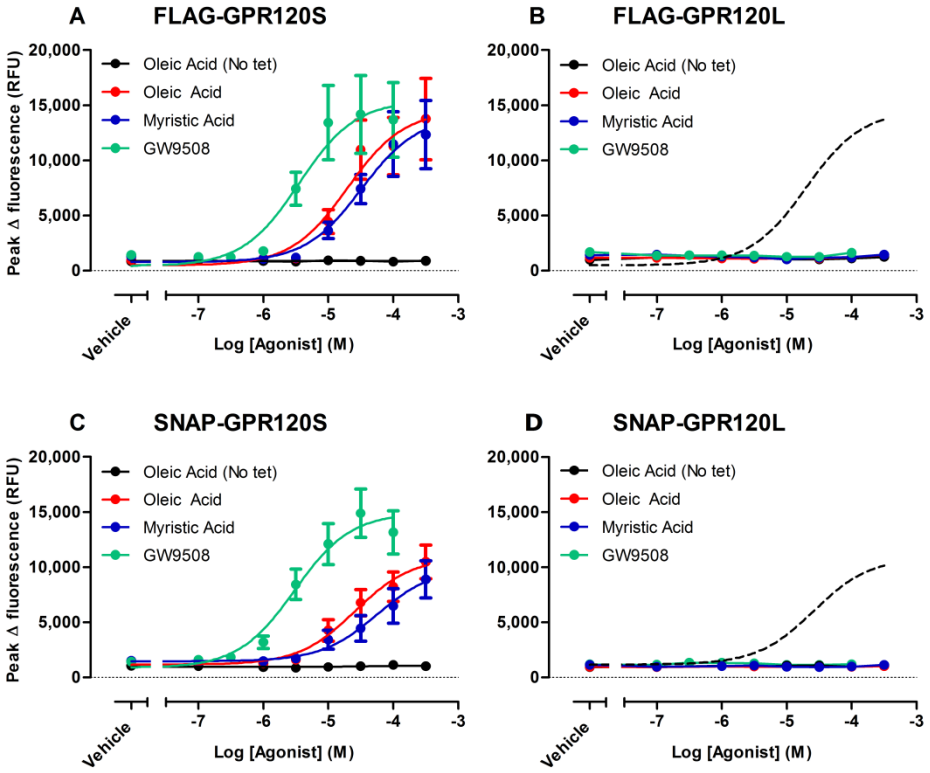

Figure 3.7 The effect of the SNAP-tag addition upon GPR120 mediated calcium mobilisation in response to agonist.

The effect of the SNAP-tag fusion upon oleic acid, myristic acid and GW9508 eliciting intracellular calcium mobilisation were measured in HEK293TR cells expressing the SNAP-GPR120S (C) or SNAP-GPR120L (D), compared to FLAG-GPR120S (A) or FLAG-GPR120L receptors (B). The dotted line shown in B and D denotes the oleic acid response at GPR120S for comparison. Data points for each experiment are the mean of triplicate readings; the data shown are pooled from the minimum of 4 individual experiments, mean ± S.E.M. RFU = relative fluorescent units.

	FLAG-GPR120S		SNAP-GPR120S	
Agonist	pEC_{50}	R_{max} (RFU)	pEC_{50}	R_{max} (RFU)
Oleic Acid	4.7 ± 0.3	13,768 ± 3,675	4.6 ± 0.2	10,493 ± 1,541
Myristic Acid	4.5 ± 0.2	12,338 ± 3,102	4.2 ± 0.3	8,901 ± 1,690
GW9508	5.5 ± 0.3	13,685 ± 3,387	5.5 ± 0.2	13,163 ± 1,949

Table 3.3 Potency and maximal responses of agonists at FLAG-GPR120S and SNAP-GPR120S as measured in the calcium mobilisation assay.

Potency and maximal responses of FLAG-GPR120S and SNAP-GPR120S in response to oleic acid, myristic acid and GW9508. Data were pooled from a minimum of 4 individual experiments, mean ± S.E.M. RFU = relative fluorescent units, peak change to agonist.

3.2.2.1 Pharmacological inhibition of calcium signalling

Next, inhibition of the calcium responses through SNAP-GPR120S activation was attempted using two compounds, PTx and 2-aminoethoxydiphenyl borate (2-APB). PTx catalyses the ADP ribosylation from nicotinamide adenine dinucleotide to the α subunit of the Gi protein, causing the blockade of Gi-dependent calcium responses (Katada and Ui, 1982). Whilst 2-APB, originally thought to block calcium signalling through blockade of IP_3 receptors (Maruyama et al., 1997), has later been found to also prevent store operated calcium entry (DeHaven et al., 2008).

Pooled time courses shown in Figure 3.8 represent calcium responses following the addition of 300 μM oleic acid or 100 μM GW9508 (at 15 seconds, dotted line) with either 100 nM PTx (Figure 3.8 A, C) or 50 μM 2-APB pre-treatment (Figure 3.8 B, D). Responses in the presence of 2-APB were significantly shortened compared to controls, for example at 60 seconds the responses were statistically different $P < 0.01$ for both oleic acid and GW9508, as tested using 2 way ANOVA with Bonferroni post tests.

100 nM PTx (Figure 3.8 E; Table 3.4; n = 4) had no significant effect upon concentration response curves, but 50 μM 2-APB (Figure 3.8 F; n = 4) inhibited peak responses to both 100 μM GW9508 and 300 μM oleic acid ($P < 0.001$ using 2 way ANOVA + Bonferroni post-tests). However although 2-APB had a significant effect upon SNAP-GPR120S mediated calcium mobilisation, it did not completely abolish it.

The FFA1 selective antagonist GW1100 was also investigated to determine its inhibition of calcium responses mediated by SNAP-FFA1. Increasing concentrations of GW1100 right shifted GW9508 concentration response curves and eventually abolished calcium signalling at SNAP-FFA1 (Figure 3.9 B; n = 4). Following Schild analysis, a slope of 2.7 ± 0.1 was obtained. A pA_2 of 6.0 ± 0.8 was also obtained, which corresponds to both the pK_B of 6.6 calculated using the Gaddum equation, and the GW1100 equilibrium dissociation constant previously estimated at 1 µM (Briscoe et al., 2006).

3.2.2.2 FFA1 non-signalling mutant, R258A

To inhibit the calcium response at SNAP-FFA1, a non-signalling receptor mutant was created, SNAP-FFA1 R258A (Smith et al., 2009; Tikhonova et al., 2007). Compared to WT, the SNAP-FFA1 R258A mutant had a decreased ability to elicit calcium responses to all agonists. (for all, $P < 0.001$ by 2 way ANOVA with Bonferroni post tests; Figure 3.9 A; Table 3.5; n = 4).

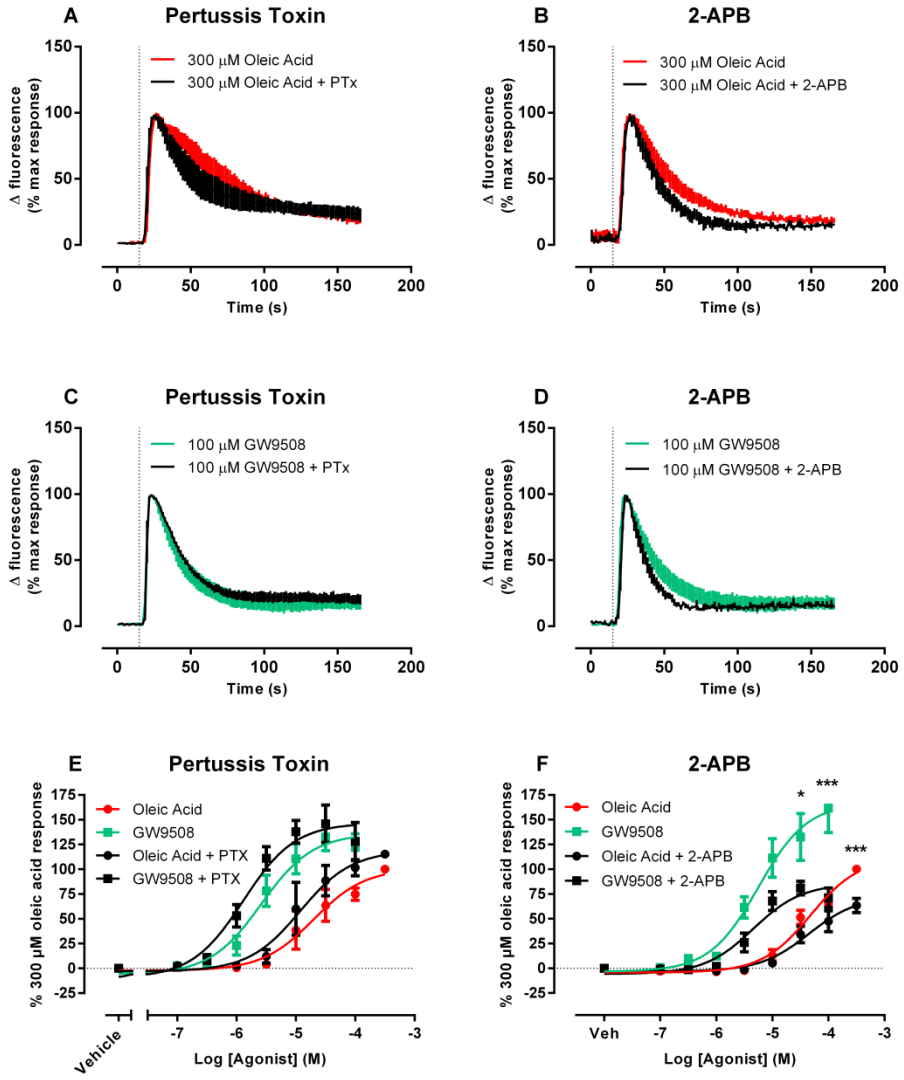

Figure 3.8 The effects of PTx and 2-APB upon potency and maximal responses of agonists at SNAP-GPR120S as measured in the calcium mobilisation assay.

The intracellular calcium mobilisation responses of SNAP-GPR120S in response to oleic acid and GW9508 following 18 hr 100 nM PTx (A, C, E) or 20 min 50 μM 2–APB (B, D, F) pre-treatment, were measured in HEK293TR cells expressing SNAP-GPR120S. A–D show the time course of response normalised to maximal response, whilst E and F show data normalised to 300 μM oleic acid response and pooled from 4 individual experiments, mean ± S.E.M. Statistical significance was measured using 2 way ANOVA plus Bonferroni post tests; *** $P < 0.001$; * $p<0.05$.

	PTx		2-APB	
Agonist	pEC_{50}	R_{max} (%)	pEC_{50}	R_{max} (%)
Oleic Acid (-)	4.7 ± 0.2	100	4.5 ± 0.1	100
Oleic Acid (+)	4.9 ± 0.2	115 ± 3	4.4 ± 0.2	64 ± 7 ***
GW9508 (-)	5.6 ± 0.1	122 ± 14	5.3 ± 0.2	162 ± 25
GW9508 (+)	5.9 ± 0.1	128 ± 19	5.3 ± 0.2	71 ± 10 ***

Table 3.4 The effects of PTx and 2-APB upon potency and maximal responses of agonists at SNAP-GPR120S as measured in the calcium mobilisation assay.

pEC_{50} and maximal responses of SNAP-GPR120S in response to oleic acid, myristic and GW9508 following 100 nM PTx or 50 μM 2–APB pre-treatment were measured in HEK293TR cells expressing SNAP-GPR120S ("+" denotes in the presence of inhibitor, whilst "-" denotes the controls in the absence of inhibitor). Data were normalised to the 300 μM oleic acid response and pooled from 4 individual experiments, mean ± S.E.M. Statistical significance was measured using 2 way ANOVA plus Bonferroni post tests *** $P < 0.001$; ** $P < 0.01$, * $P < 0.05$.

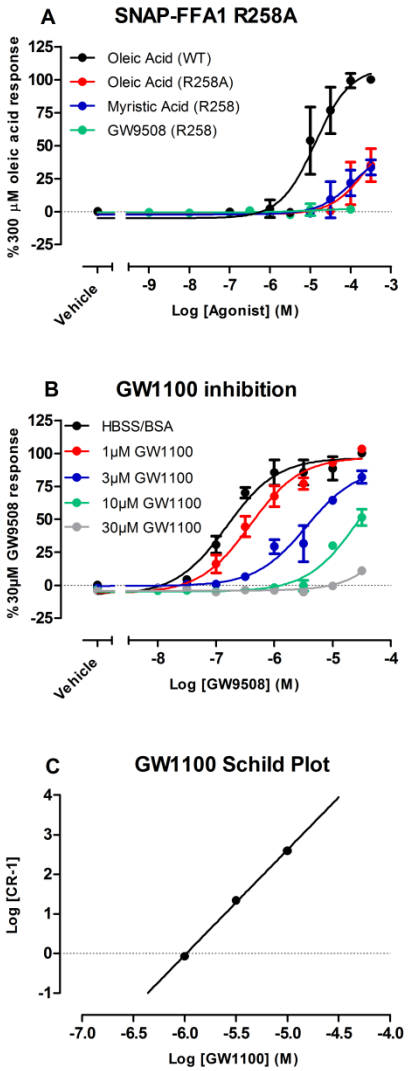

Figure 3.9 The effect of R258A mutation and GW1100 upon potency and maximal responses of agonists at SNAP-FFA1 as measured in the calcium mobilisation assay.

The intracellular calcium mobilisation responses of SNAP-FFA1 in response to oleic acid, myristic and GW9508 following R258A mutation were measured in HEK293TR cells expressing SNAP-FFA1 (A; see Figure 3.6 for full WT curves). Also measured were calcium mobilisation responses to GW9508 following pre-treatment with increasing concentrations of GW1100 (B), with data further analysed in a Schild plot (C; 30 µM data point was excluded). Data is pooled from 4 individual experiments, normalised (%) to the 300 µM oleic acid response (A) or the 30 µM GW9508 (B), mean + S.E.M.

	SNAP-FFA1		R258A	
Agonist	pEC_{50}	R_{max} (%)	pEC_{50}	R_{max} (%)
Oleic Acid	4.9 ± 0.1	100	N.D.	35 ± 6***
Myristic Acid	4.8 ± 0.1	94 ± 2	N.D.	34 ± 3***
GW9508	7.2 ± 0.1	96 ± 9	N.D.	2 ± 1***

Table 3.5 The effect of R258A mutation upon potency and maximal response values of agonists at SNAP-FFA1 as measured in the calcium mobilisation assay.

pEC_{50} values and responses of SNAP-FFA1 to 300 µM oleic acid, myristic acid and 100 µM GW9508 following both R258A mutation or following pre-treatment with increasing concentrations of GW1100 were measured in HEK293TR cells expressing SNAP-FFA1. R258A R_{max} values were determined from the maximal response at 300 µM (oleic, myristic) or 100 µM (GW9508). The concentration responses of SNAP-FFA1 and SNAP-FFA1 R258A to agonists were found to be significantly different from WT *** $P < 0.001$ using 2 way ANOVA and Bonferroni post tests. Data were normalised (%) to 300 µM oleic acid response (A) or to 30 µM GW9508 response (B), pooled from 4 individual experiments, mean ± S.E.M.

3.2.3 Integrated whole cell responses measured by DMR

Following on from the calcium mobilisation studies, the HEK293TR SNAP-GPR120 cell lines were then tested on a Corning Epic Biosensor. This is a label free system that, following automated ligand additions, measured the whole cell response by monitoring the DMR of the cellular contents (Schroder et al., 2010). After addition of ligand, large positive monophasic responses were observed at SNAP-GPR120S (Figure 3.10 A), whilst much smaller responses were observed at SNAP-GPR120L (Figure 3.10 B), with ATP used as a control compound across all cell lines.

These DMR responses were also analysed to generate concentration response curves, giving pEC_{50} values (Table 3.6). The results from this assay gave similar results to the calcium assay, of SNAP-GPR120S mediating agonist responses (Figure 3.11 A; n = 12), whilst SNAP-GPR120L did not (Figure 3.11 B; n = 10). Stimulation of cells expressing SNAP-GPR120L did give small responses, but these were no larger than those observed for the parent cell line, the HEK293TRs (Figure 3.11 C; n = 2).

Once again, the inhibitors PTx (Figure 3.12 A, B) and 2-APB (Figure 3.12 C, D) were utilised to see what effect they had upon the holistic response, as measured using DMR. Both inhibitors had a significant effect upon GW9508 potency in SNAP-GPR120S cells (Table 3.6).

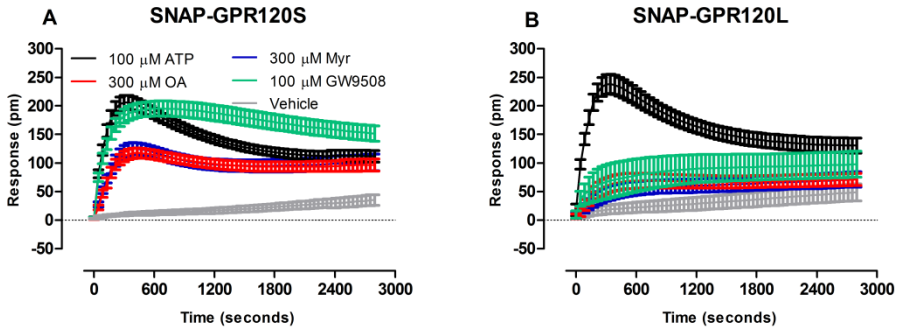

Figure 3.10 DMR time courses of SNAP-GPR120S and SNAP-GPR120L in response to agonist.

DMR measurements in HEK293TR cells expressing SNAP-GPR120S (A) or SNAP-GPR120L (B), in response to 300 μM oleic acid (OA) and myristic acid (Myr), 100 μM ATP and GW9508, and vehicle. Data shown were pooled from the minimum of 4 individual experiments, mean + S.E.M.

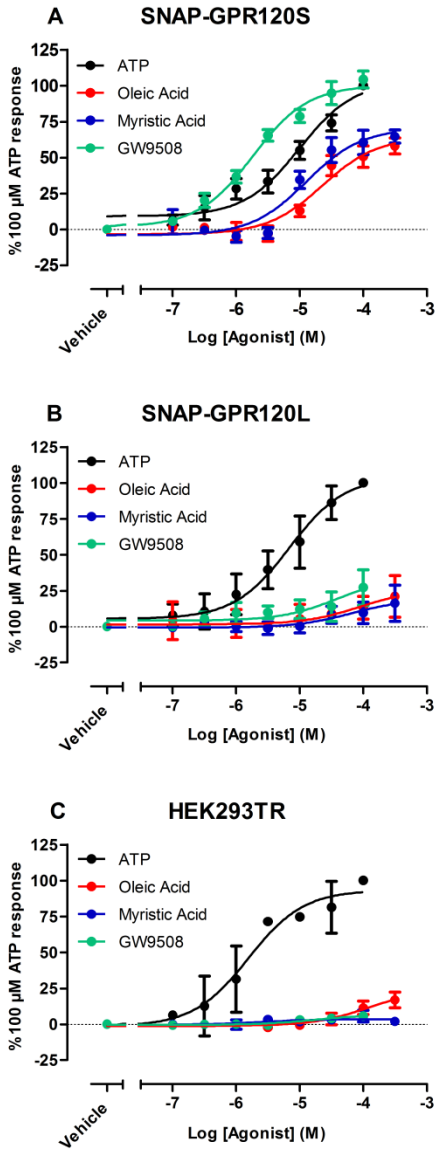

Figure 3.11 DMR concentration-dependent responses of SNAP-GPR120S and SNAP-GPR120L cells in response to agonists.

Dynamic mass redistribution concentration response curves to ATP, oleic acid, myristic and GW9508 in HEK293TR cells expressing SNAP-GPR120S (A), SNAP-GPR120L receptors (B) or non-transfected cells (C). Data shown were normalised (%) to 100 µM ATP and pooled from the minimum of 4 individual experiments, mean ± S.E.M.

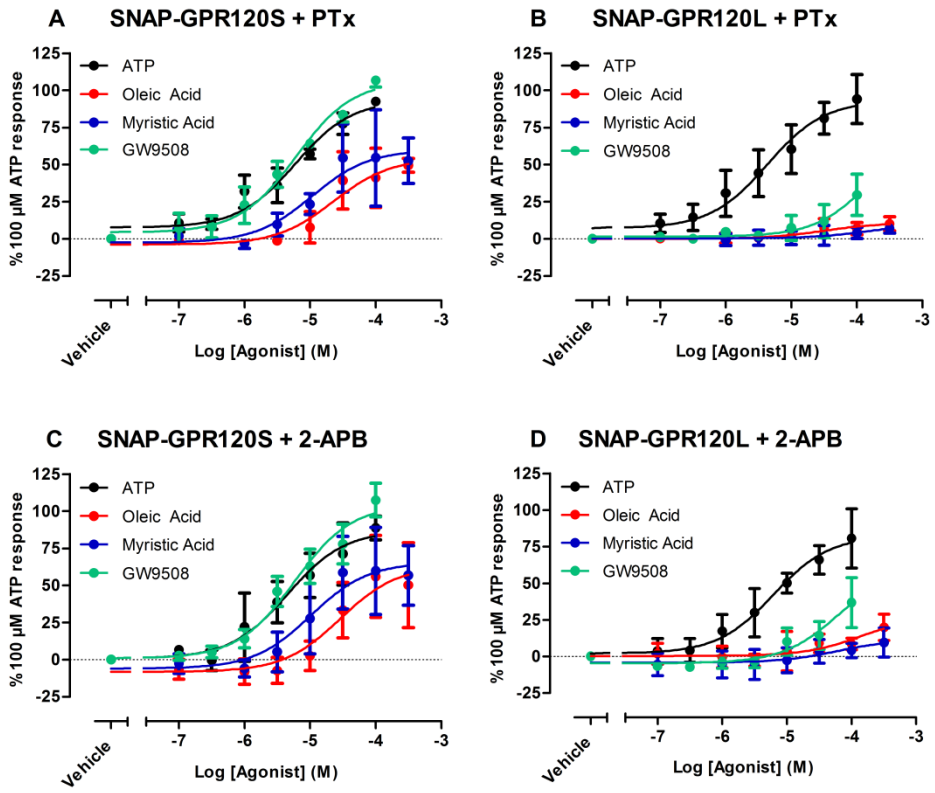

Figure 3.12 The effects of PTx and 2-APB upon potency and maximal responses of agonists at SNAP-GPR120S as measured in the DMR assay.

The DMR responses mediated by SNAP-GPR120S receptors in response to ATP, oleic acid, myristic acid and GW9508 following 100 nM PTX (A, B) or 50 µM 2–APB (C, D) pre-treatment were measured in HEK293TR cells expressing SNAP-GPR120S (A, C) or SNAP-GPR120L (B, D). Data were normalised (%) to 100 µM ATP and pooled from 3 – 5 individual experiments, mean ± S.E.M.

i			SNAP-GPR120S		SNAP-GPR120S	
Agonist	SNAP-GPR120S		100 nM PTx		50 μM 2-APB	
	pEC_{50}	R_{max}	pEC_{50}	R_{max} (%)	pEC_{50}	R_{max} (%)
ATP	5.0 ± 0.1	100	5.2 ± 0.1	92 ± 2	5.3 ± 0.2	89 ± 5
Oleic Acid	4.6 ± 0.2	58 ± 6	4.6 ± 0.2	49 ± 3	4.5 ± 0.2	50 ± 13
Myristic Acid	4.9 ± 0.2	65 ± 5	5.0 ± 0.3	53 ± 9	5.0 ± 0.2	57 ± 9
GW9508	5.7 ± 0.1	104 ± 6	5.2 ± 0.1*	107 ± 5	5.2 ± 0.2**	107 ± 11

ii			SNAP-GPR120L		SNAP-GPR120L	
Agonist	SNAP-GPR120L		100 nM PTx		50 μM 2-APB	
	pEC_{50}	R_{max}	pEC_{50}	R_{max} (%)	pEC_{50}	R_{max} (%)
ATP	5.2 ± 0.1	100	5.4 ± 0.1	94 ± 8	5.2 ± 0.1	81 ± 10
Oleic Acid	N.D.	21 ± 5	4.5 ± 0.4	10 ± 2	3.9 ± 0.4	20 ± 4
Myristic Acid	N.D.	16 ± 4	3.8 ± 0.8	7 ± 2	4.2 ± 0.6	9 ± 5
GW9508	N.D.	27 ± 12	3.7 ± 1.3	30 ± 14	4.2 ± 0.5	37 ± 17

Table 3.6 DMR potency and maximal responses of SNAP-GPR120S (i) and SNAP-GPR120L (ii) cells in response to agonists in the presence or absence of inhibitors PTx or 2-APB.

pEC_{50} and maximal responses in cells expressing SNAP-GPR120S and SNAP-GPR120L in response to oleic acid, myristic acid and GW9508 with or without 100 nM PTx or 50 μM 2–APB pre-treatment. SNAP-GPR120L R_{max} values were determined from the maximal response at 300 μM (oleic, myristic) or 100 μM (GW9508). Data were normalised (%) to 100 μM ATP and pooled from a minimum of 4 individual experiments, mean ± S.E.M; N.D. not determined.

* $P < 0.05$, ** $P < 0.01$ compared with control GW9508 pEC_{50} values in SNAP-GPR120S cells (Student's t test).

3.2.4 Arrestin interactions measured using BiFC

After measuring the holistic, whole cell responses and calcium signalling as a measure of G protein signalling, GPR120 receptor isoforms were then investigated for their ability to interact with β-arrestin2 using BiFC, and time course and concentration response curves were measured (Section 2.2.4). This assay required a different modification of the receptors; a FLAG-tagged version, with a carboxyl terminal –vYC tag to initiate the complementation. Representative images and the associated analysis are illustrated in Figure 3.13 (Kilpatrick et al., 2010).

The time course assay gave half times of interaction of 9 ± 1 min for FLAG-GPR120S-vYc with β-arrestin2-vYNL (Figure 3.14 A; n = 6) and 14 ± 1 min for FLAG-GPR120L-vYc with β-arrestin2-vYNL in response to 300 μM oleic acid (Figure 3.14 A; n = 5). Half times of interaction in response to 100 μM GW9508 for FLAG-GPR120S-vYc with β-arrestin2-vYNL were 7 ± 1 min (Figure 3.14 B; n = 6) and 8 ± 1 min for FLAG-GPR120L-vYc with β-arrestin2-vYNL (Figure 3.14 B; n = 5). In terms of concentration responses, again, both FLAG-GPR120S-vYc with β-arrestin2-vYNL (Figure 3.14 C; n = 4) and FLAG-GPR120L-vYc with β-arrestin2-vYNL (Figure 3.14 D; n = 4) had similar pEC_{50} values for oleic acid and GW9508 (Table 3.7). Therefore it was found that both GPR120 isoforms interacted with β-arrestin2, both in terms of time course and concentration response curves, equivalently (Table 3.7). In comparison, no agonist-stimulated association between FLAG-FFA1-vYC and β-arrestin2-vYNL was detected by BiFC in equivalent cell lines (data not shown).

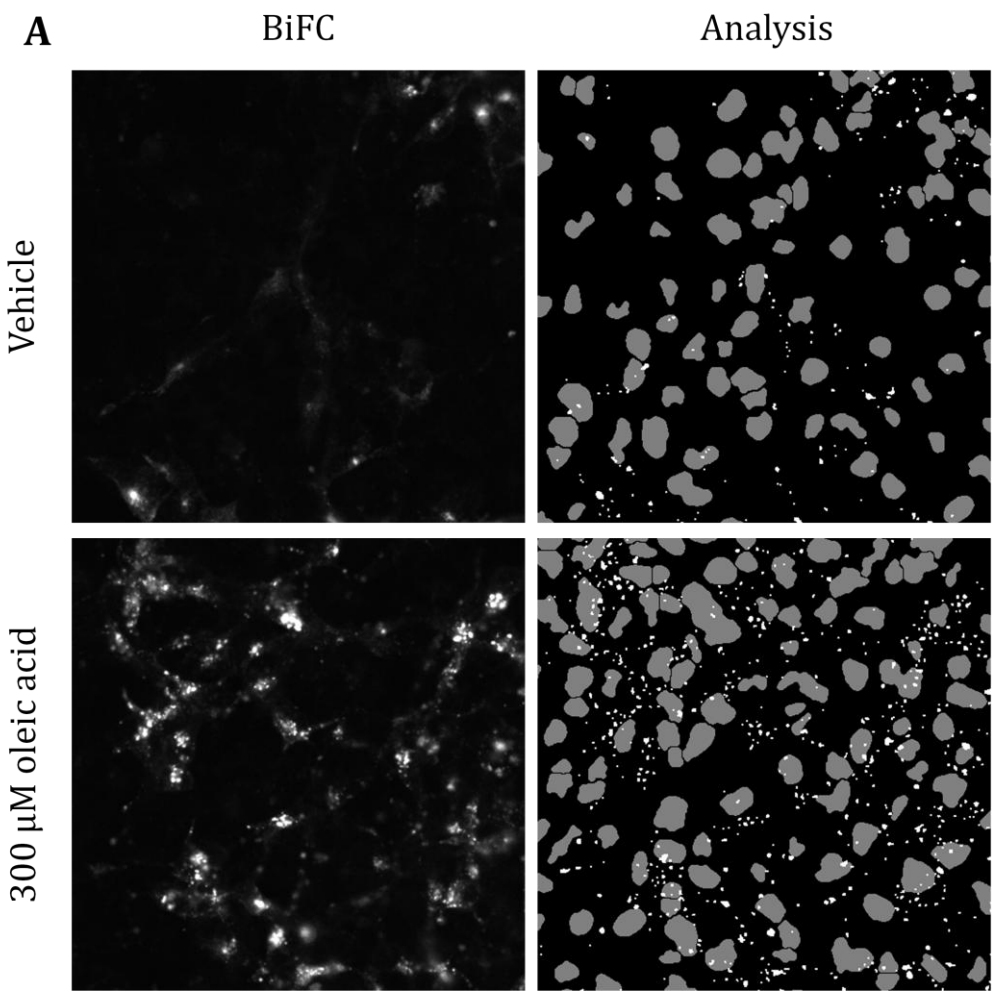
A
BiFC
Analysis
Vehicle
300 µM oleic acid

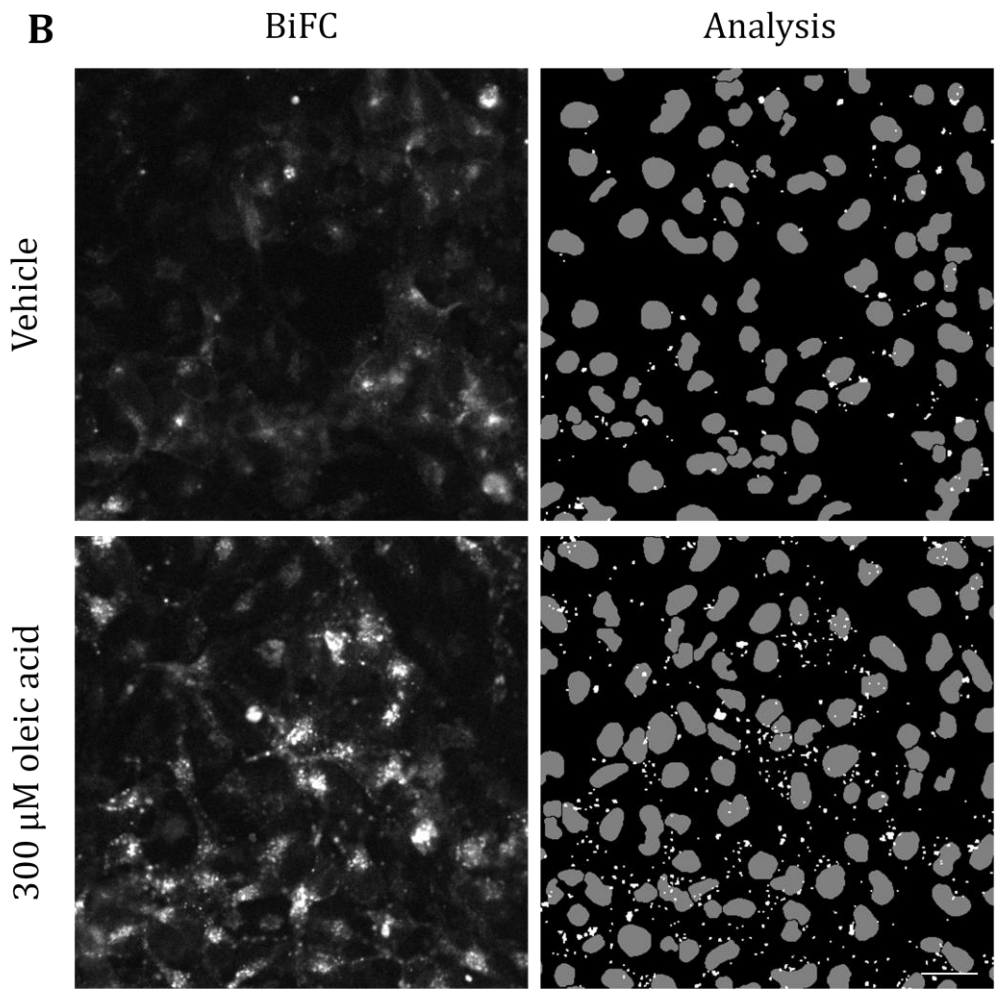

Figure 3.13 Representative images and quantitative analysis of agonist induced FLAG-GPR120S-vYC or FLAG-GPR120L-vYC interaction with β-arrestin2-vYNL.

Representative images acquired on the IX Ultra of HEK293TRs stably transfected with FLAG-GPR120S-vYC (A) or FLAG-GPR120L-vYC (B), and β-arrestin2-vYNL following 30 minute treatment with vehicle or 300 µM oleic acid at 37^{o}C. Images shown are BiFC (left panels) and the result of the granularity algorithm (right panels). Analysis identified nuclei and recomplemented YFP (white dots), with intensity thresholds set relative to positive controls present on the plate. Scale bar = 50 µm.

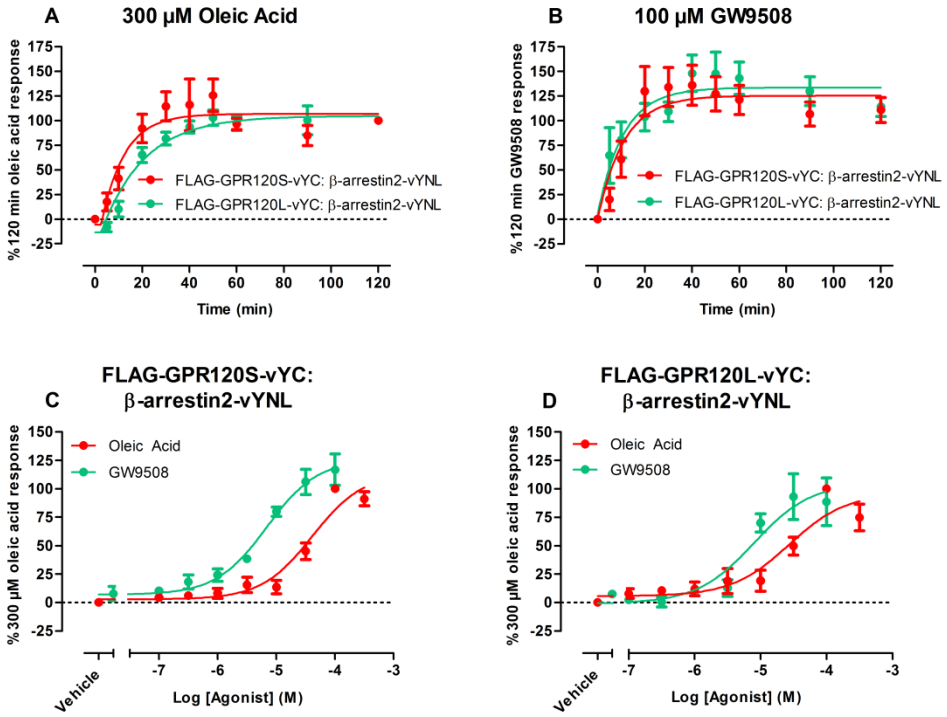

Figure 3.14 Time course and concentration response curves of FLAG-GPR120S-vYC and FLAG-GPR120L-vYC with β-arrestin2-vYNL, in response to oleic acid and GW9508 using BiFC.

120 minute time course BiFC responses of FLAG-GPR120S-vYC and FLAG-GPR120L-vYC with β-arrestin2-vYNL to 300 µM oleic acid (A) and 100 µM GW9508 (B), and concentration responses of FLAG-GPR120S-vYC (C) and FLAG-GPR120L-vYC (D) with β-arrestin2-vYNL to oleic acid and GW9508. Data were normalised (%) to the 300 µM oleic acid response and pooled from 4 – 6 individual experiments, mean ± S.E.M.

	FLAG-GPR120S-vYC: β-arrestin2-vYNL		FLAG-GPR120L-vYC: β-arrestin2-vYNL	
Agonist	pEC_{50}	R_{max} (%)	pEC_{50}	R_{max} (%)
Oleic Acid	4.4 ± 0.1	100	4.6 ± 0.2	100
GW9508	5.2 ± 0.1	118 ± 9	5.1 ± 0.2	89 ± 21

Table 3.7 Agonist potency and maximal responses for FLAG-GPR120S-vYC and FLAG-GPR120L-vYC association with β-arrestin2-vYNL.

pEC_{50} values and responses to 300 μM oleic acid or 100 μM GW9508 of FLAG-GPR120S-vYC and FLAG-GPR120L-vYC with β-arrestin2-vYNL as measured using bimolecular fluorescence complementation. Data were normalised (%) to the 300 μM oleic acid response and pooled from 4 – 6 individual experiments, mean ± S.E.M.

3.2.5 Agonist mediated endocytosis of GPR120 receptor isoforms

Next, agonist mediated endocytosis of the SNAP-GPR120 receptor was quantified using an automated imaging plate reader to image receptors labelled with SNAP-surface AF-488 (Section 2.2.4.1). Cells were then treated with agonist, and fixed prior to imaging. Firstly, the time course of agonist mediated endocytosis was measured (representative images Figure 3.15). Interestingly, time courses of agonist mediated endocytosis showed that both SNAP-GPR120 isoforms underwent internalisation, with half times in response to oleic acid of 20 ± 6 min at SNAP-GPR120S and 17 ± 2 min at SNAP-GPR120L (Figure 3.16 A; n = 4); and half times in response to GW9508 of 13 ± 1 min at SNAP-GPR120S and 21 ± 3 min at SNAP-GPR120L (Figure 3.16 B; n = 4). Half times of agonist mediated endocytosis of the isoforms to GW9508 were significantly different * $P < 0.05$ (Student's 2 tailed t test).

This in conjunction with the BiFC data, suggests that both GPR120 isoforms can interact with β-arrestin proteins and subsequently undergo agonist induced endocytosis.

Next, the internalisation assay was used to test concentration responses of the isoforms. Both isoforms underwent agonist induced endocytosis to an equivalent extent in response to maximum agonist concentrations (e.g. Figure 3.15). There was a slight variance in agonist potencies and maximum responses when measured at 30 (Figure 3.17 A, B; n = 6) versus 60 min (Figure 3.17 C, D; n = 4) especially in the responses to 100 μM GW9508 (relative to fatty acids) at SNAP-GPR120S for 30 min versus 60 min (Table 3.8).

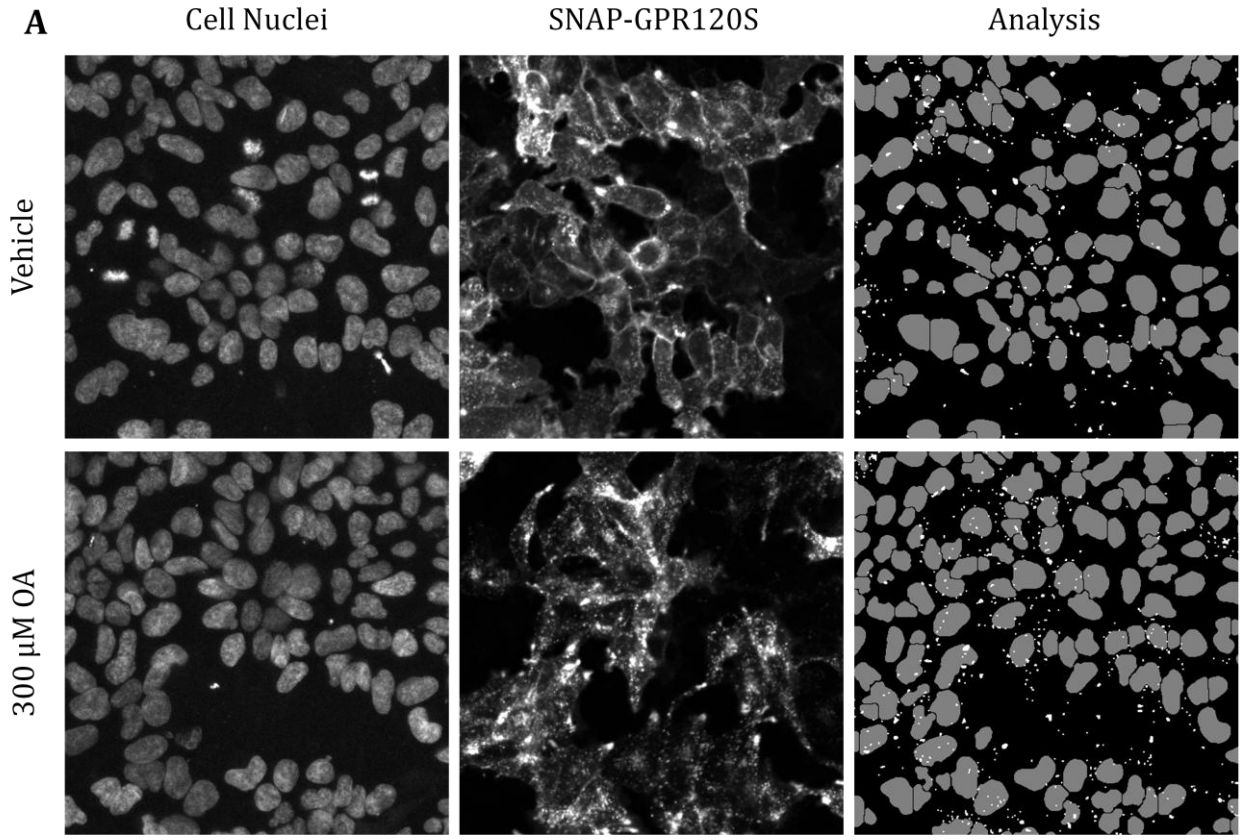
A
Cell Nuclei
SNAP-GPR120S
Analysis
Vehicle
300 µM OA

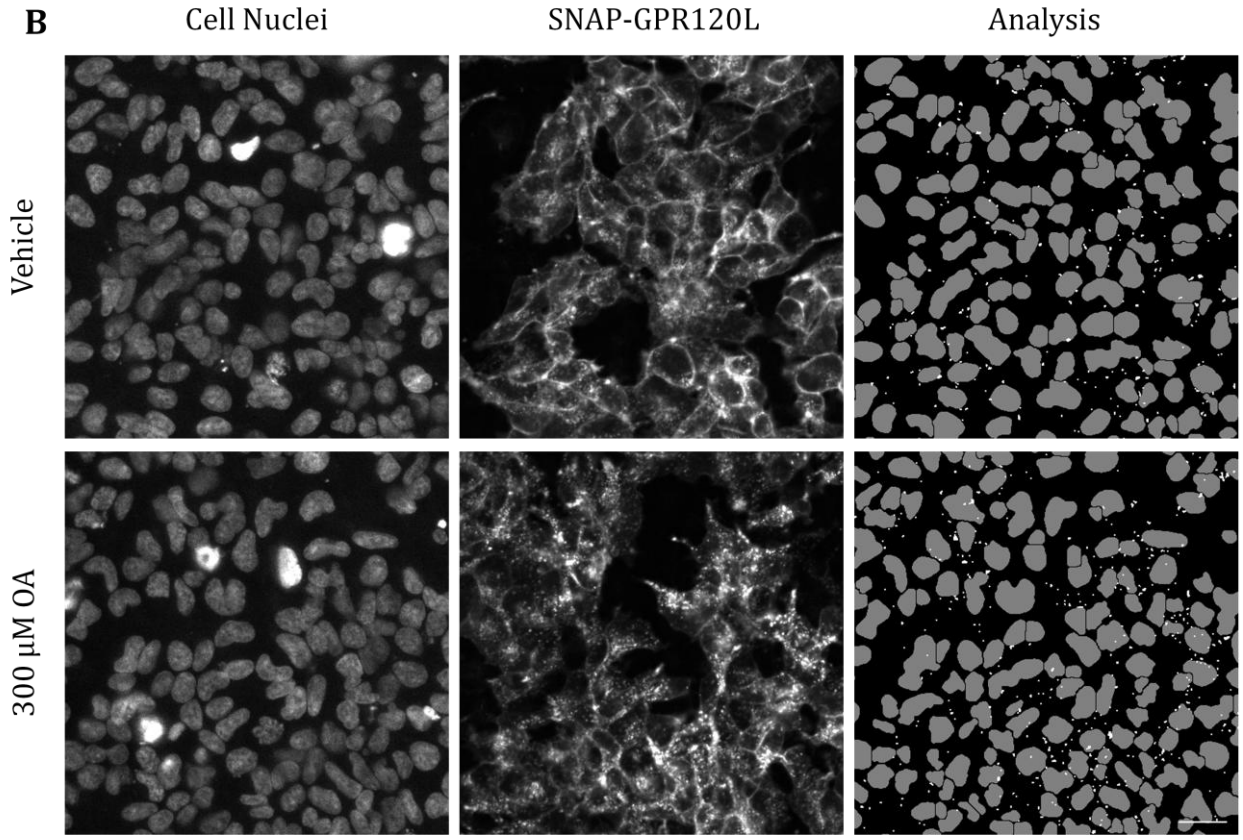
B
Cell Nuclei
SNAP-GPR120L
Analysis
Vehicle
300 μM OA

Figure 3.15 Quantitative analysis of agonist induced SNAP-GPR120S and SNAP-GPR120L endocytosis.

Representative images acquired on the IX Ultra of HEK293TRs stably transfected with SNAP-GPR120S (A) or SNAP-GPR120L (B) following 60 minute treatment with vehicle or 300 µM OA at 37^{o}C. Images shown are H33342 stained cell nuclei (left panels); SNAP-GPR120S or SNAP-GPR120L prelabelled with SNAP-surface AF-488 (middle panels; A, B respectively) and the result of the granularity algorithm (right panels). Analysis identified nuclei (grey) and internalised receptors 2-5 µm in diameter (white dots), with intensity thresholds set relative to positive and negative controls present on the plate. Scale bar = 50 µm.

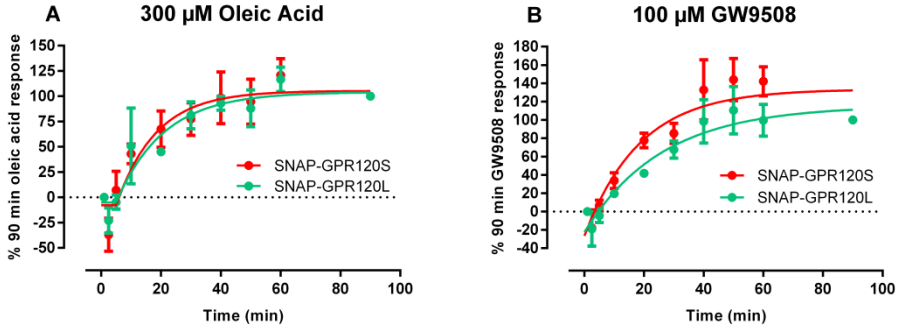

Figure 3.16 Time course of SNAP-GPR120S and SNAP-GPR120L endocytosis in response to 300 µM oleic acid and 100 µM GW9508.

Endocytosis time course responses of SNAP-GPR120S and SNAP-GPR120L to 300 µM oleic acid (A) and 100 µM GW9508 (B) as measured on the confocal plate reader. Data were normalised (%) to the 90 min response and were pooled from 4 individual experiments, mean ± S.E.M.

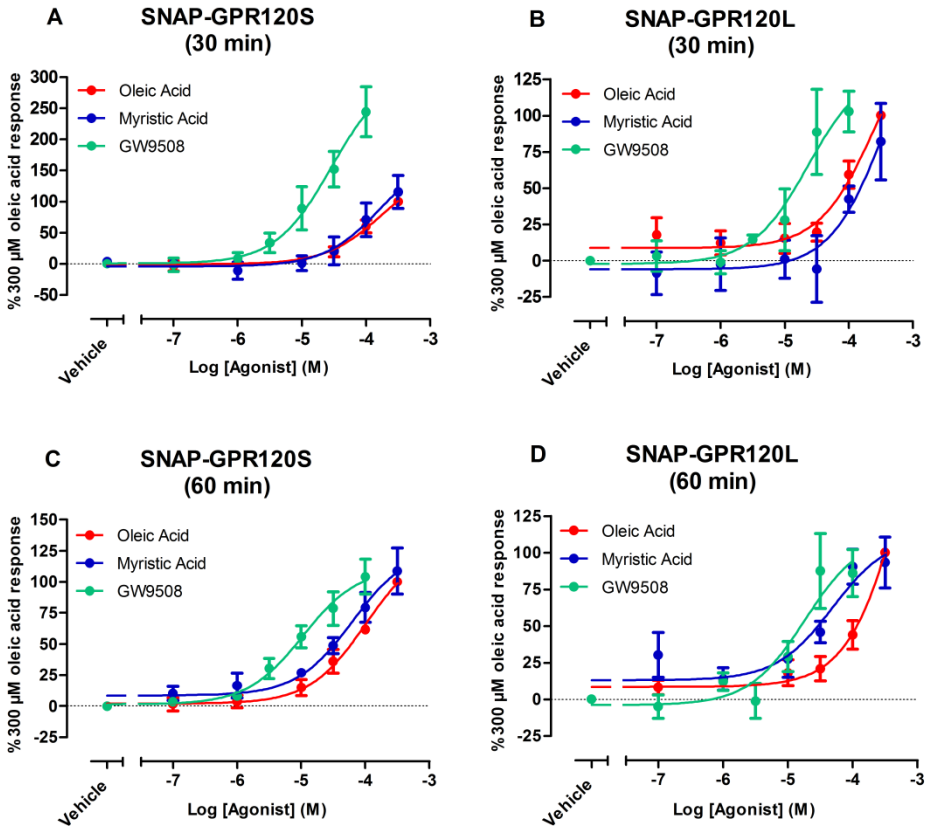

Figure 3.17 Endocytosis of SNAP-GPR120S and SNAP-GPR120L in response to agonists measured at 30 and 60 min.

Concentration response relationships of SNAP-GPR120S (A, C) and SNAP-GPR120L (B, D) internalisation to agonists at 30 (A, B) and 60 (C, D) min post addition, as measured on the confocal plate reader. Data were normalised (%) to the 300 µM oleic acid response and were pooled from 4 - 7 individual experiments, mean ± S.E.M.

i 30 min

	SNAP-GPR120S		SNAP-GPR120L	
Agonist	pEC_{50}	R_{max} (%)	pEC_{50}	R_{max} (%)
Oleic Acid	3.8 ± 0.2	100	3.8 ± 0.3	100
Myristic Acid	3.8 ± 0.4	116 ± 26	3.4 ± 0.8	82 ± 26
GW9508	4.5 ± 0.2	244 ± 40	4.6 ± 0.3	103 ± 14

ii 60 min

	SNAP-GPR120S		SNAP-GPR120L	
Agonist	pEC_{50}	R_{max} (%)	pEC_{50}	R_{max} (%)
Oleic Acid	4.0 ± 0.1	100	3.1 ± 0.4	100
Myristic Acid	4.2 ± 0.2	109 ± 19	4.3 ± 0.3	93 ± 3
GW9508	5.0 ± 0.2	104 ± 14	4.7 ± 0.3	86 ± 16

Table 3.8 Potency and maximal responses of SNAP-GPR120S and SNAP-GPR120L agonist induced endocytosis at 30 and 60 min.

Concentration responses of SNAP-GPR120S and SNAP-GPR120L to agonists at 30 min (i) and 60 min (ii) post addition, as measured on the confocal plate reader. Data were normalised (%) to the 300 µM oleic acid response and pooled from 4 – 7 individual experiments, mean ± S.E.M.

TZDs are synthetic ligands used as a treatment in type II diabetes (Section 1.4.4.1.1.4). A number of these compounds were also found to elicit responses from GPR120S, measured as calcium mobilisation (Figure 3.18 A, B; Table 3.10). SNAP-GPR120S also underwent endocytosis in response to 100 µM rosiglitazone and ciglitazone, whilst no SNAP-GPR120S endocytosis was induced by pioglitazone at up to 30 µM. However, troglitazone and pioglitazone both also induced visible changes in cell morphology at concentrations above 30 µM (Figure 3.18 C; Table 3.9; n = 4), and also TZDs were not tested on cells that had not been tet treated, therefore these may be non specific responses.

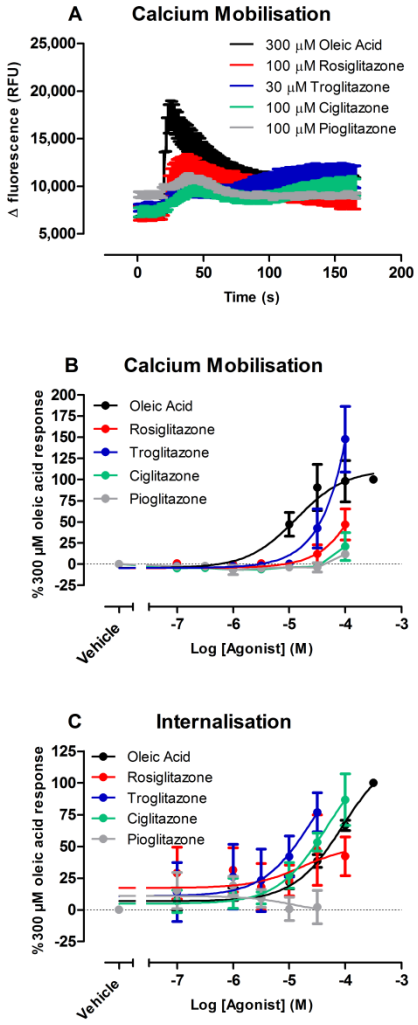

Figure 3.18 Thiazolidinediones are GPR120S agonists at high concentration.

Calcium mobilisation time courses (A) and concentration response curves (B); and internalisation concentration responses (C) of SNAP-GPR120S to thiazolidinediones. Experiments were conducted as in Figures 3.6 (calcium mobilisation) and 3.15 (internalisation). Data were normalised (%) to 300 µM oleic acid and is pooled from 4 – 5 individual experiments, mean ± S.E.M.

	Calcium		Internalisation	
Agonist	pEC_{50}	R_{max} (%)	pEC_{50}	R_{max} (%)
Oleic Acid	4.9 ± 0.1	100	4.1 ± 0.1	100
Rosiglitazone	N.D.	47 ± 8	N.D.	42 ± 15
Troglitazone	N.D.	148 ± 17	N.D.	77 ± 15
Ciglitazone	N.D.	21 ± 7	N.D.	87 ± 20
Pioglitazone	N.D.	12 ± 2	N.D.	N.D.

Table 3.9 Potency and maximal responses of SNAP-GPR120S in response to thiazolidinediones.

Calcium and internalisation potency and maximal responses of SNAP-GPR120S to different thiazolidinediones. R_{max} values were determined from the maximal response at the highest ligand concentration tested. Data were normalised (%) to the 300 μM oleic acid response and pooled from 4 - 5 individual experiments, mean ± S.E.M.

3.2.6 The subcellular trafficking of the internalised GPR120 isoforms

To determine which pathway GPR120 isoforms follow once they had undergone agonist mediated endocytosis, confocal images were taken in the presence of different pathway markers. Lysotracker red is a compound which localises to acidic organelles, such as lysosomes, and was used to mark the degradation pathway (Figure 3.19 A, B). Meanwhile, transferrin was used to label the recycling pathway, because it localises to the recycling endosomes as well as other parts of the clathrin-mediated endocytosis pathway (Figure 3.19 C, D). The extent of colocalisation of the receptors with these compounds was used as an indication of which trafficking pathway the receptors followed. From the confocal images, it appears that after stimulation oleic acid, internalised SNAP-GPR120S (Figure 3.19 A, C) and SNAP-GPR120L (Figure 3.19 B, D) predominantly colocalised with lysotracker red, to a greater extent than transferrin Figure 3.19).

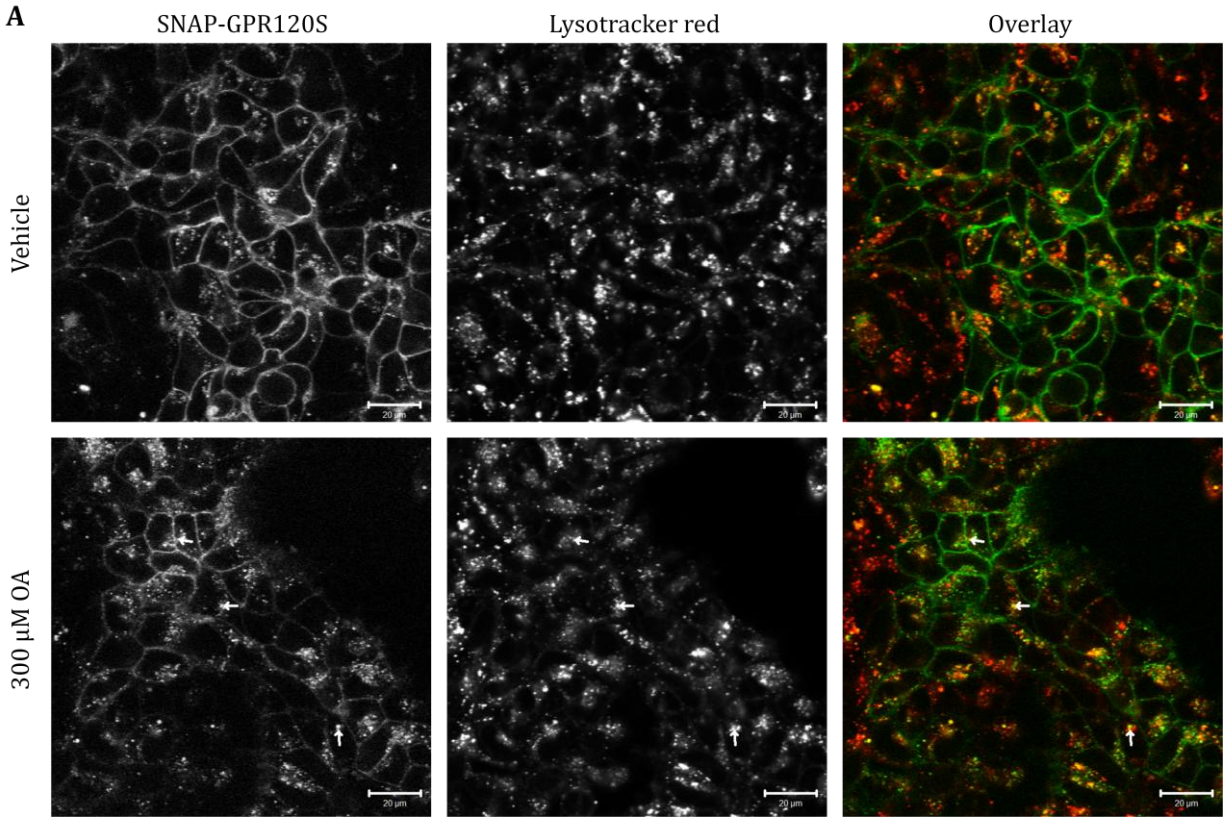
A
SNAP-GPR120S
Lysotracker red
Overlay
Vehicle
300 µM OA
20 µm

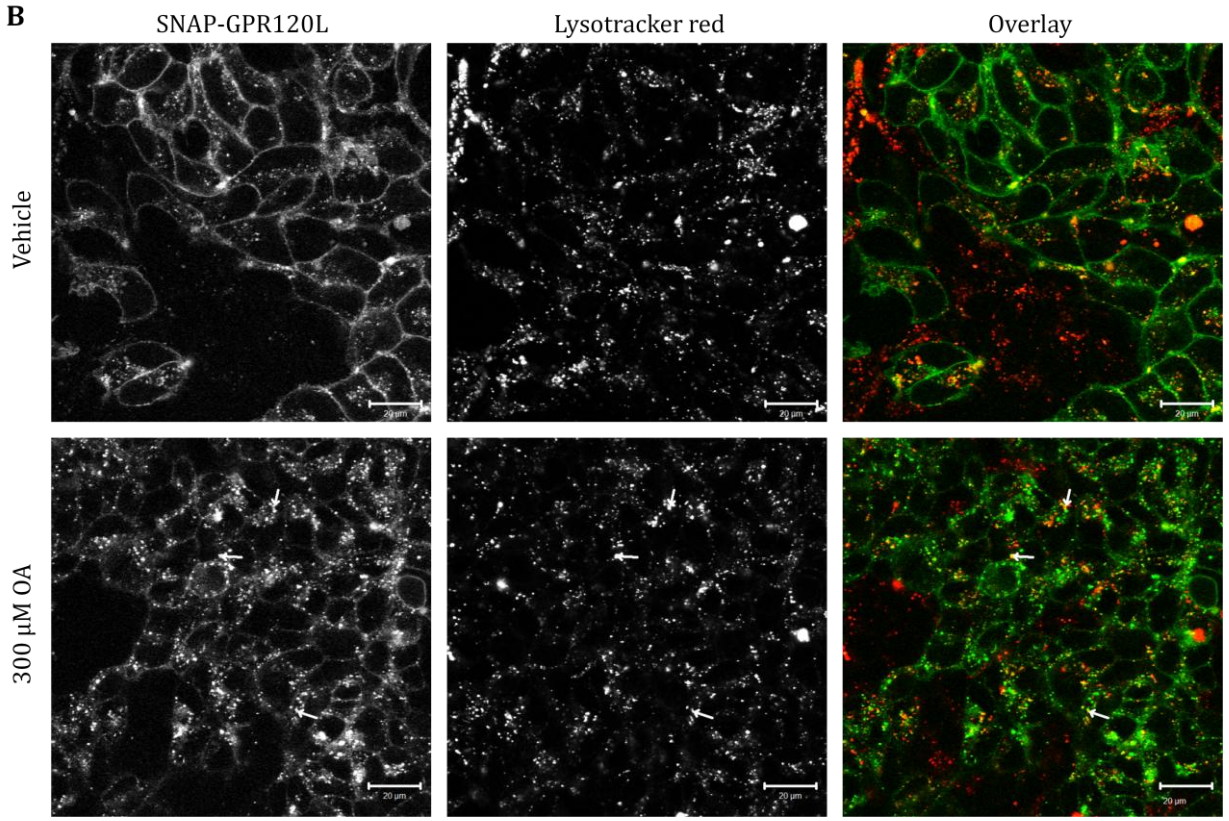
B
SNAP-GPR120L
Lysotracker red
Overlay
Vehicle
300 µM OA

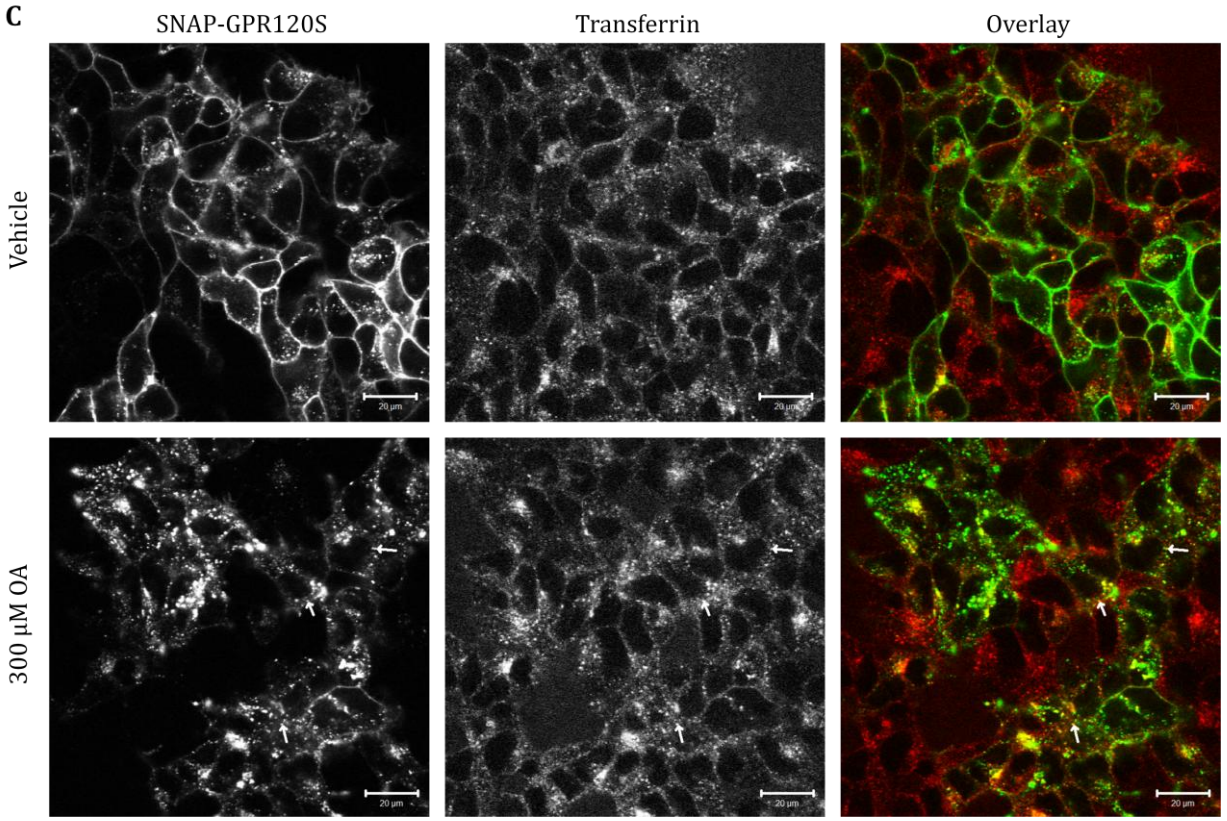
C
SNAP-GPR120S
Transferrin
Overlay
Vehicle
300 µM OA
20 µm

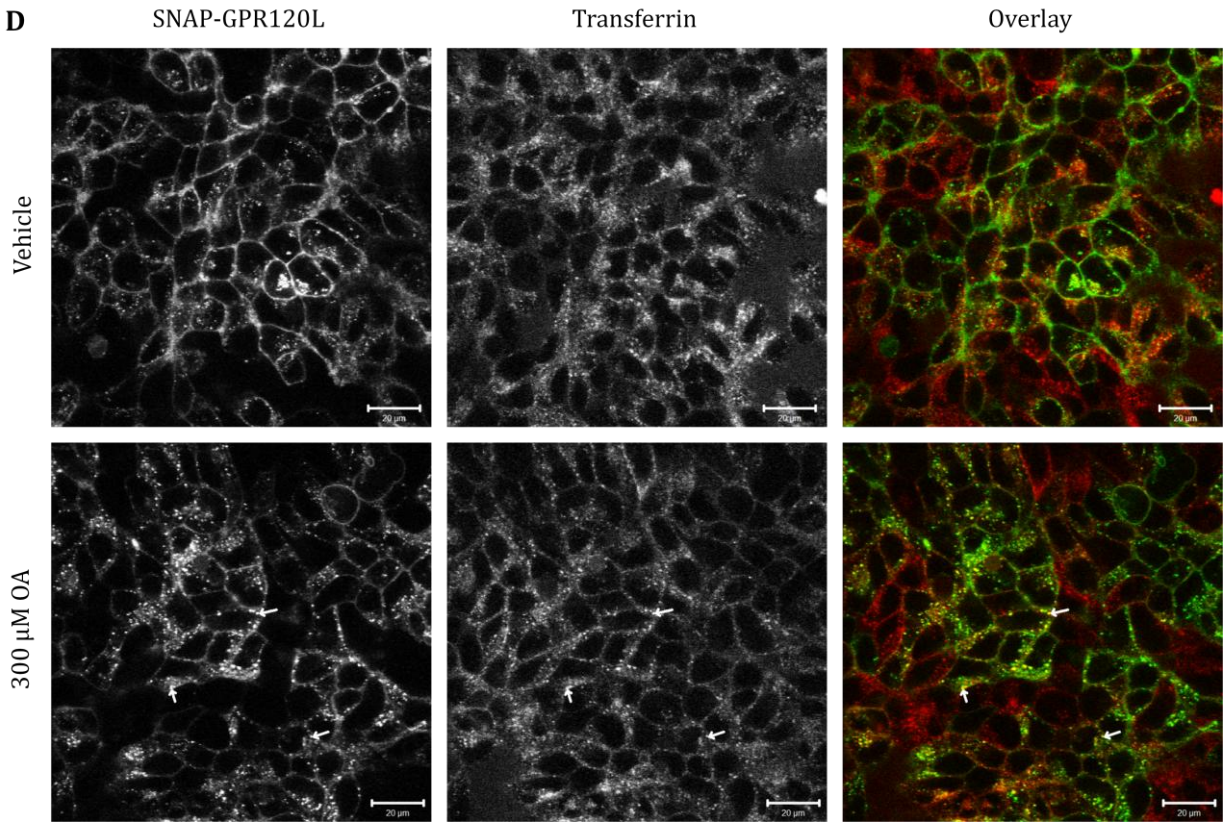
D
SNAP-GPR120L
Transferrin
Overlay
Vehicle
300 µM OA

Figure 3.19 Representative confocal colocalisation images of SNAP-GPR120S and SNAP-GPR120L in cells additionally labelled with transferrin or lysotracker red.

HEK293TRs stably transfected with SNAP-GPR120S (A, C) or SNAP-GPR120L (B, D) were treated with vehicle (top panels) or 300 µM oleic acid (OA, bottom panels) for 60 min at 37^{o}C. Images are of SNAP-surface AF-488 labelled receptor (left panels), lysotracker red (middle panels; A, B) or transferrin (middle panels; C, D) and the overlay (right panels). Images were acquired using a Zeiss LSM510 confocal microscope with laser excitation at 488 nm (SNAP-surface AF-488 labelled receptors), 543 nm (lysotracker red), or 633 nm (transferrin). Arrows denote example regions of colocalisation. Scale bar = 20 µm. Images are representative of those acquired from 4 independent experiments.

Following on from the confocal imaging studies, a quantitative strategy for measuring whether the internalised GPR120 receptors recycled back to the plasma membrane was adopted. For this, agonist was added for 30 min, the cells were washed with HBSS/0.1 % BSA (higher BSA concentration to aid in agonist removal) and then left for 5 - 60 min (the “recycling” period) without ligand.

For 300 µM oleic acid treated cells, 60 min after the wash step, at SNAP-GPR120S 74 ± 8 %, and at SNAP-GPR120L 67 ± 6 % receptors remained in internalised vesicles, i.e. they had not returned back to the cell surface (Figure 3.20 A, B respectively; n = 5). Following GW9508 addition, there was also little decrease in the percentage of receptors remaining internalised 60 min post wash, but this may be due to the 30 µM GW9508 concentration used in this assay, which induced less receptor internalisation in the first place.

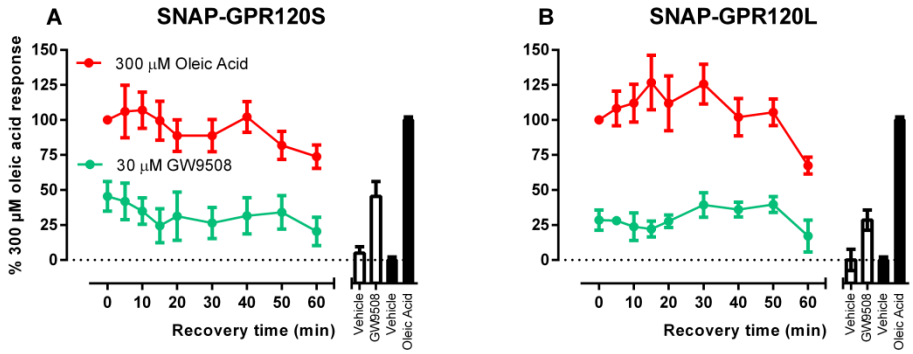

Figure 3.20 Recycling of SNAP-GPR120S and SNAP-GPR120L following 30 min stimulation with agonist.

Cells expressing SNAP-GPR120S (A) or SNAP-GPR120L (B) were treated with agonist, then underwent washes (HBSS / 0.1 % BSA) and were left 5 – 60 min, at which point they were fixed, then imaged on the confocal plate reader. Data were normalised (%) to the 300 µM oleic acid response and pooled from 5 individual experiments, mean ± S.E.M.

3.2.6.1 Role of carboxyl tail in the calcium signalling and agonist mediated endocytosis of GPR120

As discussed earlier (section 1.6.2.1), the carboxyl tail of many GPCRs is key for receptor phosphorylation, which in turn supports β-arrestin recruitment, desensitisation and internalisation. To investigate this for GPR120S, SNAP-GPR120S was modified to truncate the carboxyl tail following the leucine-346 residue (SNAP-GPR120S Δ346) and stably expressed in tet-inducible HEK293TR cells as before. The function of this mutant was then examined in calcium and internalisation assays in comparison to SNAP-120S cells. To enable comparison between the different cell lines, data for these assays were expressed as fold over basal, instead of being normalised to a reference compound.

Interestingly, the Δ346 truncation led to a significant increase in peak response amplitude of GPR120 calcium responses to agonists, and prolonged calcium responses (Figure 3.21 A). The response to 300 μM oleic acid at 30 s (measured using time course data) was significantly different $P < 0.01$ using a Student's t test (Figure 3.21 A; Table 3.10). The mutation also caused increases in agonist potency and maximum response from concentration response curves, but only the difference in myristic acid responses was significantly different, $P < 0.05$ using a Student's t test (Figure 3.21 B; Table 3.10; n = 5).

Conversely, in the internalisation assay, the same mutation led to a decrease in maximal internalisation for both time course and concentration response

curves, but surprisingly the mutation did not completely abolish agonist mediated endocytosis (representative images Figure 3.22). The SNAP-GPR120S Δ346 90 min time course maximum responses for both oleic acid and GW9508 were approximately 50 % of that for WT. This was not due to a difference in expression levels, which were not significantly different, as determined using a 2 tailed Student's t test (Figure 3.23 D; n = 4). The half time of agonist induced endocytosis in response to 300 µM oleic acid was 12 ± 1 min (compared to 15 ± 1 min for WT; Figure 3.23 A; n = 4) and to 100 µM GW9508 was 18 ± 3 min (in comparison to 12 ± 2 min for WT; Figure 3.23 B; n = 4), in each case not significantly different from WT (Student's t test). On the other hand, the response to GW9508 at 60 min was found to be significantly different between WT and GPR120S Δ346 $P < 0.05$ using a Student's t test. There was no significant difference in agonist pEC_{50} values between WT and SNAP-GPR120S Δ346 endocytosis responses (Table 3.10).

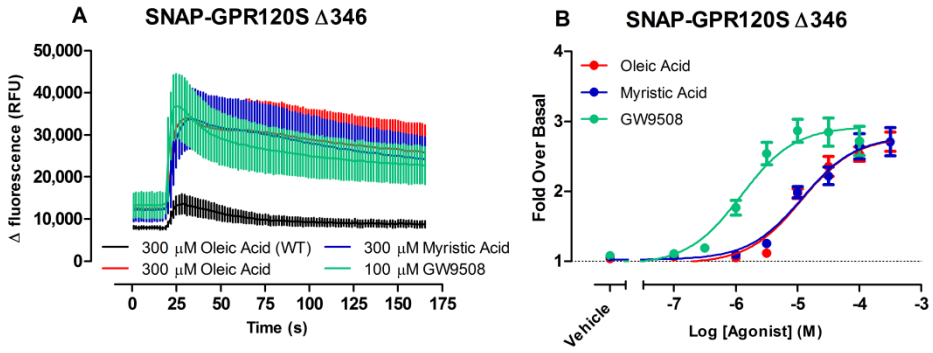

Figure 3.21 Calcium time courses and concentration responses of a mutant, SNAP-GPR120S Δ346.

Calcium time courses (A) and concentration responses (B) of SNAP-GPR120S Δ346. Data is normalised as fold over basal and is pooled from 5 individual experiments, mean ± S.E.M.

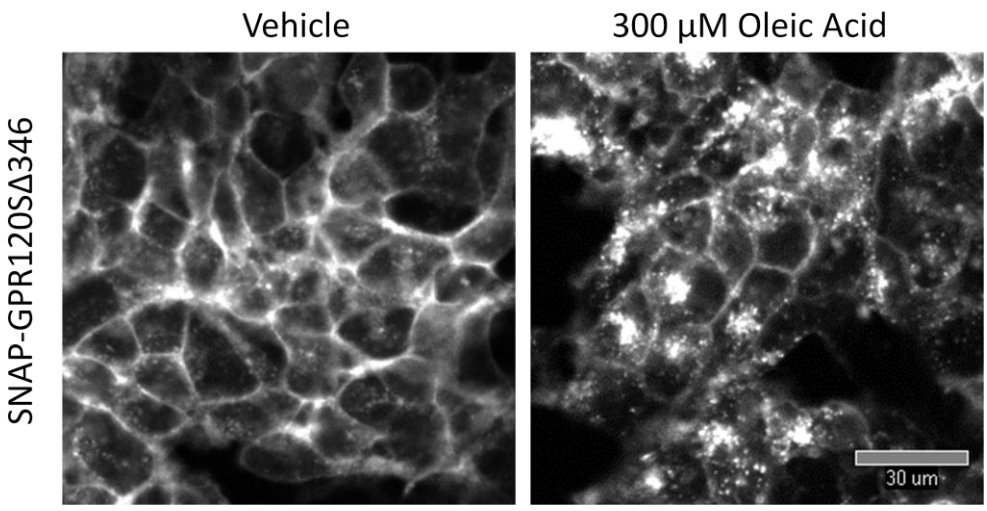

Figure 3.22 Representative images of SNAP-GPR120S Δ346 internalisation.

Images were acquired on the IX Ultra of HEK293TRs stably transfected with SNAP-GPR120S Δ346, following 30 min treatment with vehicle or 300 µM oleic acid. Scale bar = 30 µm. Refer back to Figure 3.15 for WT representative images.

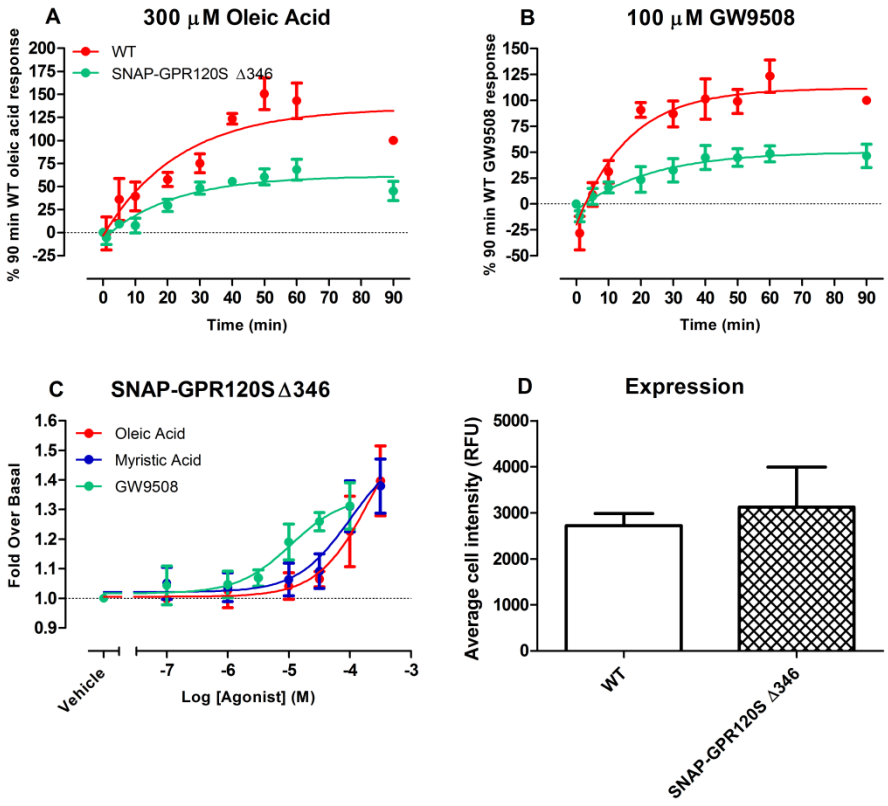

Figure 3.23 Agonist mediated endocytosis time courses and concentration responses of a truncation mutant, SNAP-GPR120S Δ346.

Internalisation time courses in response to 300 µM oleic acid (A) and 100 µM GW9508 (B), and concentration responses (C, measured at 60 min; dotted line representing WT response to oleic acid) of SNAP-GPR120S Δ346 in comparison to WT, with relative expression levels quantified (D). Data were normalised (% to 300 µM oleic acid in A, B; fold over basal in C) and pooled from 4 individual experiments, mean ± S.E.M.

	Calcium				Internalisation			
	SNAP-GPR120S		SNAP-GPR120S Δ346		SNAP-GPR120S		SNAP-GPR120S Δ346	
Agonist	pEC_{50}	R_{max} (fold over basal)	pEC_{50}	R_{max} (fold over basal)	pEC_{50}	R_{max} (fold over basal)	pEC_{50}	R_{max} (fold over basal)
Oleic Acid	4.6 ± 0.3	1.5 ± 0.2	4.9 ± 0.1	2.7 ± 0.1	4.0 ± 0.2	1.6 ± 0.1	3.7 ± 0.5	1.4 ± 0.1
Myristic Acid	4.3 ± 0.4	1.6 ± 0.2	4.9 ± 0.1*	2.7 ± 0.2*	4.3 ± 0.1	1.6 ± 0.1	4.0 ± 0.4	1.4 ± 0.1
GW9508	5.3 ± 0.3	1.9 ± 0.2	5.9 ± 0.2	2.7 ± 0.2	5.0 ± 0.1	1.6 ± 0.1	5.0 ± 0.3	1.3 ± 0.1

Table 3.10 Potency and maximal responses of SNAP-GPR120S Δ346.

pEC_{50} values and maximal responses of SNAP-GPR120S Δ346 in comparison to WT, for agonists as measured in the calcium mobilisation assay and the internalisation assay. Data were normalised as fold over basal and pooled from 4 – 5 individual experiments, mean ± S.E.M. Statistical significance determined using a Student's t test, * $P < 0.05$.

3.2.7 Potential effects of GPR120 receptor homo- and hetero-dimerisation

To investigate the potential altered pharmacology of GPR120 homo- and hetero-dimers, constrained "BiFC dimer" receptor cell lines were created. To enable this, firstly a SNAP-GPR120S-vYNL cell line was dilution cloned, and characterised in its ability to elicit calcium and internalisation responses. SNAP-GPR120S-vYNL elicited responses similar to those exhibited by SNAP-GPR120S (Figure 3.25; Table 3.11, 3.12).

The SNAP-GPR120S-vYNL cell line was then stably cotransfected with FLAG tagged GPR120S-vYC, GPR120L-vYC or FFA1-vYC. By additionally labelling the SNAP-tag with SNAP-surface BG-647 this enabled two populations to be measured at the same time in the internalisation assay: all SNAP-labelled GPR120SvYNL receptors, and the specific dimer (120S:120S, 120S: 120L or 120S:FFA1) identified by recomplemented vYFP (representative images in Figure 3.24; Table 3.12, 3.13). The calcium responses were also measured to assess whether there were any changes resulting from co-expression of the two receptors at a "population" level.

The 120S:120S cell line showed no significant difference between internalisation of the overall SNAP-labelled SNAP-GPR120S-vYNL population and the SNAP-GPR120S-vYNL:GPR120S-vYC BiFC dimer, either when measuring the time course of internalisation (Figure 3.26 A, B); or comparing concentration response curves to oleic acid or GW9508 (Representative images Figure 3.24; Figure 3.26; Table 3.12, 3.13).

Next the 120S:120L dimer was characterised (representative images Figure 3.24 B). Even though GPR120L by itself did not elicit calcium mobilisation, the co-expression of GPR120L-vYC and GPR120-SvYNL in the 120S:120L cell line did not alter agonist-stimulated calcium mobilisation significantly (Figure 3.27 A; Table 3.11).

Once again, there was no difference in internalisation between the SNAP-labelled SNAP-GPR120S-vYNL population and recomplemented vYFP "dimer" population (SNAP-GPR120S-vYNL:GPR120L-vYC) (Figure 3.27; (Figure 3.28; Table 3.12, 3.13; n = 4 - 5).

Finally, the 120S:FFA1 dimer was characterised (representative images Figure 3.24 C; Figure 3.28; Figure 3.29; Table 3.11, 3.12, 3.13). As might be expected from earlier calcium data (Figure 3.6), the additional expression of FFA1 in the cell line affected calcium signalling. The calcium data set for GW9508 fitted to a 2 site model better than a 1 site model, perhaps indicating separate FFA1 component and GPR120S components to the response. This 2 site model gave two pEC_{50} values, with 70 % of the population fitting to an pEC_{50} value of 5.5 ± 0.7, whilst the other 30 % gave an pEC_{50} value of 7.1 ± 0.7 (Figure 3.28 B), of which these responses were notably more potent than in either the FFA1 or GPR120S single population cells.

Interestingly, there was a left shift of the GW9508 internalisation response curve for the BiFC dimer SNAP-GPR120S-vYNL:FLAG-FFA1-vYC compared to SNAP labelled SNAP-GPR120S-vYNL, but this was not deemed significantly different by 2 way ANOVA (Figure 3.29 F; Table 3.12; n = 4 - 6).

120S:120S

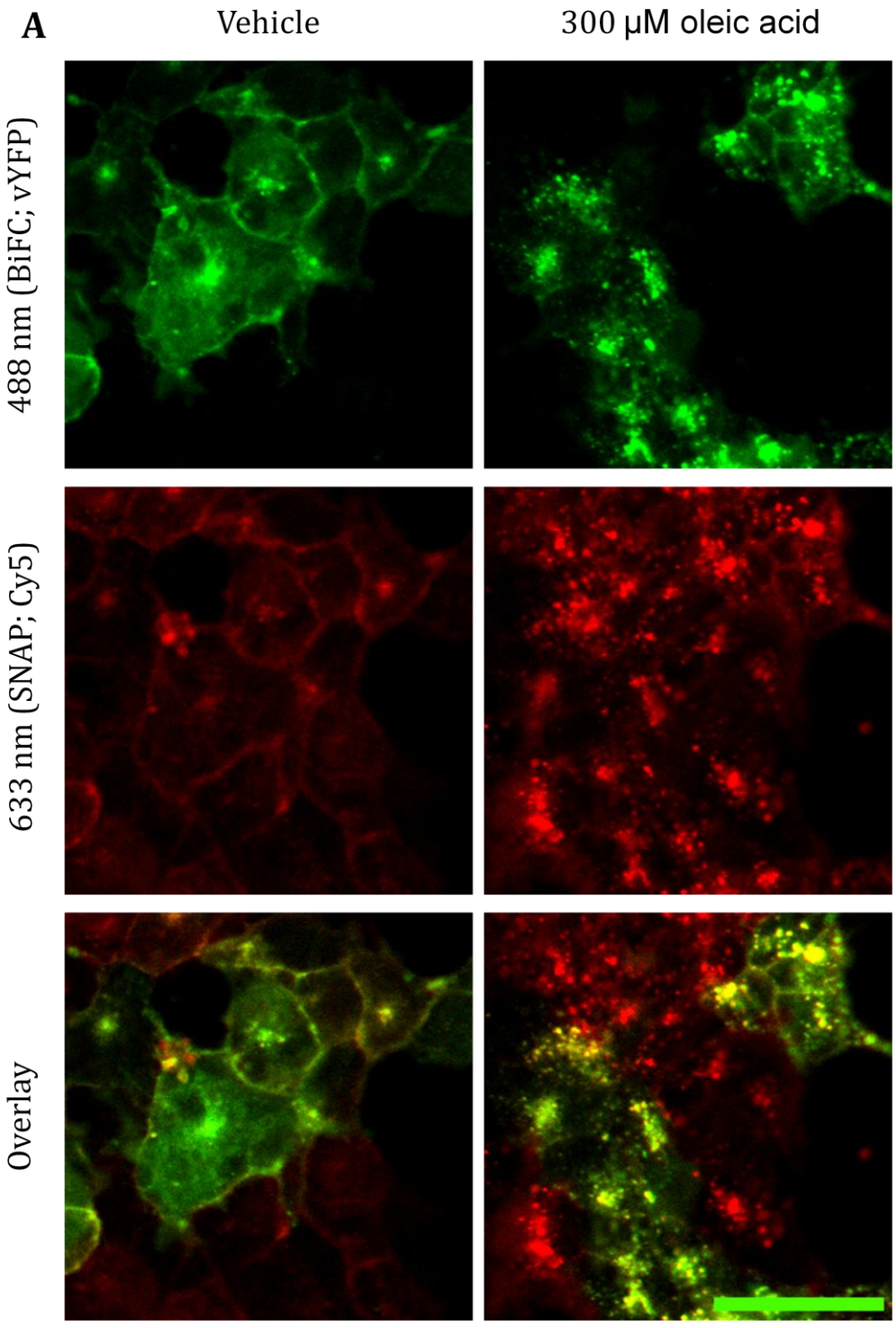
A
Vehicle
300 µM oleic acid
488 nm (BiFC; vYFP)
633 nm (SNAP; Cy5)
Overlay

120S:120L

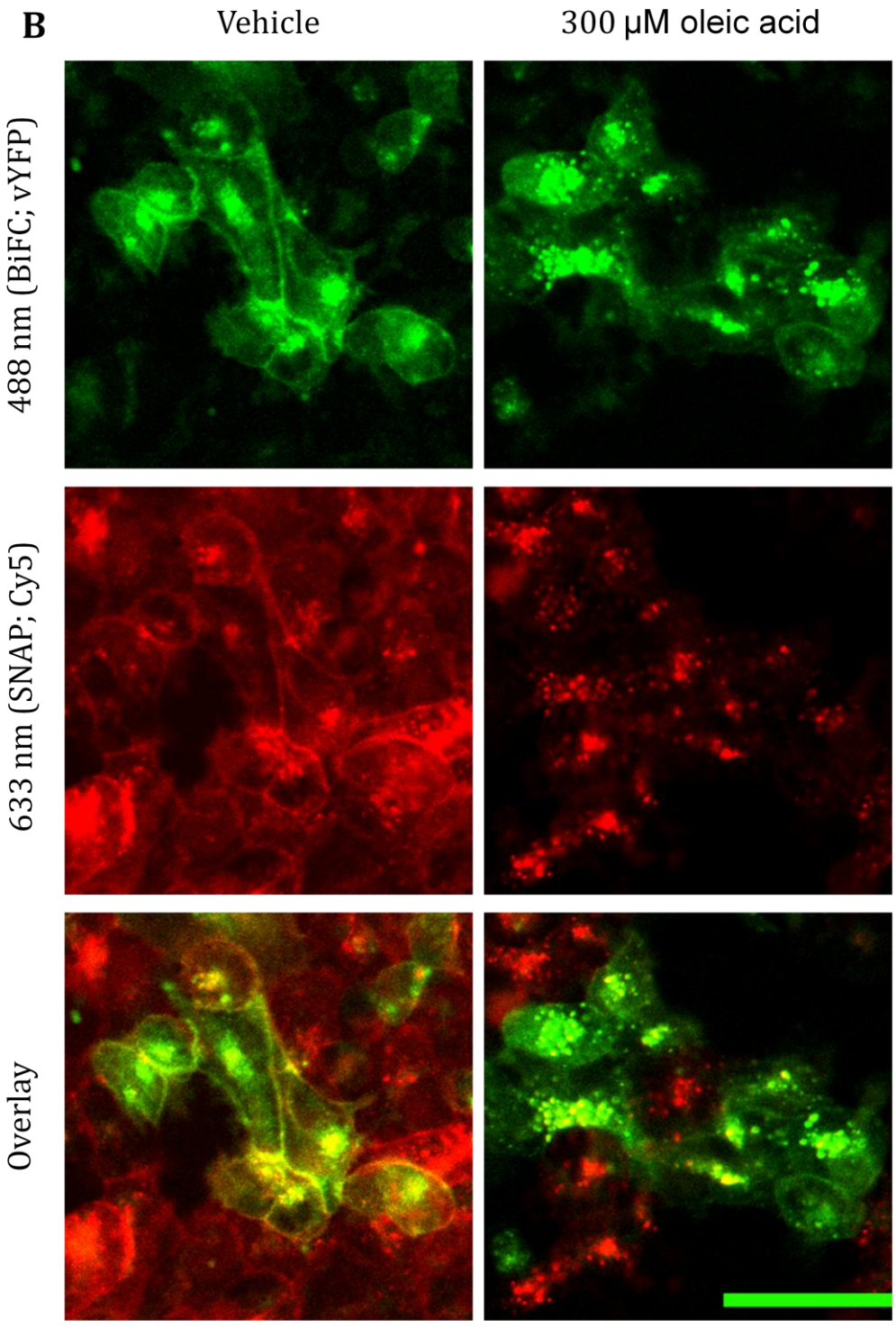
B
Vehicle
300 µM oleic acid
488 nm (BiFC; vYFP)
633 nm (SNAP; Cy5)
Overlay

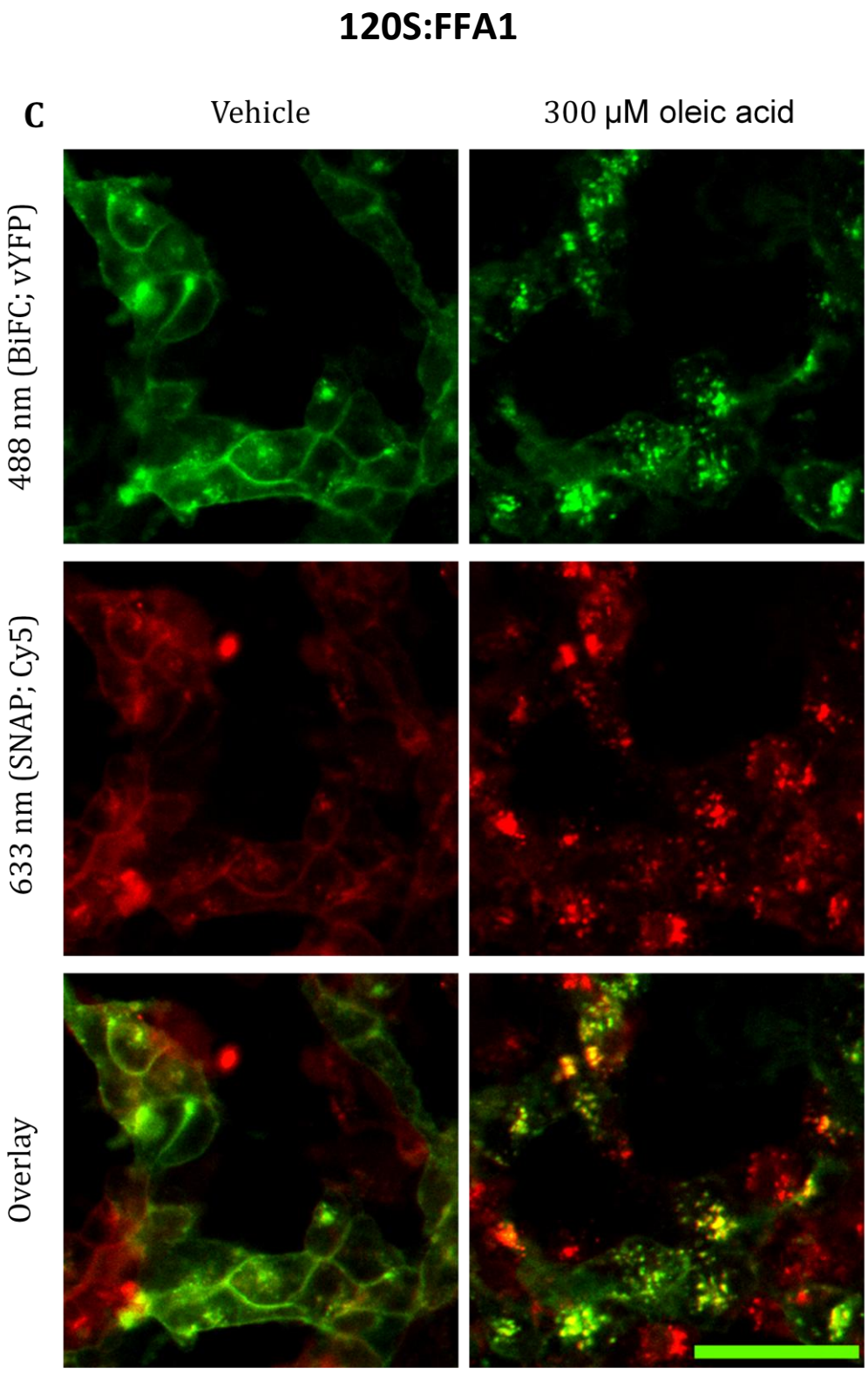
120S:FFA1
C
Vehicle
300 µM oleic acid
488 nm (BiFC; vYFP)
633 nm (SNAP; Cy5)
Overlay

Figure 3.24 Representative images of bimolecular fluorescence complementation between SNAP-GPR120S-vYNL:FLAG-GPR120S-vYC, SNAP-GPR120S-vYNL:FLAG-GPR120L-vYC and SNAP-GPR120S-vYNL:FLAG-FFA1-vYC.

Images were acquired on the IX Ultra of HEK293TRs stably transfected with SNAP-GPR120S-vYNL:FLAG-GPR120S-vYC (A), SNAP-GPR120S-vYNL:FLAG-GPR120L-vYC (B) and SNAP-GPR120S-vYNL:FLAG-FFA1-vYC (C) following 30 minute treatment with vehicle (left panels) or 300 µM oleic acid (right panels). Images show recomplemented vYFP identifying the BiFC dimer (top panels), SNAP-surface BG-647 labelled SNAP-GPR120S-vYNL receptors (middle panels) and the overlay of both images (bottom panels) Scale bar = 50 µm.

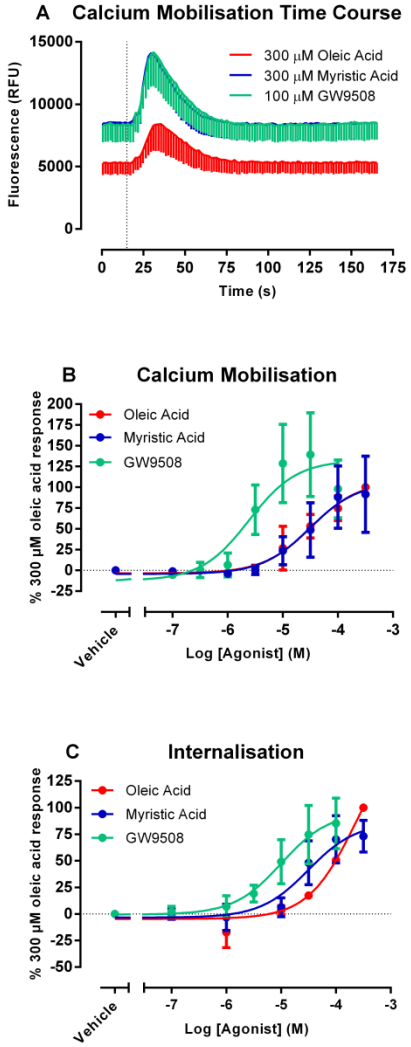

Figure 3.25 Characterisation of SNAP-GPR120S-vYNL receptors expressed in HEK293T cells.

The clonal HEK293T SNAP-GPR120S-vYNL cell line was tested for its ability to elicit calcium mobilisation, shown as time courses (A; dotted line showing time of agonist addition), and concentration response curves (B), and internalisation (B) in response to agonist. Data were normalised (%) to 300 µM oleic acid responses and pooled from 3 - 5 individual experiments, mean ± S.E.M.

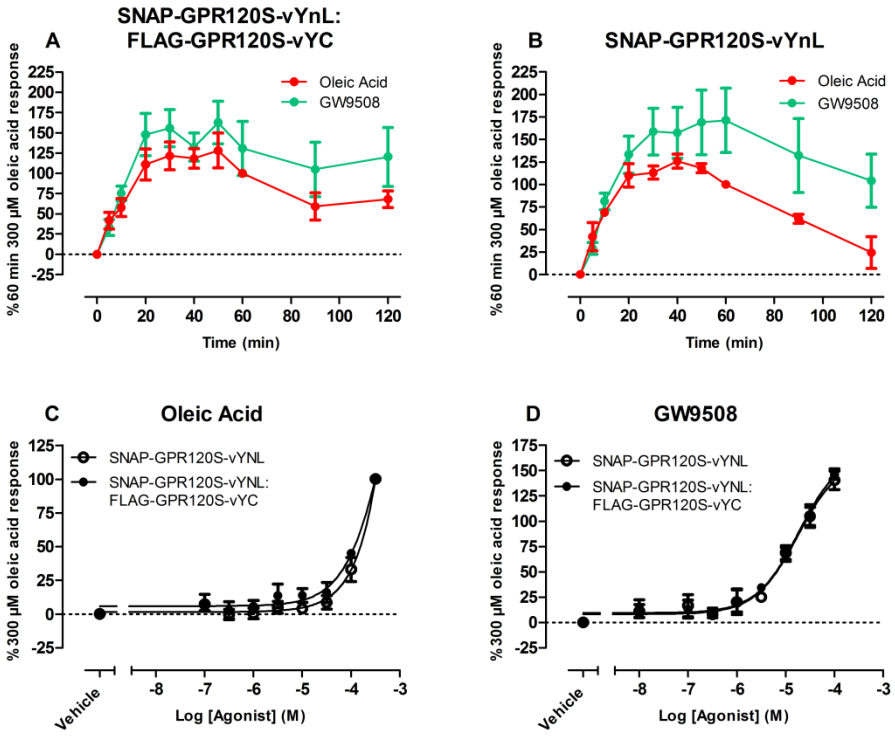

Figure 3.26 Internalisation of SNAP-GPR120S-vYNL:FLAG-GPR120S-vYC BiFC dimers in response to agonists, compared to the SNAP-GPR120SvYNL population.

The dual-transfected cell line SNAP-GPR120S-vYNL:FLAG-GPR120S-vYC was tested for its agonist-stimulated internalisation responses. Time courses of the SNAP-GPR120S-vYNL:FLAG-GPR120S-vYC population (measured by granularity analysis of the BiFC receptor images) (A) and the SNAP-surface BG-647 labelled SNAP-GPR120S-vYNL population (B) responses to 300 µM oleic acid and 100 µM GW9508; and concentration responses of the SNAP-GPR120S-vYNL:FLAG-GPR120S-vYC population and SNAP-surface BG-647 labelled SNAP-GPR120S-vYNL population to oleic acid (C) and GW9508 (D), were measured using the bimolecular fluorescence complementation assay. Data were normalised (%) to the 300 µM oleic acid response and pooled from 3 – 5 individual experiments, mean ± S.E.M.

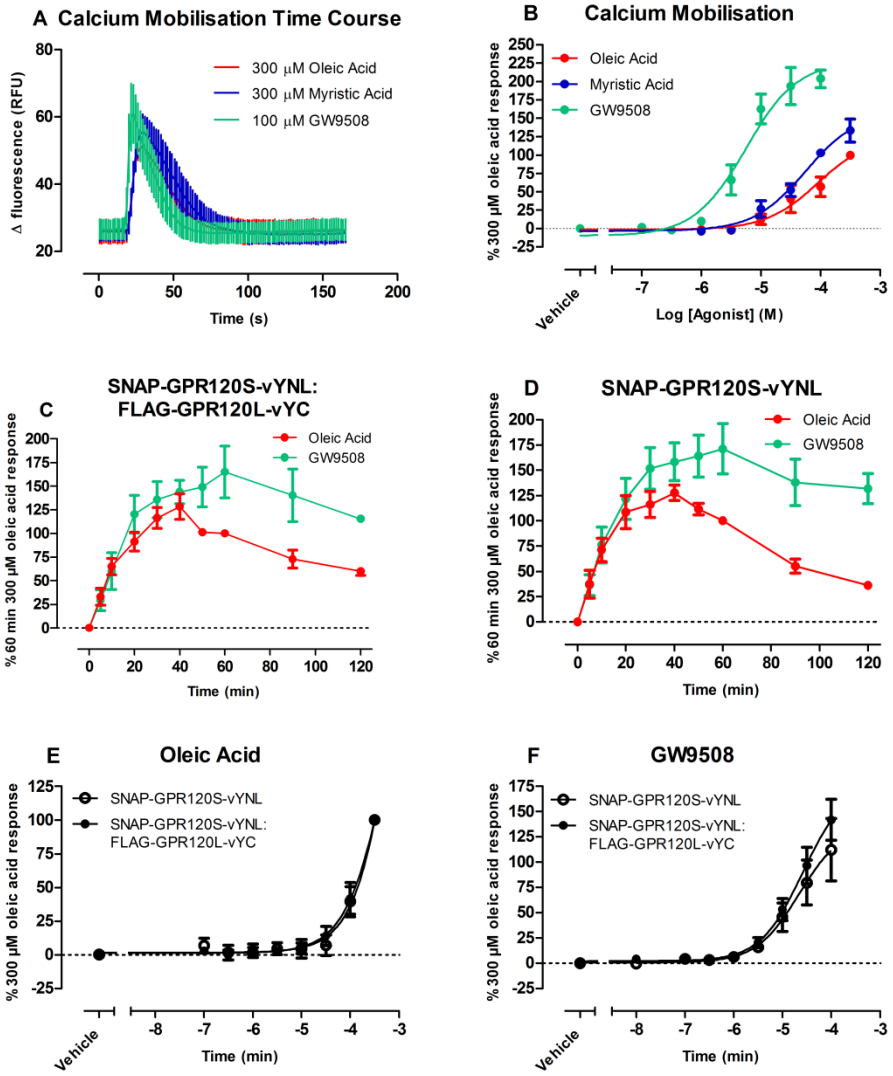
A Calcium Mobilisation Time Course
Δ fluorescence (RFU)
Time (s)
300 μM Oleic Acid
300 μM Myristic Acid
100 μM GW9508
B Calcium Mobilisation
% 300 μM oleic acid response
Log [Agonist] (M)
Vehicle
Oleic Acid
Myristic Acid
GW9508
C
SNAP-GPR120S-vYNL:
FLAG-GPR120L-vYC
% 60 min 300 μM oleic acid response
Time (min)
Oleic Acid
GW9508
D
SNAP-GPR120S-vYNL
% 60 min 300 μM oleic acid response
Time (min)
Oleic Acid
GW9508
E
Oleic Acid
% 300 μM oleic acid response
Time (min)
SNAP-GPR120S-vYNL
SNAP-GPR120S-vYNL:
FLAG-GPR120L-vYC
Vehicle
F
GW9508
% 300 μM oleic acid response
Time (min)
SNAP-GPR120S-vYNL
SNAP-GPR120S-vYNL:
FLAG-GPR120L-vYC
Vehicle

Figure 3.27 Calcium, and internalisation responses in the SNAP-GPR120S-vYNL:FLAG-GPR120L-vYC cell line in response to agonists.

The dual transfected cell line SNAP-GPR120S-vYNL:FLAG-GPR120L-vYC was tested for its calcium and internalisation responses. The calcium mobilisation time course (A) and concentration response curves (B) to oleic acid, myristic acid and GW9508 were measured using the calcium mobilisation assay. Internalisation time courses of the SNAP-GPR120S-vYNL:FLAG-GPR120L-vYC population (C) and the SNAP-surface BG-647 labelled SNAP-GPR120S-vYNL sub-population (D) responses to 300 µM oleic acid and 100 µM GW9508; and concentration responses of the SNAP-GPR120S-vYNL:FLAG-GPR120L-vYC population and SNAP-surface BG-647 labelled SNAP-GPR120S-vYNL sub-population to oleic acid (E) and GW9508 (F), were measured using the internalisation assay. Data were normalised (%) to the 300 µM oleic acid response and pooled from 4 – 5 individual experiments, mean ± S.E.M.

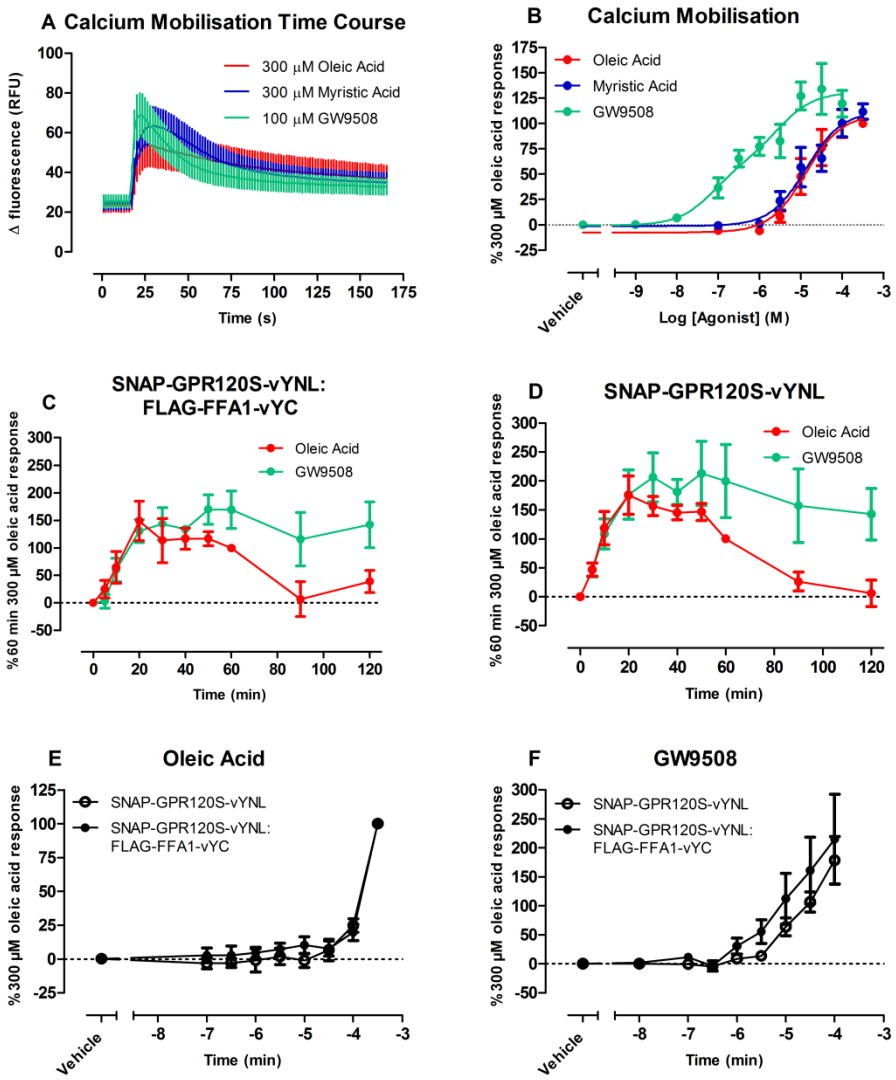
A Calcium Mobilisation Time Course
300 μM Oleic Acid
300 μM Myristic Acid
100 μM GW9508
Δ fluorescence (RFU)
Time (s)
B
Calcium Mobilisation
Oleic Acid
Myristic Acid
GW9508
% 300 μM oleic acid response
Vehicle
Log [Agonist] (M)
C
SNAP-GPR120S-vYNL:
FLAG-FFA1-vYC
Oleic Acid
GW9508
%60 min 300 μM oleic acid response
Time (min)
D
SNAP-GPR120S-vYNL
Oleic Acid
GW9508
%60 min 300 μM oleic acid response
Time (min)
E
Oleic Acid
SNAP-GPR120S-vYNL
SNAP-GPR120S-vYNL:
FLAG-FFA1-vYC
%300 μM oleic acid response
Vehicle
Time (min)
F
GW9508
SNAP-GPR120S-vYNL
SNAP-GPR120S-vYNL:
FLAG-FFA1-vYC
%300 μM oleic acid response
Vehicle
Time (min)

Figure 3.28 Calcium, and internalisation measurements of SNAP-GPR120S-vYNL:FLAG-FFA1-vYC in response to agonists.

The dual transfected cell line SNAP-GPR120S-vYnL:FLAG-FFA1-vYC was tested for its calcium and internalisation responses. The calcium mobilisation time course (A) and concentration responses (B) to oleic acid, myristic acid and GW9508 were measured using the calcium mobilisation assay. Internalisation time courses of the SNAP-GPR120S-vYNL:FLAG-FFA1-vYC BiFC dimer population (C) and the SNAP-surface BG-647 labelled SNAP-GPR120S-vYNL sub-population (D) responses to 300 µM oleic acid and 100 µM GW9508; and concentration responses of the SNAP-GPR120S-vYNL:FLAG-FFA1-vYC population and SNAP-surface BG-647 labelled SNAP-GPR120S-vYNL sub-population to oleic acid (E) and GW9508 (F), were measured using the internalisation assay. Data were normalised (%) to the 300 µM oleic acid response and pooled from 4 – 6 individual experiments, mean ± S.E.M.

	Calcium					
	GPR120S-vYNL		120S:120L		120S:FFA1	
Agonist	pEC_{50}	R_{max} (%)	pEC_{50}	R_{max} (%)	pEC_{50}	R_{max} (%)
Oleic Acid	4.5 ± 0.1	100	4.1 ± 0.2	100	4.9 ± 0.2	100
Myristic Acid	4.5 ± 0.2	92 ± 21	4.3 ± 0.1	133 ± 16	4.9 ± 0.2	112 ± 8
GW9508	5.6 ± 0.2	98 ± 16	5.3 ± 0.1	204 ± 12	HI 7.1 ± 0.7 (30%) LO 5.5 ± 0.7 (70%)	120 ± 13

Table 3.11 Potency and maximal calcium responses in SNAP-GPR120S-vYNL, SNAP-GPR120S-vYNL:GPR120L-vYC and SNAP-GPR120S-vYNL:FFA1-vYC cell lines.

pEC_{50} values and maximal responses in SNAP-GPR120S-vYNL cells and the dually transfected cell lines SNAP-GPR120S-vYNL:GPR120L-vYC (120S:120L) and SNAP-GPR120S-vYNL:FFA1-vYC (120S:FFA1) to agonist in the calcium mobilisation assay. Data were normalised (%) to the 300 µM oleic acid response and pooled from 3 – 6 individual experiments, mean ± S.E.M.

i Internalisation

GPR120S-vYNL

Agonist	pEC_{50}	R_{max} (%)
Oleic Acid	N.D.	100
Myristic Acid	4.5±0.3	73±15
GW9508	5.0±0.3	85±24

ii SNAP-labelled population

	120S:120S		120S:120L		120S:FFA1	
Agonist	pEC_{50}	R_{max} (%)	pEC_{50}	R_{max} (%)	pEC_{50}	R_{max} (%)
Oleic Acid	N.D.	100	N.D.	100	N.D.	100
GW9508	4.8 ± 0.1	140 ± 9	4.7 ± 0.2	112 ± 31	4.5 ± 0.2	179 ± 41

iii Recomplemented YFP population

	120S:120S		120S:120L		120S:FFA1	
Agonist	pEC_{50}	R_{max} (%)	pEC_{50}	R_{max} (%)	pEC_{50}	R_{max} (%)
Oleic Acid	N.D.	100	N.D.	100	N.D.	100
GW9508	4.7 ± 0.1	147 ± 5	4.6 ± 0.2	142 ± 20	4.9 ± 0.3	214 ± 78

Table 3.12 Potency and maximal responses of SNAP-GPR120S-vYNL, SNAP-GPR120S-vYNL:GPR120S-vYC , SNAP-GPR120S-vYNL:GPR120L-vYC and SNAP-GPR120S-vYNL:FFA1-vYC in response to agonists.

pEC_{50} values and maximal responses of SNAP-GPR120S-vYNL (i) and the dual transfected cell lines SNAP-GPR120S-vYNL:GPR120S-vYC (120S:120S), SNAP-GPR120S-vYNL:GPR120L-vYC (120S:120L) and SNAP-GPR120S-vYNL:FFA1-vYC (120S:FFA1) in response to agonists in the internalisation assay, with measurements taken of the SNAP-labelled population (ii) and the recomplemented YFP dimer population (iii). Oleic acid R_{max} values were determined from the maximal response at 300 µM. Data were normalised (%) to 300 µM oleic acid and pooled from 3 – 6 individual experiments, mean ± S.E.M; N.D. not determined.

	SNAP-labelled population			Recomplemented YFP population		
	120S:120S	120S:120L	120S:FFA1	120S:120S	120S:120L	120S:FFA1
Agonist	$T_{1/2}$ (min)	$T_{1/2}$ (min)	$T_{1/2}$ (min)	$T_{1/2}$ (min)	$T_{1/2}$ (min)	$T_{1/2}$ (min)
Oleic Acid	4 ± 1	5 ± 1	4 ± 1	6 ± 1	5 ± 1	8 ± 2
GW9508	8 ± 1	8 ± 1	7 ± 2	7 ± 1	8 ± 1	11 ± 4

Table 3.13 Time courses for internalisation responses in SNAP-GPR120S-vYNL:GPR120S-vYC, SNAP-GPR120S-vYNL:GPR120L-vYC and SNAP-GPR120S-vYNL:FFA1-vYC cell lines.

Internalisation time course responses of the SNAP-labelled population and the recomplemented YFP population of the dually transfected cell lines SNAP-GPR120S-vYNL:GPR120S-vYC (120S:120S), SNAP-GPR120S-vYNL:GPR120L-vYC (120S:120L) and SNAP-GPR120S-vYNL:FFA1-vYC (120S:FFA1) to agonists in the internalisation assay. Time courses appeared biphasic in nature, therefore to better fit the data to obtain half times of internalisation, curves were fitted to the first 60 minutes of the time course only. Data were pooled from 3 – 6 individual experiments, mean ± S.E.M.

3.3 Discussion

3.3.1 Summary of main findings

This study was undertaken to compare the GPR120 isoforms in terms of their signalling and trafficking, and to also investigate whether GPR120S receptor homo- and hetero-dimers had altered pharmacology.

Firstly, it was found in the calcium signalling assay that GPR120S signals in response to agonist, whilst GPR120L does not. Also, it was found that FFA1 gave absolute calcium responses that were twice the magnitude of those at GPR120S. These responses at FFA1 were inhibited by the antagonist GW1100, and by the binding site mutation R258A. The picture of GPR120S signalling and GPR120L not signalling via G proteins was reiterated in the results from the DMR assay, in which GPR120S gave monophasic responses to ligands (which could be partially inhibited using 2-APB but not PTx), whilst GPR120L did not give responses. These differences were not down to a difference in cell surface expression.

Conversely, both GPR120 isoforms were found to interact with β-arrestin2 in the BiFC assay, and also gave responses in the internalisation assay. Further to this, when the fate of the internalised receptors was determined both qualitatively and quantitatively, both receptor isoforms were found to colocalise with the marker for the degradation pathway, lysotracker red; and the receptors did not undergo recycling back to the cell surface.

These results demonstrated that, in the cell systems studied, only GPR120S is capable of G protein mediated signalling, whilst both isoforms are capable of β-arrestin2 mediated endocytosis. The carboxyl tail of GPR120S was also identified to mediate GPR120S desensitisation. Additionally, it was found by creating constrained "BiFC" homo- and hetero-dimers that dimerisation did not alter pharmacology.

3.3.2 Conclusions of studies into G protein dependent signalling

In the same host cell system (tetracycline inducible HEK293 cells), FFA1 gave absolute calcium responses that were twice the magnitude of those observed at GPR120S, whilst GPR120L did elicit calcium responses. FFA1 is known to couple predominantly to Gq/11 (Itoh et al., 2003) and weakly to Gi (Schroder et al., 2010).

These results back up previous findings in the literature of GPR120 coupling to calcium mobilisation (Hirasawa et al., 2005). Also, GPR120L was only capable of calcium signalling when expressed as a fusion protein with Gα16 (Hirasawa et al., 2005). This suggests that co-expression with an over-expressed G protein is required for GPR120L to elicit calcium responses. The only difference between the isoforms is the insertion in ICL3 (Figure 1.2), which might be the cause of steric hindrance for G protein coupling, as discussed later.

3.3.2.1 The effect of 2-APB in the calcium assay

2-APB inhibited, but did not completely abolish GPR120S calcium signalling. Calcium signalling by GPCRs is usually mediated as follows: receptor activation

leads to activation of the cognate G protein, which for calcium signalling is the Gq alpha subunit or Gβγ subunits released from Gi. The G protein activates PLC, which generates soluble IP_3 that in turn then binds to IP_3 receptors present on the endoplasmic reticulum leading to release of calcium from the intracellular stores (Charlton and Vauquelin, 2010). 2-APB, an inhibitor of calcium signalling, was originally thought to prevent calcium mobilisation through the blockade of the IP_3 receptors present on the endoplasmic reticulum (Maruyama et al., 1997); but a later study suggests it is not a consistent blocker of IP_3 receptors (Bootman et al., 2002; Gregory et al., 2001).

In fact, later research has suggested that 2-APB prevents store operated calcium entry (SOCE). SOCE occurs when a protein, ORAI1 which is part of the plasma membrane calcium channel complex, associates with STIM1 (stromal interacting molecule; acting as an endoplasmic reticulum sensor for calcium depletion from this store), resulting in calcium entry from the extracellular medium to restore intracellular calcium store levels (DeHaven et al., 2008). 2-APB blocks SOCE by preventing the migration and formation of STIM1 puncta at the plasma membrane. It was found that 2-APB did not fully block this process, which is perhaps why this compound did not completely abolish calcium signalling when tested on GPR120S responses (DeHaven et al., 2008). The concentration of 2-APB used could be increased, but only up to 200 µM, because above this 2-APB has been found to actually cause an increase in calcium concentration (Maruyama et al., 1997).

3.3.2.2 The effects of PTx in the calcium assay

The calcium responses at GPR120S were largely PTx insensitive, indicating that GPR120S coupled to the Gq/11 class of calcium signalling G proteins, as PTx only inhibits the Gi class of G proteins. The results do not exclude the possibility that GPR120 can couple to multiple G proteins, with Gq activation compensating for the inhibited Gi, therefore allowing calcium signalling to still occur. This occurs with FFA1, which has been shown to couple to Gq (Briscoe et al., 2003), and Gi (Schroder et al., 2010). The absence of G protein response with GPR120L suggests it does not couple to the G protein complement present in HEK cells, but it is also possible that GPR120S and GPR120L couple to other G proteins that exist in the sites of endogenous GPR120 expression, for example gustducin which is present in the taste cells, which will be discussed later (Section 3.4). In the same family of fatty acid receptors, PTx was also used in calcium, cAMP and ERK1/2 accumulation assays to determine that both FFA2 and FFA3 also coupled to the PTx sensitive Gi, with FFA2 additionally coupling to Gq (Le Poul et al., 2003).

3.3.2.3 Results of the DMR assay

Another assay was also used to monitor G protein mediated signalling. DMR measures the “holistic” whole cell response, which is more indicative of the receptor’s whole repertoire of G protein dependent signalling, rather than measuring one end point, which can be very close to the G protein (such as a GTPγS assay). Another advantage to DMR, is that it has been previously reported to show a signature response depending on which G protein is

involved (Schroder et al 2010). GPR120S gave large positive monophasic responses, which did not match exactly to one profile (could be consistent with Gq/11, Gi or G12/13 responses previously reported; Figure 2.9), which lead to the thought that perhaps there is multiple G protein involvement. This was the rationale for then using the inhibitors 2-APB and PTx to dissect the responses, but these inhibitors had no significant effect. This may be due to the assay being highly sensitive, detecting low levels of receptor activation due to signal amplification. Additionally, this high sensitivity means perhaps the partial inhibition may have subtly changed the functional outcome. It is also possible that GPR120S couples to more than one G protein subtype, giving rise to a unique profile; when one pathway is inhibited (e.g. Gi by PTx), the other one (e.g. Gq/11 dependent) can compensate without significantly altering the signature.

Most importantly though, the DMR assay confirmed the calcium results, in that the GPR120L isoform does not appear to elicit G protein mediated signalling in HEK293 host cells.

3.3.3 Pharmacology

The potency of agonist GW9508 was equivalent to previously published data for equivalent calcium mobilisation assays, at both FFA1 (pEC_{50} 7.1 compared to 7.3 in Briscoe et al., 2006)) and GPR120S (5.3 ± compared to 5.5 (Briscoe et al., 2006)). Similarly the pA_2 for the antagonist GW1100 at FFA1 receptors (6.0) was also similar to both its pK_B calculated using the Gaddum equation (6.6), and its published equilibrium dissociation constant 1 μM (Briscoe et al.,

2006). However Schild analysis gave a steep slope value of 2.7 ± 0.1, compared to a slope of 1 expected for a competitive reversible antagonist. This may indicate a lack of equilibrium between agonist and antagonist binding. The kinetic nature of the assay, in which peak calcium responses are measured rapidly after the agonist is added, allows very little time for equilibrium between agonist and antagonist binding to occur (Charlton and Vauquelin, 2010). In agreement with the previous study, GW1100 had no effect at GPR120 (data not shown).

FFA1 has previously been shown to respond to thiazolidinediones with an order of potency of rosiglitazone > ciglitazone = troglitazone > pioglitazone (Smith et al., 2009). The fact that GPR120S also responds to thiazolidinediones was a novel finding. The order of potency at GPR120S (as far as it could be determined) was troglitazone > ciglitazone = rosiglitazone. Pioglitazone was inactive, providing supporting evidence that these responses are indeed elicited by GPR120S rather than PPARγ. The order of potency at PPARγ is rosiglitazone > troglitazone = pioglitazone, completely different to the results found at GPR120S (Sakamoto et al., 2000). As with FFA esters, such as methyl linoleate, previously found to be inactive at GPR120 (data not shown; Hirasawa et al., 2005), thiazolidinediones also lack free carboxylate groups. However a study on their mode of action at FFA1 suggested that the 2,4-dione group on thiazolidinediones acts in a similar way to the carboxyl group (Smith et al., 2009). Additionally, pioglitazone did not elicit responses at GPR120, and a reason for this can be seen in their structures because pioglitazone, in

comparison to the active rosiglitazone contains an extra ethyl group which may occlude binding (Figure 3.29). It should be noted that the potency of all

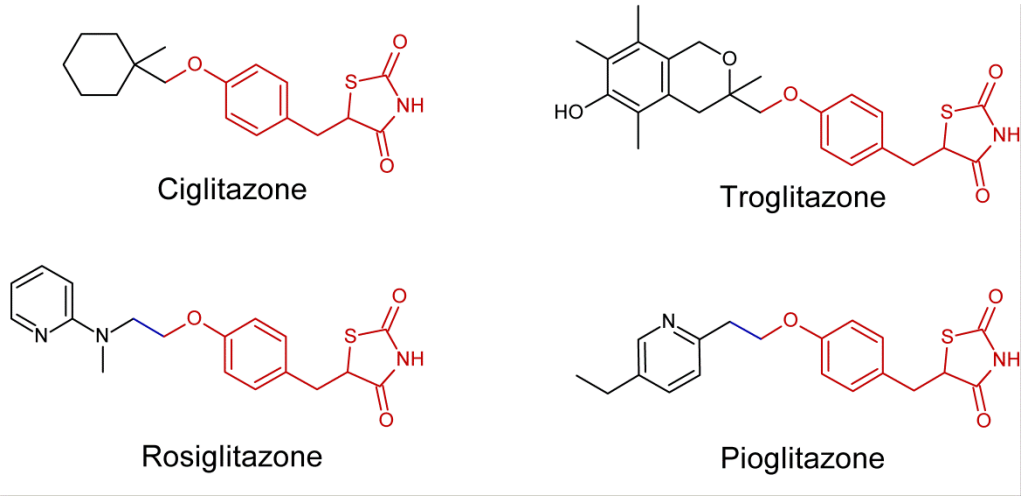

Figure 3.29 The structures of TZDs.
The TZD pharmacophore is shown in red, with structural differences shown in black.

thiazolidinediones in activating GPR120 was relatively low (10 μM and above), compared to their known mechanisms of action as PPARγ.

The use of BSA in the fatty acid preparations aided their solubility in HBSS, but also reduced "free" fatty acid concentration, as albumin contains several fatty acid binding sites (Krenzel et al., 2013). This effect was previously shown in the Hirasawa *et al* (2005) study, where the inclusion of 0.1 % BSA was clearly demonstrated to restrict α-linolenic acid mediated endocytosis of GPR120 (Hirasawa et al., 2005). This effect was also seen when treating FFA1 with lauric acid in the presence of increasing concentrations of BSA and monitoring calcium responses (Stoddart et al., 2007). Also, in one study on the creation of novel FFA1 agonists and their optimisation, it was found that some substituents were favourable for FFA1 receptor binding, i.e. they increased agonist activity, but not for binding BSA, i.e. they reduced the inhibitory shift in potency in the presence of serum (Sasaki et al., 2011). This knowledge led to the optimisation of BSA concentrations (0.1 vs. 0.02 % BSA) and 0.02 % BSA (~3 μM) was selected as optimal. This concentration led to the observation of 3-10 fold reductions in FFA potency compared to previous work (Briscoe et al., 2006; Hirasawa et al., 2005), but also minimised the amount of vehicle (e.g. DMSO) required to solubilise the FFAs at maximum response concentrations.

3.3.4 Novel findings regarding GPR120 arrestin recruitment and internalisation

There were advantages and disadvantages to using the novel technique of BiFC to identify the association between GPR120 and β-arrestin2. Firstly, the

subcellular localisation of these components increased the specificity of the experiment. This is because the receptor was localised at the plasma membrane, whilst β-arrestin2 was in a diffuse pattern in the cytosol (Bychkov et al., 2012), thus remain separated until agonist had been added. It also used live cells at the physiologically relevant temperature and gave quantitative pharmacological data for comparison of potency values obtained in the internalisation assay. A disadvantage to this system was that the YFP maturation step is slow, so measurements are not real time, and also the formation of the BiFC complex is irreversible, so all interactions were caught with no indication whether the interaction was a transient or more long lasting one (Kilpatrick et al., 2010; Rose et al., 2010).

The first interesting finding here was that GPR120S more readily interacted with β-arrestin2 than FFA1. Also, in contrast to the results from studying G protein mediated responses, agonist stimulated GPR120L also interacted with β-arrestin2 in an equivalent manner to GPR120S. This suggests that the DMR assay does not appear to pick up GPCR:β-arrestin interactions, consistent with findings in Schroder et al., (2010). Following on from the β-arrestin assay, agonist induced endocytosis was then measured. This gave the similar results to β-arrestin BiFC, that both GPR120 isoforms underwent internalisation in contrast to the assays that measured G protein mediated responses, and also in contrast to the fact that FFA1 did not undergo agonist induced endocytosis to such a clear extent as GPR120.

These internalisation assays used the SNAP-tag to visualise GPR120 and FFA1 receptors, having verified that when compared to the FLAG-tagged receptors, there was no functional impact upon calcium signalling. A key advantage of the SNAP-tag modification is that it allows the receptor to be labelled with any wavelength SNAP-surface label and can be used on live cells (Keppler et al., 2003). Both membrane permeant and impermeant labels are available, and an advantage of using the impermeant label (SNAP-surface) is that it only labels cell surface expressed receptors capable of undergoing agonist stimulated internalisation. The reaction which attaches the label to the receptor is specific, rapid and irreversible, and the label is fairly photostable. Another advantage of the SNAP-tag system over other visualisation methods like GFP, is that the SNAP-tag modification is on the amino terminus, compared to the carboxyl tail for GFP, and so it avoids potential effects on phosphorylation sites on the carboxyl tail, or on interactions with other intracellular effector proteins. Disadvantages of the SNAP-tag are that it still requires genetic modification of the receptor, and the large (~20kDa) modification is on the amino terminus, which could potentially affect ligand binding. However, here the SNAP-tagged receptor was as equally functional as the FLAG-tagged receptor.

The BiFC and internalisation assay potency values are slightly right shifted relative to calcium and DMR assays. This could be because of the varying degrees of receptor reserve in each assay, for example a lower receptor reserve (expected in receptor internalisation or direct receptor:β-arrestin interaction assays) results in agonists being less potent, with EC_{50} values closer

to the 50 % occupancy level for the receptor Kd. In contrast assays that measure downstream effects of G protein signalling measure an endpoint that has undergone signal amplification, and are therefore predicted to show increased receptor reserve, and agonist potency. There was a correlation between the pEC_{50} values acquired from β-arrestin binding and internalisation, which may be as expected if GPR120 internalisation is β-arrestin dependent, but this mechanism was not explicitly identified.

Confocal imaging in conjunction with the use of intracellular markers transferrin (to label recycling compartments) and lysotracker red (to label lysosomes) was undertaken to determine the intracellular sorting of GPR120 following internalisation. These images showed colocalisation with lysotracker red, suggesting a non-recycling trafficking profile. This was investigated further using a recycling protocol on the platereader, which further confirmed this non-recycling profile.

3.3.5 Potential molecular basis for GPR120 isoform specific signalling

These experiments showed an interesting result of the short isoform undergoing both G protein dependent and β-arrestin2 mediated endocytosis, whilst the long isoform only elicited β-arrestin2 mediated endocytosis. This must be due to the 16 residues inserted into ICL3 of GPR120L (Figure 3.10).

How does such a small change make such a large difference to the protein-protein interactions? Similar to GPR120, a 29 residue insert in ICL3 is all that differs between the long and short isoforms of the dopamine D_2 receptor. Point mutations within ICL3 of the short dopamine D_2 receptor changed G

protein coupling specificity, suggesting that this area is important for G protein interactions (Senogles et al., 2004). Also, a study in which the dopamine D_3 receptor had 12 residues from the carboxyl tail of ICL3 replaced with equivalent residues from the long dopamine D_{2L} receptor, found that this chimera then acquired promiscuity in G protein coupling, similar to WT D_{2L} (Lane et al., 2008). Additionally, mutation of residues at the M_2 muscarinic receptor TM5:ICL3 interface (close to the insert position in GPR120L) altered its G protein coupling specificity (Kostenis et al., 1997), again showing the importance of residues within this region for G protein coupling. Meanwhile, the ICL3 fragment of the glucagon-like peptide-1 receptor stimulated all G proteins tested (Bavec et al., 2003), and the ICL3 of the μ-opioid receptor is thought to mediate interactions with its G protein (Chaipatikul et al., 2003).

Interestingly, both isoforms had equivalent β-arrestin and internalisation profiles, which is backed up by previous work showing no difference in agonist induced phosphorylation of the isoforms (Burns and Moniri, 2010). This shows that the ICL3 insert does not affect interactions with β-arrestin. The classical model of receptor desensitisation is of threonine and serine residues in the carboxyl tail and intracellular loops becoming phosphorylated by GRKs and protein kinases, which then allow β-arrestin to bind. The binding of β-arrestin prevents G proteins binding, thus preventing signalling; and β-arrestin also acts as a scaffold for the proteins required for internalisation and desensitisation of the receptor (Ferguson et al., 1996). However there are also examples that show that for some receptors, ICL3 or carboxyl tail phosphorylation is not an absolute requirement for arrestin recruitment. In

the μ-opioid receptor, serine and threonine residues in the carboxyl tail and ICL3 were not required for arrestin mediated desensitisation (Celver et al., 2001).

Instead, there is some evidence to suggest that there is a contiguous recognition site of ten proximal residues in intracellular loop 2 of GPCRs, termed the "activation sensor", that one part of β-arrestin2 binds to in a phosphorylation independent manner (Marion et al., 2006). This is in conjunction with a second site, dubbed the "phosphorylation" sensor, that β-arrestin2 also recognises and binds to in a phosphorylation dependent manner. For most GPCRs, both sites must be engaged for internalisation (Gurevich and Gurevich, 2006).

In the study on the μ-opioid receptor, ICL2 was also the site of the critical GRK phosphorylation site (Thr180) required for arrestin recruitment, again showing a role for ICL2 in mediating receptor interactions with β-arrestin (Celver et al., 2001).

A previous study has shown that GPR120 activates two independent signalling pathways. In adipocytes, agonist treatment activated signalling through Gq to cause glucose uptake, whilst in the macrophage, agonist treatment instead elicited anti-inflammatory effects through β-arrestin2 (Oh et al., 2010). Another GPCR, PAR2 has also been shown to activate two signalling pathways, via Gq and β-arrestin2 independently (Zoudilova et al., 2007), as has the archetypal GPCR β_2AR (Drake et al., 2008). Perhaps GPR120 activation of

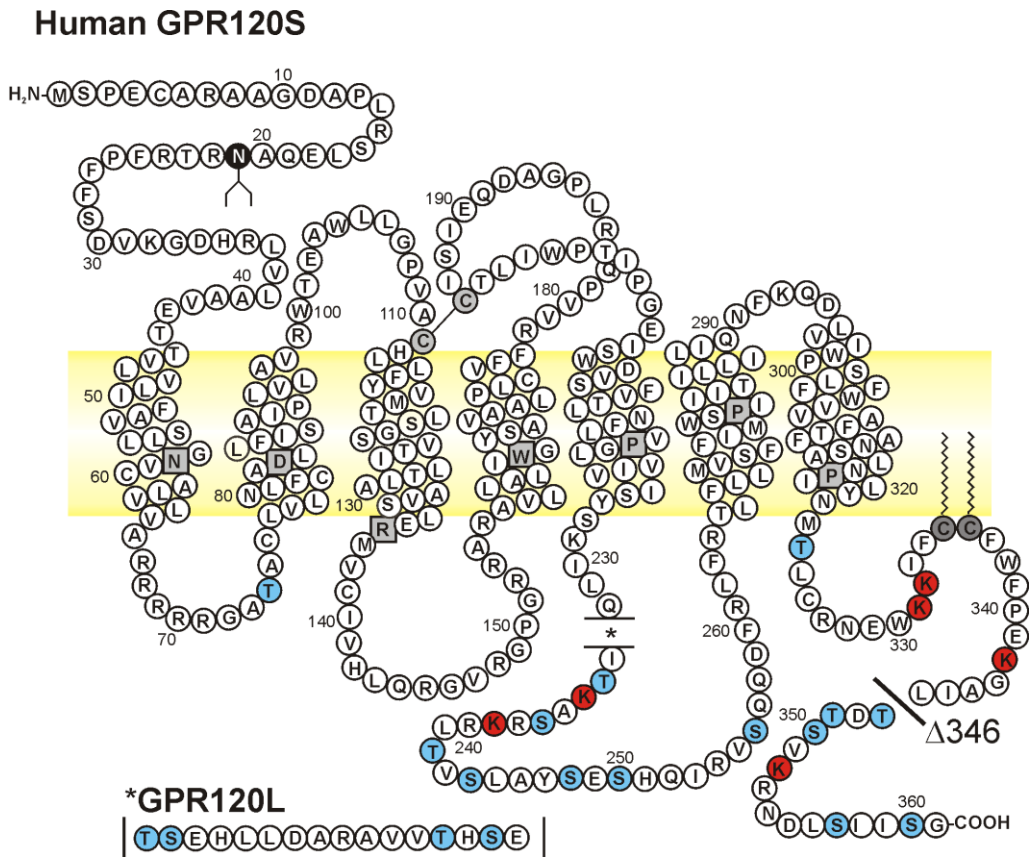

Figure 3.30 The structure of GPR120 showing the position of sites of interest. This structure of GPR120 shows the potential sites of phosphorylation at Ser/Thr residues (shown in blue) and potential ubiquitination sites at Lys (shown in red), together with the position of the Δ346 truncation.

these two pathways is isoform specific. Future work should determine whether GPR120L is endogenously expressed in different cell types in an isoform specific manner, and if so, where, and to confirm whether these pathways are isoform specific. These expression studies are critical, because some work has shown no evidence for the expression of the long isoform in humans (CP, Briscoe, Janssen Pharmaceuticals, private communication).

3.3.6 Role of the GPR120 carboxyl tail

As there was no effect of isoform ICL3 differences when the β-arrestin interactions and internalisation responses were measured, the carboxyl tail was examined as an alternative regulatory domain in GPR120. This was achieved by truncating the tail at amino acid position 346, to remove 5 Ser/Thr residues (Figure 3.30). The carboxyl tail was found to be critical for GPR120 G protein signal desensitisation, as the calcium data demonstrated. This also revealed that GPR120S calcium responses undergo rapid desensitisation. This may account for the difference in profile observed between GPR120S and FFA1, even though they both predominantly couple to the same class of G protein, Gq/11. Following removal of the carboxyl tail, i.e. the desensitisation domain, the peak response of GPR120S became as robust as that of FFA1.

Additionally, these residues in the distal carboxyl tail also appear critical for internalisation, as their removal reduced the extent of internalisation but interestingly did not prevent internalisation. These results were unusual, because they suggest a separation of desensitisation and internalisation that

is in contrast to the dogma that desensitisation and internalisation are sequential and both dependent upon β-arrestin proteins.

Previous work on the follicle stimulating hormone receptor has shown it to have separate sites for phosphorylation required for uncoupling (desensitisation) present on ICL3, whilst phosphorylation sites for internalisation are thought to be on ICL1 predominantly, with a little involvement of sites on ICL3 (Nakamura et al., 1998a). Also, agonist induced activation and phosphorylation were found not to be essential for internalisation (Malecz et al., 1998), whilst an interaction with β-arrestin was required for internalisation (Nakamura et al., 1998b). Also, one residue, S421 found in the carboxyl tail of the $5HT_{2A}$ serotonin receptor has shown to be key for facilitating desensitisation (Gray et al., 2003). Recent evidence for β_2AR suggests a "phosphorylation barcode" system (Butcher et al., 2011; Nobles et al., 2011), where differential phosphorylation signals for different receptor outcomes (Budd et al., 2001). Another example of differential phosphorylation is found with the melanocortin 1 receptor. When GRK2 phosphorylated, it did not undergo internalisation (only desensitisation), whilst GRK6 caused internalisation (Sanchez-Laorden et al., 2007). Another study, on the *N*-formyl peptide receptor demonstrated no correlation between the binding of β-arrestin and the processes of receptor desensitisation and internalisation (Potter et al., 2006).

Taken together, perhaps something similar is also true for GPR120, suggesting a paradigm of differential phosphorylation, whereby phosphorylation of residues in the distal carboxyl tail are responsible for desensitisation and

uncoupling, whilst residues elsewhere in the proximal carboxyl tail or on the intracellular loops are required for receptor internalisation. Whilst β-arrestin dependent mechanisms of internalisation are expected to predominate, GPCRs can also internalise though β-arrestin independent mechanisms (Mundell et al., 2006).

3.3.7 Pharmacology of constrained fatty acid receptor dimers

The BiFC technique was again utilised to test the influence of fatty acid receptor dimerisation of pharmacology, by creating constrained dimers. The key advantage of using BiFC is that it allowed specific GPR120S homo- or hetero-dimers to be visualised and their pharmacology assessed in the internalisation assay in comparison to the overall SNAP-GPR120S-vYNL population in the same cells. There are also limitations to this technique, chiefly that BiFC is an irreversible process and thus has potential to generate dimers that might otherwise not exist (or exist transiently) for endogenous receptors. The extent of measured dimerisation can vary depending on the GPCR being studied and the technique used, for example reconstitution of GPCRs into lipid discs discovered the μ opioid receptor to be in monomeric form (Kuszak et al., 2009); whilst TIRF found only a proportion of antagonist-occupied M1 muscarinic receptors formed dimers (Hern et al., 2010). Additionally, there is evidence for both β_1AR transient dimerisation and sustained β_2AR dimer formation (Dorsch et al., 2009), discussed in more detail in section 1.6.5.

This study of constrained FFA dimers was important, because in pharmacologically relevant and important tissues, for example the colonic L cells in the gut, GPR120S (Hirasawa et al., 2005) and FFA1 (Edfalk et al., 2008) are both expressed. If these receptors undergo heterodimerisation in these sites, with altered pharmacology, any drugs designed to target either receptor may have limited effectiveness. Alternatively, this BiFC assay could be used to discover more effective “hetero-dimer” specific compounds.

In the calcium assay, when measuring responses of the co-expressed receptor populations, the receptor subtypes could be acting independently, e.g. in GPR120S:GPR120L, the presence of GPR120L does not prevent calcium mobilisation, but the calcium signal could be due to GPR120S acting alone. Also, the GPR120S:FFA1 cells had a 2 component calcium response to GW9508, with both components approximately fitting to the pEC_{50} values for each receptor when expressed alone i.e. 7.1 at FFA1 and 5.5 at GPR120S.

In the internalisation assay, GW9508 was found to be more potent in the GPR120S:FFA1 “dimer”, which is noteworthy because FFA1 does not readily undergo agonist induced endocytosis alone (data not shown). These data suggest binding of GW9508 to the higher affinity FFA1 binding site can support greater internalisation of the BiFC heterodimer, but require further work for confirmation.

Future work on the heterodimerisation cell lines could be to use more ligands, for example GW1100 is an antagonist at FFA1 but is inactive at GPR120 (Briscoe et al., 2006). GW1100 would therefore be interesting to use on

GPR120S:FFA1, to see what pharmacology it produced in terms of both calcium and internalisation responses. It would also be interesting to use additional more selective agonists that have differing orders of potency at each receptor, to see what effect the "dimer" has on their responses, for example Met36 (Chapter 4) (Ma et al., 2010). The use of a biophysical technique, such as FRET (Herrick-Davis et al., 2004) or BRET (Babcock et al., 2003) has also been popular in the study of dimerisation, in conjunction with a biochemical technique such as Western blotting. BRET is advantageous because it can be done in living cells without the use of laser excitation, whilst FRET can be utilised to determine the subcellular localisation of the signal (Herrick-Davis et al., 2004). TR-FRET has also been shown to be undertaken successfully in native tissues (Albizu et al., 2010), which was of great importance because other techniques, including the ones used here, rely upon overexpression of a receptor in an artificial, recombinant system and may also require a good native antibody or a good fluorescent ligand (Chapter 5).

3.4 Future work

A crucial next step in this work will be to determine the expression of endogenous human GPR120 isoforms, confirm that the longer isoform is expressed, and whether the isoforms have differential expression to physiologically match their different signalling profiles in various cell types.

Future work could also be undertaken on the role Gα gustducin (a Gi related protein) plays in relation to FFA receptors. Gustducin was originally found in

the taste cells, but has also been found in gut enteroendocrine K and L cells and has been implicated in the secretion of GLP-1 (Jang et al., 2007), which is intriguing as GPR120 is known to promote the release of GLP-1 (Hirasawa et al., 2005) and CCK (Tanaka et al., 2008a). Perhaps gustducin is the link between FFA receptors and incretin secretion, as gustducin was found to be co-expressed in 17 % of GPR120 cells and 40 % of FFA1 cells (Li et al., 2013). Additionally, lipids suppress ghrelin levels post prandial to promote satiety. Further work could be to ascertain whether this signalling involves FFA receptors because one study has found that GPR120 may also be involved in ghrelin signalling to cause cessation of ghrelin initiation of hunger sensations (Janssen et al., 2012).

Another area of interest is to ascertain the domains involved in GPR120 signalling and trafficking. To continue the interesting results from the carboxyl tail data, a more targeted study could be undertaken to ascertain the roles of individual Ser/Thr residues within the carboxyl tail region of deletion, and see whether they could represent a "phosphorylation barcode". Also, GPR120 internalisation could be further studied by confirming GPR120 internalisation is β-arrestin2 dependent using siRNA approaches (Abrisqueta et al., 2013). In addition to that, further analysis could be carried out on the confocal images depicting trafficking of the receptors to the lysosomes, by applying a colocalisation algorithm.

Chapter Four: Investigation of the GPR120 binding site using mutagenesis

4.1 Introduction

FFA1 and GPR120 are potential therapeutic targets for type II diabetes and obesity (chapter 1). So far, a number of synthetic ligands have been developed and tested, but these are mainly agonists at FFA1. This has mostly been carried out in the absence of any detailed knowledge of the FFA receptor family binding site, aside from theoretical modelling. Therefore, elucidating more detail about these binding sites especially for GPR120 is key, and this will potentially allow for the design of ligands with greater selectivity for GPR120.

4.1.1 Structure activity relationships for synthetic ligands at FFA1 and GPR120

Generally, both FFA1 (Briscoe et al., 2003) and GPR120 (Hirasawa et al., 2005) are activated by long chain fatty acids, 6–22 and 14-22 carbons in length respectively. Other synthetic ligands such as GW9508 and Metabolex compound 36 (Met36; Figure 4.1) have a similar length of the ligand backbone, suggesting that there is an optimum carbon chain length, presumably for sitting correctly within the binding pockets.

The key characteristic of both FFAs and most synthetic agonists at FFA1 and GPR120 is the requirement for a carboxylate group (Figure 4.1; Table 4.1). This is particularly shown by comparison of the activity of fatty acids to the

inactivity of the corresponding FFA esters that lack this group, e.g. in GPR120 (Hirasawa et al., 2005), see also Chapter 1). Interestingly, TZDs do not contain a carboxylate, but have a 2,4-dione group that does the same function for FFA1 (Smith et al., 2009) and GPR120 agonism (see Chapter 3). In addition both Banyu patented GPR120 agonists lack functional acid groups entirely (Arakawa et al., 2010; Hashimoto et al., 2010).

Moving along the structure, the majority of FFA1 and GPR120 agonists then contain an aromatic moiety (e.g. phenyl ring) at a structurally defined 3 carbon position from the terminal carboxylate group. For example, this phenyl group in GW9508 was proposed to mimic the conformational restriction of carbon double bonds in unsaturated FFAs, such as linolenic acid (Briscoe et al., 2006). An equivalent aromatic-dione spacing is also shared in TZDs, which formed the structural template for FFA1 agonists such as Merck compound B (Figure 4.1). A central oxygen (ether) or nitrogen (amino) links this pharmacophore with a second bulky aromatic group in majority of agonists, including TZDs and the Banyu derivatives (Figure 4.1). In the TUG series of FFA1 agonists however (e.g. Christiansen et al., 2008), this is substituted by an ethyne triple bond.

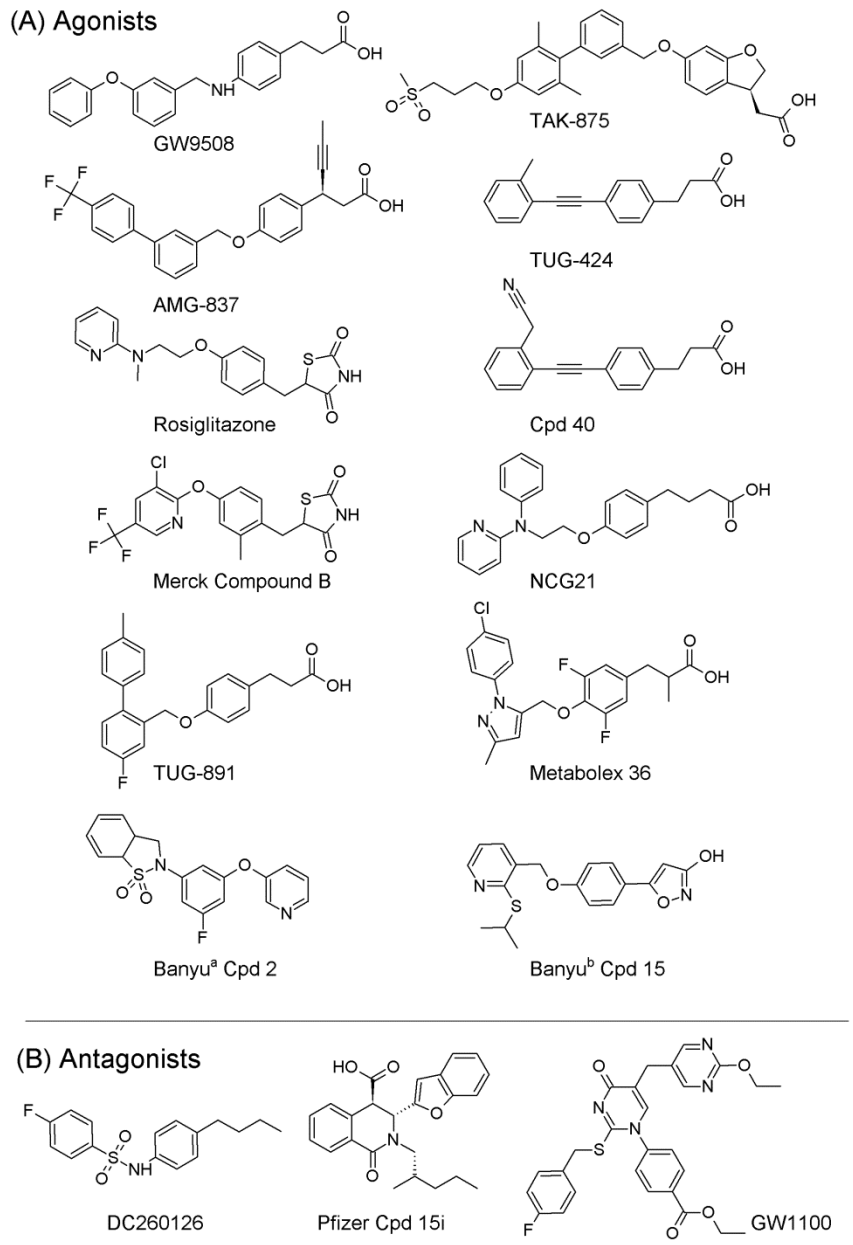

Figure 4.1 Chemical structures of example FFA GPCR agonists (A) and antagonists (B). Information on agonist pharmacology, with references, is provided in Table 1. The structure of Met36 is reproduced from the relevant GPR120 agonist patent (Ma et al., 2010) and two Banyu compounds are shown from isoindolin-1-one derivatives[a] (cpd 2; Arakawa et al., 2010) and the phenyl-isoxazol-3-ol series[b] (cpd 15; Hashimoto et al., 2010). GW1100 (Briscoe et al., 2006), Pfizer compound 15i (Humphries et al., 2009) and DC260126 (Hu et al., 2009) inhibited agonist stimulated FFA1 receptor calcium responses in transfected cells with respective pIC_{50} values of 6.0, 7.7, and 6.0.

Agonist	FFA1 pEC_{50}	GPR120 pEC_{50}	Selectivity and comments	References
Example FFAs				
Palmitic Acid (C16:0)	5.2-5.3	4.3	Several actions as nutrients and signalling molecules. Potency observed highly dependent on assay constituents (e.g. BSA)	(Briscoe et al., 2003; Hirasawa et al., 2005; Itoh et al., 2003)
Oleic Acid (C18:1)	4.4-5.7	4.5		
DHA(C22:6)	5.4-6.0	5.4		
PPARγ agonists				
Rosiglitazone	5.0-5.6[a]	N.D.	GPR40 activity shared by related TZDs such as Troglitazone, Ciglitazone and Pioglitazone. Low potency GPR120 agonism for Rosiglitazone (at 100 μM)	(Hara et al., 2009a; Kotarsky et al., 2003; Smith et al., 2009; Watson et al., 2012)
FFA1 agonists				
MEDICA16	5.5-5.9[a]	<5.0		(Hara et al., 2009b; Kotarsky et al., 2003)
GW9508	6.6-7.3	5.5	GPR40 activity 100 fold selective over a panel of 360 other targets. pEC_{50} values for PPARα, δ and γ were 4.0, 4.0 and 4.9 respectively	(Briscoe et al., 2006; Smith et al., 2009; Sum et al., 2007)
Cpd B	7.1	N.D.	Lead compound of series inactive at PPARs (< 10 μM). GPR40 knockout abolished effects of Cpd B and C on insulin secretion *in vivo*	(Tan et al., 2008; Zhou et al., 2010)
Cpd C	6.8			

TUG424	7.5[b]	N.D.	No activity at FFA2 and FFA3 reported (TUG424). Cpd 37 has 100 fold selectivity for FFA1 over FFA2, FFA3 and PPARs, with improved pharmacokinetic properties owing to reduced lipophilicity	(Christiansen et al., 2012; Christiansen et al., 2008)
Cpd 37	7.1[b]			
TAK-875	7.1[c]	N.D.		(Sasaki et al., 2011; Tsujihata et al., 2011)
AMG-837	7.9[a]	> 5.0	Partial agonist at FFA1, increases GSIS and lowered post-prandial glucose levels (0.05 mg / kg) in normal rats	(Lin et al., 2011)
Cpd 40	7.7	N.D.		(Christiansen et al., 2013)
GPR120 agonists				
Grifolic acid	N.D.	N.D.	Weak GPR120 partial agonist without GPR40 activity (at 100 μM).	(Hara et al., 2009b)
NCG21 (Cpd 12)	4.7	5.9	Lacks PPARα, γ, δ agonist activity (at 100 μM)	(Sun et al., 2010; Suzuki et al., 2008)
Isoindolin-1-one series (Cpd 2)	N.D.	6.7	Banyu patent	(Arakawa et al., 2010)
Phenyl-isoxazol-3-ol series (Cpd 15)	N.D.	7.2	Banyu patent	(Hashimoto et al., 2010)
Met36 (Cpd 36)	N.D.	> 6.0	Cpd 36 (100 mg / kg) reduced glucose excursion by 45 % after an oral glucose tolerance test in lean C57Bl/6J mice	(Ma et al., 2010)
TUG 891 (Cpd 43)	4.2	7.4	No activity at FFA2 and FFA3	(Shimpukade et al., 2012)

Table 4.1 Summary of long chain FFA GPCR agonist pharmacology

Agonist pEC_{50} values quoted were obtained from fluorescent indicator measurements of Ca^{2+} mobilization, except [a]Smith et al.(2009) compared TZD agonism for FFA1 ERK activation, while Kotarsky et al.(2003) and Lin et al (2011) measured FFA1 Ca^{2+} signalling using an aequorin reporter gene; [b]measurement of insulin secretion/DMR assay; [c]measurement of inositol phosphate accumulation; Shimpukade et al (2012) used a BRET assay. N.D. not determined; pEC_{50} values have not been published.

All agonists contain a terminal aromatic group (phenyl or biphenyl group) which connects to the rest of the molecule via the phenylproprionic acid moiety (the ether or amino group). There is limited information on this terminal aromatic group; for example TUG-424 and compound 42 (Figure 4.1) had the highest potency in their compound series, thought to be due to the methyl group being in the ortho position (Christiansen et al., 2008).

Interestingly, as far as can be deduced, GPR120 selective compounds such as Met36 and TUG-891 appear to be characterised by the bulky aromatic groups in the ortho position, which creates a structural "kink" in the structure in contrast to the FFA1 selective GW9508 (Figure 4.1).

Conversely, there are very few antagonists for the FFA receptors, with micromolar affinity, for example GW1100 at FFA1 (Briscoe et al., 2006). The three antagonists in the public domain (Figure 4.1) are structurally diverse, thus there is no clear SAR yet. Additionally, there are no antagonists for GPR120.

Allosteric modulation of FFA receptors may also be possible. Allosteric compounds target an alternative binding site to the orthosteric FFA binding site to influence receptor activation (e.g. by the endogenous agonist) and they have the advantage of improving receptor selectivity, e.g. between FFA1 and GPR120 (May et al., 2007). Allosteric compounds have been discovered for another receptor in the FFA family, FFA2 (Lee et al., 2008), and as will be discussed in Chapter 5, an allosteric component to the action of some existing FFA1 agonists (e.g. GW9508) has been suggested.

4.1.2 Ligand binding to lipid GPCRs

Although no FFA receptor has yet been crystallised, a high resolution structure of one lipid GPCR, the sphingosine-1-phosphate (S1P) receptor, has been obtained (Hanson et al., 2012). This structure showed that the amino terminus appears to fold over the top of the receptor, which in combination with the positions of ECL1 and 2, forms a barrier that appears to limit "downwards" ligand access to the binding pocket. Uniquely this suggested that the ligand access is only through partitioning into the hydrophobic environment of the plasma membrane, through a gap between TM 1 and TM 7. Once the ligand is "docked" into the binding pocket (located in the extracellular half of the receptor transmembrane domains), the polar phosphate headgroup is orientated towards the top of the binding pocket, coordinating with positive polar TM residues of Asn and Arg. This parallels the models of ligand binding with FFA1 (Sum et al., 2007) and GPR120 (Suzuki et al., 2008), as suggested by the inactivating effects of mutations of these residues (e.g. Arg 258 in FFA1, Chapter 3) The hydrophobic tail of the S1P (identical to a FFA carbon chain) sits in the binding pocket (Hanson et al., 2012), reaching the highly conserved residue W6.48 (Ballesteros-Weinstein numbering system (Figure 4.2)) that is thought to play a key role in GPCR activation (see Chapter 1) (Holst et al., 2010).

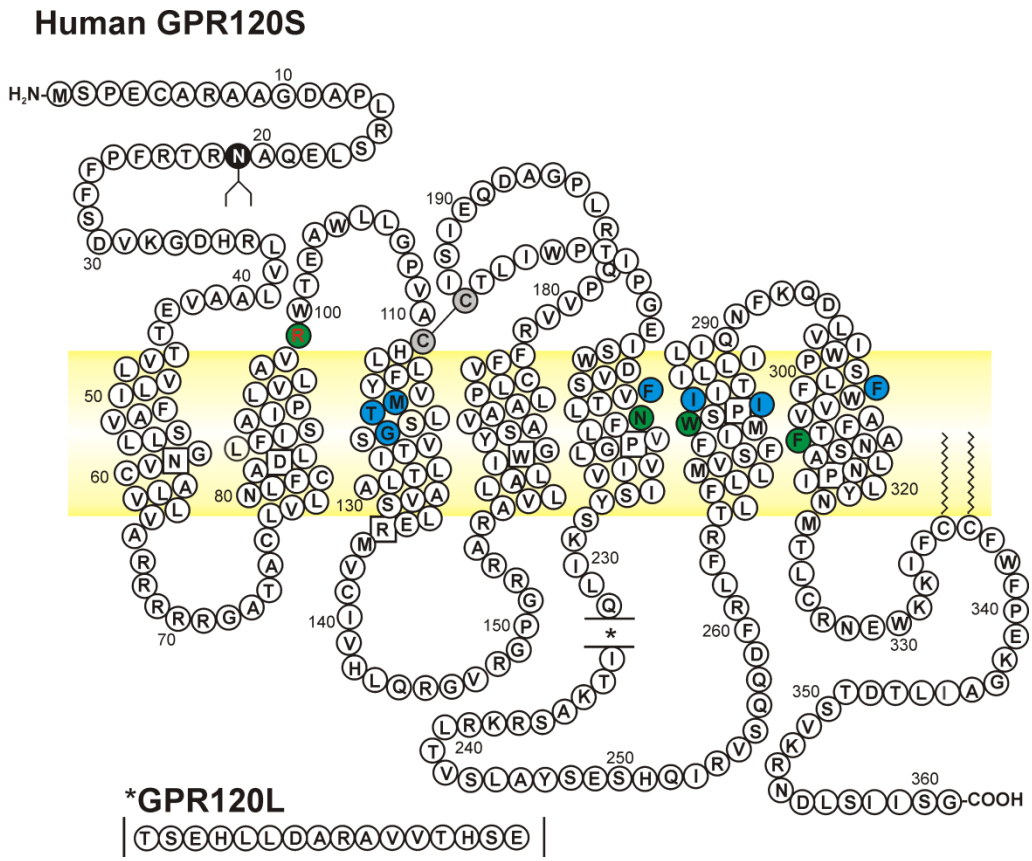

Figure 4.2 The structure of GPR120 showing the position of the most conserved residue in each TM helix and the sites of mutation in this study.
The Ballesteros-Weinstein system of numbering allows comparison of a residue in an equivalent position between different GPCRs, The most conserved residue is set as "x.50" (shown in squares), with this number decreasing for residues closer to the amino terminus or increasing if closer to the carboxyl terminus (Ballesteros and Weinstein, 1995). The sites of mutation made in this study are in green, and the sites of other residues of interest in the Ulven model are shown in blue (Shimpukade et al., 2012).

4.1.3 The key features of the FFA1 receptor binding site

Although the crystal structure of FFA1 or GPR120 has not yet been determined, homology studies have developed models of the binding sites by mapping the receptor sequences onto crystal structures of other class A GPCRs, such as β_2AR. For FFA1, recent investigations have also begun to test such models using site directed mutagenesis.

4.1.3.1 Docking of carboxylate on the ligand into the binding site

The negatively charged carboxylate group present on the majority of agonists was proposed to dock into the positive residues Arg183 and Arg258 on FFA1 (Sum et al., 2007; Tikhonova et al., 2007), although one study suggests that Arg258 is thought to be solely important for binding linoleic acid (Takeuchi et al., 2013). The importance of Arg258 for oleic acid and GW9508 FFA1 responses was confirmed in Chapter 3. In the Sum *et al*. (2007) investigation, mutation of Arg183 (TM 5), Asn244 (ECL3) and Arg258 (TM 7; Figure 4.2) all reduced the magnitude of response to linoleic acid, whilst mutation of R183A or R258A removed all responses to GW9508. The positive Arg residues, located at the top of the TM domains are thought to play a role in orientation of the agonist so that the lipophilic portion sits in the lower hydrophobic binding pocket (Sum et al., 2007; Sun et al., 2010). There is thought to be additional anchorage from His137 for GW9508, because the 3-phenoxy portion of GW9508 forms a hydrophobic interaction with His137 (Tikhonova et al., 2008; Tikhonova et al., 2007), and/or His86 and His 98 (Sum et al.,

2007), but this is not universally agreed (Smith et al., 2009), highlighting the difficulty of using mutagenesis studies to determine and confirm binding sites.

4.1.3.2 Role of ECL2 in ligand binding at FFA1

From an FFA1 homology model based on the inactive β_2AR, ECL2 residues Glu145 and Glu172, along with aforementioned Arg183 and Arg258 were found to control FFA1 activation by agonists (Sum et al., 2009). Glu145 (ECL2; postulated to face into the binding pocket) formed a constraining hydrogen bond with Arg183 (TM 5), whilst Glu172 (ECL2) formed a hydrogen bond with Arg258 (TM 7). These residues appear important because these interactions hold the receptor in an inactive state and so are disrupted following the binding of GW9508 or linoleic acid. Then the negatively charged carboxylate of the ligand instead undergoes interactions with the positively charged binding site of Arg183, Arg258 and Asn244, causing the receptor to adopt the active conformation. It was also suggested that perhaps antagonists, without the requisite carboxylate groups, are unable to cause release of this ionic lock (Sum et al., 2009). Other GPCRs also contain a negatively charged Glu or Asp residue in ECL2 (a Cx(E/D) motif) which corresponds to Glu172 to FFA1. It has been postulated that these negative charges form a counter ion to the positively charged residues in the agonist binding pocket. This extracellular loop ionic lock also appears to be conserved in other class A purinergic and muscarinic GPCRs (Costanzi et al., 2005; Scarselli et al., 2007). Such residues thus appear to be involved in receptor activation, but not in direct ligand binding interactions (Sum et al., 2009).

4.1.3.3 Published models of GPR120 binding site

In contrast to FFA1 with its multiple Arg sites in the receptor binding site, GPR120 contains a single predicted coordinating residue, Arg99 at the top of TM 2 (Suzuki et al., 2008). Two untested homology models have been published on GPR120, one using bovine rhodopsin (Sun et al., 2010) and the other using the β_2AR structure as the template (Shimpukade et al., 2012). The β_2AR "Ulven" model shows Met118, Thr119, Gly122, Phe211, Asn215, Trp277, Ile280, and Ile281 forming a narrow lipophilic binding pocket (Figure 4.2). Met, Ile and Val are hydrophobic residues, predicted to make hydrophobic contacts with the biphenyl moiety on the ligand, whilst Trp277 is the Trp 6.48 that is highly conserved throughout class A GPCRs, and appears to be key for forming a hydrogen-bond with the ether-oxygen present in the agonist TUG-891 (Figure 4.1). Additionally, the phenylpropionate group present in some agonists is predicted to interact with Phe304 on the top side and Phe311 on the bottom side (Shimpukade et al., 2012).

In the rhodopsin-based model, the hydrophobic residues that were suggested to form interactions between the ligand and the binding pocket were Met115, Leu187 and Phe202 which interacted with the phenyl ring on the ligand. Also in this model, ECL2 was modelled showing contact with the ligand, perhaps through Trp198 (Sun et al., 2010), whilst ECL2 was not mentioned in the Ulven model (Shimpukade et al., 2012).

Of note with both GPR120 models and the sphingosine 1-phosphate receptor structure, was that the agonist compounds penetrated quite deeply into the

TM domains of the receptor, which contrasts with the antagonist carazolol, which was bound at a relatively shallow position within the TM helices of β_2AR (Cherezov et al., 2007).

4.1.4 AstraZeneca model of GPR120 binding site

In this study, the AstraZeneca (AZ) model of GPR120 was used (provided by Dr. Graeme Robb, CVGI, Alderley Park), based on the crystal structure of the *active* β2-adrenoceptor (Rasmussen et al., 2011) and docked with various agonists including Met36 (Figure 4.1). Using the active structure has the potential advantage that in studying agonist binding to an activated receptor, this will give more relevant information for the design of therapeutically relevant GPR120 agonists.

This model also defined the narrow lipophilic pocket as containing Met118, Thr119, Gly122, Phe211, Asn215, Ile280, Ile281 and Trp277, similar to the Ulven model (Shimpukade et al., 2012). The AZ model also contained Trp277, the highly conserved Trp 6.48, which was thought to interact via a water molecule to the nitrogen in the ring of Met36. As with the Ulven model of GPR120, the phenylpropionate moiety of Met36 forms stacking interactions with both Phe311 in the AZ model (Figure 4.3, 4.4), and Phe304 (G. Robb, personal communication).

Finally, Asn215 was implicated in a second form of the AstraZeneca model, in mediating polar interactions with the pyrazole ring of Met36 instead of the water molecule shown in Figure 4.3.

There are also similarities between the AstraZeneca model and the crystal structure of S1PR (section 4.1.5). The S1PR ligand, ML056 sits in the binding pocket in the same orientation as the postulated orientation of oleic acid in GPR120 in the AZ model, with the phosphate head interacting with Arg120 in TM 3. The phenyl acyl tail of ML056 also sits in a hydrophobic pocket that is lined with aromatic residues, 4 of which predicted to interact with the ligand (Hanson et al., 2012), which is also similar to the AZ model of GPR120 (Figure 4.5).

4.1.5 Aims

Currently, with the exception of GPR120 Arg99 (Sun et al., 2010; Watson et al., 2012), all evidence for GPR120 ligand binding is based on modelling, whilst the FFA1 models have been tested by mutagenesis. Therefore, the aim of this work was to re-address this situation, by mutating key interactions, as identified by the AZ model, and study their effects upon GPR120S receptor activation using calcium signalling and internalisation assays with 4 representative agonist compounds. The residues studied were Arg99 (2.64), Arg178 (4.65), Asn244 (5.46), Trp277 (6.48) and Phe311 (7.43), with the numbers in brackets referring to their Ballesteros-Weinstein numbering. In the rest of the chapter, the mutants will be referred to by their numbering from the GPR120S sequence (Figure 4.2).

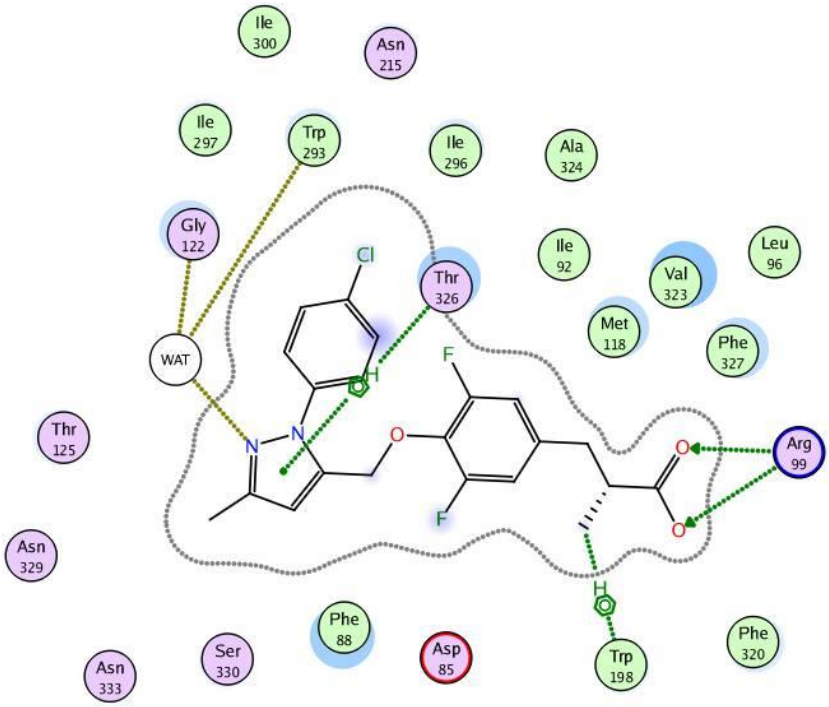

Figure 4.3 Model of Met36 within the GPR120 binding site.

The known interaction of Arg99 with the carboxylate is shown. Another interaction is Trp277 (Trp293 in figure) and Gly122 (a backbone residue in GPR120) with a water molecule interacting with the pyrazole (the nitrogen containing ring) present in Met36. The model also implicated Phe311 (Phe327 in figure, which uses GPR120L numbering) in forming an aromatic stacking interaction with the ligand. An alternative hypothesis had Asn215 as an interaction in place of the water molecule. Figure provided by Dr G. Robb (AZ).

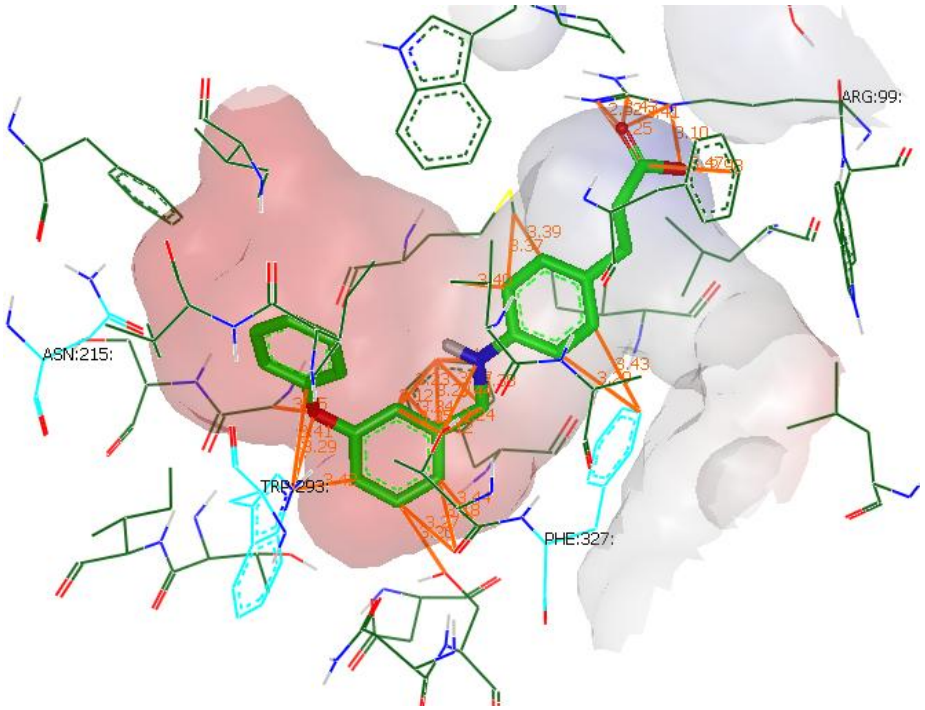

Figure 4.4 GW9508 docked into GPR120 binding site, with key residues from model highlighted.

This shows the synthetic ligand, GW9508 (green stick figure, with space filling) undergoing interactions with the three residues to be tested from the mode: Asn215, Trp277 (labelled as Trp293) and Phe311 (labelled as Phe327, for GPR120L isoform). Figure provided by Dr. G. Robb (AZ).

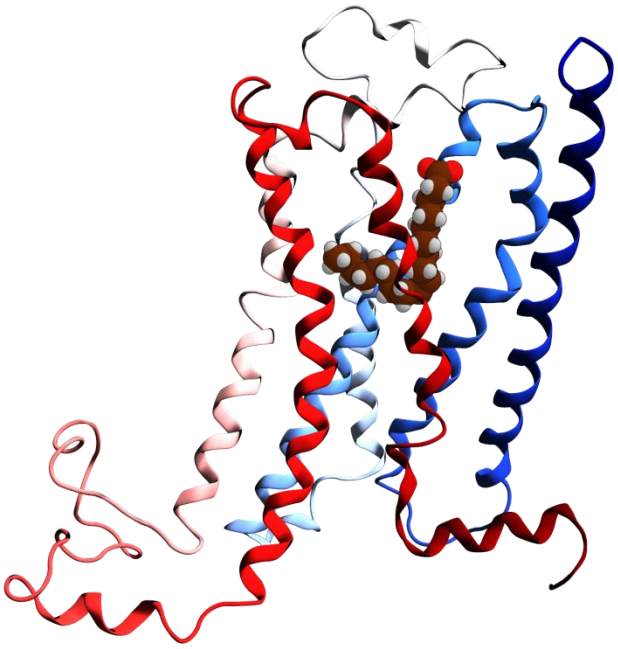

Figure 4.5 Oleic acid docked into GPR120.
This shows oleic acid (space filling) sitting within the whole homology modelled receptor. Figure provided by Dr. G. Robb (AZ).

4.2 Results

4.2.1 Quantification of GPR120S mutant expression levels

Alanine SNAP-GPR120S mutants were constructed at Arg99 (R99A), Arg178 (R178A), Asn215 (N215A), Trp277 (W277A) and Phe311 (F311A) and Trp277 was also substituted with a more conservative amino acid, phenylalanine (W277F). Receptor cDNAs were stably and inducibly expressed as mixed populations in HEK293TR cells, and their function compared with the cell line expressing WT SNAP-GPR120S (see Chapter 3). The expression levels of the mutants reaching the plasma membrane were determined using platereader imaging of SNAP-surface labelled receptors (Figure 4.6) and quantified using a cell scoring algorithm (see section 2.2.9.3.2 and chapter 3). In Figure 4.7 (and in the images used for quantification, Figure 4.6), the same acquisition settings were used (and brightness/contrast image adjustments) to compare cell lines. As the SNAP-surface fluorophore used is membrane impermeant, fluorescent labelling of the receptor indicates that it has the ability to reach the cell surface. This was done to ascertain that the mutation had not prevented receptor folding and expression, and so that any functional effects were relevant with respect to ligand binding and/or activation.

The R99A mutant had reduced cell surface expression and also underwent constitutive internalisation. W277A also had significantly lower cell surface expression than WT. Conversely, W277F had significantly increased expression relative to WT (Figure 4.7; representative images Figure 4.6). All other receptor mutants had similar expression levels to WT, were predominantly

cell surface localised when vehicle treated and underwent some agonist induced endocytosis.

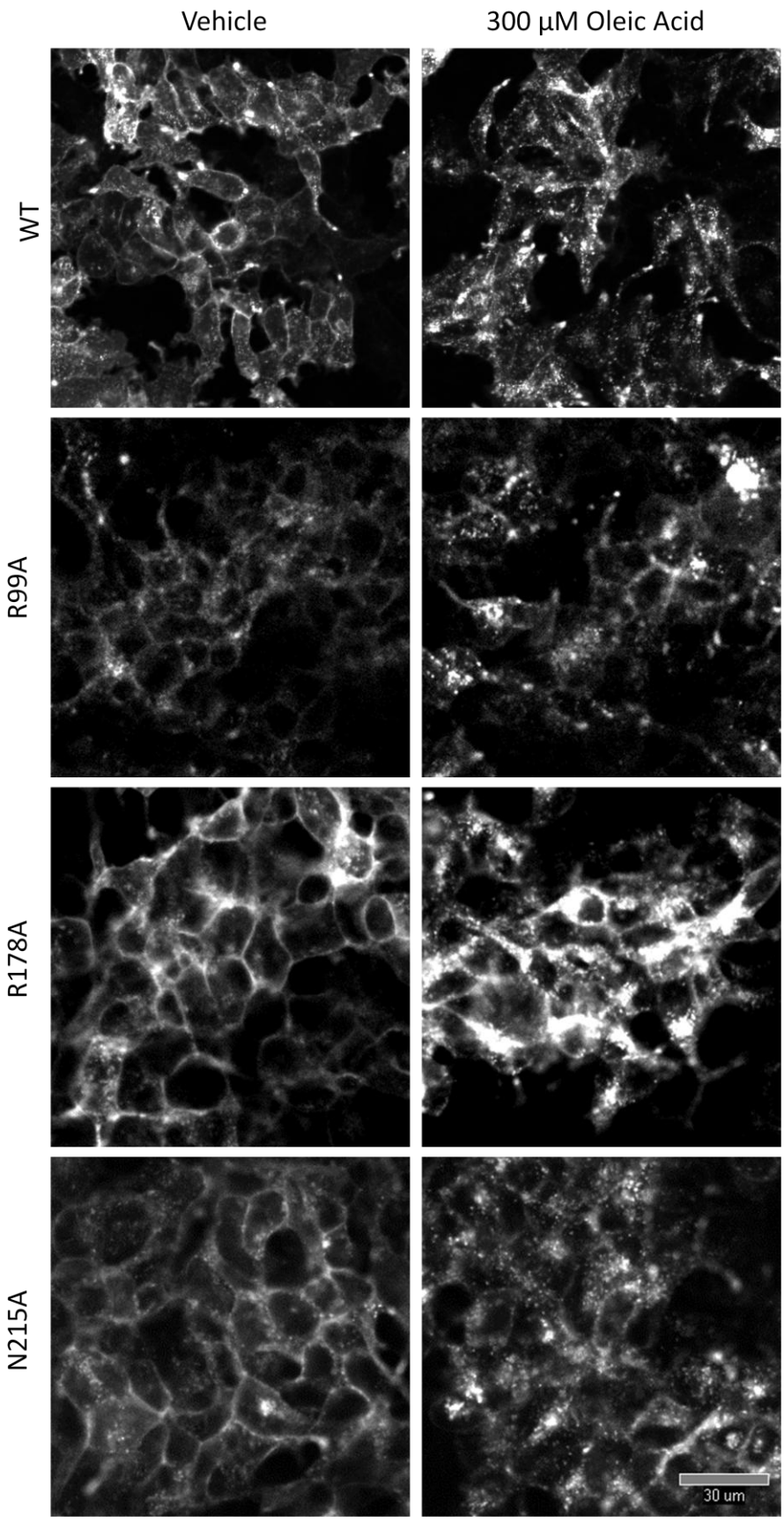
Vehicle
300 µM Oleic Acid
WT
R99A
R178A
N215A
30 um

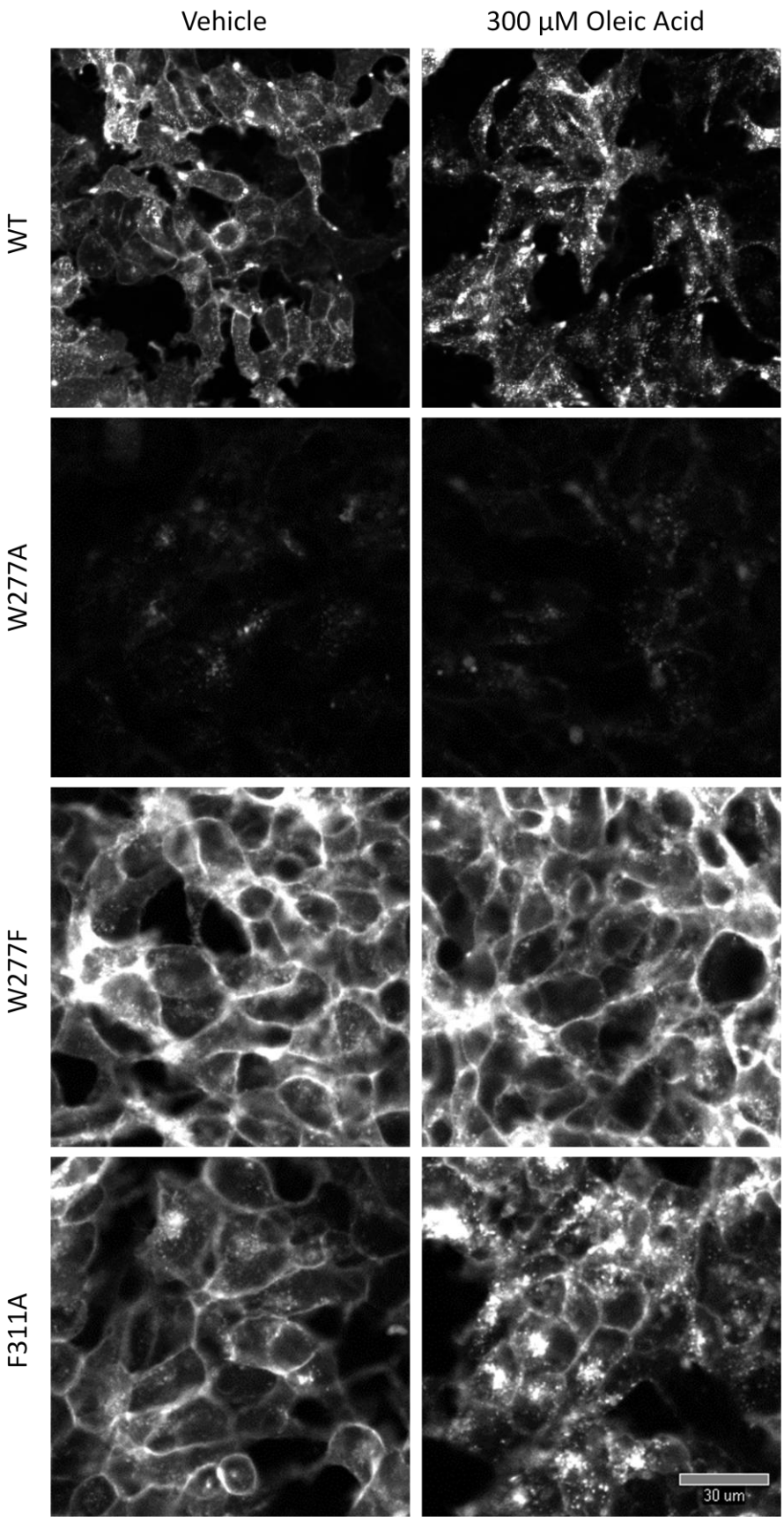
Vehicle
300 µM Oleic Acid
WT
W277A
W277F
F311A
30 um

Figure 4.6 Representative images of GPR120S mutant expression levels.

Images were acquired on the IX Ultra of HEK293TRs stably transfected with the SNAP-GPR120S mutant as indicated, following SNAP-surface AF-488 labelling (0.1 μM) and treatment with vehicle or 300 μM oleic acid for 60 min at 37^{o}C. Images (here showing 25 % of the original Ultra image) were acquired using the same laser power and gain settings, and have undergone identical level adjustments to enable comparison between cell lines. Scale bar = 30 μm.

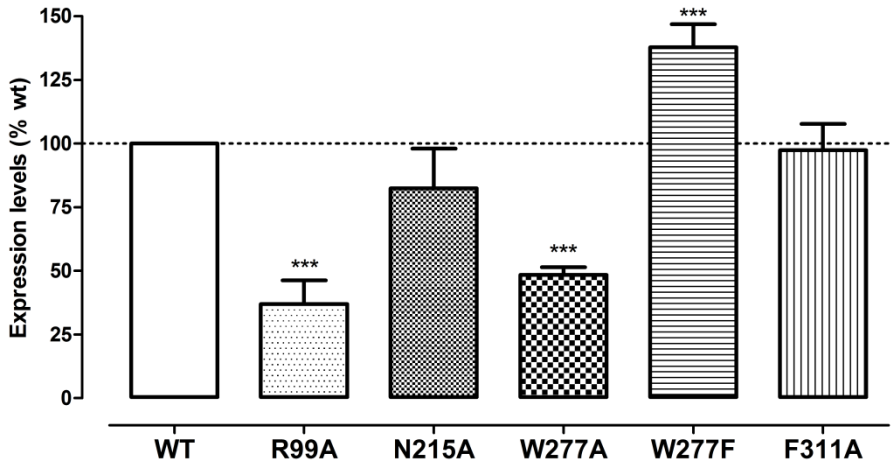

Figure 4.7 Relative expression levels of the SNAP-GPR120S mutants.

Using images acquired on the IX Ultra of HEK293TRs stably transfected with the mutants (Figure 4.5), relative expression levels of each mutant relative to WT could be determined using a multiwavelength cell scoring algorithm. The mutant data from each experiment shown was normalised (%) to GPR120S WT cells on the same plate, and then pooled from 4 - 6 individual experiments, mean ± S.E.M. Significance was measured using Student's t test; *** $p < 0.001$.

4.2.2 Calcium responses of GPR120 mutants

Next, the mutants were tested in a traditional signalling assay, for their ability to elicit calcium responses in response to unsaturated oleic acid (C18:1), saturated myristic acid (C14:0), GW9508 or Met36. Concentration response curves to the four agonists were constructed from peak responses and expressed as fold over basal levels.

R99A and W277A substitutions completely inhibited SNAP-GPR120S calcium responses to all agonists, whilst the R178A mutant stimulated calcium mobilisation in an equivalent manner to WT (Figure 4.8; Figure 4.9; Table 4.2).

Interestingly (and in contrast to the effects of W277A), W277F increased GPR120S responses to FFAs (significantly for 300 µM myristic acid), had no effect on GW9508 concentration response curves, and reduced the potency of Met36. Equally the N215A mutant had a significantly decreased response to 100 µM Met36, reducing its potency, but had no significant effect on responses to other agonists. F311A substitution did not alter SNAP-GPR120S calcium responses significantly, but there was a slight right shifting in the response curve to Met36 (Figure 4.8; Table 4.2; n = 4).

The time courses of GPR120S calcium responses were also compared to maximum agonist concentrations (myristic acid responses omitted for clarity). N215A responses to oleic acid and GW9508 were more transient than WT (significant at 60 s); whilst W277F responses to GW9508 was also significantly reduced at 60 s compared to WT (Figure 4.10; Table 4.3; n = 4).

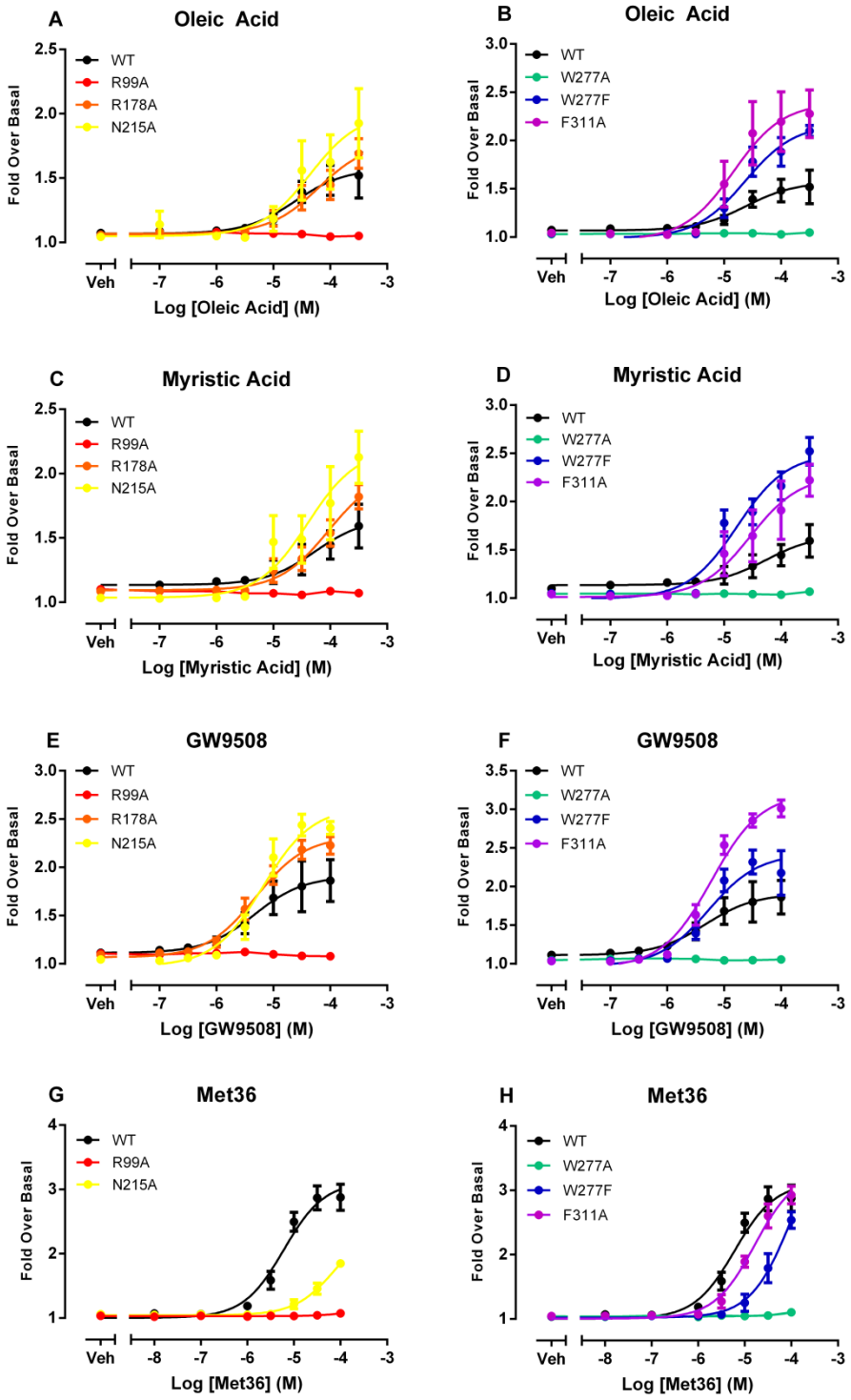
A
Oleic Acid
WT
R99A
R178A
N215A
Fold Over Basal
Log [Oleic Acid] (M)
B
Oleic Acid
WT
W277A
W277F
F311A
Fold Over Basal
Log [Oleic Acid] (M)
C
Myristic Acid
WT
R99A
R178A
N215A
Fold Over Basal
Log [Myristic Acid] (M)
D
Myristic Acid
WT
W277A
W277F
F311A
Fold Over Basal
Log [Myristic Acid] (M)
E
GW9508
WT
R99A
R178A
N215A
Fold Over Basal
Log [GW9508] (M)
F
GW9508
WT
W277A
W277F
F311A
Fold Over Basal
Log [GW9508] (M)
G
Met36
WT
R99A
N215A
Fold Over Basal
Log [Met36] (M)
H
Met36
WT
W277A
W277F
F311A
Fold Over Basal
Log [Met36] (M)

Figure 4.8 The effects of the SNAP-GPR120S mutations upon the calcium concentration responses to oleic acid, myristic acid, GW9508 and Met36.

HEK293TRs expressing SNAP-GPR10S WT, R99A, R178A, N215A, W277A/F or F311A were treated with oleic acid (A-B), myristic acid (C-D), GW9508 (E-F) or Met36 (G-H). The peak calcium responses were measured by changes in Fluo4 fluorescence on a FlexStation III, were analysed as fold over basal and pooled from 4-6 individual experiments, mean ± S.E.M.

	Calcium							
	pEC_{50}				R_{max} (fold over basal)			
Agonist	Oleic Acid	Myristic Acid	GW9508	Met36	Oleic Acid	Myristic Acid	GW9508	Met36
WT	4.2 ± 0.3	N.D.	5.4 ± 0.2	4.7 ± 0.1	1.5 ± 0.2	1.6 ± 0.2	1.9 ± 0.2	3.5 ± 0.1
Mutant								
R99A	N.D.	N.D.	N.D.	N.T.	1.1 ± 0.1	1.1 ± 0.1	1.1 ± 0.1*	N.T.
R178A	N.D.	N.D.	5.2 ± 0.2	N.T.	1.7 ± 0.1	1.8 ± 0.1	2.2 ± 0.1	N.T.
N215A	4.4 ± 0.4	N.D.	5.2 ± 0.1	N.D.	1.9 ± 0.3	2.1 ± 0.2	2.4 ± 0.1	1.9 ± 0.1***
W277A	N.D.	N.D.	N.D.	N.T.	1.1 ± 0.1	1.1 ± 0.1	1.1 ± 0.1*	N.T.
W277F	4.8 ± 0.2	4.9 ± 0.2	5.4 ± 0.2	N.D.	1.1 ± 0.1	2.5 ± 0.1***	2.0 ± 0.3	2.3 ± 0.1***
F311A	4.8 ± 0.3	4.4 ± 0.3	5.2 ± 0.2	4.8 ± 0.1	2.1 ± 0.3	2.1 ± 0.2	2.8 ± 0.2**	2.9 ± 0.1**

Table 4.2 Potency and maximal calcium responses of GPR120S mutants to different agonists.

EC_{50} values and maximal responses of GPR120 mutants in response to agonist as measured using the calcium assay (see concentration response curves in Figure 4.8). The responses shown were analysed as fold over basal, and pooled from 4 - 5 individual experiments, mean ± S.E.M. Statistical significance was defined using one way ANOVA and Dunnett's post test, * $P < 0.05$; ** $P < 0.01$. N.D.-not determined, N.T.-not tested.

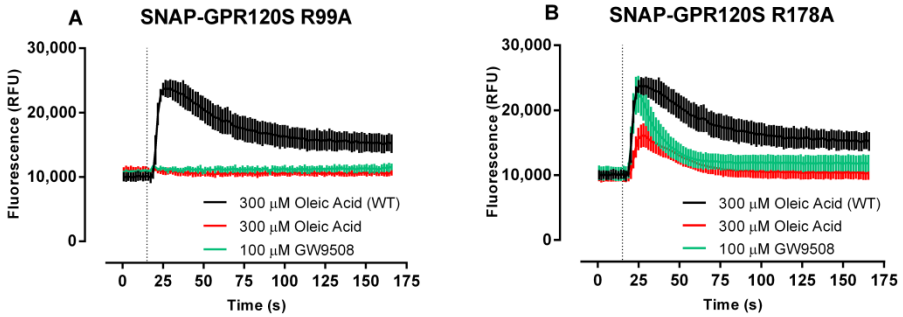

Figure 4.9 The effect of R99A or R178A mutations upon the time course of SNAP-GPR120S stimulated calcium mobilisation in response to 300 µM oleic acid and 100 µM GW9508.

HEK293TRs expressing SNAP-GPR120S WT, R99A or R178A were treated with 300 µM oleic acid or 100 µM GW9508 and their calcium response recorded over 165 s. Dotted line indicates the time of agonist addition. The data shown were pooled from the raw fluorescence values (as relative fluorescence units, RFU) from 4-5 individual experiments, mean ± S.E.M. N.B. these data were not normalised in the same way as Figure 4.10 because of the lack of response at R99A.

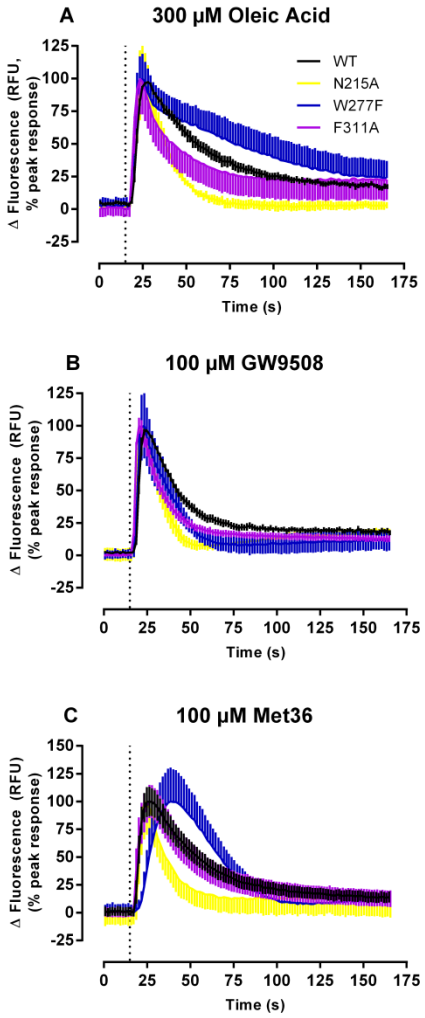

Figure 4.10 The effect of N215A, W277F and F311A mutations upon the time course of GPR120S stimulated calcium mobilisation in response to agonists compared to WT.

HEK293TRs expressing SNAP-GPR120S WT, N215A, W277F or F311A were treated with 300 µM oleic acid, 100 µM GW9508 or 100 µM Met36, and the calcium response followed over 165 s. Dotted line indicates the time of agonist addition. For clarity, W277F responses to oleic acid and Met36 are shown with error bar above, whilst F311A response to oleic acid and N215A response to Met36 are shown error bar below. The data shown were normalised to peak response, pooled from 4 - 5 individual experiments, mean ± S.E.M.

	Time Course		
Agonist	Oleic Acid	GW9508	Met36
Mutant			
N215A	**	*	N.S.
W277F	N.S.	***	N.S.
F311A	N.S.	N.S.	N.S.

Table 4.3 Summary of statistical significance between calcium responses at 60 s time point in Figure 4.10.

Statistical significance between the calcium time course of GPR120S WT and mutants, N215A, W277F and F311A in response to 300 µM oleic acid, 100 µM GW9508 or 100 µM Met36 (Figure 4.10) was determined at 60 s using 1 way ANOVA + Dunnett's post tests, N.S.-not significant, * $P < 0.05$, ** $P < 0.01$, *** $P < 0.001$.

4.2.3 Internalisation responses of GPR120 mutants

The GPR120S mutants were then imaged on the automated IX Ultra platereader, and receptor internalisation was quantified by SNAP-surface AF-488 labelling and 60 min agonist treatment as previously described (section 2.2.3.4; representative images of receptor internalisation are shown in Figure 4.11). Concentration response curve data (Figure 4.12) were expressed as fold over basal instead of normalisation to a reference compound, to allow comparison between different cell lines and thus different mutants. Potency and maximal responses for the different agonists are summarised in Table 4.4.

The R99A mutant underwent low levels of agonist stimulated internalisation compared to WT in response to the highest concentrations of oleic acid and myristic acid, but did give a small concentration response curve to GW9508 (Table 4.4; Figure 4.12; n = 5).

Meanwhile, R178A, N215A and F311A did not significantly alter agonist-promoted GPR120S internalisation (Figure 4.12; Table 4.4; n = 4 - 6).

Interestingly, only agonist promoted internalisation of SNAP-GPR120S W277A and W277F mutants, compared to WT were significantly inhibited (Table 4.4; Figure 4.12; n = 6).

For the responses where agonist pEC_{50} values could be determined, none were significantly altered by mutation (Figure 4.12; Table 4.4; n = 4).

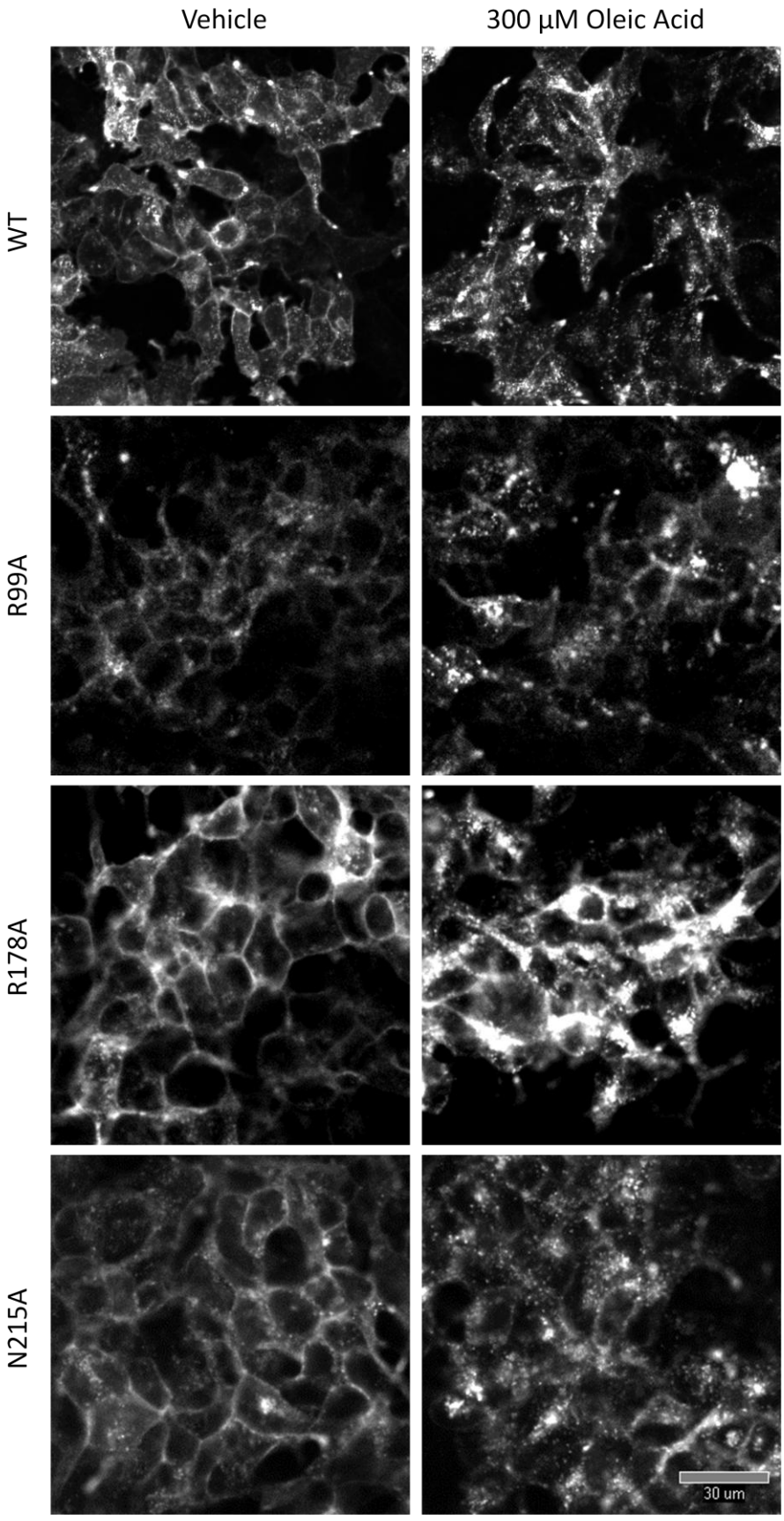
Vehicle
300 µM Oleic Acid
WT
R99A
R178A
N215A
30 um

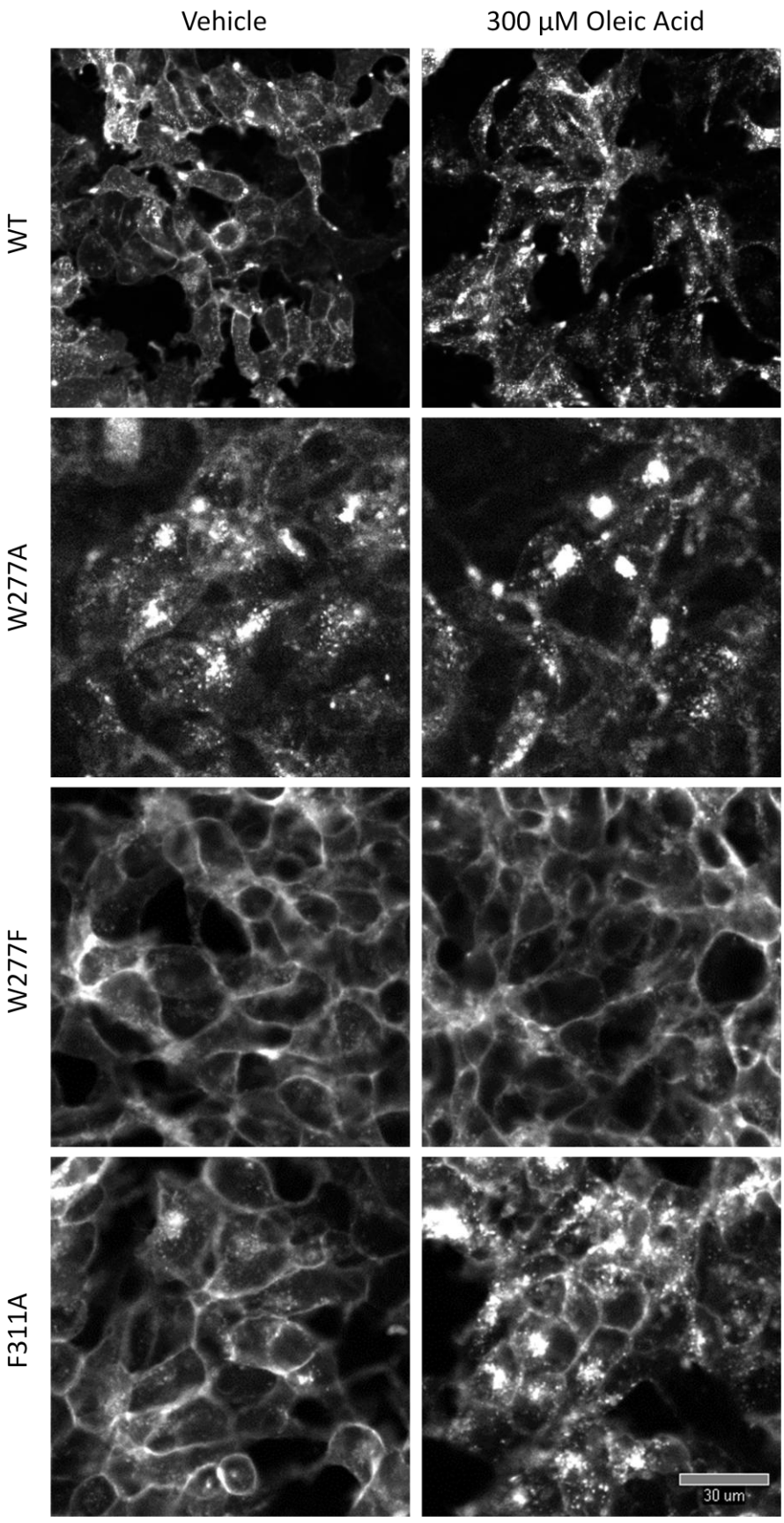
Vehicle
300 µM Oleic Acid
WT
W277A
W277F
F311A
30 um

Figure 4.11 Representative images of GPR120S mutant internalisation in response to vehicle or 300 µM oleic acid.

Images (25 % of total image shown here) were acquired on the IX Ultra of HEK293TRs stably transfected with the SNAP-GPR120S mutant as indicated, after SNAP-surface AF-488 labelling and treatment with vehicle or 300 µM oleic acid for 60 min at 37^{o}C. In contrast to Figure 4.6, image level adjustments were kept constant for vehicle and oleic acid images within each mutant, to highlight agonist-stimulated receptor internalisation if present. Scale bar = 30 µm.

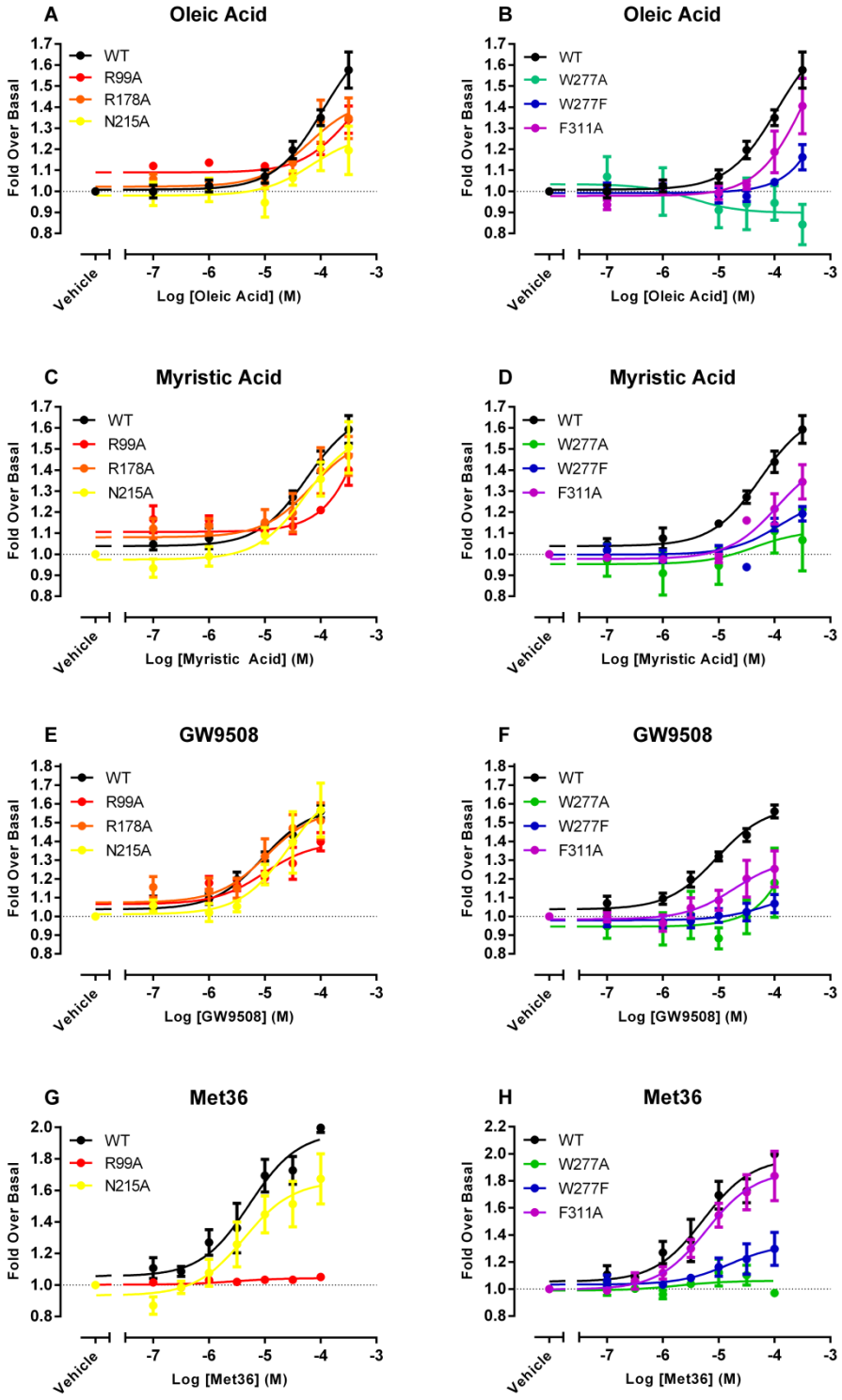

Figure 4.12 Internalisation of the GPR120 mutants in response to agonists.

HEK293TRs expressing SNAP-GPR120S WT, R99A, R178A, N215A, W277A, W277F or F311A were treated with oleic acid (A-B), myristic acid (C-D), GW9508 (E-F) or Met36 (G-H) and internalisation concentration response relationships were measured by image granularity analysis (as described in

section 2.2.9.3.1). The responses shown were analysed as fold over basal and pooled from 4 - 6 individual experiments, mean ± S.E.M. (Met36 data set provided by N. Holliday).

	Internalisation							
	pEC_{50}				R_{max} (fold over basal)			
Agonist	Oleic Acid	Myristic Acid	GW9508	Met36	Oleic Acid	Myristic Acid	GW9508	Met36
WT	4.0 ± 0.2	4.3 ± 0.1	5.0 ± 0.1	5.3 ± 0.2	1.6 ± 0.1	1.6 ± 0.1	1.6 ± 0.1	2 ± 0.1
Mutant								
R99A	3.5 ± 0.5	N.D.	5.0 ± 0.3	N.D.	1.3 ± 0.1	1.4 ± 0.1	1.4 ± 0.1	1.1 ± 0.1
R178A	4.2 ± 0.4	4.2 ± 0.4	5.0 ± 0.3	N.T.	1.4 ± 0.1	1.5 ± 0.1	1.5 ± 0.1	N.T.
N215A	4.2 ± 0.6	4.3 ± 0.3	4.6 ± 0.3	4.2 ± 0.3	1.2 ± 0.1	1.5 ± 0.1	1.6 ± 0.1	1.7 ± 0.3
W277A	5.5 ± 1.5	4.4 ± 1.8	N.D.	N.D.	0.8 ± 0.1***	1.1 ± 0.2**	1.2 ± 0.2	1.0 ± 0.1
W277F	N.D.	3.9 ± 0.4	4.1 ± 1.3	N.D.	1.2 ± 0.1	1.2 ± 0.1*	1.1 ± 0.1*	1.3 ± 0.1
F311A	3.4 ± 0.6	4.0 ± 0.3	4.7 ± 0.5	5.2 ± 0.1	1.4 ± 0.1	1.3 ± 0.1	1.3 ± 0.1	2.1 ± 0.1

Table 4.4 Potency and maximal internalisation responses of GPR120 mutants to agonists.

EC_{50} values and maximal responses of GPR120 mutants (from Figure 4.12) undergoing internalisation in response to agonist as measured using the confocal plate reader assay. The responses were analysed as fold over basal and pooled from 4 - 6 individual experiments, mean ± S.E.M. Statistical significance was defined using one way ANOVA and Dunnett's post test, * $P < 0.05$; ** $P < 0.01$, *** $P < 0.001$. N.D.-not determined. N.T. - not tested (Met36 data provided by N. Holliday).

4.3 Discussion

4.3.1 Key points from mutagenesis study of GPR120S binding site

The key findings were that R99A abolished GPR120S calcium signalling to both FFAs and synthetic agonists, therefore supporting its role in docking the negative carboxylate group on the ligand, whereas R178A had no effect upon signalling and as such does not play this role. Asn215 appears to be key for interacting with Met36 but not other ligands, whilst F311A had a small non-significant effect on activation, but not as dramatic as perhaps the AZ model suggested. W277A and W277F both suggest that Trp277 has a significant role in GPR120S ligand binding and activation. It should be kept in mind that there are limitations to studying binding sites by comparing signalling responses in different cell lines, even when normalised as fold over basal. Many factors can affect agonist potency and maximum response, such as receptor expression level (which has been monitored in this study) and the efficiency of a receptor coupling to a response can vary, for example in the calcium versus internalisation assays. Other limitations will be covered later in the discussion.

4.3.2 Arg99: the residue that interacts with the acid group of ligands

The R99A mutation, present at the top of TM 2, was postulated to be key for coordination of the carboxylate group on both FFAs and the synthetic GW9508 into the binding site (Sun et al., 2010; Suzuki et al., 2008). As expected, this mutation abolished all calcium signalling. Interestingly, R99A had small fold over basal responses in the internalisation assay. Perhaps this

mutation still allowed some ligand entry bilaterally from the membrane to allow receptor activation as seen in the lipid receptor S1P (Hanson et al., 2012). Additionally, the Banyu compounds lack this carboxylate group (Figure 4.1) but still act as GPR120 agonists. Therefore, there must be other interactions in the agonist binding site that still support binding and activation, so Arg99 may not be essential for all ligands. R99A did affect receptor expression and this would have impacted upon the signalling assays, especially in reducing the receptor reserve which results in agonists being less potent and having reduced maximal responses. However, some GPR120 R99A receptors were still cell surface expressed, so it is therefore unlikely that R99A would have abolished signalling by expression effects alone (Schwartz et al., 1997). However, the low level of R99A expression and the high levels of basal endocytosis might have had an impact upon assessing the agonist-stimulated internalisation of this mutant reliably.

4.3.3 Arg178 does not play a similar role to Arg99

The rationale for creating the R178A mutation was that it was the only other positive residue in the upper half of the GPR120 TM domains, at the top of TM 4 (aside from R99A), and it was thought that perhaps this residue could play a similar role to R99A. In the AZ model, this residue was found to point outwards from the TM bundle and away from the putative binding site, and therefore it was of no surprise that this mutation had no significant effect upon signalling. Therefore this residue does not play a role in interacting with the agonist carboxylate groups. Additionally, this also appears to rule out the

possibility that agonists can interact with different positively charged residues in GPR120 in a ligand selective manner, as has been suggested for the multiple Arg contact points present in FFA1 (Sum et al., 2009; Sum et al., 2007; Tikhonova et al., 2008).

4.3.4 Phe311 was predicted to interact with the phenyl group in the ligand

In the model, Phe311 was shown to be an important feature of the ligand binding site, forming either pi-pi stack interactions (aromatic face to face) in combination with Phe304 either side of the phenyl ring present in nearly all synthetic agonists, or (C-H)-pi donation (edge to face). In the experimental study, this residue made relatively little difference to GPR120S calcium signalling or endocytosis. It may still contribute to docking the ligand into the correct orientation in the pocket and stabilising it there, but has a small effect when compared to other key residues such as Arg99. These small effects included somewhat more transient calcium timecourses in SNAP-GPR120S F311A cells, for example to oleic acid. Perhaps the AZ model overestimates the importance of this residue, for example by basing the structure on a particular "active" β_2AR conformation, rather than the inactive GPCR structures used previously (Shimpukade et al., 2012; Sun et al., 2010). Another issue could be that signal amplification in the calcium assay might compensate for mutation effects, but equally the F311A mutation had no significant effect in the internalisation assay where lower receptor reserve is expected.

4.3.5 The highly conserved Trp277, implicated in class A GPCR activation

Trp277 (Trp 6.48) is in the highly conserved C**W**xP "rotomer" switch, which has been implicated in GPCR activation. When this residue was mutated in β_2AR, NK1, ghrelinR, GPR119 and GPR39 (Holst et al., 2010), the 5-hydroxytrytamine 4 receptor (Pellissier et al., 2009) and the A_3 adenosine receptor (Gao et al., 2002) it abolished agonist induced receptor activation. Interestingly, mutation of this residue in the B_2 bradykinin receptor affected antagonist, but not agonist binding, thought to be due to the antagonist undergoing aromatic interactions with Trp (Marie et al., 2001).

The Trp277 also appears to be an important interaction in the AZ model of GPR120, forming either a hydrogen-bond with the ether-oxygen present in GW9508 or undergoing a charge-donation effect from the pi-orbital of the central aromatic ring present in other synthetic agonists. Additionally, mutation of Trp269 (6.48) in the S1P receptor abolished ERK signalling mediated by CYM-5442 but not S1P, suggesting an interaction between the phenyl ring in the synthetic CYM-5442 structure and the aromatic ring in Trp269 (Hanson et al., 2012).

The W277A mutation had significantly reduced expression levels, but as with R99A, some mutant receptor still reached the plasma membrane, so the lack of function appears to be a real result, and suggests that Trp277 is a key residue in the binding site, in agreement with the AZ model and the previously published model (Shimpukade et al., 2012). This agrees with the idea that agonists are agonists because they have the ability to reach down into the

binding pocket and “knock” the Trp residue, causing receptor activation (see section 1.5.1).

Interestingly the more conservative substitution W277F had no effect on FFA or GW9508 activation of GPR120S calcium signalling, but reduced the potency of Met36 in this assay. This implies the Phe substitution can still undergo pi-pi interactions and maintain receptor activation for some agonists, but was less able to do so with Met36. These decreases in Met36 responses were despite GPR120S W277F receptors being more highly expressed than wild type.

Larger effects of the W277F mutation, for all agonists, were observed when receptor internalisation was the endpoint rather than calcium responses. This may be a consequence of receptor reserve, because for example in a β-arrestin dependent internalisation, 50 % receptors may need to be occupied for a 50 % endocytosis response, if using the canonical stoichiometry of one β-arrestin to one activated receptor (Bayburt et al., 2011; Hanson et al., 2007). In contrast, only a small percentage of the receptors being activated may be required for a full calcium response due to signal amplification, which may mask some mutation effects. Another possibility is that W277F had a greater pathway-dependent effect upon the internalisation pathway, for example like a D_2 dopamine mutant that still mediated G protein signalling, but was incapable of β-arrestin binding (Lan et al., 2009).

4.3.6 Asn215 supports an alternative model for Met36 binding

The original AZ model (Figure 4.3) incorporated a water molecule interacting with the pyrazole (nitrogen ring) of Met36, but in an alternative arrangement

this interaction was mediated by direct contact with Asn215. A previous GPR120 model also implicated this residue in TUG-891 binding (Shimpukade et al., 2012). In addition, this Asn residue flanks the TM 5 Phe216 residue thought to involved in forming and stabilising an interaction with the Trp277 (6.48) rotomer toggle in TM 6, and the N215A mutation could also influence this (Holst et al., 2010).

Consistent with a role for N215A in the calcium signalling assay, N215A selectively inhibited Met36 responses, whilst GW9508 and FFA responses were relatively unaffected (although interestingly all the calcium time courses showed GPR120S N215A desensitising more rapidly than WT). The model supports the idea that GW9508 and Met36 have different conformations of the bi-aromatic rings in the GPR120S binding site. Perhaps, the pyrazole-phenyl of Met36 sits “closer” to Asn215 than the biphenyl of GW9508. Also, perhaps this difference could be key to the change in selectivity from FFA1 selective ligands (such as GW9508) to the GPR120 selective ligands such as Met36 and TUG-891 (Figure 4.13). There was little effect of the N215A mutant in the receptor internalisation assay. This was unexpected because with a reduced receptor reserve in this assay there should have been a greater effect, for example in inhibiting Met36 responses. Perhaps there was a greater level of basal endocytosis of N215A compared to WT, which influenced the results. Another explanation could be that this mutation had a pathway specific effect, that this time was directed against the G protein mediated pathway but not the internalisation pathway.

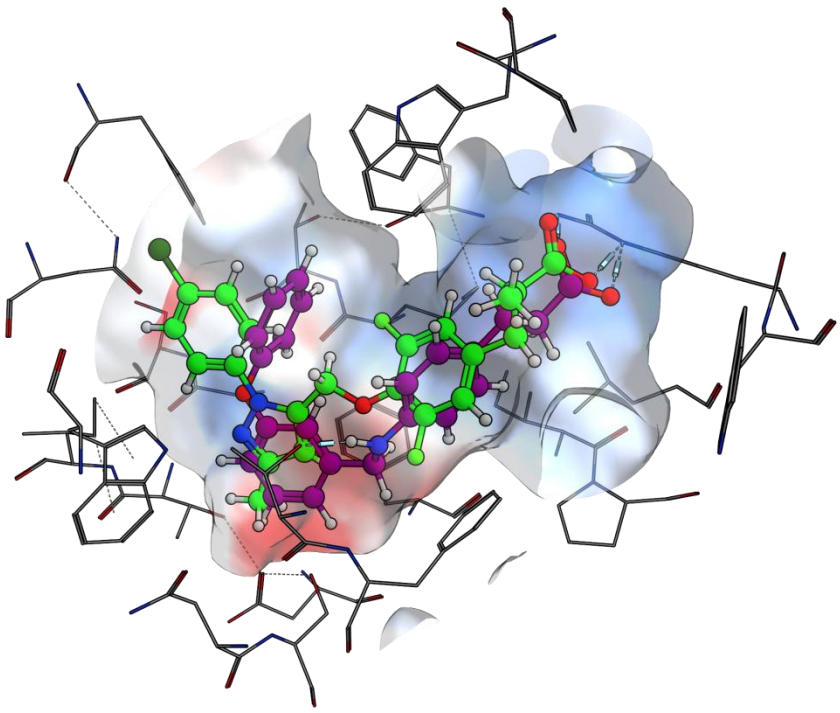

Figure 4.13 The GPR120 binding site with both GW9508 (purple) and Met36 (green) within.

Shows the position of GW9508 (purple ball and stick) versus the position of Met36 (green ball and stick) within the binding pocket of GPR120. Figure provided by Graeme Robb (AZ).

Overall these data broadly support the AZ model of ligand binding, suggesting that Trp277 is implicated in the activation of GPR120 in response to all types of ligand as expected, whilst Asn215 is more involved in interacting with Met36 than fatty acids and GW9508, and Phe311 had relatively little effect.

4.3.7 Limitations of modelling

In one previous study of FFA1, the mutation of Tyr12 abolished all responses to GW9508 and linoleic acid. It was suggested that it does not interact directly with the ligand, but instead contributes to holding the receptor in the correct conformation required for activation (Sum et al., 2007). This brings in the interesting points of if an agonist no longer activates the receptor following mutation, it could be that the mutation has had an effect upon multiple things such as: preventing receptor folding and expression, conformation changes required for activation, coupling between the receptor and effector; *or* has affected the binding site. This highlights the difficulty of using mutagenesis to study binding sites, whereas a direct binding assay would be better (Chapter 5).

Some of these limitations were controlled for in this study, by monitoring receptor expression; and using two assays to measure two signalling pathways, that had both different levels of receptor reserve and were dependent upon coupling with different effectors.

Also, these results have shown that another limitation of receptor modelling is that it is good at defining the overall site, but can sometimes overstate one the importance of one residue, for example Phe311. This may be because the

model is based on the agonist activated β_2AR (Rasmussen et al., 2011a), which gives two main issues. Firstly, that β_2AR is not necessarily that similar to GPR120; and also that protein modifications were introduced into β_2AR to allow for crystallisation, therefore may have altered one of the many "active" conformations of the receptor.

This also brings up the question of whether activated receptors undergo conformational induction or conformational selection, and so which structural template (inactive versus active) is most appropriate for studying agonists which stimulate such conformational changes. Conformation induction is when the agonist plays a role in changing the inactive conformation of the receptor into the active one. Mutations could prevent the agonist from inducing the active conformation of the receptor. Meanwhile, conformational selection is when the receptor spontaneously adopts the active conformation and the ligand binding to this increases the proportion of active conformations, leading to a response. Mutations could alter the equilibrium at which the receptor spontaneously forms the active conformation (Kenakin, 1995). This shows the complications of the use of mutagenesis in the study of binding sites, because effects measured from functional assays may be due to issues such as above, rather than the mutation knocking out the actual binding site *per se*. Arguably though, whilst this study was based upon an active structural template, and a previous study was based upon an inactive one (Shimpukade et al., 2012), a similar range of residues were identified as key in both models, albeit with different agonists used in their identification.

Again, this demonstrates why binding assays are crucial for these types of studies (chapter 5), rather than solely relying on read outs from functional assays.

4.4 Future work

Future work could be to test the effects of the mutations on additional GPR120 signalling pathways, such as GTPγS as a measure of G protein activation, or ERK activation, as GPR120 has been shown previously to signal through ERK (Hirasawa et al., 2005), to give better evidence on whether W277F or N215A substitutions are pathway specific. For example W277F had a greater effect upon agonist stimulated internalisation in comparison to its selective action on Met36 calcium signalling. Additionally, the internalisation results could be complemented by measuring the association of the mutant receptors with β-arrestin2.

Similarly, it would be of interest to test further GPR120 selective compounds, such as the Banyu compounds, to see if compounds without the carboxylate retain activity at R99A. Additionally, other compounds such as NCG21 (Sun et al., 2010) and TUG-891 (Shimpukade et al., 2012) could also be tested, particularly in evaluating the selective effects of N215A on Met36 signalling, in comparison to GW9508. GW9508 and Met36 were shown by the model to have different conformations due to the position of the biphenyl rings (the end phenyl of Met36 sits “closer” to the Phe311 and Asn215 than the end phenyl ring of GW9508), which might explain these differences. Therefore future work could also be to generate a double mutant of N215A and F311A

to give more information on the difference in results between GW9508 and Met36. Mutation of Phe216 could also test the theory that N215A has effects due to affecting the interaction between Phe216 in TM 5 and the Trp277 in TM 6.

Further analysis of the model showed two more key interactions that are predicted to be selective for GW9508 (and not Met36) binding. Phe88 is predicted to undergo phenyl-phenyl ring stacking with the GW9508 biphenyl moiety and Thr310 may interact with the amine linker specific to GW9508.

In the absence of a large effect of F311A, Phe304 could also be mutated, to test the theory that this residue, in conjunction with Phe311, forms stacking interactions with the phenyl proprionic acid pharmacophore of the synthetic ligands. Other residues mentioned in the literature such as Met118 (3.32), Thr119 (3.33), Gly122 (3.36), Phe211 (5.42), Ile280 (6.51) and Ile281 (6.52) imply a large hydrophobic patch, and point mutation of these residues individually may have limited effects.

Chapter Five: Development and characterisation of a novel fluorescent FFA1 agonist

5.1 Introduction

Ligand binding techniques are important for the study of receptor pharmacology because they are one of the main ways to attain the affinity of a ligand for the receptor, by determining Kd, the equilibrium dissociation constant. This is fundamental to the comparison of the activity of different ligands in the drug discovery process, or in exploring the way that a ligand binds to its receptor.

For FFA receptors such as FFA1 and GPR120, using traditional radioligands is difficult, but not impossible as shown by a recent study on determining the binding sites of FFA1 (Lin et al., 2012). This difficulty of determining binding was highlighted in the previous chapter, whereby the binding site of GPR120 had to be investigated indirectly using signalling assays, rather than being able to measure the affinity of the mutant receptors for their agonists directly (Chapter 4). A possible solution to this is using fluorescent ligands. These ligands potentially offer a way of visualising ligand binding at these receptors, and allowing separation of “specific” binding from non-specific interactions such as with cellular membranes.

5.1.1 Advantages of fluorescent ligands for studying GPCR pharmacology

5.1.1.1 The opportunity for single cell pharmacology

The ability to visualise fluorescent ligands, using various microscopy techniques, helps fulfil a need for pharmacology at the "single cell" level rather than a whole population study. This is useful because receptor populations can be heterogeneous, both within cell populations, and even within single cells. For example GPCRs have been shown to exist in signalling scaffolds associated with microdomains such as lipid rafts (Padgett and Slesinger, 2010). FCS is advantageous for measuring these microdomains in the membrane (Cordeaux et al., 2008; He and Marguet, 2011), because it measures the diffusion of a labelled species, and this diffusion can be altered due to the presence of these lipid rafts or other cytoskeletal structures in the plasma membrane, which then allows the extraction of biological information about the underlying receptor interactions.

Fluorescent ligand imaging can also be used to study cell heterogeneity in receptor expression levels, for example in native tissues, and still be able to derive data from the subpopulation of receptor expressing cells (Pramanik et al., 2001). In addition to this, fluorescent ligands have also previously been employed to determine binding kinetics (May et al., 2011), and in high content screening (Stoddart et al., 2012).

5.1.1.2 The study of ligand-receptor complexes

Firstly, fluorescent ligands can be used in the place of a radiolabelled ligand as a probe in a traditional binding assay. A high content screening format is used

on an automated platereader, resulting in images which are then analysed to produce competition curves to obtain IC_{50} estimates for the unlabelled ligands (Stoddart et al., 2012). Additionally, fluorescent ligands can be used in the measurement of binding kinetics on single cells, which in this case also provided additional information about allosteric interactions across a homo-dimer interface (May et al., 2011).

FCS (section 2.2.8), in conjunction with a fluorescent ligand, can also be applied to studying ligand-receptor interactions, due to the nature of the differing speeds of diffusion of different species (Pramanik et al., 2001). As discussed below, this is because the free fluorescent ligand in solution moves faster than ligand in complex with the receptor, which diffuses more slowly through the plasma membrane (Briddon and Hill, 2007). FCS can even be used to undertake binding style studies (Pramanik et al., 2001), and derive dissociation kinetics (Pramanik and Rigler, 2001). FCS has been used to study the diffusion of a variety of GPCRs in complex with a ligand, including β_2AR (Hegener et al., 2004), the galanin receptor (Pramanik et al., 2001) and the adenosine family of receptors (Briddon et al., 2004; Cordeaux et al., 2008).

FCS can also be carried out without the use of modified receptors, for example by measuring the fluorescent ligand instead, because receptors labelled using GFP, SNAP-tag or an antibody are a larger species, with potentially different interactions with cell partners such as the cytoskeleton, which then impact on their diffusion speed. This, together with the fact that FCS is a sensitive technique, also offers potential to measure native receptors

in native cells, such as the A_3 adenosine receptor in neutrophils (Dr. R. Corriden, University of Nottingham, personal communication).

5.1.1.3 Discrimination between modes of binding

FCS also has the ability to discriminate between different modes of binding (Pramanik et al., 2001), especially when using fluorescent ligands compared to the more traditional pharmacology of using radiolabelled ligands. One example of this is where a fluorescent antagonist for the H_1 histamine receptor was demonstrated to significantly associate with the plasma membrane lipids, as well as binding to the receptor (Rose et al., 2012). This is particularly relevant for the study of lipid GPCR binding, where "sideways" entry of the ligand by first entering the cell membrane has been suggested by the crystal structure of the S1P receptor (Hanson et al., 2012).

5.1.2 Principles of fluorescent ligand design

There can be some difficulty in designing fluorescent ligands for GPCRs, which will be discussed in this section. The basic considerations when designing a fluorescent ligand are in 3 parts: pharmacophore, linker and fluorophore (Kozma et al., 2013).

5.1.2.1 Pharmacophore

The pharmacophore represents the molecular features of a ligand that allow it to bind to the binding site of the receptor. This affinity should be maintained when designing a fluorescent ligand, but there is difficulty with designing fluorescent ligands for GPCRs. This is because some receptors have a TM

localised binding site combined with a ligands of low molecular weight, with one example of this being the design of XAC-BY630 for the A_1 adenosine receptor (Briddon et al., 2004). Both the fluorophore and the linker significantly increase the size of the ligand, and this may disrupt the binding of the pharmacophore, or may even form interactions of its own with receptor proteins and other cell constituents.

Additionally, especially for receptors such as the adenosine family, the desired receptor selectivity should be maintained (Kozma et al., 2013). The choice of linker point in the parent compound is also an important consideration, because this chemical manipulation should aim to disrupt affinity as little as possible (Briddon et al., 2011; Kozma et al., 2013).

5.1.2.2 Fluorophore

There are a few determining factors for consideration when choosing a fluorophore for a fluorescent ligand. Firstly, the fluorophore can influence the receptor-pharmacophore interaction due to its size, which can be in the region of 400 to 1,000 Da, and can double the size of the molecule (Briddon et al., 2011). Also, at the A_1 adenosine receptor, it was found that different fluorophores can significantly alter receptor binding of the resultant ligands, whereby a BODIPY labelled ligand was found to have the greatest affinity (Baker et al., 2010). Also, the choice of fluorophore may be dependent upon the experiments that it will be used for, for example the colour may be important if the ligand will be used in conjunction with a labelled receptor.

Also, for FCS, photo physical properties such as excitation and emission spectra are important considerations (Briddon et al., 2011).

Other properties of the fluorophore may be advantageous, for example BODIPY fluorophores are quenched in aqueous solution, which is preferable for live cell experiments; ”free” BODIPY-based fluorescent ligands in solution emit less fluorescence that receptor-bound ligands in a hydrophobic environment (Briddon et al., 2011). BODIPY fluorophores also have a low rate of photobleaching, and there are derivatives (such as BODIPY-630/650), which like Cy5, have far-red fluorescence clearly distinguishable from cellular auto fluorescence (Kozma et al., 2013). Cy5 is less lipophilic than BODIPY630/650, which could be advantageous in minimising non-specific ligand binding to the plasma membrane and other cell lipid environments.

5.1.2.3 Linker

In most cases, the linker region has to be long enough to extend beyond the pharmacophore binding pocket, which can vary from receptor to receptor. For example, peptide receptors have a binding domain on the extracellular amino terminus or extracellular loops, whilst aminergic receptors have binding sites buried deep within the TM helices, that would require a longer linker region.

The linker can also influence the pharmacophore, alter affinity or efficacy (Vernall et al., 2012), and influence the intensity of fluorescent labelling (Middleton et al., 2007). For example, during the design of a fluorescent ligand used at the A_1 adenosine receptor, the linker length was found to affect its pharmacology, whereby ligands derived from the agonist N-ethyl

carboxamido adenosine (NECA) conjugated to a dansyl fluorophore had an increase in affinity and/or efficacy as the linker chain length increased, whilst was opposite was true when the fluorophore was BODIPY-630/650 (Baker et al., 2010).

In summary, fluorescent ligands have their own pharmacological properties such as affinity, efficacy, and subtype selectivity if applicable, which may differ considerably from the parent pharmacophore. They must therefore be treated and characterised as entirely new ligands (Briddon et al., 2011; Middleton et al., 2007).

5.1.3 Principles of FCS and PCH analysis

5.1.3.1 FCS

In FCS, the confocal spot focuses on a small area of interest, such the plasma membrane (area 0.1 – 0.3 μm^2), defining a detection volume (~0.25fl), which is Gaussian in shape. Within this volume, fluctuations in fluorescent intensity are measured as for example fluorescently labelled receptor or ligand diffuse through (Figure 2.15). Autocorrelation analysis of these fluctuations gives quantitative data on the fluorescent particles present. This includes the average number of particles and their average dwell time, τ_D, which in conjunction with knowledge of the size of the confocal volume can then be used to calculate the particle concentration and diffusion co-efficients (D) of the fluorescent species respectively. Autocorrelation analysis is covered in more depth in section 2.2.9.5.1.

Briefly, autocorrelation analysis takes the size of the deviation in a fluctuation (δI) from average intensity at time T and compares it with a subsequent fluctuation at time T + τ. Using the whole range of τ values gives the autocorrelation function, G(τ), which is normalised to the square of the mean intensity, <I>, resulting in an autocorrelation decay curve (see Figure 2.15 C). The dwell time, τ_D, is derived from the halfway point of the G(τ) decay of the autocorrelation function, whilst the particle number, *N*, is derived from its inverse relationship to the amplitude of G_0 (Briddon and Hill, 2007). In an experiment, calibration with a fluorophore of a known diffusion co-efficient, e.g. Cy5 (*D* 3.16 x10^{-10} m^2 s^{-1}), allows the confocal volume and radius ($\omega_0 = 4D_{Cy5}\tau_D)^{1/2}$ to be calculated. This then allows the diffusion co-efficient of the labelled receptor or ligand to be calculated from individual τ_D values using the equation $D=\omega^2_0/4\tau_D$; and the particle concentration can be calculated using $N/(\pi\omega^2_0)$. These values are therefore "normalised" and allow comparison between data sets.

Where multiple fluorescent species are present, with sufficiently different diffusion rates, the resultant autocorrelation curves can be modelled with additive components to obtain estimates of the relevant particle concentrations and dwell times (e.g. τ_{D1}, τ_{D2}, τ_{D3}). In particular these quantitative data are useful because they give information on both the free and receptor bound fluorescent ligand, and multiple receptor diffusing components if present. For example, Cordeaux et al. (2008) used a fluorescent agonist in FCS studies of the adenosine A_3 receptor, in which autocorrelation curves showed three components: τ_{D1} (~ 60 μs) representing diffusion of the

free ligand; together with receptor bound components τ_{D2}, usually in the region of 1-10 ms, and τ_{D3} is >50 ms (Cordeaux et al., 2008). Generally, there are also additional short lived components to be accounted in the autocorrelation curves, that derive from fluorophore photophysics. These can range from 1 – 10 μs (for fluorophores such as Cy5), to up to 1 ms (for fluorescent proteins such as GFP or YFP).

There are some limiting factors to measuring receptor diffusion. When studying membrane localised receptors, there is also a limit to the two dimensional model because it assumes a "flat" 2D plasma membrane, that in reality is a more complex three dimensional structure with molecules that diffuse in 3D within it. Additionally, there is a limit to the separation of species with differing diffusion rates based solely on molecular weight, due to the cube root relationship between the change in mass causing a change in diffusion co-efficient (Briddon and Hill, 2007). For example an 8 fold change in molecular mass of the species being measured will only result in a ~2 fold change in the diffusion co-efficient. For small molecular weight fluorescent ligands, the diffusion co-efficient can distinguish between free ligand and ligand-bound to receptor, because this change in molecular mass is large enough to cause a detectable change in the diffusion co-efficient. However, FCS is not generally appropriate to determine the presence of receptor dimers versus monomers (2 fold change in mass). However this is also why small changes in measured D can still result from significant changes in the molecular composition of receptor complexes. The measurement of particle concentration works best at low particle concentrations (because the

fluctuations in intensity are relatively larger and generate a higher amplitude of the autocorrelation curve), and this means FCS is sensitive enough to study low fluorescent ligand or receptor concentrations, for example in native cells, where more traditional binding methods would be challenging. Finally, the largest limitation with FCS is that in order to be detected, the fluorescent species must be moving to generate fluctuations. Therefore, stationary receptors, for example attached to the static cytoskeleton, would not be detected by FCS.

5.1.3.2 PCH

From the same fluorescence intensity data set collected over time (e.g. 15 s), photon counting histogram (PCH; covered in depth in section 2.2.9.5.2) analysis can also be applied. Briefly, PCH analysis depends upon the variation in amplitude rather than over time (in comparison to FCS autocorrelation analysis) and can provide a different calculation of the particle concentration. In addition, it also gives information on molecular brightness (ε), the brightness of each species (Chen et al., 1999).

This analysis is useful because it is perhaps more sensitive in determining the stoichiometry of the fluorescent complexes, because if the fluorescent species contains 2 labelled receptors instead of 1, the diffusion co-efficient might not change significantly (see above), but ε is expected to double.

5.1.4 Aims

One of the issues with fatty acid receptor drug discovery, for example at FFA1 and GPR120, is the highly lipophilic nature of their ligands which poses problems in the generation of specific, high-affinity radiolabelled ligands. Without these, traditional pharmacology such as radioligand binding is more challenging, preventing generation of data key to drug discovery such as equilibrium dissociation constants measuring ligand affinity. This study hoped to address this for FFA1 and GPR120, by replicating the traditional binding assay through characterisation of a novel fluorescent ligand based on GW9508, before exploring the mechanism of fluorescent ligand:receptor interactions by FCS and PCH techniques.

5.2 Results

5.2.1 Ligand characterisation in terms of calcium responses

CellAura technologies (Nottingham, UK) synthesised a number of analogues of GW9508 with 3 different types of linker and 2 different fluorophores (BODIPY630/650 and Cy5). These were screened for FFA1 activity in preliminary calcium signalling assays (data not shown). This process led to the choice of the ligand 40Ag-Cy5, which was then examined in more detail. The detailed structure of 40Ag-Cy5 is not shown for confidentiality reasons.

Firstly, this ligand, along with its precursor congener (the ligand without the fluorescent Cy5 addition; abbreviated to 40Ag-Cg) were both tested for their ability to stimulate calcium responses via both FFA1 and GPR120. Calcium responses were observed in HEK293TR FLAG-tagged FFA1 cells to 40Ag-Cy5 and its congener (in HBSS in the absence of BSA), with pEC_{50} values of 5.7 ± 0.1 and 7.8 ± 0.4 respectively, compared to a pEC_{50} of 8.3 ± 0.6 for GW9508 responses. No responses were observed to 40Ag-Cy5 when cells were not pre-treated with tetracycline to induce FFA1 expression (Figure 5.1 A; n=4). The presence of 0.02 % BSA in this assay, had little effect on the ligand pEC_{50} values at FFA1 (Figure 5.1 B; Table 5.1; n=4). In contrast 40Ag-Cy5 was inactive at FLAG-tagged GPR120S, at up 10 µM, compared to the GW9508 pEC_{50} of 6.0±0.2 (Figure 5.1 C; n=4). This showed that 40Ag-Cy5 retained GW9508 selectivity for FFA1 over GPR120S.

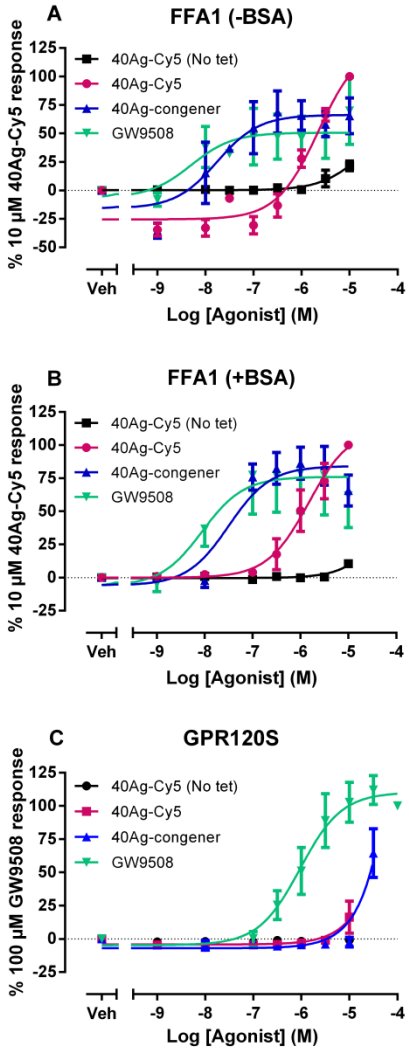

Figure 5.1 Calcium mobilisation responses of FLAG-tagged FFA1 and GPR120S to 40Ag-Cy5, its congener and GW9508 show 40Ag-Cy5 selectivity at FFA1 over GPR120S.

The ability of 40Ag-Cy5 and its congener to elicit intracellular calcium responses at FFA1, both in the absence (A) and presence (B; 0.02 %) of BSA and also at GPR120 (C) was measured in tetracycline (tet) inducible HEK293TR cells by Fluo4 mobilisation. The FFA1 data were normalised (%) to the 10 µM 40Ag-Cy5 response, whilst the GPR120S data were normalised (%) to the 100 µM GW9508 response. These peak responses were pooled from a minimum of 4 individual experiments, mean ± S.E.M.

	pEC_{50} with 0.02 % BSA	pEC_{50} without BSA
40Ag-Cy5	5.8 ± 0.2	5.7 ± 0.1
40Ag-Congener	7.5 ± 0.3	7.8 ± 0.4
GW9508	8.1 ± 0.5	8.3 ± 0.6

Table 5.1 Potency values of 40Ag-Cy5, its congener and GW9508 at FLAG tagged FFA1 receptors from the characterisation of the fluorescent ligand in the calcium assay.

pEC_{50} values were obtained from the concentration response curves in Figure 5.1 A and B, pooled from a minimum of 4 individual experiments, mean ± S.E.M.

5.2.2 Using the fluorescent ligand 40Ag-Cy5 in a binding assay format

Next 40Ag-Cy5 was used in a binding assay using HEK293TR FLAG-FFA1 cells, to test the theory that this fluorescent ligand could be used in an assay analogous to radioligand binding. The principle is similar to radioligand binding. HEK293TR FLAG-FFA1 cells were first briefly pre-treated (5 min; to try to ensure true equilibrium conditions) with a non-fluorescent competing ligand. 40Ag-Cy5 was then added and allowed to reach equilibrium binding (optimised as 30 min at 37°C, data not shown), then the cells were imaged live on an automated plate reader (Stoddart et al., 2012). From the images (Figure 5.2), it can be seen that as the concentration of the competing ligand increased, fluorescent 40Ag-Cy5 binding decreased. To these images, a modified version of the granularity analysis was applied to maximise the signal to noise ratio when quantifying fluorescence intensity. Small "pits" quantified cell-bound fluorescent ligand, predominantly localised to the cell surface (granules 1-2 µm in diameter); while larger "vesicles" excluded the larger, non-bound aggregates of ligand (granules > 5 µm in diameter; Figure 5.3). Cells without tetracycline treatment displayed low levels of fluorescent ligand binding and were used to set the negative control (0 %), whilst the totals (tet treated cells, with no competing ligand) were set as the positive control (100%; Figure 5.2, 5.3).

Firstly, the assay was optimised, by comparing 40Ag-Cy5 binding and its displacement in HBSS buffer with 0.02 % BSA and without BSA. Interestingly, in comparison to the calcium signalling assay, in which 0.02 % BSA had no

effect upon ligand potency, here it can be seen that the addition of BSA, reduced total cellular binding in the presence of 100 nM 40Ag-Cy5 (Figure 5.2). Subsequently, binding experiments were performed in the absence of BSA, unless otherwise stated. Following this, paired competition curves were carried out using the antagonist GW1100 (Figures 5.3, 5.4). This allowed for the estimation of the dissociation constant of 40Ag-Cy5. Two sets of displacements were carried out (in the absence of BSA) using 1 µM or 100 nM 40Ag-Cy5. This gave two IC_{50} values for GW1100, of 2.2 ± 0.2 and 1.1 ± 0.2 µM respectively, from the pooled data (Figure 5.4). This allowed for the simultaneous solution of the Cheng-Prusoff equation (section 2.2.9.4) for each curve, resulting in an estimation of 0.6 µM for the dissociation constant (K_{FL}) of 40Ag-Cy5 at FFA1 receptors. This knowledge of the dissociation constant of 40Ag-Cy5 at FFA1 in principle allowed for K_i values to be estimated for the competing ligands, again using the Cheng-Prusoff equation for conversion from the IC_{50}s of the displacement curves. A selection of known FFA1 synthetic agonists (GW9508, TZDs) and an antagonist were tested as competing ligands in this assay to test for their displacement of 40Ag-Cy5 binding (Figure 5.5), and pIC_{50} values and K_is were calculated (Table 5.2). Interestingly, oleic acid did not displace 40Ag-Cy5 binding at concentrations up to 300 µM, and in fact the presence of oleic acid led to increased 40-AgCy5 binding in the assay. Increasing the oleic acid pre-treatment time (to either 15 min or 30 min) did not alter the lack of 40Ag-Cy5 displacement observed (data not shown).

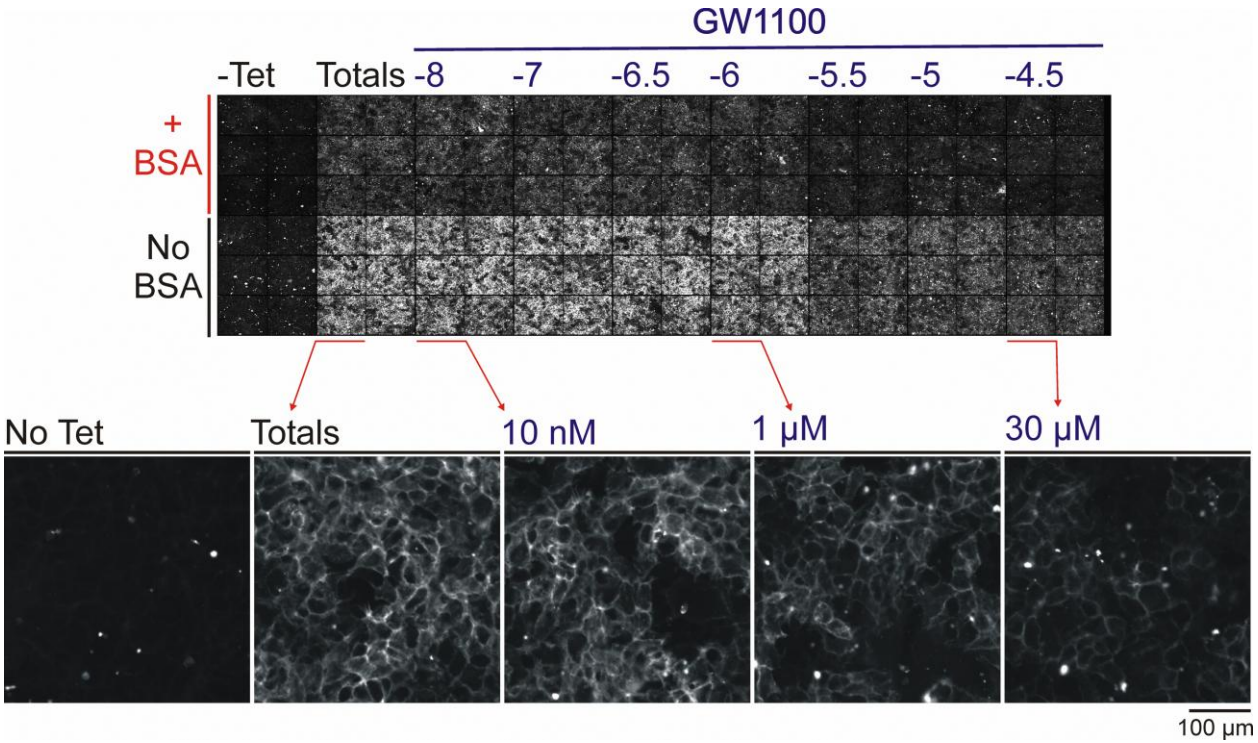
GW1100
-Tet
Totals
-8
-7
-6.5
-6
-5.5
-5
-4.5
+
BSA
No
BSA
No Tet
Totals
10 nM
1 µM
30 µM
100 µm

Figure 5.2 A representative plate map showing increasing concentrations of GW1100 displacing 40Ag-Cy5 from binding.

HEK293TR FLAG-FFA1 cells were pre-treated with unlabelled ligand for 5 min at 37°C, followed by 1 µM 40Ag-Cy5 for 30 min at 37°C in HBSS in the presence or absence of 0.02 % BSA. Cells were immediately imaged live on the IX Ultra platereader (2 horizontal sites / well, < 10 min read time), without an intervening wash step. The top section shows the plate map (10 wells (20 sites) x 6 wells), with the top 3 rows in the presence of BSA and the bottom 3 rows in the absence of BSA. The far left column shows low fluorescent ligand binding in the absence of receptor expression (-tet), whilst the next column depicts the "totals" which is 40Ag-Cy5 binding in the absence of any competing ligand. The following 7 columns show the displacement of 40Ag-Cy5 binding in the presence of increasing concentrations of GW1100 (indicated as log M). The bottom section shows enlarged individual images, with identical level adjustments, to show 40Ag-Cy5 binding and its displacement with greater clarity.

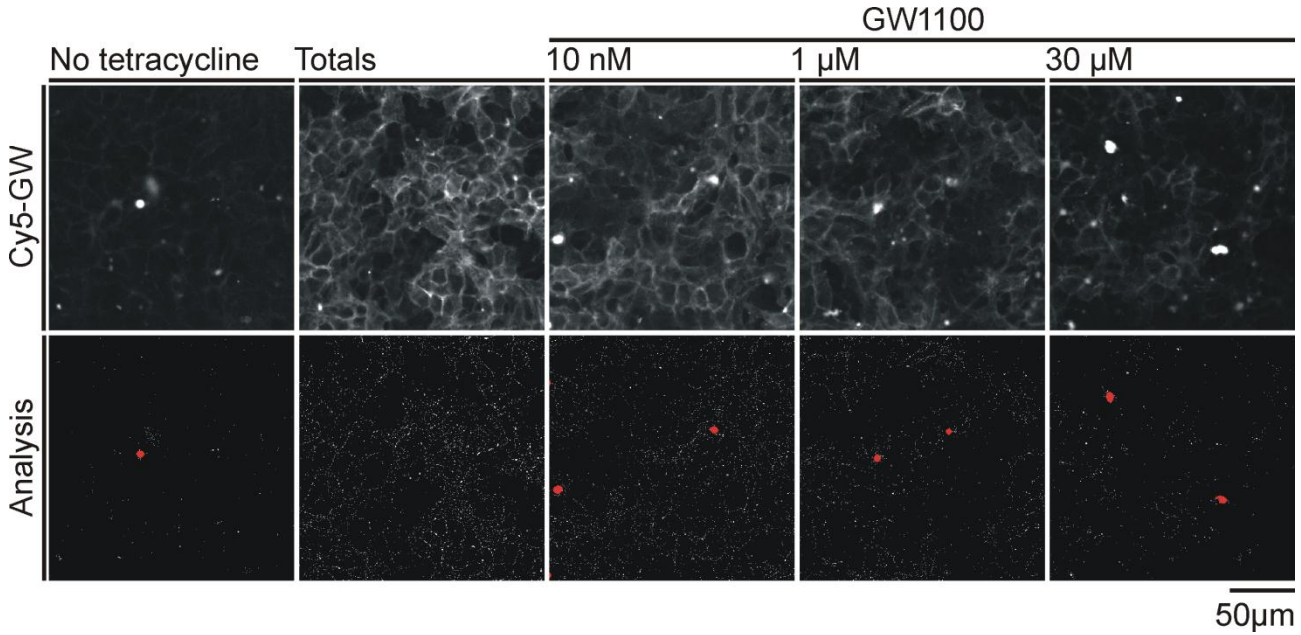

Figure 5.3 Representative images and quantitative analysis of specific 40Ag-Cy5 binding to FFA1 receptors.

Images illustrate an example experiment performed as described in Figure 5.3, using 100 nM 40AG-Cy5 and incubation media lacking BSA. The top row shows (L-R) (i) HEK293TR FLAG-FFA1 cells that have not undergone tetracycline induction of FFA1 expression; (ii) tetracycline-induced cells labelled by 40AG-Cy5 that have not undergone competing ligand treatment (totals) and (iii) competition for 40Ag-Cy5 binding by increasing concentrations of GW1100 as indicated. The bottom row shows representative granularity analysis applied to these images. This analysis measured fluorescent ligand binding as the pit count ("white dots," granules 1-2 µm in diameter) whilst excluding the larger aggregates ("red dots", > 5 µm in diameter). When quantifying and pooling data, binding in the absence of tetracycline was set as the negative control (0 %), whilst the totals were set as the positive control (100 %).

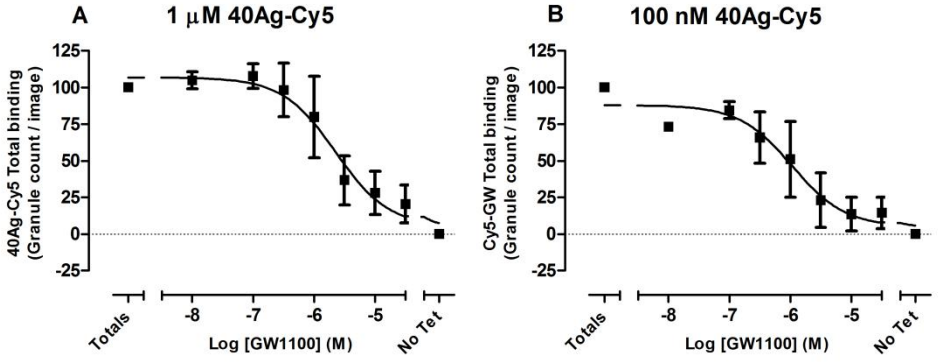

Figure 5.4 Paired GW1100 competition curves enable estimation of 40Ag-Cy5 dissociation constant at FFA1 receptors.

Two displacement curves (no BSA) were performed by pre-treating tetracycline induced HEK293TR cells expressing FFA1 with increasing concentrations of GW1100 for 5 min at 37^{o}C, followed by 30 min treatment at 37^{o}C with 1 μM or 100 nM 40Ag-Cy5. These paired curves gave GW1100 IC_{50} values of 2.2 and 1.1 μM respectively. Simultaneous solution of the Cheng-Prusoff equations for each curve (shown in text, section 2.2.9.4), gave an estimate of the 40Ag-Cy5 dissociation constant for FFA1 receptor (K_{FL}) of 0.6 μM. The data were normalised (%) to the 1 μM (A) or 100 nM (B) 40Ag-Cy5 "total" response and were pooled from 2 individual experiments, mean ± S.E.M.

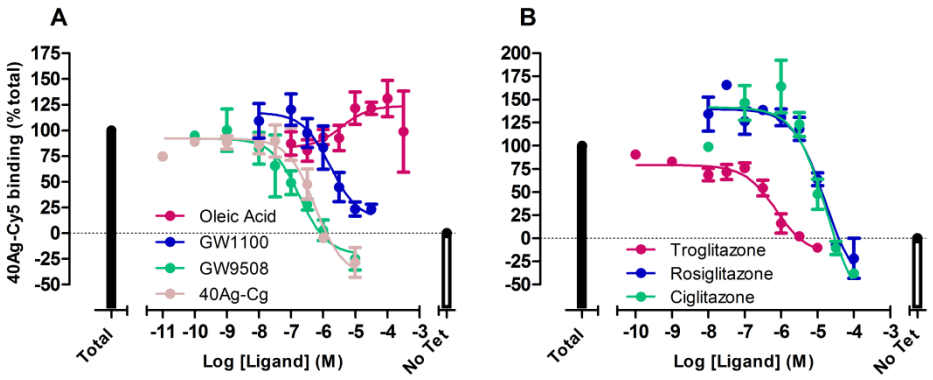

Figure 5.5 Binding curves show the displacement of 40Ag-Cy5 binding to FLAG-tagged FFA1 receptors following the pre-treatment of a competing ligand.

HEK293TR cells induced to expressing FFA1 were pre-treated for 5 min at 37^{o}C with competing ligands: oleic acid, GW1100, GW9508 or 40Ag-congener (A) or the thiazolidinediones troglitazone, rosiglitazone and ciglitazone (B). They were then treated with 40Ag-Cy5 for 30 min at 37^{o}C and were immediately imaged live. The data were normalised (%) to the 100 nM 40Ag-Cy5 "total" response and were pooled from a minimum of 3 individual experiments, mean ± S.E.M. Fitted IC_{50} curves yielded the affinity estimates in Table 5.2.

Ligand	pIC_{50} (-Log M)	K_i (μM)
GW1100	5.8 ± 0.3	1.42
40Ag-Congener	6.1 ± 0.2	0.66
GW9508	6.8 ± 0.2	0.13
Troglitazone	6.1 ± 0.2	0.62
Rosiglitazone	4.8 ± 0.2	13.5
Ciglitazone	4.8 ± 0.2	14.6
Oleic Acid	N.D.	N.D.

Table 5.2 pIC_{50} and K_i values of competing ligands at the human FFA1 receptor. pIC_{50} values were fitted from the pooled displacement (n = 3+) curves in Figure 5.5. The estimation of K_{fl} from the paired GW1100 displacement curves (Figure 5.4) was also used to apply the Cheng-Prusoff conversion to competing ligand IC_{50} values, yielding the indicated K_i estimates. N.D. no displacement obtained.

5.2.3 Diffusion of FFA1 using FCS of SNAP-labelled receptors and bound 40Ag-Cy5

5.2.3.1 Optimisation of FCS at SNAP-surface labelled FFA1 receptors

To obtain reference measurements of FFA1 receptor diffusion, FCS was first performed using SNAP-surface BG-647 (0.1 or 0.5 µM) labelled HEK293TR cells expressing SNAP-tagged FFA1 receptors (representative FCS read in Figure 5.6). Firstly, the position of the upper and lower plasma membrane was determined by performing a confocal z scan by positioning the scan in xy on the nucleus (Figure 5.6 A). The confocal volume was placed on the upper plasma membrane for FCS readings (dotted line in 5.6 A). Next, the fluorescent fluctuations were recorded, typically 3 x 15 s reads at 0.7 % laser power, following a 15 s prebleach at 0.5 % laser power (Figure 5.6 B). These data were then fitted to an autocorrelation 2 component 2 dimensional model (Figure 5.6 C), and the deviation from this fit was also plotted (Figure 5.6 D).

In evaluating this model, the fast τ_{D1} component 1 (~100 µs dwell time) was interpreted as free SNAP-surface label that remained after washing the cells, whilst τ_{D2} (component 2) was interpreted as labelled SNAP-FFA1 receptors in the membrane. From the autocorrelation analysis, diffusion co-efficients (D) were derived, which normalised the dwell time (τ_{D1} or τ_{D2}) to the confocal volume calculated in the calibration for that day's experiment, and allows for comparison with estimates for other labelled receptors. As expected, D for component 1 or 2 did not alter when SNAP-surface fluorophore concentration

was increased from 0.1 to 0.5 µM (Figure 5.7 A&B). Interestingly, there was a statistically significant increase in particle concentration in component 2 following the increase in SNAP-surface label concentration (Figure 5.7 D; 53 – 69 cells from 5 individual experiments).

In the course of these experiments, the laser power used to measure fluorescent fluctuations was also optimised. Four different laser powers at 633 nm were used: 0.5 % (0.249 µW), 0.7 % (0.423 µW), 1 % (0.748 µW) and 2 % (1.410 µW; laser power determination carried out by Dr. S.J. Briddon, University of Nottingham). Component 2 D, which measured the diffusion co-efficient of SNAP-surface labelled FFA1 receptors, significantly increased when laser power was increased from 0.5 % to 2 %, as expected because higher laser powers would be predicted to increase fluorophore bleaching, and shorten the apparent dwell time of the species in the confocal volume (Figure 5.8 B). Also, the particle concentration of component 2 significantly decreased when laser power was increased from 0.5 % to 2 % (Figure 5.8 D). From this, 0.5 µM SNAP-surface BG-647 was the chosen concentration to label the SNAP-FFA1 receptors, and 0.7 % laser power was subsequently used to measure the fluorescence fluctuations. Finally the effect of agonist (1 µM GW9508, pre-treated for 5 min at 22°C) on SNAP-FFA1 receptor diffusion was assessed. This treatment significantly increased the particle concentration for this component (Figure 5.9 B; 58 cells from 4 individual experiments).

These data were also analysed using a 2 component PCH analysis, which determined the molecular brightness and concentration of the diffusing

species. Representative traces show that the 2 component model fit the control data (receptors labelled with 0.1 µM / 0.5 µM SNAP-surface BG-647) better than the 1 component model (Figure 5.10 A). Since the bin time chosen (1 ms) should exclude the contribution of free SNAP-surface label to the PCH histogram (component 1 described in FCS traces above), both PCH components were interpreted as SNAP-surface labelled receptor-containing particles. Interestingly, when 0.5 µM SNAP-surface BG-647 was used to label FFA1, this shifted the curve further right, as would be expected with increased particle concentration (Figure 5.10 B). Indeed, the estimated particle concentration of both component 1 and 2 were found to be significantly increased for 0.5 µM SNAP-surface BG-647 labelled FFA1 (Figure 5.10 C & D). Also, the molecular brightness for component 1 (SNAP-surface labelled FFA1 receptors) was found to almost double as the SNAP-surface BG-647 labelling concentration increased from 0.1 to 0.5 µM, from 2486 ± 275 to 4126 ± 948 cpm s^{-1} (Figure 5.10 E & F; 59 – 66 cells from 5 individual experiments). PCH analysis found no significant difference when BG-647 labelled FFA1 was treated with 1 µM GW9508 compared to vehicle (Figure 5.11; 58 – 61 cells from 4 individual experiments).

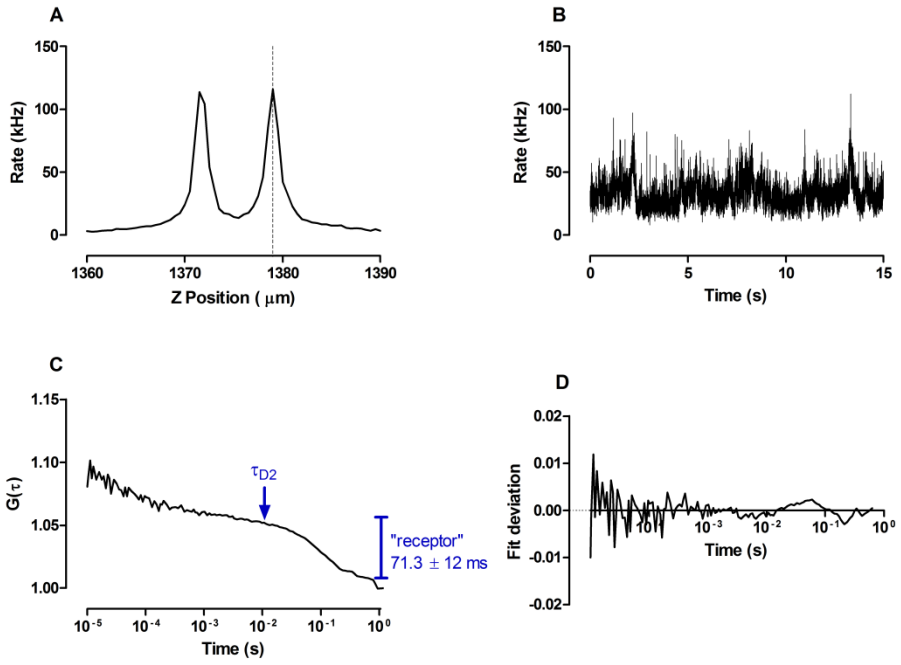

Figure 5.6 FCS measurements of the lateral mobility of SNAP-FFA1 receptors labelled with 0.5 µM SNAP-surface BG-647.

A shows the confocal Z scan, which identified the upper and lower plasma membrane in SNAP-surface BG-647 labelled HEK293TR SNAP-FFA1 cells, with the dotted line showing where the confocal volume was placed for FCS readings. Next, fluorescent fluctuations were recorded 3 x 15 sec at 0.7 % laser power on the upper plasma membrane, following a 15 sec prebleach at 0.5 % laser power, all at 22^{o}C (an example record shown in B). Finally, the data were fitted to an autocorrelation curve using a 2 component 2 dimensional diffusional model (C) and also the deviation from the fit of the autocorrelation (D). This resulted in a SNAP-FFA1 receptor dwell time (τ_{D2} of 71.3 ± 12 ms; 53 cells from 5 individual experiments).

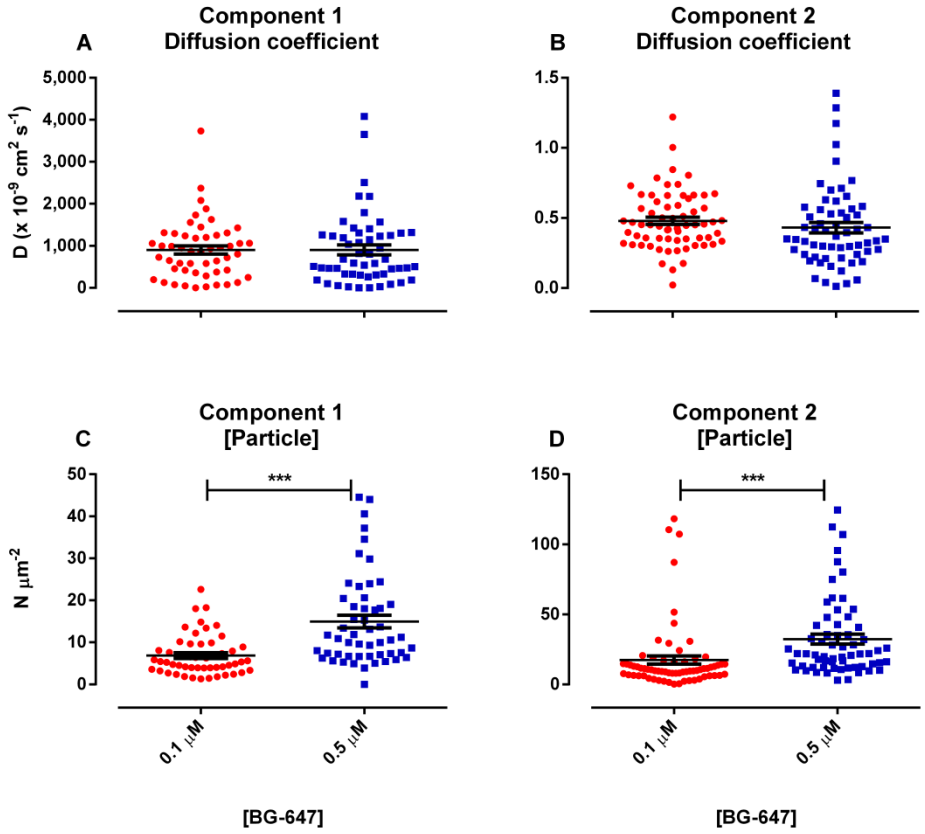

Figure 5.7 HEK293TR cells expressing FFA1 were labelled with either 0.1 or 0.5 µM SNAP-surface BG-647, and their diffusion measured using FCS.
Scatter plots show the pooled data points (individual values, and mean ± s.e.m.) for diffusion co-efficients (abbreviated to D) for component 1 (A, interpreted as free SNAP-surface label) and 2 (B, interpreted as SNAP-FFA1 diffusion) derived from the model; and the particle concentrations for component 1 (C) and 2 (D) from FCS experiments in HEK293TR cells expressing FFA1 (53 – 69 cells from 5 individual experiments) and labelled with 0.1 and 0.5 µM SNAP-surface BG-647. Statistical significance was determined using a Matt-Whitney test, *** P <0.001.

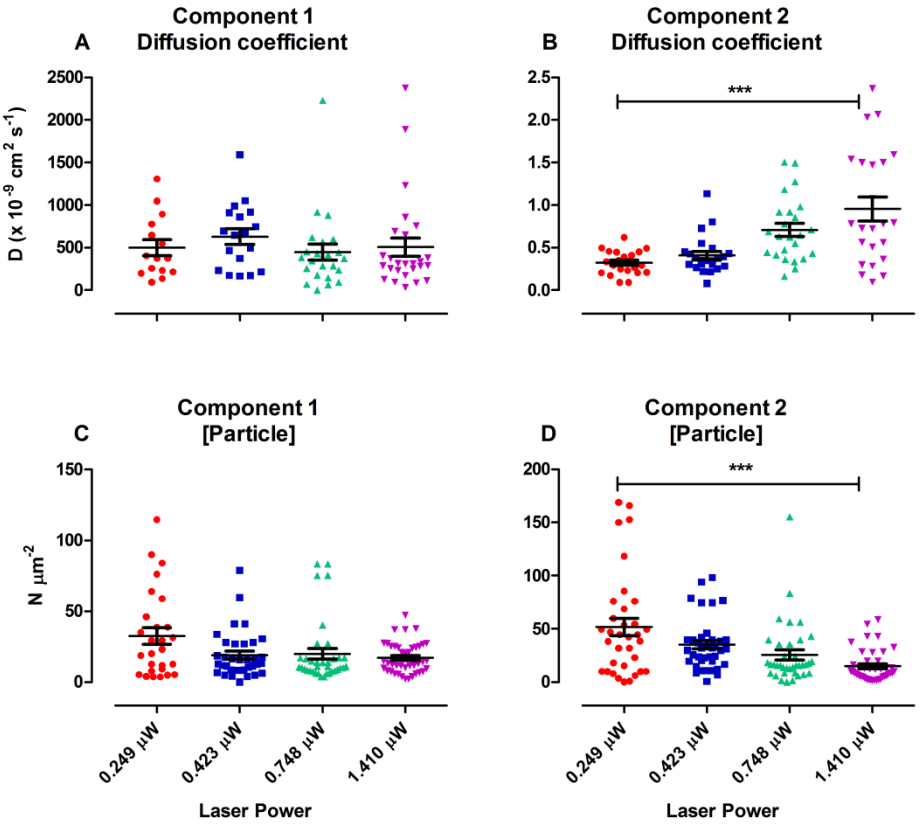

Figure 5.8 HEK293TR cells expressing FFA1 were labelled with 0.5 µM SNAP-surface BG-647 and their diffusion measured using FCS at 0.5, 0.7, 1 and 2 % laser power.

Scatter plots show the pooled data for diffusion co-efficients (abbreviated to D) for component 1 (A) and 2 (B) derived from the autocorrelation model; and the particle concentrations for component 1 (C) and 2 (D) from FCS experiments in HEK293TR cells expressing FFA1 (15 – 42 cells from 2 individual experiments) and labelled with 0.5 µM SNAP-surface BG-647. Statistical significance was determined using a Kruskal Wallis test with Dunn's multiple comparisons post test, *** $P < 0.001$.

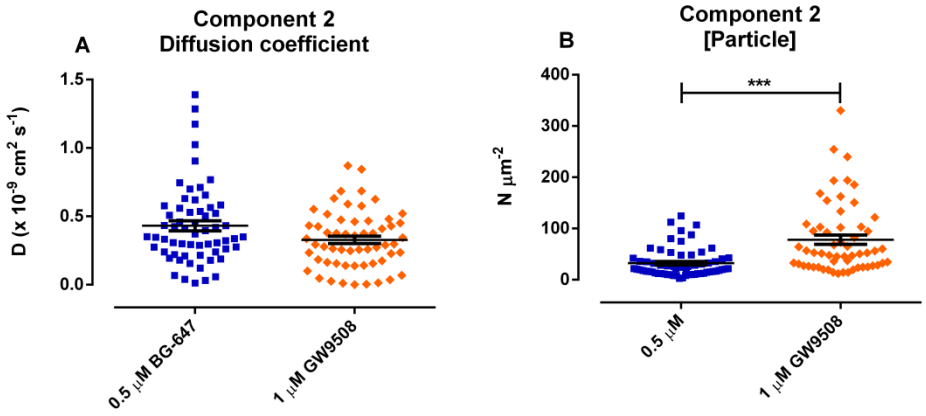

Figure 5.9 Effect of 1 µM GW9508 agonist treatment on the lateral mobility of SNAP-FFA1 receptors in HEK293TR cells, measured by FCS.

Scatter plots show the pooled data for diffusion co-efficients for component 2 (A) of the model; and the particle concentration for component 2 (B) from FCS experiments in HEK293TR cells expressing SNAP-FFA1 receptors (58 – 61 cells from 4 individual experiments), pre-labelled with 0.5 µM SNAP-surface BG-647 and treated with vehicle or 1 µM GW9508. Statistical significance was determined using a Kruskal Wallis test with Dunn's multiple comparisons post test, *** $P < 0.001$.

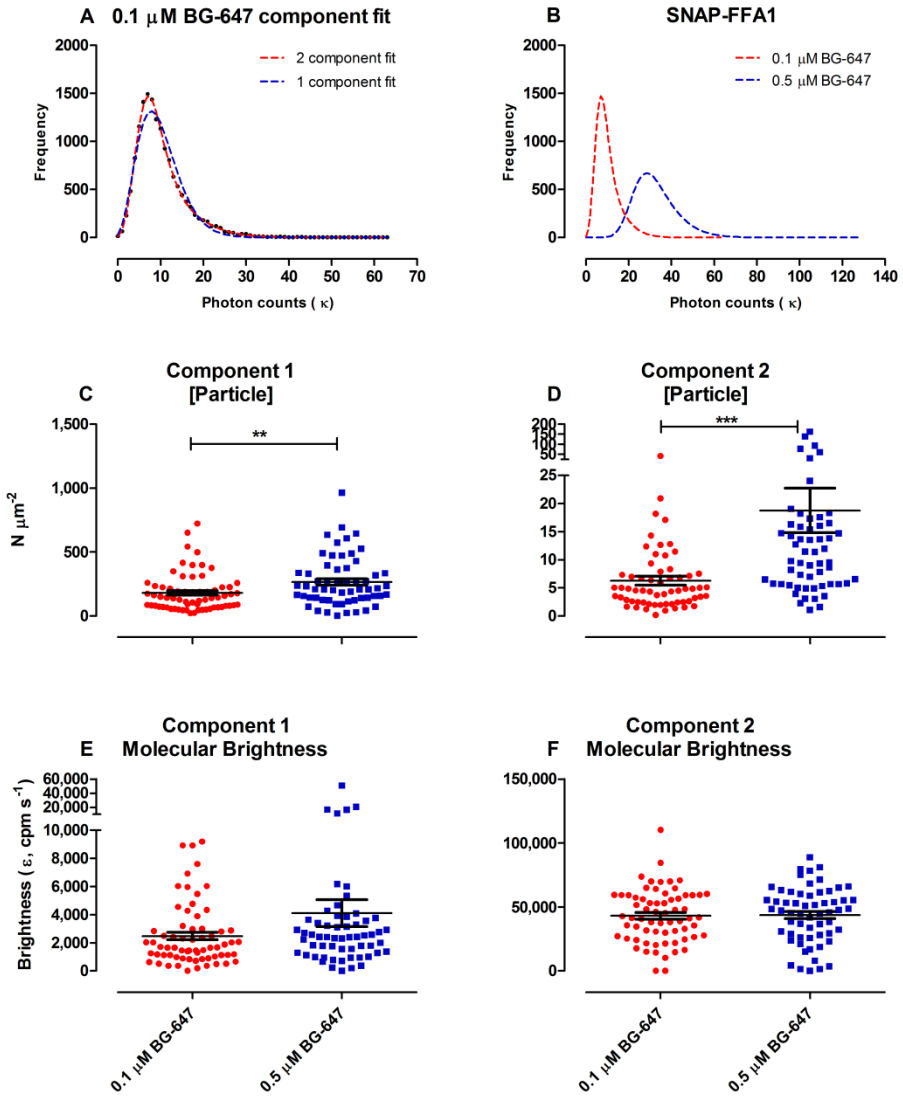

Figure 5.10 Photon counting histogram (PCH) analysis estimates of particle concentration and molecular brightness of 0.1 or 0.5 µM SNAP-surface BG-647 labelled SNAP-FFA1 receptors in HEK293TR cells.

Representative 1 and 2 component fits of PCH analysis of HEK293TR cells expressing SNAP-FFA1 and labelled with 0.1 µM SNAP-surface BG-647 (A); whilst representative traces of the 2 component fits to data from SNAP-FFA1 cells labelled with 0.1 or 0.5 µM SNAP-surface BG-647 labelled FFA1 (B). From this analysis, scatter plots show pooled data for the PCH obtained particle concentrations for component 1 (C) and 2 (D) – both of which were interpreted as SNAP-surface labelled receptor species; and the molecular brightness for component 1 (E) and 2 (F) (59 – 66 cells from 5 individual experiments). In the PCH analysis, bin time was set to 1 ms. Statistical significance was determined using a Matt-Whitney test, ** $P < 0.01$, *** $P < 0.001$.

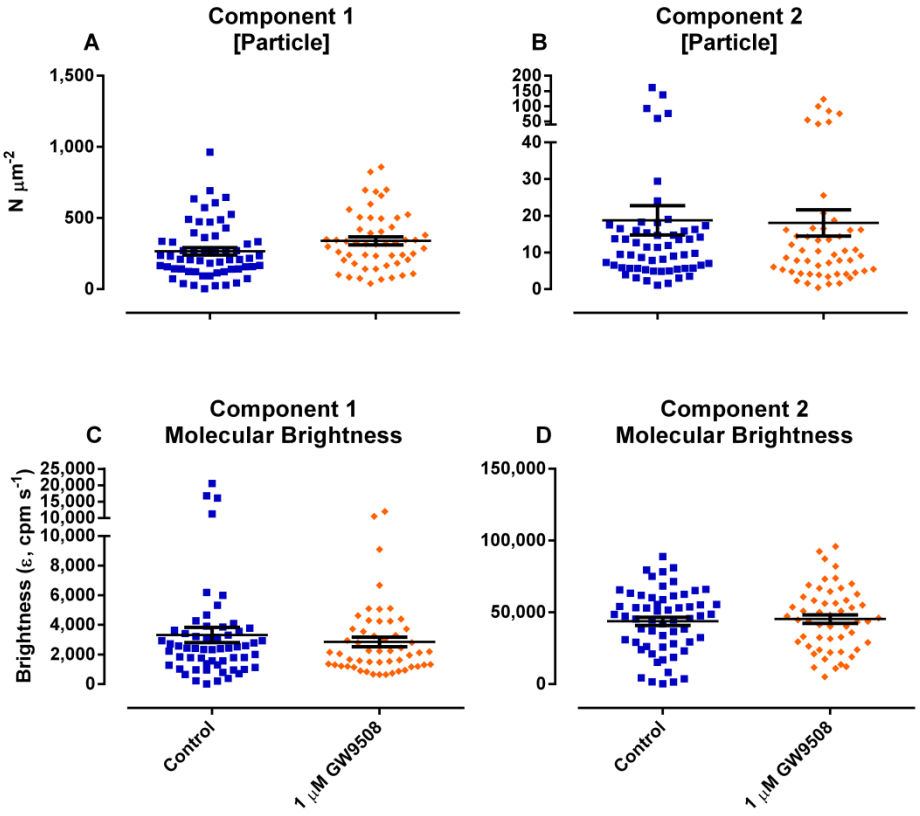

Figure 5.11 Photon counting histogram (PCH) analysis of particle concentration and molecular brightness of SNAP-FFA1 receptors in cells treated with vehicle or 1 µM GW9508.

Scatter plots show the pooled data for particle concentrations for component 1 (A) and 2 (B); and the molecular brightness for component 1 (C) and 2 (D) from FCS experiments in HEK293TR cells expressing FFA1 (58 – 61 cells from 4 individual experiments), labelled with 0.5 µM SNAP-surface BG-647 and treated with vehicle or 1 µM GW9508. In the PCH analysis, bin time was set to 1 ms.

5.2.4 FCS studies of 40Ag-Cy5 at SNAP-surface labelled FFA1

Next, diffusion of the fluorescent ligand, 40Ag-Cy5 was measured free in HBSS solution. The diffusion of both 10 and 100 nM 40Ag-Cy5 were measured in the absence and presence of 0.02 % BSA. As expected, a ten fold increase in ligand concentration from 10 nM (+ 0.02 % BSA) to 100 nM (+ 0.02 % BSA) caused a concomitant 10 fold increase in particle concentration, from 3.5 ± 0.2 to 33.7 ± 2.8 N/μm^2 (Figure 5.12; 31 – 45 cells from 3 - 5 individual experiments). At the highest concentration (100 nM), the presence of BSA increased the dwell time (Figure 5.12 A) and also reduced the diffusion co-efficient of 40Ag-Cy5 in solution. From these data, the dwell time of 112 ± 22 µs, as measured for 100 nM without BSA, was used as the constant for "free ligand" in later autocorrelation data from cells.

Then, HEK293TR cells expressing SNAP-FFA1 were labelled with 40Ag-Cy5 (5 min at 22°C) in HBSS in the absence of BSA and FCS recordings made. Pre-labelling of SNAP-FFA1 with SNAP-surface AF-488 was also undertaken to enable easy identification by initial epifluorescence microscopy, and to remove any bias in selecting fluorescent ligand labelled (or unlabelled) cells. This wavelength was also used to measure the confocal z scan and determine the position of the upper plasma membrane. In these experiments, the confocal volume was placed one 0.5 µm step above the upper membrane, to take into account the differences between 488 nm (SNAP-surface labelled FFA1) and 633 nm (40Ag-Cy5) laser lines.

Representative FCS traces from SNAP-FFA1 receptor cells treated with 100 nM 40Ag-Cy5, in the absence or presence of 1 μM GW1100 (10 min at 22^{o}C) are shown in Figure 5.13 and Figure 5.14 respectively. In each figure, the confocal z scan for a representative cell is shown (A), complete with the position of where the confocal volume was placed, which was offset slightly above the upper membrane (dotted line in A). Also shown are the raw fluorescent fluctuations of FFA1 treated with 100 nM 40Ag-Cy5 (B), the autocorrelation curve (C) of the data fitted to a model that encompassed 3 dimensional diffusion of the ligand with a single component 2 dimensional diffusion of the receptor (unless otherwise stated), and the deviation from this model (D). τD1 (the fast 3D component representing free ligand) was set constant at 112 μs from earlier measurements of 40Ag-Cy5 in solution (Figure 5.11 A) whilst τ_{D2} was interpreted as 40Ag-Cy5-bound receptor.

In the pooled FCS data (Figure 5.15), increasing concentrations of 40Ag-Cy5, from 25 – 100 nM, resulted in higher observed particle concentrations for both free ligand (component 1) and bound ligand (component 2), but did not change the diffusion co-efficient of the FFA1 receptor bound ligand significantly (Figure 5.15 B). These diffusion co-efficient estimates were approximately 4 times faster than those measured for SNAP-surface BG-647 labelled SNAP-FFA1 receptors (compare Figure 5.9 A). Pre-treatment with a Kd concentration of the antagonist, GW1100 (1 μM for 5 min), as expected reduced the percentage proportion of the autocorrelation curve represented by τ_{D2} (compare Figure 5.13 and 5.14; pooled data in Figure 5.15), but this was not statistically significant; whilst the measured component 2 diffusion co-

efficient remained unaffected (Figure 5.15; 31 – 45 cells from 3 -5 individual experiments). Unexpectedly there was also a significant increase in component 2 particle concentration for 40Ag-Cy5 labelled SNAP-FFA1 that had been pre-treated with 1 µM GW1100 (Figure 5.15 F). PCH analysis, with bin time again set to 1 ms, showed large increases in both component 1 and 2 particle concentration as the concentration of 40Ag-Cy5 was increased. The only conditions that did not have significant differences were from 25 to 50 nM 40Ag-Cy5 and from 100 nM 40Ag-Cy5 to 100 nM 40Ag-Cy5 + 1 µM GW1100 (Figure 5.16 C & D; 34 – 54 cells from 4 individual experiments). As for SNAP-surface BG-647 labelled FFA1 receptors (Figure 5.10), there was also an approximate doubling in molecular brightness of component 1 when labelling SNAP-FFA1 receptors with 50 nM 40Ag-Cy5, compared to 25 nM, from 2453 ± 207 to 4400 ± 400 cpm s^{-1} (Figure 5.16 E; **, $P < 0.01$ from Kruskal Wallis with Dunn's multiple comparison post test). Pre-incubation with 1µM GW1100 had no significant effect upon molecular brightness of component 1 (Figure 5.16 E), but did significantly reduce the brightness of component 2, in cells labelled with 100 nM 40Ag-Cy5 (Figure 5.16 F).

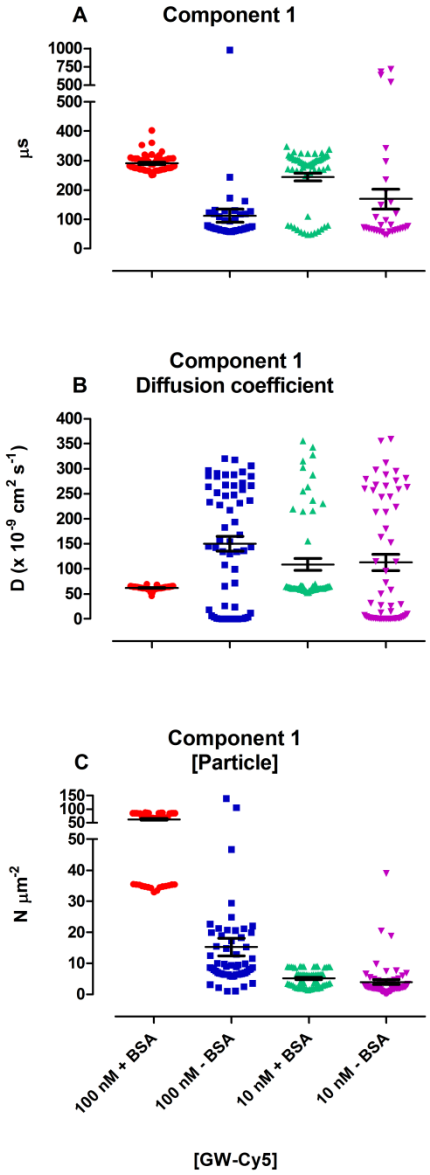

Figure 5.12 FCS measurements of 10 or 100 nM 40Ag-Cy5 freely diffusing in HBSS solution in the absence or presence of 0.02 % BSA.

Scatter plots show the pooled autocorrelation data for dwell times calculated from a single component 3D autocorrelation model (A); the resultant diffusion co-efficients (B; abbreviated to D); and the calculated particle concentrations (C) from FCS experiments (60 readings from 4 individual experiments).

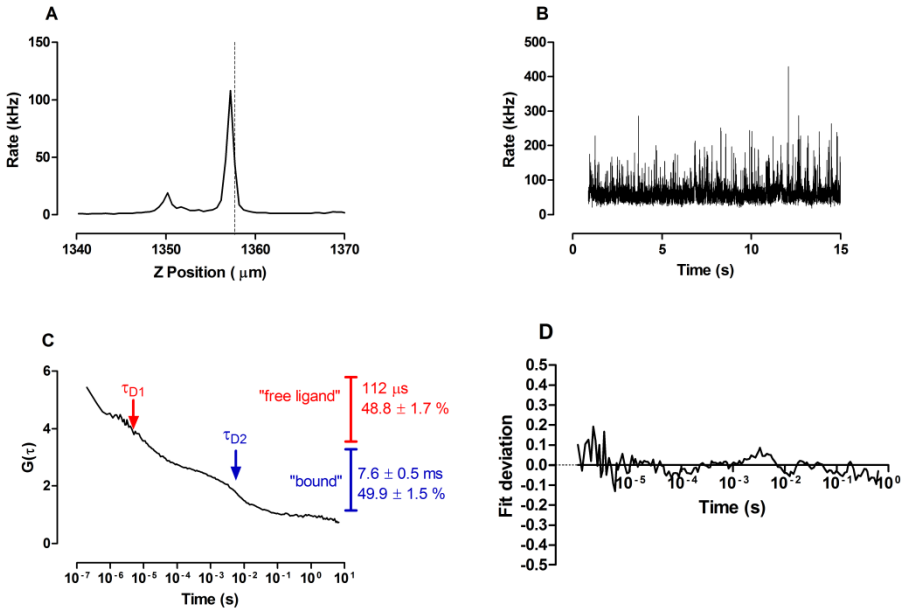

Figure 5.13 FCS measurements depicting the lateral mobility of 100 nM 40Ag-Cy5 treated (5 min at 22°C) SNAP-FFA1.

The confocal z scan identified the upper and lower plasma membrane based on SNAP-surface AF-488 labelling of the cells, with the dotted line showing where the confocal volume was placed for FCS readings (A). Fluorescent fluctuations were recorded 3 x 15 sec at 0.7 % laser power on the upper plasma membrane, following a 15 sec prebleach at 0.5 % laser power, all at 22°C (example record, B). Finally, the data were fitted to an autocorrelation curve using a 2 component (1x 3D, 1x 2D) diffusional model (C; 45 cells from 4 individual experiments), and also shown is the deviation from the fit of the autocorrelation curve (D). This resulted in a "ligand-bound receptor" diffusion time of 7.6 ± 0.5 ms.

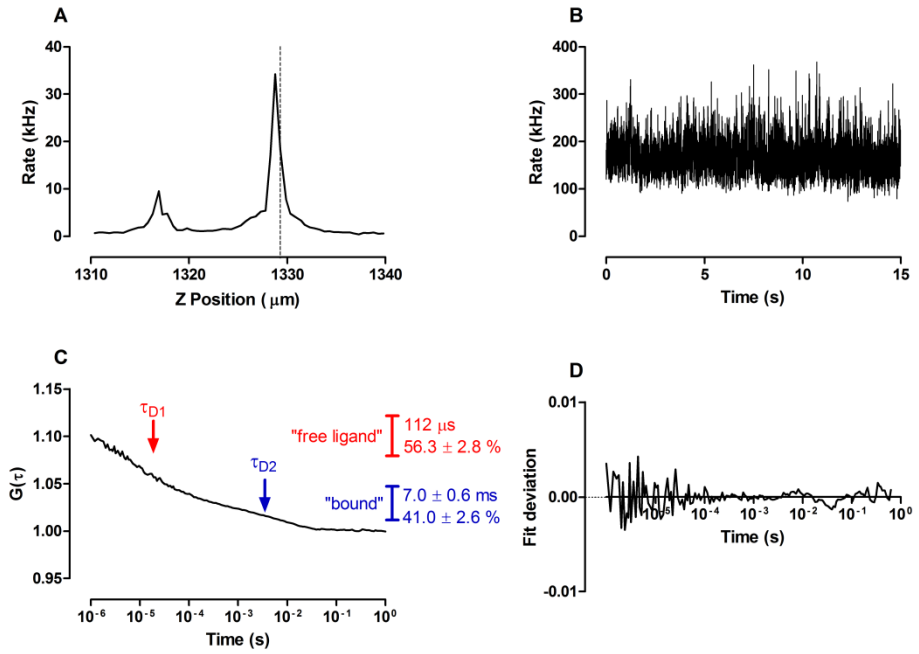

Figure 5.14 FCS measurements depicting the lateral mobility of SNAP-FFA1 labelled treated with 100 nM 40Ag-Cy5 (5 min at 22°C) after antagonist, 1 μM GW1100 pre-treatment (10 min at 22°C).

The confocal z scan identified the upper and lower plasma membrane, with the dotted line showing where the confocal volume was placed for FCS readings (A). Fluorescent fluctuations were recorded 3 x 15 sec at 0.7 % laser power on the upper plasma membrane, following a 15 sec prebleach at 0.5 % laser power, all at 22°C (example record, B). Finally, the data were fitted to an autocorrelation curve using a 2 component diffusional model (1x3D, 1x2D, C; 40 cells from 4 individual experiments), and also shown is the deviation from the fit of the autocorrelation (D). This resulted in a “ligand-bound receptor” (component 2) diffusion time of 7.0 ± 0.6 ms.

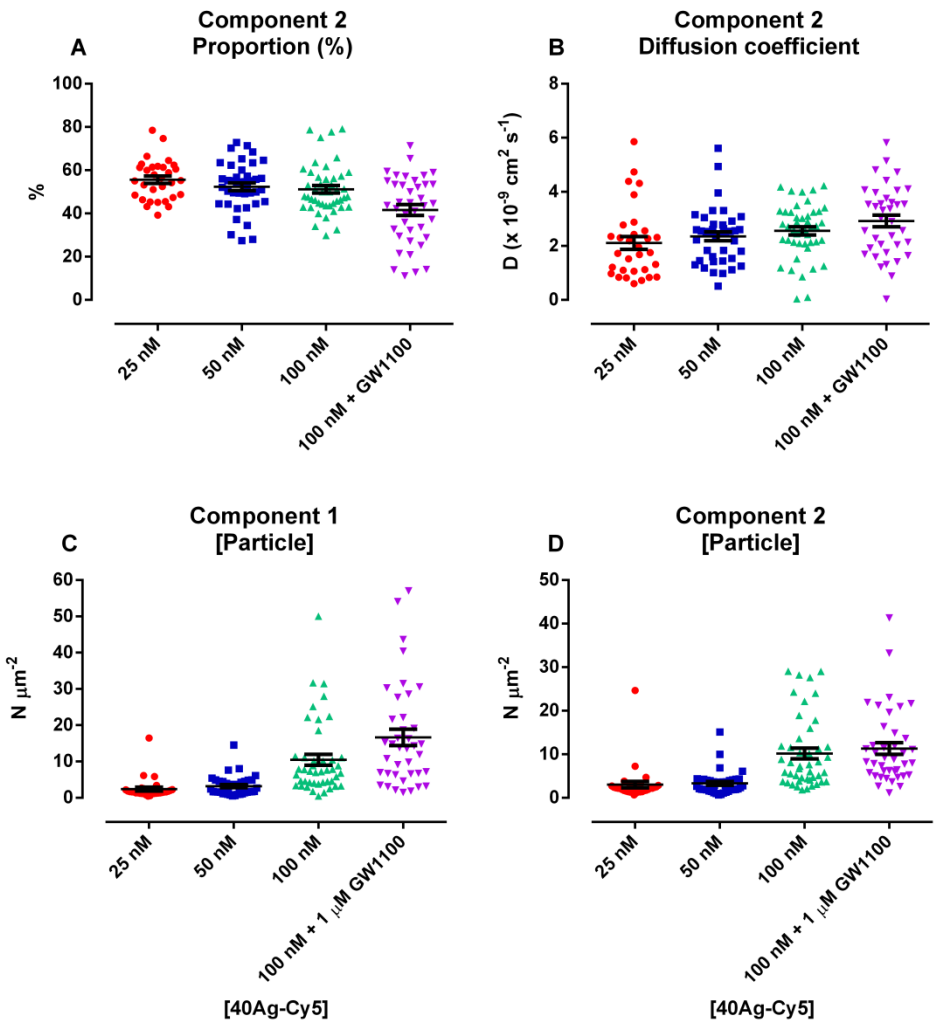

Figure 5.15 FCS measurements of HEK293TR cells expressing SNAP-FFA1 treated with 25 and 50 nM 40Ag-Cy5; and 100 nM 40Ag-Cy5 (5 min at 22°C), with or without the pre-treatment of antagonist, 1 µM GW1100 (10 min at 22°C).

Scatter plots show the pooled autocorrelation data for percentage proportion of the autocorrelation curve corresponding component 2 (A); the diffusion co-efficient of component 2 (B); and the particle concentration of component 1 (free ligand, with fixed diffusion co-efficient) (C) and 2 (D) from FCS experiments (31-45 readings from 4 individual experiments).

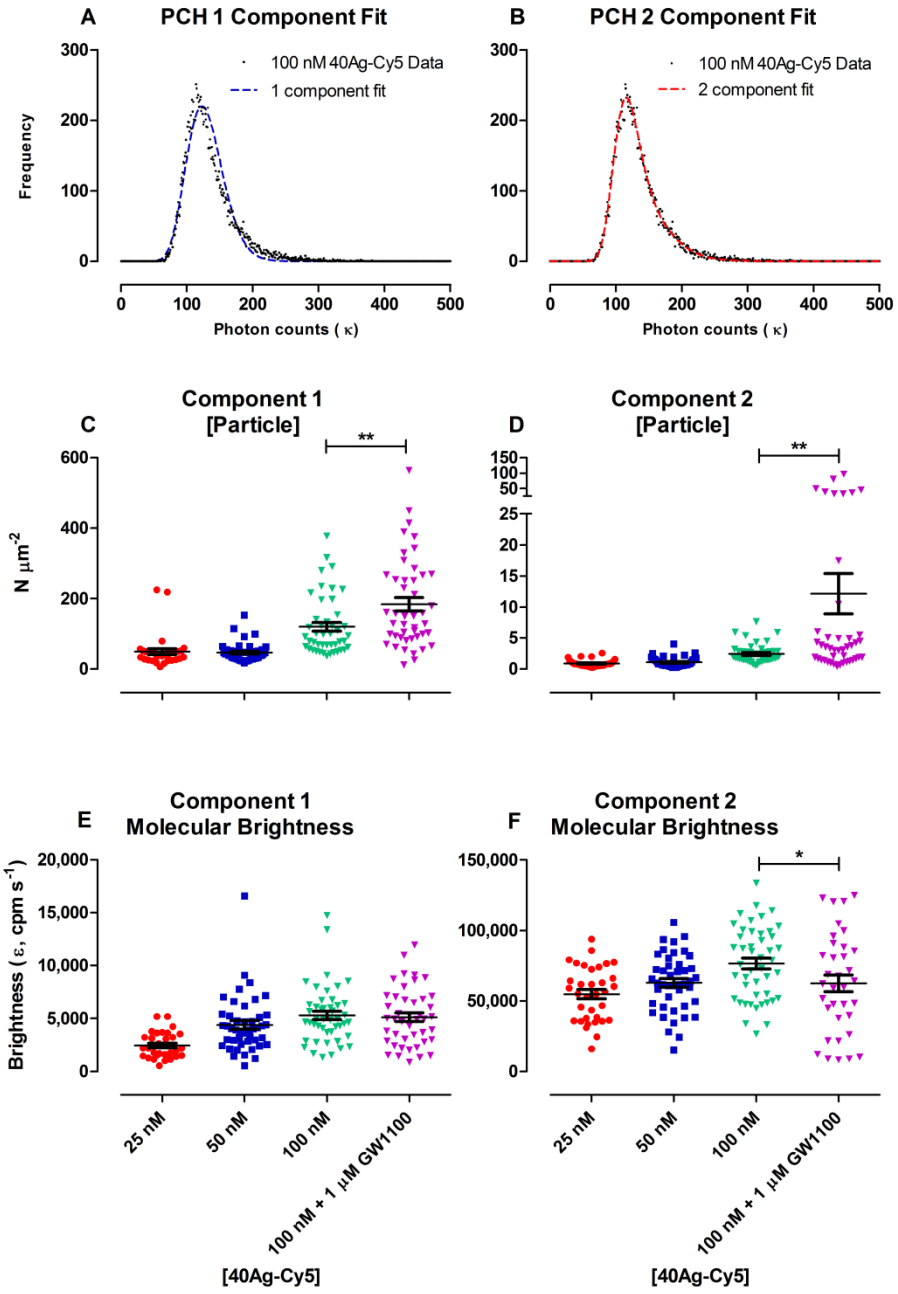

Figure 5.16 Photon counting histogram (PCH) analysis estimates of particle concentration and molecular brightness of FFA1 treated with 25 and 50 nM 40Ag-Cy5; and 100 nM 40Ag-Cy5 (5 min at 22°C), with or without the pre-treatment of antagonist GW1100 (10 min at 22°C).

Representative 1 and 2 component fits of PCH analysis of FFA1 treated with 100 nM 50Ag-Cy5 are shown in A and B respectively. Using the 2 component fits (both of were interpreted as "FFA1 bound" species), scatter plots show the pooled data for particle concentrations obtained for component 1 (C) and 2 (D); and the molecular brightness for component 1 (E) and 2 (F) from FCS experiments in HEK293TR cells expressing SNAP-FFA1 (34 – 54 cells from 4

individual experiments) and treated with the ligands as indicated. Bin time was set to 1 ms, to exclude contributions from the fast diffusing free ligand Statistical significance between all groups was defined using a Kruskal-Wallis test with Dunn's multiple comparison post-tests; whilst comparison between 100 nM 40Ag-Cy5 and 100 nM 40Ag-Cy5 + 1 µM GW1100 was defined using a Student's unpaired t test * $P < 0.05$, ** $P < 0.01$.

5.3 Discussion

The objective of this study was to use a fluorescent ligand to measure and determine the binding affinities of ligands at FFA1. Following the synthesis of 40Ag-Cy5, it was found to have sub-micromolar affinity and selectivity for FFA1. 40Ag-Cy5 was able to be used in imaging competition assays to identify the binding affinities of other FFA1 ligands. FCS studies using both SNAP-surface and 40Ag-Cy5 labelled FFA1 seem to suggest that FFA1 receptors exist as oligomers as well as monomers. In the future, this study could be expanded to examine the route of association and dissociation of the fluorescent ligand, to identify whether the route is via the membrane, as is the case for the S1P receptor (Hanson et al., 2012)

5.3.1 Advantages and disadvantages of the 40Ag-Cy5 fluorescent ligand

A range of fluorescent fatty acids are already commercially available and examples of these ligands, such as BODIPY558/568-C12, act as FFA1 agonists (Dr N Holliday, personal communication). However, despite one report of a fluorescent fatty acid binding assay (Hara et al., 2009a), these ligands have several disadvantages when imaging their binding; for example they have low FFA1/GPR120 affinity, readily label cellular membranes in the absence of FFA1 or GPR120 receptors non-specifically, and they are rapidly incorporated into other cellular lipids (such as triglycerides; Dr N Holliday, personal communication).

Thus the rationale for using a more stable synthetic high affinity ligand, GW9508, as the starting point for fluorescent ligand generation was to

improve the ultimate selectivity and affinity of 40Ag-Cy5 for FFA receptors. Indeed this ligand was a selective FFA1 agonist, with potency and estimated affinity in the low μM range. In imaging studies it also had greater apparent selectivity for binding FFA1, rather than binding to other hydrophobic elements present in the plasma membrane such as fatty acid binding proteins, or partitioning into the lipid bilayer. This may be a consequence of reduced 40Ag-Cy5 lipophilicity due to the use of the more hydrophilic Cy5 fluorophore, compared to BODIPY630/650, which may also make the ligand more membrane impermeant.

There were some limitations with this study. 40Ag-Cy5 was still 100 fold less potent that GW9508 at FFA1 (pEC_{50} is 10 nM), and was completely inactive at GPR120 (compared to GW9508 pEC_{50} of 1 μM). This meant that unfortunately 40Ag-Cy5 could not be used to complement the GPR120 mutagenesis study (chapter 4). Additionally, 40Ag-Cy5 is an agonist, therefore it could be suggested that it might label a subset of "active" receptor conformations. Also, it could potentially result in FFA1 internalisation which would complicate the binding studies, but there were no observations of this, as the ligand stayed on the plasma membrane during the $37^{o}C$ incubations (and as discussed in Chapter 3, relatively little agonist stimulated SNAP-FFA1 receptor internalisation could be detected). Finally, there is also the possibility that 40Ag-Cy5 does not still hit the same binding site as either free fatty acids or even the parent compound GW9508 (Lin et al., 2012), which will be discussed later.

5.3.2 Imaging analysis of 40Ag-Cy5 binding

Using this fluorescent ligand, successful competition binding assays could be performed at FFA1 with high content imaging approaches (Stoddart et al., 2012). This assay showed 40Ag-Cy5 had specific FFA1 receptor binding, because whole cell membrane binding was largely (though not exclusively) dependent upon the tetracycline induction of the expression of FFA1. This was in direct comparison to high levels of non specific binding that occurred when using a radioligand, [^{3}H]TAK-875 at FFA1 (Dr A.J.H. Brown, AZ, personal communication) (Negoro et al., 2012). Also, two radiolabelled compounds, partial agonist [^{3}H] AMG837 and agonist [^{3}H] AM1638 were successfully used to study FFA1 binding, but details of any non-specific binding were not included in the published data (Lin et al., 2012).

Another key advantage to using a fluorescent ligand instead of a radioligand, is that the fluorescent ligand did not require washing off to measure the binding. Therefore binding could be monitored in real time at “true” equilibrium, without first separating bound from free ligand.

However, there was still some background 40Ag-Cy5 membrane staining present in the no tetracycline controls and in the presence of high concentrations of competing ligand, suggesting some residual non-specific background binding into the plasma membrane. Also, as expected, total binding of 40Ag-Cy5 was reduced by the presence of BSA, because albumin has multiple fatty acid and drug binding sites (Krenzel et al., 2013), and was

confirmed by the FCS solution studies (Figure 5.12) to interact with 100 nM 40Ag-Cy5.

This binding assay was also validated because both the IC_{50} value for GW1100 that was determined with this assay; and the rank order of potency of the thiazolidinediones of troglitazone > rosiglitazone, ciglitazone; were both comparable to results previously published using other functional assays (Briscoe et al., 2006; Smith et al., 2009) (e.g. GW1100 pKb in the same FFA1 cell line calculated in Chapter 3).

There were some unusual findings from the FFA1 competition binding assay, which will now be discussed. Firstly, competition with synthetic ligands did not in general displace 40Ag-Cy5 binding to 0 % levels, as defined by cells in the absence of tetracycline induction of the FFA1 receptor. For agonists such as TZDs, GW9508 or the 40Ag-Cy5 congener, the maximum competition observed was greater than this. This might be explained (given the GW9508 pharmacophore of the 40Ag-Cy5 ligand) by the presence of additional non-FFA1 membrane binding sites for 40Ag-Cy5, which can be competed for by these ligands.

In contrast, the antagonist GW1100 did not fully displace 40Ag-Cy5 binding to the low levels seen in no tet controls. This might arise because the presence of FFA1 itself elevates non-specific membrane binding in these cells (e.g. because dissociation of 40Ag-Cy5 from FFA1 provides a route for this ligand into the plasma membrane). Alternatively, it might indicate allosteric

interactions between GW1100 and the 40Ag-Cy5, discussed further below (Lin et al., 2012).

Most interestingly, the endogenous free fatty acid agonists (oleic and myristic acid) did not displace 40Ag-Cy5 binding at concentrations up to 300 µM. While this could perhaps be due to low mM affinity of FFAs, one could argue that there was actually an increase in 40Ag-Cy5 binding with increasing oleic acid concentration (and potentially, this was also evident with low concentrations of TZDs). This suggests perhaps that oleic acid binds to a different site on FFA1 to 40Ag-Cy5 and there is positive allosteric co-operativity between these two binding sites. Recent findings from an FFA1 binding study support the existence of such mechanisms (Lin et al., 2012). Using radiolabelled partial agonist [^{3}H]AMG837, or full agonist [^{3}H]AM1638, these authors uncovered complex allosteric interactions at FFA1 between these ligands, other members of the compound series (e.g. AM8182; structurally related to GW9508 (chapter 4)), and endogenous FFAs (DHA). A summary of the postulated FFA1 binding interactions found in Lin et al., (2012) is shown in Figure 5.16. In particular, the authors demonstrated that the free fatty acid DHA *increased* [^{3}H]AM1638 binding at FFA1 (Lin et al., 2012), in an identical fashion to the observations between oleic acid and 40Ag-Cy5 in this study.

This possibility of allosteric interactions thus requires further experiments to investigate (section 5.4).

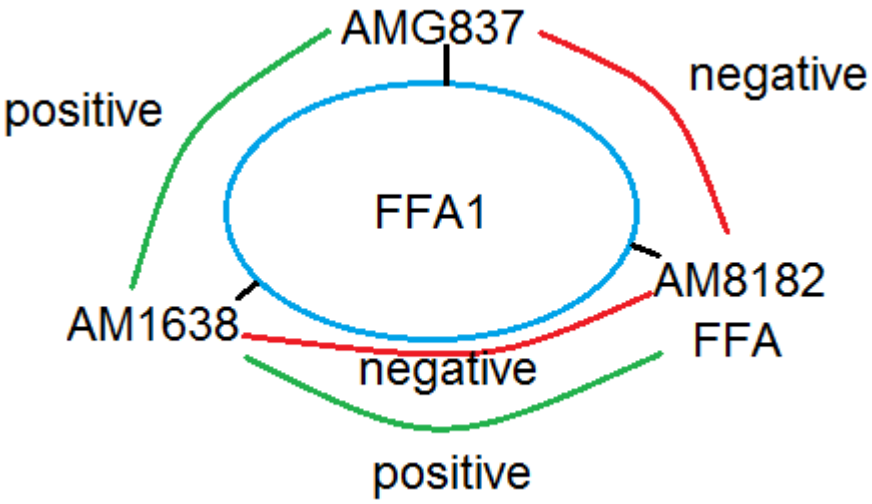

Figure 5.16 Three postulated FFA1 binding sites and the potential allosteric modulation between them

Based on the recent Lin et al. (2012) study, the partial FFA1 agonist AMG837 binds to a site different to full agonists AM1638 and AM8182, and positive and negative cooperative binding effects are shown as green or red lines respectively. A point to note is that although there is negative binding co-operativity between the AMG837 site and the AM8182 site shown here, a contrasting positive cooperative effect is observed in the functional Ca^{2+} signalling assay (Lin et al., 2012).

5.3.3 FCS and PCH analysis of SNAP-FFA1 receptor diffusion

SNAP-surface BG-647 was used to label SNAP-tagged FFA1 receptors and measure their diffusion using FCS. The advantages of this method, compared to the use of GFP-tagged receptor proteins, are that there are less effects from fluorophore photophysics; and that the far red fluorophore is resistant to photobleaching compared to fluorescent proteins, at a wavelength which minimises cellular auto fluorescence compared to at 488 nm (Kozma et al., 2013). Using SNAP-surface BG-647 labelled proteins also allowed more direct comparison with the 40Ag-Cy5 ligand data, as acquisition involved the same calibration and beam path settings, from the same confocal volume. The optimisation of the laser power was also important, because higher laser powers can cause shorter dwell times, for example of τ_{D2}, due to the fact that the fluorophore is more likely to become bleached before the labelled molecules can fully traverse the confocal volume, resulting in the shorter, artificially “faster” dwell times. This was demonstrated by the component 2 diffusion co-efficient, interpreted as the SNAP-surface BG-647 labelled receptors, undergoing a significant increase when laser power was increased from 0.5 % to 2 %. The particle concentration of component 2 also significantly decreased when laser power was increased from 0.5 % to 2 %, and this may also have been due to bleaching.

The decrease in diffusion coefficient from component 1 to component 2 of SNAP-surface BG-647 labelled FFA1 is to be expected, and is in line with the proposal that component 1 measured the fast moving free SNAP-surface label

(with similar *D* to freely diffusing fluorophores such as Cy5 used for calibration), whilst component 2 measured the SNAP-surface labelled receptor which would diffuse much slowly. Component 1 particle concentration increased when SNAP-surface BG-647 concentration was increased from 0.1 to 0.5 µM. Equally there was also a significant increase in component 2 particle concentration when increasing SNAP-surface BG-647 from 0.1 to 0.5 µM, which indicates that not all SNAP-tagged FFA1 receptor proteins were labelled at the lower concentration.

The calculation of diffusion co-efficients allows for comparison with other receptors and other labels, and it was found that the diffusion co-efficient for SNAP-FFA1 was comparable to other GPCRs expressed in the same cell line, even though these studies used fluorescent protein tags fused to the receptors. Such examples include the neuropeptide Y Y1 receptor (Kilpatrick et al., 2012) and bradykinin 2 receptor (Philip et al., 2007).

Diffusion rates derived from other methods, such as fluorescence recovery after photobleaching (FRAP) are still consistent with other methods, for example the mobility of β_2AR (Hegener et al., 2004; Kaya et al., 2011). However, some diffusion rates from FRAP (e.g. for the Y1 receptor) have been found to be an order of magnitude lower than those from FCS. This is thought to be because FRAP measurements cover a larger area of the plasma membrane compared to FCS, therefore cytoskeletal factors limiting diffusion might become more noticeable (Kilpatrick et al., 2012).

The addition of 1 μM GW9508 caused a decrease in the diffusion co-efficient of the receptor mediated component 2. This would be expected if the binding of GW9508 increased the mass of FFA1 receptor complexes sufficiently, or changed the interactions with cellular components such as the cytoskeleton to slow their diffusion. The extent with which agonists can affect receptor diffusion is very variable, for example NPY slowed the receptor diffusion of the neuropeptide Y1 receptor (Kilpatrick et al., 2012); meanwhile, agonist treatment resulted in two differently diffusing populations of the A_3 adenosine receptor (Cordeaux et al., 2008); whilst agonists had no effect upon the diffusion of the A1 adenosine receptor (Briddon et al., 2008) or opioid receptors (Golebiewska et al., 2011). However, in Kilpatrick et al., (2012), this slowing in receptor diffusion was thought to be associated with receptors clustering prior to endocytosis. This is unlikely here because FFA1 less readily undergoes endocytosis.

The observed SNAP-FFA1 particle concentration also significantly increased following GW9508 treatment. This could be explained either by dissociation of receptor clusters into smaller units, or the agonist increasing the mobility of an inactive pool of immobile FFA1 receptors invisible to FCS. PCH analysis of SNAP-surface labelled FFA1 receptor records revealed two “receptor” components of very different molecular brightness, with a minority of very bright FFA1 receptor “clusters” (10x the component 1 “unit” brightness). However 1 μM GW9508 did not alter the relative proportions of these PCH components.

The calculated particle concentration for the predominant FFA1 receptor component in PCH analysis (component 1) was ~5 fold higher than that estimated by FCS as component 2, but the PCH analysis still showed the same increase in particle concentration between 0.1 and 0.5 μM SNAP-surface BG-647 labelled FFA1 as was found in the FCS analysis. The difference in calculated values may be due to the fact that the FCS data are fitted to a 2D model, whilst the PCH data is fitted to the currently available 3D model (Chen et al., 1999). There are limitations to either model because the model is based on a 2D bilayer that in reality will also contain components diffusing in 3D. In addition, the PCH analysis may also incorporate some measurement of immobile particles, but this would not contribute to the FCS time dependent fluctuation data (Kilpatrick et al., 2012).

5.3.4 FCS analysis of 40Ag-Cy5 diffusion

5.3.4.1 Free diffusion of 40Ag-Cy5 in solution

Diffusion of the free 40Ag-Cy5 ligand (100 nM) was affected by the addition of 0.02 % BSA, which was as expected because BSA contains binding sites for drugs and fatty acids (Krenzel et al., 2013), and the parent compound GW9508 binds albumin (Dr. G. Robb, AZ, personal communication). Theoretically, there would a 64 fold change in mass upon the ligand binding BSA because the molecular mass of ligand is 1,038 Da, whilst BSA is ~66,000 Da, therefore should result in a 4 fold change in dwell time, but the observed result was only a ~2 fold change in dwell time which suggests a mix of free ligand and ligand bound to BSA was present. Other things that may cause this

discrepancy are that the ligand in solution may not all be monomeric, and that the ligand may not bind BSA in a 1:1 stoichiometry.

5.3.4.2 40Ag-Cy5 binding to HEK293TR cells expressing FFA1

Membrane binding of 100 nM 40Ag-Cy5 to cells expressing FFA1 receptors was clearly observed as the appearance of an additional slow diffusing component (τ_{D2} ~ 8 ms) in the autocorrelation curve, interpreted as FFA1 receptor bound 40Ag-Cy5, in addition to free ligand. However a discrepancy in the studies of 40Ag-Cy5 binding to FFA1 was that the apparent diffusion co-efficient of FFA1 bound 40Ag-Cy5 was 5-6 times faster than the measurements using the SNAP-labelled receptor alone. One suggestion for this could be that the fluorescent agonist selectively labels a fast moving population of receptors when compared to SNAP-surface which labels all receptors, as suggested to explain the "fast" τ_{D2} and "slow" τ_{D3} components described for A_3 receptor bound fluorescent agonists (Cordeaux et al., 2008). A more likely scenario (given the relatively low affinity of the ligand) is that 40Ag-Cy5 only binds to the FFA1 receptor for short time before dissociating, and this length of time is less than the time taken for the receptor molecules to diffuse completely across the confocal volume. This is also the latest theory for the A_3 adenosine receptor data (Dr S.J. Briddon, University of Nottingham, personal communication). The addition of 1µM GW1100, expected to displace 40Ag-Cy5 binding by ~ 50 %, did decrease the proportion of the τ_{D2} bound component slightly without significantly changing the diffusion co-efficient, which could suggest that 40Ag-Cy5 was partly displaced. However, this was not significant, and there was also no change in particle concentration of

component 2. To exclude artefacts from experimenter bias, cells were not chosen on the basis of their 40Ag-Cy5 labelling in these studies, but on the basis of the SNAP-surface AF-488 labelling of FFA1. The apparent "free" concentration of 40Ag-Cy5 as determined from component 1 particle concentration did increase following GW1100 treatment, though not significantly, suggesting some displacement of 40Ag-Cy5 from FFA1. Interestingly, there was also a significant increase in component 2 particle concentration following GW1100 (and this was evident in the PCH analysis for receptor bound components), showing that GW1100 does appear to have some sort of effect upon 40Ag-Cy5 binding to FFA1, though these early data are not entirely consistent with the clear competition observed in the binding study.

Perhaps these less than conclusive results are due to the experiment not being carried out at equilibrium, because in contrast to the binding studies, the cells were treated with 40Ag-Cy5 for only 5 min at 22^{o}C, compared to 30 min at 37^{o}C. Also, in the binding experiments 1 μM GW1100 only gave 30-50 % displacement of 40Ag-Cy5, which could result in the limited effect seen here in the FCS data, therefore, the experiments should be repeated with an increased GW1100 concentration. Another limitation with this study is that a minority of very bright particles may skew the τ_{D2} parameter, and the relative contributions to different τ_D components, and one effect of GW1100 was to increase the proportion of these large 40Ag-Cy5 bound clusters observed as component 2 in PCH analysis.

5.3.5 PCH data suggests presence of FFA1 dimer/oligomer formation

PCH analysis applied to either SNAP-surface BG-647 labelled FFA1, or 40Ag-Cy5 labelled FFA1 receptors, also measured the molecular brightness of the SNAP-FFA1 receptor containing particles. In addition to defining both "unit" (component 1) and clustered, very bright particles (component 2), in both cases the brightness of the "unit" component 1 was increased by increasing the concentration of the SNAP label or 40AG-Cy5 ligand. Thus, when the SNAP-surface concentration was increased from 0.1 to 0.5 μM BG-647 there was almost a doubling in molecular brightness of component 1, though this was not found to be statistically significant. Equally, the molecular brightness of component 1 was significantly increased when FFA1 cells were exposed to 100 nM 40Ag-Cy5 compared to 25 nM 40Ag-Cy5. In both cases, this increase suggests the presence of dimers or higher order receptor oligomers within the membrane. If FFA1 receptors were **only** monomeric, it would either be labelled (by SNAP-surface or 40Ag-Cy5) or not, i.e. 1 or 0, thus increasing label concentration would increase particle concentration but not brightness. If in contrast, some FFA1 receptors were oligomers (e.g. a dimer) one or two protomers within a particular particle could be labelled, i.e. the brightness could be 1 or 2, theoretically causing an approximate doubling in molecular brightness for the particle as the labelling concentration is increased, and an increase in molecular brightness overall for the population. This is the first evidence for dimerisation occurring in the FFA receptor family. It also indicates another way in which FCS and PCH can be used to determine the oligomerisation of receptors in conjunction with the use of SNAP-surface

labels, in comparison to other studies, in which PCH measurements for Y1 or opioid receptors have been altered in the presence of agonists (Golebiewska et al., 2011; Kilpatrick et al., 2012).

Additionally, this demonstration of FFA1 dimerisation indicates another possible explanation for the allosteric "cross-talk" between binding sites in each protomer (Lin et al., 2011). This allosteric co-operativity across a homodimer has previously been demonstrated for both the A_3 adenosine (May et al., 2011) and D_2 dopamine receptor (Han et al., 2009). Another interesting example is with the chemokine receptor, where it was found that the binding of a specific ligand to one receptor in the oligomer prevented radiolabelled chemokine binding to the other protomer. Additionally, there was evidence of negative co-operativity across a heterodimer, where the binding of a specific antagonist to one protomer inhibited chemokine binding to the other protomer (Sohy et al., 2009).

5.4 Future work

5.4.1 Binding

Future studies on the binding assay would be to carrying it out using a native tissue such as pancreatic islet β cells, immune cells or colonic endocrine cells, as this would show the applicability of using a fluorescent ligand to study native FFA1 receptors in the absence of suitable antibodies and could also localise receptors to specific cells, for example α or β cells in the pancreatic islets, in addition to studying pharmacology by binding assays.

5.4.2 FCS

Future work is necessary to determine that component 2 identified in 40Ag-Cy5 FCS studies is definitively FFA1 receptor bound. One option would be to carry out FCS measurements on HEK293TR cells that have not undergone tetracycline induction of FFA1 expression. The expected result from treating these cells with 40Ag-Cy5 would be that component 2 disappears. This was attempted unsuccessfully (results not shown) by using DiO labelled cells to locate the membrane, but hopefully with further optimisation these issues could be resolved.

Another further FCS experiment that could be carried out would be to pre-treat with GW9508 as a competing ligand, then treat with 40Ag-Cy5. This is because GW9508 would be expected to bind at the same site as 40Ag-Cy5, therefore this could then be compared with the GW1100 data. Additionally, the GW1100 studies could be repeated using a higher concentration of GW1100, predicted to fully displace the 40Ag-Cy5 ligand. These studies might also lead to greater understanding of potential allosteric interactions between these ligands, but also begin to determine whether 40Ag-Cy5 binds FFA1 through the extracellular, aqueous solution or via the membrane as was suggested for the S1P receptor (Hanson et al., 2012).

A future study that would complement the FCS work, would be to carry out FRAP on the SNAP-labelled receptors. This technique measures the proportion of receptors that are immobile, because a limitation of FCS is that it only detects moving species (Kilpatrick et al., 2012).

5.4.3 Testing allosteric interactions

The possibility of allosteric interactions could be investigated using other radio- or fluorescently labelled ligands (Leach et al., 2011; Lin et al., 2012). These ligands could also be used in the technique of perfusion (May et al., 2011). In this study, perfusion was used to detect allosteric interactions by comparing the dissociation kinetics of a fluorescent ligand using infinite dilution conditions, or in the presence of other ligands. Cells expressing the receptor of interest were imaged under constant switchable perfusion in buffer, buffer with fluorescent ligand or buffer with unlabelled ligand. Images were then analysed to quantify association and dissociation kinetics of the fluorescent ligand binding. Allosteric interactions between protomers were detected by the fact that the unlabelled ligand accelerated the dissociation rate of the labelled ligand (May et al., 2011), compared to infinite dilution conditions.

Chapter Six: Overall discussion

6.1 Discussion

Investigating the pharmacology of FFA receptors is important because there is a rising worldwide prevalence of both obesity (Ogden et al., 2006; Rennie and Jebb, 2005) and type II diabetes (Wild et al., 2004), and particularly for obesity, a very limited amount of pharmacological options licensed for treatment. Therefore the investigation of novel therapeutic targets in these area is a key element to meeting this growing need.

Since their deorphanisation, both GPR120 (Hirasawa et al., 2005) and FFA1 (Briscoe et al., 2003) have been researched for their possibility as novel targets for obesity and type II diabetes. FFA1 has already been validated as a target for type II diabetes, due to the success of the agonist TAK-875 in ongoing clinical trials (Kaku et al., 2013), and is known for modulating GSIS in the presence of FFAs, due to it predominantly being expressed in the pancreatic β cell (Briscoe et al., 2003). GPR120 is also of interest because it is predominantly expressed in the gut and its activation causes the release of incretins, aka satiety hormones, such as GLP-1 (Hirasawa et al., 2005) and CCK (Tanaka et al., 2008a). It is also expressed in the tongue (Matsumura et al., 2009), suggesting the possibility of GPR120 acting as a dietary fat sensor.

Although GPR120 exists in 2 splice isoforms, no full isoform specific characterisation had been carried out. This study aimed to readdress this situation (chapter 3). Using a variety of assays, it was found that GPR120S can

respond in a G protein dependent manner, as measured using calcium and dynamic mass redistribution (DMR; (Schroder et al., 2010)), whilst GPR120L gave no responses. Additionally, the G protein mediated responses by GPR120S were insensitive to the effects of PTx, therefore these responses are mediated independently of Gi, probably through Gq as previously hinted at (Hirasawa et al., 2005). Unfortunately, although DMR is known for giving unique signatures depending upon the G protein coupling of the receptor (Schroder et al., 2010), the GPR120S responses did not correlate precisely to one of these signatures.

Interestingly, it was found that both GPR120S and GPR120L signal in a G protein independent manner, as elucidated using both an internalisation assay and BiFC to measure the interactions between receptor and β-arrestin (Kilpatrick et al., 2010). Additionally, as part of this work, the novel finding that GPR120S undergoes calcium signalling and internalisation in response to nuclear PPARγ agonists, thiazolidinediones, was discovered.

Following internalisation, both receptors were also observed to undergo trafficking, predominantly to the lysosomes and did not undergo significant recycling back to the cell surface. All that differs between the isoforms is a 16 residue insert in the third intracellular loop, which must result in the selective difference in G protein dependent signalling.

Following on from this, a mutant of GPR120S was created, to examine the possibility that the carboxyl tail was an alternative regulatory domain in GPR120, because both isoforms had similar trafficking profiles therefore there

must be no effect of the ICL3 insertion upon this pathway. This mutant was truncated at the carboxyl tail at residue 346, thus removing 5 Ser/Thr residues. This mutation resulted in a lack of desensitisation in calcium signalling, resulting in larger calcium responses of the same magnitude of FFA1 expressed in the same cell background. Interestingly, in contrast to the dogma of sequential desensitisation and internalisation, this mutation appeared to have less of an effect upon the internalisation pathway.

Further work needs to be carried out to determine if GPR120L is expressed in humans, in which tissues, and under what circumstances (e.g. adult versus during development). Some preliminary data has struggled to find any evidence of its expression (Dr C.P. Briscoe, Janssen Pharmaceuticals, personal communication). If it is expressed in humans, further work then needs to determine whether the expression profiles of the isoforms differ, to see if these findings of differential signalling have *in vivo* relevance. An intriguing study found that GPR120 underwent differential signalling depending on which tissue it is expressed in. In the adipocyte GPR120 signalled through Gq to cause glucose uptake; whilst in the macrophage it signalled through β-arrestin2 to mediate anti-inflammatory effects (Oh et al., 2010). It could be tantalising to postulate that this is due to GPR120S being expressed in the adipocyte, whilst GPR120L was expressed in the macrophage; but there is no evidence for this so far. If it turns out that such an expression profile exists, this gives additional possibilities for GPR120 as a therapeutic target, and potential use of "biased" agonists. One example could be if GPR120S was expressed in a tissue that required glucose uptake, a ligand could be used to

target this G protein mediated effect; or if on the other hand, an anti-inflammatory effect was required, a ligand that was bias towards β-arrestin2 signalling could be used to target that pathway instead.

Additionally, GPR120 and FFA1 are known to have some overlapping sites of expression in the GI tract (Hirasawa et al., 2005; Stoddart et al., 2008). This degeneracy is interesting, considering they are activated by a similar range of FFAs. Therefore, these receptors were constrained into heterodimers to investigate whether they underwent novel pharmacology in response to agonist, because if so, this could complicate designing drugs to target these receptors in the gut. However these results did not show "heterodimer" specific pharmacology for the limited range of ligands tested. There is also the possibility of FFA1 and GPR120 coupling to the Gα protein, gustducin within these endocrine cells in the GI tract (Kinnamon, 2012).

This characterisation of GPR120 showed it to still be an exciting drug target, but to design drugs to target GPR120, more information on the binding site is required. This is especially relevant to design drugs to be selective for GPR120 over FFA1, considering their overlap in human expression sites, and this is what led to the rationale to investigate the GPR120 binding site (chapter 4).

Firstly, two modelling studies, with the model based on rhodopsin, identified R99 placed at the top of TM 2, to be the positive counter ion to the negative carboxylate group found on the endogenous agonists, FFAs (Sun et al., 2010; Suzuki et al., 2008). Along with R99, R178 was also tested, because like R99, it is at the top of a TM helix 4, and may also have been a counter ion to the

carboxyl group. It was found that R99 was key for this role, whilst R178 was not. In addition to this, a later modelling study, this time based on the active structure of β_2AR (Rasmussen et al., 2011a), indentified a hydrophobic pocket comprised of Met118, Thr119, Gly122, Phe211, Asn215, Ile280, Ile281 and Trp277. This study also identified F304 and F311 to form interactions with the phenylpropionate moiety of the ligand (Shimpukade et al., 2012).

Meanwhile, Graeme Robb (AZ) also modelled the GPR120 binding site, again using the active crystal structure of β_2AR (Rasmussen et al., 2011a), and identified Asn215, Trp277 and Phe311 as being important for ligand binding. Therefore, a mutagenesis study was carried out, comprising of testing the SNAP-tagged GPR120S mutants N215A, W277A, W277F and F311A on both a calcium and an internalisation assay, in the same background. It was found that N215 interacts selectively with the synthetic agonist Met36, and is suggested to be key for this class of ligands which have selectivity for GPR120 over FFA1. W277 meanwhile, is highly conserved in all class A GPCRs and is implicated in the toggle switch activation of receptors (Holst et al., 2010). It was found to be important for stabilising both endogenous FFA activation and synthetic ligands, for example either hydrogen bonding with the ether-oxygen group present in GW9508, or undergo charge-donation effect from the pi-orbital of the central aromatic ring present in Met36. On the other hand, F311 was found to be overestimated by model, because its mutation had little effect on agonist activation of GPR120S. It was postulated to contribute to docking the ligand in the binding site in combination with F304 (Shimpukade et al., 2012), so perhaps this is an explanation for the lack of effect by itself.

The residue Phe311 being overestimated by the model shows some limitations in the modelling approach and mutagenesis to determine the binding site. Firstly, the model is flawed because there is no x-ray structure of GPR120, and is instead based on the crystal structure of β_2AR (and as discussed in Chapter 1, there may be significant differences in this template, even for class A GPCRs). Secondly, the effects of the mutants are measured by signalling assays, which is also flawed because results can be affected by cell surface expression levels of the receptor (though this was monitored in this study). Additionally, using a signalling assay such as measuring calcium also has flaws because the effect of a mutant may be hidden by the fact that the calcium signalling assay has signal amplification, but this is why the internalisation assay was also employed in this study for comparison. If a mutant is found to have an effect upon signalling, there are still limitations to interpretation because if an agonist no longer activates the receptor following mutation, this could be due to a myriad of factors. The mutation, e.g. Trp "toggle switch" could have prevented receptor conformational changes required for activation, or prevented the coupling between the receptor and effector protein. These factors may be in addition to or instead of the role of the residue in mediating ligand-receptor interactions in the binding site. This highlights the difficulty of using mutagenesis and signalling assays to study GPCR binding sites, and a ligand binding assay would be another way to investigate this.

This example of the need for a binding assay at FFA receptors is also emphasised by the current lack of information about ligand affinity for these

receptors (rather than indirect potency estimates). Normally, affinity estimates are key for drug discovery (chapter 5), for example in considering structure activity relationships.

Since there are no radiolabelled ligands of suitable selectivity or affinity, a fluorescent ligand 40Ag-Cy5, based on a known agonist at FFA1 was synthesised (by CellAura, Nottingham) and characterised. 40Ag-Cy5 was found to be selective for FFA1 (sub μM affinity) over GPR120. 40Ag-Cy5 was used successfully in a whole cell ligand binding imaging assay, and could be specifically competed from the FFA1 receptor by a collection of known ligands at FFA1 (Stoddart et al., 2012). This also showed that a traditional radioligand binding assay could be replicated using a fluorescent ligand, because its results agreed with those already in the literature, such as the order of potency of TZDs (Smith et al., 2009); and the pIC_{50} of the antagonist GW1100 (Briscoe et al., 2006).

Then, to further confirm ligand binding, the technique of FCS was used. This firstly measured the diffusion of the SNAP-tagged receptor alone (dwell time 71 ± 12 ms). Then FFA1 was treated with 40Ag-Cy5, which was demonstrated to bind to the receptor (dwell time 7.6 ± 0.5 ms), and that this binding could be partly displaced by the pre-treatment of FFA1 with an antagonist, GW1100 without affecting the dwell time. The apparent formation of FFA1 dimers was shown by the fact that the molecular brightness assumed to correspond to the main receptor component, as measured from PCH analysis, appeared to almost double, when either increasing SNAP-surface BG-647 labelling

concentration (labelling the SNAP-tagged receptor irreversibly) or increasing the concentration of 40Ag-Cy5. This in conjunction with the findings from the constrained dimers (chapter 3), suggests that perhaps FFA1 can indeed exist as oligomers, and potentially heterodimers, e.g. with GPR120.

In the future, if a fluorescent ligand for GPR120 were to become available, it would be of interest to test ligand binding at the mutants created in this study (chapter 4), and also to determine the Ki values for ligands at the wild type receptor. Also, the existence of GPR120:FFA1 dimers could be validated using either a FRET based assay or the perfusion system.

6.2 General conclusion

In conclusion, this investigation into the FFA receptors GPR120 and FFA1 has found novel findings regarding the differential G protein signalling of the GPR120 isoforms, even though they underwent similar intracellular trafficking. The ligand binding site of GPR120 was also probed using a mutagenesis study, validating the proposed molecular model for the general mode of binding of the different types of GPR120 agonists, but with some limitations. A binding assay would be a better approach to identifying residues key for ligand binding, and measuring ligand affinity at these receptor directly (for example to generate structure activity relationships during drug discovery). A traditional pharmacological binding assay was achieved at FFA1 using a fluorescent ligand *in lieu* of a radiolabelled ligand. This ligand was then also utilised to investigate the binding of FFA1 using another technique, FCS, as well as to define its diffusion characteristics.

Therefore, this investigation shows the utility of using a fluorescent ligand in the place of a radiolabelled ligand to characterise FFA receptors. Overall, it has revealed new avenues for exploiting FFA receptors as pharmacological targets. In particular, this has been by validating a new mechanism for measuring ligand binding at these receptors using fluorescent tools. It has also revealed future possibilities to increase FFA ligand selectivity by targeting FFA receptor dimers or isoform-specific signalling pathways.

References

Abrisqueta M, Herraiz C, Perez Oliva AB, Sanchez-Laorden BL, Olivares C, Jimenez-Cervantes C and Garcia-Borron JC (2013) Differential and competitive regulation of human melanocortin 1 receptor signaling by beta-arrestin isoforms. *J Cell Sci*.

Ahn S, Maudsley S, Luttrell LM, Lefkowitz RJ and Daaka Y (1999) Src-mediated tyrosine phosphorylation of dynamin is required for beta2-adrenergic receptor internalization and mitogen-activated protein kinase signaling. *J Biol Chem* **274**(3): 1185-1188.

Ahn S, Shenoy SK, Wei H and Lefkowitz RJ (2004) Differential kinetic and spatial patterns of beta-arrestin and G protein-mediated ERK activation by the angiotensin II receptor. *J Biol Chem* **279**(34): 35518-35525.

Ahren B (2013) Avoiding hypoglycemia: a key to success for glucose-lowering therapy in type 2 diabetes. *Vasc Health Risk Manag* **9**: 155-163.

Albizu L, Cottet M, Kralikova M, Stoev S, Seyer R, Brabet I, Roux T, Bazin H, Bourrier E, Lamarque L, Breton C, Rives ML, Newman A, Javitch J, Trinquet E, Manning M, Pin JP, Mouillac B and Durroux T (2010) Time-resolved FRET between GPCR ligands reveals oligomers in native tissues. *Nat Chem Biol* **6**(8): 587-594.

Albu JB, Heilbronn LK, Kelley DE, Smith SR, Azuma K, Berk ES, Pi-Sunyer FX and Ravussin E (2010) Metabolic changes following a 1-year diet and exercise intervention in patients with type 2 diabetes. *Diabetes* **59**(3): 627-633.

Alquier T, Peyot ML, Latour MG, Kebede M, Sorensen CM, Gesta S, Ronald Kahn C, Smith RD, Jetton TL, Metz TO, Prentki M and Poitout V (2009) Deletion of GPR40 impairs glucose-induced insulin secretion in vivo in mice without affecting intracellular fuel metabolism in islets. *Diabetes* **58**(11): 2607-2615.

Altenbach C, Kusnetzow AK, Ernst OP, Hofmann KP and Hubbell WL (2008) High-resolution distance mapping in rhodopsin reveals the pattern of helix movement due to activation. *Proc Natl Acad Sci U S A* **105**(21): 7439-7444.

Appleyard SM, Celver J, Pineda V, Kovoor A, Wayman GA and Chavkin C (1999) Agonist-dependent desensitization of the kappa opioid receptor by G protein receptor kinase and beta-arrestin. *J Biol Chem* **274**(34): 23802-23807.

Arakawa K, Nishimura T, Sugimoto Y, Takahashi H and Shimamura T (2010) Novel isoindolin-1-one derivative. *International Patent WO 2010/104195*.

Arora KK, Sakai A and Catt KJ (1995) Effects of second intracellular loop mutations on signal transduction and internalization of the gonadotropin-releasing hormone receptor. *J Biol Chem* **270**(39): 22820-22826.

Arunlakshana O and Schild HO (1959) Some quantitative uses of drug antagonists. *Br J Pharmacol Chemother* **14**(1): 48-58.

Attramadal H, Arriza JL, Aoki C, Dawson TM, Codina J, Kwatra MM, Snyder SH, Caron MG and Lefkowitz RJ (1992) Beta-arrestin2, a novel member of the arrestin/beta-arrestin gene family. *J Biol Chem* **267**(25): 17882-17890.

Audet N, Charfi I, Mnie-Filali O, Amraei M, Chabot-Dore AJ, Millecamps M, Stone LS and Pineyro G (2012) Differential association of receptor-Gbetagamma complexes with beta-arrestin2 determines recycling bias and potential for tolerance of delta opioid receptor agonists. *J Neurosci* **32**(14): 4827-4840.

Avlani VA, Gregory KJ, Morton CJ, Parker MW, Sexton PM and Christopoulos A (2007) Critical role for the second extracellular loop in the binding of both orthosteric and allosteric G protein-coupled receptor ligands. *J Biol Chem* **282**(35): 25677-25686.

Azzi M, Charest PG, Angers S, Rousseau G, Kohout T, Bouvier M and Pineyro G (2003) Beta-arrestin-mediated activation of MAPK by inverse agonists reveals distinct active conformations for G protein-coupled receptors. *Proc Natl Acad Sci U S A* **100**(20): 11406-11411.

Babcock GJ, Farzan M and Sodroski J (2003) Ligand-independent dimerization of CXCR4, a principal HIV-1 coreceptor. *J Biol Chem* **278**(5): 3378-3385.

Baillie GS, Sood A, McPhee I, Gall I, Perry SJ, Lefkowitz RJ and Houslay MD (2003) beta-Arrestin-mediated PDE4 cAMP phosphodiesterase recruitment regulates beta-adrenoceptor switching from Gs to Gi. *Proc Natl Acad Sci U S A* **100**(3): 940-945.

Baker JG, Hall IP and Hill SJ (2003) Agonist and inverse agonist actions of beta-blockers at the human beta 2-adrenoceptor provide evidence for agonist-directed signaling. *Mol Pharmacol* **64**(6): 1357-1369.

Baker JG, Middleton R, Adams L, May LT, Briddon SJ, Kellam B and Hill SJ (2010) Influence of fluorophore and linker composition on the pharmacology of fluorescent adenosine A1 receptor ligands. *Br J Pharmacol* **159**(4): 772-786.

Balaraman GS, Bhattacharya S and Vaidehi N (2010) Structural insights into conformational stability of wild-type and mutant beta1-adrenergic receptor. *Biophys J* **99**(2): 568-577.

Ballesteros JA, Jensen AD, Liapakis G, Rasmussen SG, Shi L, Gether U and Javitch JA (2001) Activation of the beta 2-adrenergic receptor involves disruption of an ionic lock between the cytoplasmic ends of transmembrane segments 3 and 6. *J Biol Chem* **276**(31): 29171-29177.

Ballesteros JA and Weinstein H (1995) Integrated methods for modeling G-protein coupled receptors. *Methods Neurosci* **25**.

Baneres JL and Parello J (2003) Structure-based analysis of GPCR function: evidence for a novel pentameric assembly between the dimeric leukotriene B4 receptor BLT1 and the G-protein. *J Mol Biol* **329**(4): 815-829.

Barak LS, Ferguson SS, Zhang J and Caron MG (1997) A beta-arrestin/green fluorescent protein biosensor for detecting G protein-coupled receptor activation. *J Biol Chem* **272**(44): 27497-27500.

Batterham RL, Cohen MA, Ellis SM, Le Roux CW, Withers DJ, Frost GS, Ghatei MA and Bloom SR (2003) Inhibition of food intake in obese subjects by peptide YY3-36. *N Engl J Med* **349**(10): 941-948.

Bavec A, Hallbrink M, Langel U and Zorko M (2003) Different role of intracellular loops of glucagon-like peptide-1 receptor in G-protein coupling. *Regul Pept* **111**(1-3): 137-144.

Bayburt TH, Leitz AJ, Xie G, Oprian DD and Sligar SG (2007) Transducin activation by nanoscale lipid bilayers containing one and two rhodopsins. *J Biol Chem* **282**(20): 14875-14881.

Bayburt TH, Vishnivetskiy SA, McLean MA, Morizumi T, Huang CC, Tesmer JJ, Ernst OP, Sligar SG and Gurevich VV (2011) Monomeric rhodopsin is sufficient for normal rhodopsin kinase (GRK1) phosphorylation and arrestin-1 binding. *J Biol Chem* **286**(2): 1420-1428.

Beaulieu JM, Sotnikova TD, Marion S, Lefkowitz RJ, Gainetdinov RR and Caron MG (2005) An Akt/beta-arrestin 2/PP2A signaling complex mediates dopaminergic neurotransmission and behavior. *Cell* **122**(2): 261-273.

Belfort R, Berria R, Cornell J and Cusi K (2010) Fenofibrate reduces systemic inflammation markers independent of its effects on lipid and glucose metabolism in patients with the metabolic syndrome. *J Clin Endocrinol Metab* **95**(2): 829-836.

Bhattacharya S, Hall SE, Li H and Vaidehi N (2008a) Ligand-stabilized conformational states of human beta(2) adrenergic receptor: insight into G-protein-coupled receptor activation. *Biophys J* **94**(6): 2027-2042.

Bhattacharya S, Hall SE and Vaidehi N (2008b) Agonist-induced conformational changes in bovine rhodopsin: insight into activation of G-protein-coupled receptors. *J Mol Biol* **382**(2): 539-555.

Birdsall NJ (2010) Class A GPCR heterodimers: evidence from binding studies. *Trends Pharmacol Sci* **31**(11): 499-508.

Birnboim HC and Doly J (1979) A rapid alkaline extraction procedure for screening recombinant plasmid DNA. *Nucleic Acids Res* **7**(6): 1513-1523.

Bjarnadottir TK, Fredriksson R, Hoglund PJ, Gloriam DE, Lagerstrom MC and Schioth HB (2004) The human and mouse repertoire of the adhesion family of G-protein-coupled receptors. *Genomics* **84**(1): 23-33.

Bjork K and Svenningsson P (2011) Modulation of monoamine receptors by adaptor proteins and lipid rafts: role in some effects of centrally acting drugs and therapeutic agents. *Annu Rev Pharmacol Toxicol* **51**: 211-242.

Blin N, Yun J and Wess J (1995) Mapping of single amino acid residues required for selective activation of Gq/11 by the m3 muscarinic acetylcholine receptor. *J Biol Chem* **270**(30): 17741-17748.

Bluml K, Mutschler E and Wess J (1994) Identification of an intracellular tyrosine residue critical for muscarinic receptor-mediated stimulation of phosphatidylinositol hydrolysis. *J Biol Chem* **269**(1): 402-405.

Bockaert J and Pin JP (1999) Molecular tinkering of G protein-coupled receptors: an evolutionary success. *EMBO J* **18**(7): 1723-1729.

Boggiano MM, Chandler PC, Oswald KD, Rodgers RJ, Blundell JE, Ishii Y, Beattie AH, Holch P, Allison DB, Schindler M, Arndt K, Rudolf K, Mark M, Schoelch C, Joost HG, Klaus S, Thone-Reineke C, Benoit SC, Seeley RJ, Beck-Sickinger AG, Koglin N, Raun K, Madsen K, Wulff BS, Stidsen CE, Birringer M, Kreuzer OJ, Deng XY, Whitcomb DC, Halem H, Taylor J, Dong J, Datta R, Culler M, Ortmann S, Castaneda TR and Tschop M (2005) PYY3-36 as an anti-obesity drug target. *Obes Rev* **6**(4): 307-322.

Bolen S, Feldman L, Vassy J, Wilson L, Yeh HC, Marinopoulos S, Wiley C, Selvin E, Wilson R, Bass EB and Brancati FL (2007) Systematic review: comparative effectiveness and safety of oral medications for type 2 diabetes mellitus. *Ann Intern Med* **147**(6): 386-399.

Boneva NB, Kikuchi M, Minabe Y and Yamashima T (2011) Neuroprotective and ameliorative actions of polyunsaturated fatty acids against neuronal diseases: implication of fatty acid-binding proteins (FABP) and G protein-coupled receptor 40 (GPR40) in adult neurogenesis. *J Pharmacol Sci* **116**(2): 163-172.

Bootman MD, Collins TJ, Mackenzie L, Roderick HL, Berridge MJ and Peppiatt CM (2002) 2-aminoethoxydiphenyl borate (2-APB) is a reliable blocker of store-operated Ca2+ entry but an inconsistent inhibitor of InsP3-induced Ca2+ release. *FASEB J* **16**(10): 1145-1150.

Borg CM, le Roux CW, Ghatei MA, Bloom SR, Patel AG and Aylwin SJ (2006) Progressive rise in gut hormone levels after Roux-en-Y gastric bypass suggests gut adaptation and explains altered satiety. *Br J Surg* **93**(2): 210-215.

Briaud I, Kelpe CL, Johnson LM, Tran PO and Poitout V (2002) Differential effects of hyperlipidemia on insulin secretion in islets of langerhans from hyperglycemic versus normoglycemic rats. *Diabetes* **51**(3): 662-668.

Briddon SJ, Gandia J, Amaral OB, Ferre S, Lluis C, Franco R, Hill SJ and Ciruela F (2008) Plasma membrane diffusion of G protein-coupled receptor oligomers. *Biochim Biophys Acta* **1783**(12): 2262-2268.

Briddon SJ and Hill SJ (2007) Pharmacology under the microscope: the use of fluorescence correlation spectroscopy to determine the properties of ligand-receptor complexes. *Trends in Pharmacological Sciences* **28**(12): 637-645.

Briddon SJ, Kellam B and Hill SJ (2011) Design and use of fluorescent ligands to study ligand-receptor interactions in single living cells. *Methods Mol Biol* **746**: 211-236.

Briddon SJ, Middleton RJ, Cordeaux Y, Flavin FM, Weinstein JA, George MW, Kellam B and Hill SJ (2004) Quantitative analysis of the formation and diffusion of A1-adenosine receptor-antagonist complexes in single living cells. *Proc Natl Acad Sci U S A* **101**(13): 4673-4678.

Briscoe CP, Peat AJ, McKeown SC, Corbett DF, Goetz AS, Littleton TR, McCoy DC, Kenakin TP, Andrews JL, Ammala C, Fornwald JA, Ignar DM and Jenkinson S (2006) Pharmacological regulation of insulin secretion in MIN6 cells through the fatty acid receptor GPR40: identification of agonist and antagonist small molecules. *Br J Pharmacol* **148**(5): 619-628.

Briscoe CP, Tadayyon M, Andrews JL, Benson WG, Chambers JK, Eilert MM, Ellis C, Elshourbagy NA, Goetz AS, Minnick DT, Murdock PR, Sauls HR, Jr., Shabon U, Spinage LD, Strum JC, Szekeres PG, Tan KB, Way JM, Ignar DM, Wilson S and Muir AI (2003) The orphan G protein-coupled receptor GPR40 is activated by medium and long chain fatty acids. *J Biol Chem* **278**(13): 11303-11311.

Brown AJ, Goldsworthy SM, Barnes AA, Eilert MM, Tcheang L, Daniels D, Muir AI, Wigglesworth MJ, Kinghorn I, Fraser NJ, Pike NB, Strum JC, Steplewski KM, Murdock PR, Holder JC, Marshall FH, Szekeres PG, Wilson S, Ignar DM, Foord SM, Wise A and Dowell SJ (2003) The Orphan G protein-coupled receptors GPR41 and GPR43 are activated by propionate and other short chain carboxylic acids. *J Biol Chem* **278**(13): 11312-11319.

Bruno MJ, Koeppe RE, 2nd and Andersen OS (2007) Docosahexaenoic acid alters bilayer elastic properties. *Proc Natl Acad Sci U S A* **104**(23): 9638-9643.

Brzobohaty B and Kovac L (1986) Factors enhancing genetic transformation of intact yeast cells modify cell wall porosity. *J Gen Microbiol* **132**(11): 3089-3093.

Buckley JD and Howe PR (2010) Long-chain omega-3 polyunsaturated fatty acids may be beneficial for reducing obesity-a review. *Nutrients* **2**(12): 1212-1230.

Budd DC, Willars GB, McDonald JE and Tobin AB (2001) Phosphorylation of the Gq/11-coupled m3-muscarinic receptor is involved in receptor activation of the ERK-1/2 mitogen-activated protein kinase pathway. *J Biol Chem* **276**(7): 4581-4587.

Bunemann M, Frank M and Lohse MJ (2003) Gi protein activation in intact cells involves subunit rearrangement rather than dissociation. *Proc Natl Acad Sci U S A* **100**(26): 16077-16082.

Burns RN and Moniri NH (2010) Agonism with the omega-3 fatty acids alpha-linolenic acid and docosahexaenoic acid mediates phosphorylation of both the short and long isoforms of the human GPR120 receptor. *Biochem Biophys Res Commun* **396**(4): 1030-1035.

Burstein ES, Spalding TA, Hill-Eubanks D and Brann MR (1995) Structure-function of muscarinic receptor coupling to G proteins. Random saturation mutagenesis identifies a critical determinant of receptor affinity for G proteins. *J Biol Chem* **270**(7): 3141-3146.

Buse JB, Rosenstock J, Sesti G, Schmidt WE, Montanya E, Brett JH, Zychma M and Blonde L (2009) Liraglutide once a day versus exenatide twice a day for type 2 diabetes: a 26-week randomised, parallel-group, multinational, open-label trial (LEAD-6). *Lancet* **374**(9683): 39-47.

Butcher AJ, Prihandoko R, Kong KC, McWilliams P, Edwards JM, Bottrill A, Mistry S and Tobin AB (2011) Differential G-protein-coupled receptor phosphorylation provides evidence for a signaling bar code. *J Biol Chem* **286**(13): 11506-11518.

Bychkov E, Zurkovsky L, Garret MB, Ahmed MR and Gurevich EV (2012) Distinct cellular and subcellular distributions of G protein-coupled receptor kinase and arrestin isoforms in the striatum. *PLoS One* **7**(11): e48912.

Cai K, Itoh Y and Khorana HG (2001) Mapping of contact sites in complex formation between transducin and light-activated rhodopsin by covalent crosslinking: use of a photoactivatable reagent. *Proc Natl Acad Sci U S A* **98**(9): 4877-4882.

Cai K, Klein-Seetharaman J, Hwa J, Hubbell WL and Khorana HG (1999) Structure and function in rhodopsin: effects of disulfide cross-links in the cytoplasmic face of rhodopsin on transducin activation and phosphorylation by rhodopsin kinase. *Biochemistry* **38**(39): 12893-12898.

Campos C (2012) Chronic hyperglycemia and glucose toxicity: pathology and clinical sequelae. *Postgrad Med* **124**(6): 90-97.

Canals M, Scholten DJ, de Munnik S, Han MK, Smit MJ and Leurs R (2012) Ubiquitination of CXCR7 controls receptor trafficking. *PLoS One* **7**(3): e34192.

Cao TT, Deacon HW, Reczek D, Bretscher A and von Zastrow M (1999) A kinase-regulated PDZ-domain interaction controls endocytic sorting of the beta2-adrenergic receptor. *Nature* **401**(6750): 286-290.

Castro-Fernandez C and Conn PM (2002) Regulation of the gonadotropin-releasing hormone receptor (GnRHR) by RGS proteins: role of the GnRHR carboxyl-terminus. *Mol Cell Endocrinol* **191**(2): 149-156.

Caulfield MP and Birdsall NJ (1998) International Union of Pharmacology. XVII. Classification of muscarinic acetylcholine receptors. *Pharmacol Rev* **50**(2): 279-290.

Cavuoto P, McAinch AJ, Hatzinikolas G, Cameron-Smith D and Wittert GA (2007) Effects of cannabinoid receptors on skeletal muscle oxidative pathways. *Mol Cell Endocrinol* **267**(1-2): 63-69.

Celver JP, Lowe J, Kovoor A, Gurevich VV and Chavkin C (2001) Threonine 180 is required for G-protein-coupled receptor kinase 3- and beta-arrestin 2-mediated desensitization of the mu-opioid receptor in Xenopus oocytes. *J Biol Chem* **276**(7): 4894-4900.

Chabre M, Deterre P and Antonny B (2009) The apparent cooperativity of some GPCRs does not necessarily imply dimerization. *Trends Pharmacol Sci* **30**(4): 182-187.

Chabre M and le Maire M (2005) Monomeric G-protein-coupled receptor as a functional unit. *Biochemistry* **44**(27): 9395-9403.

Chaipatikul V, Loh HH and Law PY (2003) Ligand-selective activation of mu-oid receptor: demonstrated with deletion and single amino acid mutations of third intracellular loop domain. *J Pharmacol Exp Ther* **305**(3): 909-918.

Chakrabarti S, Liu NJ and Gintzler AR (2010) Formation of mu-/kappa-opioid receptor heterodimer is sex-dependent and mediates female-specific opioid analgesia. *Proc Natl Acad Sci U S A* **107**(46): 20115-20119.

Chao J, Leung Y, Wang M and Chang RC (2012) Nutraceuticals and their preventive or potential therapeutic value in Parkinson's disease. *Nutr Rev* **70**(7): 373-386.

Charest PG, Oligny-Longpre G, Bonin H, Azzi M and Bouvier M (2007) The V2 vasopressin receptor stimulates ERK1/2 activity independently of heterotrimeric G protein signalling. *Cell Signal* **19**(1): 32-41.

Charlton SJ and Vauquelin G (2010) Elusive equilibrium: the challenge of interpreting receptor pharmacology using calcium assays. *Br J Pharmacol* **161**(6): 1250-1265.

Chen CK, Zhang K, Church-Kopish J, Huang W, Zhang H, Chen YJ, Frederick JM and Baehr W (2001) Characterization of human GRK7 as a potential cone opsin kinase. *Mol Vis* **7**: 305-313.

Chen Y, Muller JD, So PT and Gratton E (1999) The photon counting histogram in fluorescence fluctuation spectroscopy. *Biophys J* **77**(1): 553-567.

Cheng Y and Prusoff WH (1973) Relationship between the inhibition constant (K1) and the concentration of inhibitor which causes 50 per cent inhibition (I50) of an enzymatic reaction. *Biochem Pharmacol* **22**(23): 3099-3108.

Cherezov V, Rosenbaum DM, Hanson MA, Rasmussen SG, Thian FS, Kobilka TS, Choi HJ, Kuhn P, Weis WI, Kobilka BK and Stevens RC (2007) High-resolution crystal structure of an engineered human beta2-adrenergic G protein-coupled receptor. *Science* **318**(5854): 1258-1265.

Christiansen E, Due-Hansen ME, Urban C, Grundmann M, Schmidt J, Hansen SV, Hudson BD, Zaibi M, Markussen SB, Hagesaether E, Milligan G, Cawthorne MA, Kostenis E, Kassack MU and Ulven T (2013) Discovery of a potent and selective free fatty acid receptor 1 agonist with low lipophilicity and high oral bioavailability. *J Med Chem* **56**(3): 982-992.

Christiansen E, Due-Hansen ME, Urban C, Grundmann M, Schroder R, Hudson BD, Milligan G, Cawthorne MA, Kostenis E, Kassack MU and Ulven T (2012) Free fatty acid receptor 1 (FFA1/GPR40) agonists: mesylpropoxy appendage lowers lipophilicity and improves ADME properties. *J Med Chem* **55**(14): 6624-6628.

Christiansen E, Urban C, Merten N, Liebscher K, Karlsen KK, Hamacher A, Spinrath A, Bond AD, Drewke C, Ullrich S, Kassack MU, Kostenis E and Ulven T (2008) Discovery of potent and selective agonists for the free fatty acid receptor 1 (FFA(1)/GPR40), a potential target for the treatment of type II diabetes. *J Med Chem* **51**(22): 7061-7064.

Collier CA, Bruce CR, Smith AC, Lopaschuk G and Dyck DJ (2006) Metformin counters the insulin-induced suppression of fatty acid oxidation and stimulation of triacylglycerol storage in rodent skeletal muscle. *Am J Physiol Endocrinol Metab* **291**(1): E182-189.

Comps-Agrar L, Kniazeff J, Norskov-Lauritsen L, Maurel D, Gassmann M, Gregor N, Prezeau L, Bettler B, Durroux T, Trinquet E and Pin JP (2011) The oligomeric state sets GABA(B) receptor signalling efficacy. *EMBO J* **30**(12): 2336-2349.

Cook WS, Yeldandi AV, Rao MS, Hashimoto T and Reddy JK (2000) Less extrahepatic induction of fatty acid beta-oxidation enzymes by PPAR alpha. *Biochem Biophys Res Commun* **278**(1): 250-257.

Cordeaux Y, Briddon SJ, Alexander SP, Kellam B and Hill SJ (2008) Agonist-occupied A3 adenosine receptors exist within heterogeneous complexes in membrane microdomains of individual living cells. *FASEB J* **22**(3): 850-860.

Cornish J, MacGibbon A, Lin JM, Watson M, Callon KE, Tong PC, Dunford JE, van der Does Y, Williams GA, Grey AB, Naot D and Reid IR (2008) Modulation of osteoclastogenesis by fatty acids. *Endocrinology* **149**(11): 5688-5695.

Costa T, Lang J, Gless C and Herz A (1990) Spontaneous association between opioid receptors and GTP-binding regulatory proteins in native membranes: specific regulation by antagonists and sodium ions. *Mol Pharmacol* **37**(3): 383-394.

Costanzi S, Joshi BV, Maddileti S, Mamedova L, Gonzalez-Moa MJ, Marquez VE, Harden TK and Jacobson KA (2005) Human P2Y(6) receptor: molecular modeling leads to the rational design of a novel agonist based on a unique conformational preference. *J Med Chem* **48**(26): 8108-8111.

Damian M, Martin A, Mesnier D, Pin JP and Baneres JL (2006) Asymmetric conformational changes in a GPCR dimer controlled by G-proteins. *EMBO J* **25**(24): 5693-5702.

Damke H, Baba T, Warnock DE and Schmid SL (1994) Induction of mutant dynamin specifically blocks endocytic coated vesicle formation. *J Cell Biol* **127**(4): 915-934.

Dasgupta P, Rastogi S, Pillai S, Ordonez-Ercan D, Morris M, Haura E and Chellappan S (2006) Nicotine induces cell proliferation by beta-arrestin-mediated activation of Src and Rb-Raf-1 pathways. *J Clin Invest* **116**(8): 2208-2217.

Davies MN, Gloriam DE, Secker A, Freitas AA, Mendao M, Timmis J and Flower DR (2007) Proteomic applications of automated GPCR classification. *Proteomics* **7**(16): 2800-2814.

De Feyter HM, Praet SF, van den Broek NM, Kuipers H, Stehouwer CD, Nicolay K, Prompers JJ and van Loon LJ (2007) Exercise training improves glycemic control in long-standing insulin-treated type 2 diabetic patients. *Diabetes Care* **30**(10): 2511-2513.

De Lean A, Stadel JM and Lefkowitz RJ (1980) A ternary complex model explains the agonist-specific binding properties of the adenylate cyclase-coupled beta-adrenergic receptor. *J Biol Chem* **255**(15): 7108-7117.

DeFea KA (2011) Beta-arrestins as regulators of signal termination and transduction: how do they determine what to scaffold? *Cell Signal* **23**(4): 621-629.

DeFea KA, Zalevsky J, Thoma MS, Dery O, Mullins RD and Bunnett NW (2000) beta-arrestin-dependent endocytosis of proteinase-activated receptor 2 is required for intracellular targeting of activated ERK1/2. *J Cell Biol* **148**(6): 1267-1281.

DeHaven WI, Smyth JT, Boyles RR, Bird GS and Putney JW, Jr. (2008) Complex actions of 2-aminoethyldiphenyl borate on store-operated calcium entry. *J Biol Chem* **283**(28): 19265-19273.

Despres JP, Golay A and Sjostrom L (2005) Effects of rimonabant on metabolic risk factors in overweight patients with dyslipidemia. *N Engl J Med* **353**(20): 2121-2134.

Deupi X (2012) Quantification of structural distortions in the transmembrane helices of GPCRs. *Methods Mol Biol* **914**: 219-235.

Dormandy JA, Charbonnel B, Eckland DJ, Erdmann E, Massi-Benedetti M, Moules IK, Skene AM, Tan MH, Lefebvre PJ, Murray GD, Standl E, Wilcox RG, Wilhelmsen L, Betteridge J, Birkeland K, Golay A, Heine RJ, Koranyi L, Laakso M, Mokan M, Norkus A, Pirags V, Podar T, Scheen A, Scherbaum W, Schernthaner G, Schmitz O, Skrha J, Smith U and Taton J (2005) Secondary prevention of macrovascular events in patients with type 2 diabetes in the PROactive Study (PROspective pioglitAzone Clinical Trial In macroVascular Events): a randomised controlled trial. *Lancet* **366**(9493): 1279-1289.

Dorsch S, Klotz KN, Engelhardt S, Lohse MJ and Bunemann M (2009) Analysis of receptor oligomerization by FRAP microscopy. *Nat Methods* **6**(3): 225-230.

Drake MT, Violin JD, Whalen EJ, Wisler JW, Shenoy SK and Lefkowitz RJ (2008) beta-arrestin-biased agonism at the beta2-adrenergic receptor. *J Biol Chem* **283**(9): 5669-5676.

Dunham TD and Farrens DL (1999) Conformational changes in rhodopsin. Movement of helix f detected by site-specific chemical labeling and fluorescence spectroscopy. *J Biol Chem* **274**(3): 1683-1690.

Eckert GP, Renner K, Eckert SH, Eckmann J, Hagl S, Abdel-Kader RM, Kurz C, Leuner K and Muller WE (2012) Mitochondrial dysfunction--a pharmacological target in Alzheimer's disease. *Mol Neurobiol* **46**(1): 136-150.

Edfalk S, Steneberg P and Edlund H (2008) Gpr40 is expressed in enteroendocrine cells and mediates free fatty acid stimulation of incretin secretion. *Diabetes* **57**(9): 2280-2287.

Egan JM, Clocquet AR and Elahi D (2002) The insulinotropic effect of acute exendin-4 administered to humans: comparison of nondiabetic state to type 2 diabetes. *J Clin Endocrinol Metab* **87**(3): 1282-1290.

El-Assaad W, Buteau J, Peyot ML, Nolan C, Roduit R, Hardy S, Joly E, Dbaibo G, Rosenberg L and Prentki M (2003) Saturated fatty acids synergize with elevated glucose to cause pancreatic beta-cell death. *Endocrinology* **144**(9): 4154-4163.

Ernst OP, Gramse V, Kolbe M, Hofmann KP and Heck M (2007) Monomeric G protein-coupled receptor rhodopsin in solution activates its G protein transducin at the diffusion limit. *Proc Natl Acad Sci U S A* **104**(26): 10859-10864.

Farrens DL, Altenbach C, Yang K, Hubbell WL and Khorana HG (1996) Requirement of rigid-body motion of transmembrane helices for light activation of rhodopsin. *Science* **274**(5288): 768-770.

Feng H, Zheng L, Feng Z, Zhao Y and Zhang N (2012) The role of leptin in obesity and the potential for leptin replacement therapy. *Endocrine*.

Ferguson SS, Barak LS, Zhang J and Caron MG (1996) G-protein-coupled receptor regulation: role of G-protein-coupled receptor kinases and arrestins. *Can J Physiol Pharmacol* **74**(10): 1095-1110.

Ferguson SS, Menard L, Barak LS, Koch WJ, Colapietro AM and Caron MG (1995) Role of phosphorylation in agonist-promoted beta 2-adrenergic receptor sequestration. Rescue of a sequestration-defective mutant receptor by beta ARK1. *J Biol Chem* **270**(42): 24782-24789.

Field BC, Wren AM, Peters V, Baynes KC, Martin NM, Patterson M, Alsaraf S, Amber V, Wynne K, Ghatei MA and Bloom SR (2010) PYY3-36 and oxyntomodulin can be additive in their effect on food intake in overweight and obese humans. *Diabetes* **59**(7): 1635-1639.

Filippatos TD, Derdemezis CS, Gazi IF, Nakou ES, Mikhailidis DP and Elisaf MS (2008) Orlistat-associated adverse effects and drug interactions: a critical review. *Drug Saf* **31**(1): 53-65.

Flint A, Raben A, Astrup A and Holst JJ (1998) Glucagon-like peptide 1 promotes satiety and suppresses energy intake in humans. *J Clin Invest* **101**(3): 515-520.

Floyd ZE and Stephens JM (2012) Controlling a master switch of adipocyte development and insulin sensitivity: covalent modifications of PPARgamma. *Biochim Biophys Acta* **1822**(7): 1090-1095.

Fong TM, Huang RRC and Strader CD (1992) LOCALIZATION OF AGONIST AND ANTAGONIST BINDING DOMAINS OF THE HUMAN NEUROKININ-1 RECEPTOR. *Journal of Biological Chemistry* **267**(36): 25664-25667.

Fotiadis D, Liang Y, Filipek S, Saperstein DA, Engel A and Palczewski K (2003) Atomic-force microscopy: Rhodopsin dimers in native disc membranes. *Nature* **421**(6919): 127-128.

Frank M, Thumer L, Lohse MJ and Bunemann M (2005) G Protein activation without subunit dissociation depends on a G{alpha}(i)-specific region. *J Biol Chem* **280**(26): 24584-24590.

Fredriksson R, Hoglund PJ, Gloriam DE, Lagerstrom MC and Schioth HB (2003a) Seven evolutionarily conserved human rhodopsin G protein-coupled receptors lacking close relatives. *FEBS Lett* **554**(3): 381-388.

Fredriksson R, Lagerstrom MC, Lundin LG and Schioth HB (2003b) The G-protein-coupled receptors in the human genome form five main families. Phylogenetic analysis, paralogon groups, and fingerprints. *Mol Pharmacol* **63**(6): 1256-1272.

Freedman NJ, Liggett SB, Drachman DE, Pei G, Caron MG and Lefkowitz RJ (1995) Phosphorylation and desensitization of the human beta 1-adrenergic receptor. Involvement of G protein-coupled receptor kinases and cAMP-dependent protein kinase. *J Biol Chem* **270**(30): 17953-17961.

Fritze O, Filipek S, Kuksa V, Palczewski K, Hofmann KP and Ernst OP (2003) Role of the conserved NPxxY(x)5,6F motif in the rhodopsin ground state and during activation. *Proc Natl Acad Sci U S A* **100**(5): 2290-2295.

Fujita T, Matsuoka T, Honda T, Kabashima K, Hirata T and Narumiya S (2011) A GPR40 agonist GW9508 suppresses CCL5, CCL17, and CXCL10 induction in keratinocytes and attenuates cutaneous immune inflammation. *J Invest Dermatol* **131**(8): 1660-1667.

Fukunaga S, Setoguchi S, Hirasawa A and Tsujimoto G (2006) Monitoring ligand-mediated internalization of G protein-coupled receptor as a novel pharmacological approach. *Life Sci* **80**(1): 17-23.

Gagnon AW, Kallal L and Benovic JL (1998) Role of clathrin-mediated endocytosis in agonist-induced down-regulation of the beta2-adrenergic receptor. *J Biol Chem* **273**(12): 6976-6981.

Gales C, Rebois RV, Hogue M, Trieu P, Breit A, Hebert TE and Bouvier M (2005) Real-time monitoring of receptor and G-protein interactions in living cells. *Nat Methods* **2**(3): 177-184.

Gales C, Van Durm JJ, Schaak S, Pontier S, Percherancier Y, Audet M, Paris H and Bouvier M (2006) Probing the activation-promoted structural rearrangements in preassembled receptor-G protein complexes. *Nat Struct Mol Biol* **13**(9): 778-786.

Galvez T, Duthey B, Kniazeff J, Blahos J, Rovelli G, Bettler B, Prezeau L and Pin JP (2001) Allosteric interactions between GB1 and GB2 subunits are required for optimal GABA(B) receptor function. *EMBO J* **20**(9): 2152-2159.

Gao ZG, Chen A, Barak D, Kim SK, Muller CE and Jacobson KA (2002) Identification by site-directed mutagenesis of residues involved in ligand recognition and activation of the human A3 adenosine receptor. *J Biol Chem* **277**(21): 19056-19063.

Gardner EL and Vorel SR (1998) Cannabinoid transmission and reward-related events. *Neurobiol Dis* **5**(6 Pt B): 502-533.

Gautam N, Downes GB, Yan K and Kisselev O (1998) The G-protein beta gamma complex. *Cellular Signalling* **10**(7): 447-455.

Ge H, Li X, Weiszmann J, Wang P, Baribault H, Chen JL, Tian H and Li Y (2008) Activation of G protein-coupled receptor 43 in adipocytes leads to inhibition of lipolysis and suppression of plasma free fatty acids. *Endocrinology* **149**(9): 4519-4526.

George SR, Fan T, Xie Z, Tse R, Tam V, Varghese G and O'Dowd BF (2000) Oligomerization of mu- and delta-opioid receptors. Generation of novel functional properties. *J Biol Chem* **275**(34): 26128-26135.

Gerber BO, Meng EC, Dotsch V, Baranski TJ and Bourne HR (2001) An activation switch in the ligand binding pocket of the C5a receptor. *J Biol Chem* **276**(5): 3394-3400.

Gether U, Lin S and Kobilka BK (1995) Fluorescent labeling of purified beta 2 adrenergic receptor. Evidence for ligand-specific conformational changes. *J Biol Chem* **270**(47): 28268-28275.

Ghanouni P, Steenhuis JJ, Farrens DL and Kobilka BK (2001) Agonist-induced conformational changes in the G-protein-coupling domain of the beta 2 adrenergic receptor. *Proc Natl Acad Sci U S A* **98**(11): 5997-6002.

Golebiewska U, Johnston JM, Devi L, Filizola M and Scarlata S (2011) Differential response to morphine of the oligomeric state of mu-opioid in the presence of delta-opioid receptors. *Biochemistry* **50**(14): 2829-2837.

Goodman OB, Jr., Krupnick JG, Santini F, Gurevich VV, Penn RB, Gagnon AW, Keen JH and Benovic JL (1996) Beta-arrestin acts as a clathrin adaptor in endocytosis of the beta2-adrenergic receptor. *Nature* **383**(6599): 447-450.

Gotoh C, Hong YH, Iga T, Hishikawa D, Suzuki Y, Song SH, Choi KC, Adachi T, Hirasawa A, Tsujimoto G, Sasaki S and Roh SG (2007) The regulation of adipogenesis through GPR120. *Biochem Biophys Res Commun* **354**(2): 591-597.

Grace CR, Perrin MH, DiGruccio MR, Miller CL, Rivier JE, Vale WW and Riek R (2004) NMR structure and peptide hormone binding site of the first extracellular domain of a type B1 G protein-coupled receptor. *Proc Natl Acad Sci U S A* **101**(35): 12836-12841.

Graciano MF, Valle MM, Kowluru A, Curi R and Carpinelli AR (2011) Regulation of insulin secretion and reactive oxygen species production by free fatty acids in pancreatic islets. *Islets* **3**(5): 213-223.

Granier S, Manglik A, Kruse AC, Kobilka TS, Thian FS, Weis WI and Kobilka BK (2012) Structure of the delta-opioid receptor bound to naltrindole. *Nature* **485**(7398): 400-404.

Gray JA, Compton-Toth BA and Roth BL (2003) Identification of two serine residues essential for agonist-induced 5-HT2A receptor desensitization. *Biochemistry* **42**(36): 10853-10862.

Gregory RB, Rychkov G and Barritt GJ (2001) Evidence that 2-aminoethyl diphenylborate is a novel inhibitor of store-operated Ca2+ channels in liver cells, and acts through a mechanism which does not involve inositol trisphosphate receptors. *Biochem J* **354**(Pt 2): 285-290.

Gullapalli A, Wolfe BL, Griffin CT, Magnuson T and Trejo J (2006) An essential role for SNX1 in lysosomal sorting of protease-activated receptor-1: evidence for retromer-, Hrs-, and Tsg101-independent functions of sorting nexins. *Mol Biol Cell* **17**(3): 1228-1238.

Gurevich EV, Tesmer JJ, Mushegian A and Gurevich VV (2012) G protein-coupled receptor kinases: more than just kinases and not only for GPCRs. *Pharmacol Ther* **133**(1): 40-69.

Gurevich VV and Gurevich EV (2006) The structural basis of arrestin-mediated regulation of G-protein-coupled receptors. *Pharmacol Ther* **110**(3): 465-502.

Gurevich VV and Gurevich EV (2008) GPCR monomers and oligomers: it takes all kinds. *Trends Neurosci* **31**(2): 74-81.

Habib AM, Richards P, Rogers GJ, Reimann F and Gribble FM (2013) Co-localisation and secretion of glucagon-like peptide 1 and peptide YY from primary cultured human L cells. *Diabetologia*.

Haga H, Yamada R, Ohnishi Y, Nakamura Y and Tanaka T (2002) Gene-based SNP discovery as part of the Japanese Millennium Genome Project: identification of 190,562 genetic variations in the human genome. Single-nucleotide polymorphism. *J Hum Genet* **47**(11): 605-610.

Hamid YH, Vissing H, Holst B, Urhammer SA, Pyke C, Hansen SK, Glumer C, Borch-Johnsen K, Jorgensen T, Schwartz TW, Pedersen O and Hansen T (2005) Studies of relationships between variation of the human G protein-coupled receptor 40 Gene and Type 2 diabetes and insulin release. *Diabetic Medicine* **22**(1): 74-80.

Hamm HE (1998) The many faces of G protein signaling. *J Biol Chem* **273**(2): 669-672.

Han Y, Moreira IS, Urizar E, Weinstein H and Javitch JA (2009) Allosteric communication between protomers of dopamine class A GPCR dimers modulates activation. *Nat Chem Biol* **5**(9): 688-695.

Hanson MA, Roth CB, Jo E, Griffith MT, Scott FL, Reinhart G, Desale H, Clemons B, Cahalan SM, Schuerer SC, Sanna MG, Han GW, Kuhn P, Rosen H and Stevens RC (2012) Crystal structure of a lipid G protein-coupled receptor. *Science* **335**(6070): 851-855.

Hanson SM, Gurevich EV, Vishnivetskiy SA, Ahmed MR, Song X and Gurevich VV (2007) Each rhodopsin molecule binds its own arrestin. *Proc Natl Acad Sci U S A* **104**(9): 3125-3128.

Hara T, Hirasawa A, Sun Q, Koshimizu TA, Itsubo C, Sadakane K, Awaji T and Tsujimoto G (2009a) Flow cytometry-based binding assay for GPR40 (FFAR1; free fatty acid receptor 1). *Mol Pharmacol* **75**(1): 85-91.

Hara T, Hirasawa A, Sun Q, Sadakane K, Itsubo C, Iga T, Adachi T, Koshimizu T, Hashimoto T, Asakawa Y and Tsujimoto G (2009b) Novel selective ligands for free fatty acid receptors GPR120 and GPR40. *Naunyn-Schmiedebergs Archives of Pharmacology* **380**(3): 247-255.

Harmon JS, Gleason CE, Tanaka Y, Poitout V and Robertson RP (2001) Antecedent hyperglycemia, not hyperlipidemia, is associated with increased islet triacylglycerol content and decreased insulin gene mRNA level in Zucker diabetic fatty rats. *Diabetes* **50**(11): 2481-2486.

Hashimoto M and Hossain S (2011) Neuroprotective and ameliorative actions of polyunsaturated fatty acids against neuronal diseases: beneficial effect of docosahexaenoic acid on cognitive decline in Alzheimer's disease. *J Pharmacol Sci* **116**(2): 150-162.

Hashimoto N, Sasaki Y, Nakama C and Ishikawa M (2010) Novel phenyl-isoxazol-3-olderivative. *US Patent 2010/0130559*.

He HT and Marguet D (2011) Detecting nanodomains in living cell membrane by fluorescence correlation spectroscopy. *Annu Rev Phys Chem* **62**: 417-436.

Heal DJ, Aspley S, Prow MR, Jackson HC, Martin KF and Cheetham SC (1998) Sibutramine: a novel anti-obesity drug. A review of the pharmacological evidence to differentiate it from d-amphetamine and d-fenfluramine. *Int J Obes Relat Metab Disord* **22 Suppl 1**: S18-28; discussion S29.

Hegener O, Prenner L, Runkel F, Baader SL, Kappler J and Haberlein H (2004) Dynamics of beta2-adrenergic receptor-ligand complexes on living cells. *Biochemistry* **43**(20): 6190-6199.

Hein P, Frank M, Hoffmann C, Lohse MJ and Bunemann M (2005) Dynamics of receptor/G protein coupling in living cells. *EMBO J* **24**(23): 4106-4114.

Hellmann J, Zhang MJ, Tang Y, Rane M, Bhatnagar A and Spite M (2013) Increased Saturated Fatty Acids in Obesity Alter Resolution of Inflammation in Part by Stimulating Prostaglandin Production. *J Immunol*.

Hern JA, Baig AH, Mashanov GI, Birdsall B, Corrie JE, Lazareno S, Molloy JE and Birdsall NJ (2010) Formation and dissociation of M1 muscarinic receptor dimers seen by total internal reflection fluorescence imaging of single molecules. *Proc Natl Acad Sci U S A* **107**(6): 2693-2698.

Herrick-Davis K, Grinde E, Harrigan TJ and Mazurkiewicz JE (2005) Inhibition of serotonin 5-hydroxytryptamine2c receptor function through heterodimerization: receptor dimers bind two molecules of ligand and one G-protein. *J Biol Chem* **280**(48): 40144-40151.

Herrick-Davis K, Grinde E and Mazurkiewicz JE (2004) Biochemical and biophysical characterization of serotonin 5-HT2C receptor homodimers on the plasma membrane of living cells. *Biochemistry* **43**(44): 13963-13971.

Herzig S, Hedrick S, Morantte I, Koo SH, Galimi F and Montminy M (2003) CREB controls hepatic lipid metabolism through nuclear hormone receptor PPAR-gamma. *Nature* **426**(6963): 190-193.

Hinshaw JE and Schmid SL (1995) Dynamin self-assembles into rings suggesting a mechanism for coated vesicle budding. *Nature* **374**(6518): 190-192.

Hirasawa A, Tsumaya K, Awaji T, Katsuma S, Adachi T, Yamada M, Sugimoto Y, Miyazaki S and Tsujimoto G (2005) Free fatty acids regulate gut incretin glucagon-like peptide-1 secretion through GPR120. *Nat Med* **11**(1): 90-94.

Hlavackova V, Goudet C, Kniazeff J, Zikova A, Maurel D, Vol C, Trojanova J, Prezeau L, Pin JP and Blahos J (2005) Evidence for a single heptahelical domain being turned on upon activation of a dimeric GPCR. *EMBO J* **24**(3): 499-509.

Holman RR, Paul SK, Bethel MA, Matthews DR and Neil HA (2008) 10-year follow-up of intensive glucose control in type 2 diabetes. *N Engl J Med* **359**(15): 1577-1589.

Holst B, Nygaard R, Valentin-Hansen L, Bach A, Engelstoft MS, Petersen PS, Frimurer TM and Schwartz TW (2010) A conserved aromatic lock for the tryptophan rotameric switch in TM-VI of seven-transmembrane receptors. *J Biol Chem* **285**(6): 3973-3985.

Hong YH, Nishimura Y, Hishikawa D, Tsuzuki H, Miyahara H, Gotoh C, Choi KC, Feng DD, Chen C, Lee HG, Katoh K, Roh SG and Sasaki S (2005) Acetate and propionate short chain fatty acids stimulate adipogenesis via GPCR43. *Endocrinology* **146**(12): 5092-5099.

Houze JB, Zhu L, Sun Y, Akerman M, Qiu W, Zhang AJ, Sharma R, Schmitt M, Wang Y, Liu J, Medina JC, Reagan JD, Luo J, Tonn G, Zhang J, Lu JY, Chen M, Lopez E, Nguyen K, Yang L, Tang L, Tian H, Shuttleworth SJ and Lin DC (2012) AMG 837: a potent, orally bioavailable GPR40 agonist. *Bioorg Med Chem Lett* **22**(2): 1267-1270.

Hu CD, Chinenov Y and Kerppola TK (2002) Visualization of interactions among bZIP and Rel family proteins in living cells using bimolecular fluorescence complementation. *Mol Cell* **9**(4): 789-798.

Hu H, He LY, Gong Z, Li N, Lu YN, Zhai QW, Liu H, Jiang HL, Zhu WL and Wang HY (2009) A novel class of antagonists for the FFAs receptor GPR40. *Biochem Biophys Res Commun* **390**(3): 557-563.

Hu J, Thor D, Zhou Y, Liu T, Wang Y, McMillin SM, Mistry R, Challiss RA, Costanzi S and Wess J (2012) Structural aspects of M(3) muscarinic acetylcholine receptor dimer formation and activation. *FASEB J* **26**(2): 604-616.

Hu J, Wang Y, Zhang X, Lloyd JR, Li JH, Karpiak J, Costanzi S and Wess J (2010) Structural basis of G protein-coupled receptor-G protein interactions. *Nat Chem Biol* **6**(7): 541-548.

Huang B, Perroud TD and Zare RN (2004) Photon counting histogram: one-photon excitation. *Chemphyschem* **5**(10): 1523-1531.

Huang J, Chen S, Zhang JJ and Huang XY (2013) Crystal structure of oligomeric beta-adrenergic G protein-coupled receptors in ligand-free basal state. *Nat Struct Mol Biol*.

Hundal RS, Krssak M, Dufour S, Laurent D, Lebon V, Chandramouli V, Inzucchi SE, Schumann WC, Petersen KF, Landau BR and Shulman GI (2000) Mechanism by which metformin reduces glucose production in type 2 diabetes. *Diabetes* **49**(12): 2063-2069.

Huwiler A and Pfeilschifter J (2009) Lipids as targets for novel anti-inflammatory therapies. *Pharmacol Ther* **124**(1): 96-112.

Ichimura A, Hirasawa A, Poulain-Godefroy O, Bonnefond A, Hara T, Yengo L, Kimura I, Leloire A, Liu N, Iida K, Choquet H, Besnard P, Lecoeur C, Vivequin S, Ayukawa K, Takeuchi M, Ozawa K, Tauber M, Maffeis C, Morandi A, Buzzetti R, Elliott P, Pouta A, Jarvelin MR, Korner A, Kiess W, Pigeyre M, Caiazzo R, Van Hul W, Van Gaal L, Horber F, Balkau B, Levy-Marchal C, Rouskas K, Kouvatsi A, Hebebrand J, Hinney A, Scherag A, Pattou F, Meyre D, Koshimizu TA, Wolowczuk I, Tsujimoto G and Froguel P (2012) Dysfunction of lipid sensor GPR120 leads to obesity in both mouse and human. *Nature*.

Imasawa T, Koike K, Ishii I, Chun J and Yatomi Y (2010) Blockade of sphingosine 1-phosphate receptor 2 signaling attenuates streptozotocin-induced apoptosis of pancreatic beta-cells. *Biochem Biophys Res Commun* **392**(2): 207-211.

Ish-Horowicz D and Burke JF (1981) Rapid and efficient cosmid cloning. *Nucleic Acids Res* **9**(13): 2989-2998.

Itoh Y, Cai K and Khorana HG (2001) Mapping of contact sites in complex formation between light-activated rhodopsin and transducin by covalent crosslinking: use of a chemically preactivated reagent. *Proc Natl Acad Sci U S A* **98**(9): 4883-4887.

Itoh Y, Kawamata Y, Harada M, Kobayashi M, Fujii R, Fukusumi S, Ogi K, Hosoya M, Tanaka Y, Uejima H, Tanaka H, Maruyama M, Satoh R, Okubo S, Kizawa H, Komatsu H, Matsumura F, Noguchi Y, Shinohara T, Hinuma S, Fujisawa Y and Fujino M (2003) Free fatty acids regulate insulin secretion from pancreatic beta cells through GPR40. *Nature* **422**(6928): 173-176.

Iwata K, Ito K, Fukuzaki A, Inaki K and Haga T (1999) Dynamin and rab5 regulate GRK2-dependent internalization of dopamine D2 receptors. *Eur J Biochem* **263**(2): 596-602.

Izumi M, Miyazawa H, Kamakura T, Yamaguchi I, Endo T and Hanaoka F (1991) Blasticidin S-resistance gene (bsr): a novel selectable marker for mammalian cells. *Exp Cell Res* **197**(2): 229-233.

Jaakola VP, Griffith MT, Hanson MA, Cherezov V, Chien EY, Lane JR, Ijzerman AP and Stevens RC (2008) The 2.6 angstrom crystal structure of a human A2A adenosine receptor bound to an antagonist. *Science* **322**(5905): 1211-1217.

James JR, Oliveira MI, Carmo AM, Iaboni A and Davis SJ (2006) A rigorous experimental framework for detecting protein oligomerization using bioluminescence resonance energy transfer. *Nat Methods* **3**(12): 1001-1006.

James WP, Caterson ID, Coutinho W, Finer N, Van Gaal LF, Maggioni AP, Torp-Pedersen C, Sharma AM, Shepherd GM, Rode RA and Renz CL (2010) Effect of sibutramine on cardiovascular outcomes in overweight and obese subjects. *N Engl J Med* **363**(10): 905-917.

Jang HJ, Kokrashvili Z, Theodorakis MJ, Carlson OD, Kim BJ, Zhou J, Kim HH, Xu X, Chan SL, Juhaszova M, Bernier M, Mosinger B, Margolskee RF and Egan JM (2007) Gut-expressed gustducin and taste receptors regulate secretion of glucagon-like peptide-1. *Proc Natl Acad Sci U S A* **104**(38): 15069-15074.

Janssen S, Laermans J, Iwakura H, Tack J and Depoortere I (2012) Sensing of fatty acids for octanoylation of ghrelin involves a gustatory G-protein. *PLoS One* **7**(6): e40168.

Jensen AD, Guarnieri F, Rasmussen SG, Asmar F, Ballesteros JA and Gether U (2001) Agonist-induced conformational changes at the cytoplasmic side of transmembrane segment 6 in the beta 2 adrenergic receptor mapped by site-selective fluorescent labeling. *J Biol Chem* **276**(12): 9279-9290.

Johnston JM, Aburi M, Provasi D, Bortolato A, Urizar E, Lambert NA, Javitch JA and Filizola M (2011) Making structural sense of dimerization interfaces of delta opioid receptor homodimers. *Biochemistry* **50**(10): 1682-1690.

Jones KA, Borowsky B, Tamm JA, Craig DA, Durkin MM, Dai M, Yao WJ, Johnson M, Gunwaldsen C, Huang LY, Tang C, Shen Q, Salon JA, Morse K, Laz T, Smith KE, Nagarathnam D, Noble SA, Branchek TA and Gerald C (1998) GABA(B) receptors function as a heteromeric assembly of the subunits GABA(B)R1 and GABA(B)R2. *Nature* **396**(6712): 674-679.

Jordan BA and Devi LA (1999) G-protein-coupled receptor heterodimerization modulates receptor function. *Nature* **399**(6737): 697-700.

Jordan BA, Trapaidze N, Gomes I, Nivarthi R and Devi LA (2001) Oligomerization of opioid receptors with beta 2-adrenergic receptors: a role in trafficking and mitogen-activated protein kinase activation. *Proc Natl Acad Sci U S A* **98**(1): 343-348.

Joseph JW, Koshkin V, Saleh MC, Sivitz WI, Zhang CY, Lowell BB, Chan CB and Wheeler MB (2004) Free fatty acid-induced beta-cell defects are dependent on uncoupling protein 2 expression. *J Biol Chem* **279**(49): 51049-51056.

Kabadi MU and Kabadi UM (2003) Efficacy of sulfonylureas with insulin in type 2 diabetes mellitus. *Ann Pharmacother* **37**(11): 1572-1576.

Kaku K, Araki T and Yoshinaka R (2013) Randomized, double-blind, dose-ranging study of TAK-875, a novel GPR40 agonist, in Japanese patients with inadequately controlled type 2 diabetes. *Diabetes Care* **36**(2): 245-250.

Kammerer RA, Frank S, Schulthess T, Landwehr R, Lustig A and Engel J (1999) Heterodimerization of a functional GABAB receptor is mediated by parallel coiled-coil alpha-helices. *Biochemistry* **38**(40): 13263-13269.

Kang DS, Kern RC, Puthenveedu MA, von Zastrow M, Williams JC and Benovic JL (2009) Structure of an arrestin2-clathrin complex reveals a novel clathrin binding domain that modulates receptor trafficking. *J Biol Chem* **284**(43): 29860-29872.

Karaki S, Mitsui R, Hayashi H, Kato I, Sugiya H, Iwanaga T, Furness JB and Kuwahara A (2006) Short-chain fatty acid receptor, GPR43, is expressed by enteroendocrine cells and mucosal mast cells in rat intestine. *Cell Tissue Res* **324**(3): 353-360.

Karaki S, Tazoe H, Hayashi H, Kashiwabara H, Tooyama K, Suzuki Y and Kuwahara A (2008) Expression of the short-chain fatty acid receptor, GPR43, in the human colon. *J Mol Histol* **39**(2): 135-142.

Katada T and Ui M (1982) Direct modification of the membrane adenylate cyclase system by islet-activating protein due to ADP-ribosylation of a membrane protein. *Proc Natl Acad Sci U S A* **79**(10): 3129-3133.

Katsuma S, Hatae N, Yano T, Ruike Y, Kimura M, Hirasawa A and Tsujimoto G (2005) Free fatty acids inhibit serum deprivation-induced apoptosis through GPR120 in a murine enteroendocrine cell line STC-1. *J Biol Chem* **280**(20): 19507-19515.

Kaupmann K, Malitschek B, Schuler V, Heid J, Froestl W, Beck P, Mosbacher J, Bischoff S, Kulik A, Shigemoto R, Karschin A and Bettler B (1998) GABA(B)-receptor subtypes assemble into functional heteromeric complexes. *Nature* **396**(6712): 683-687.

Kaya AI, Ugur O, Altuntas O, Sayar K and Onaran HO (2011) Long and short distance movements of beta(2)-adrenoceptor in cell membrane assessed by photoconvertible fluorescent protein dendra2-beta(2)-adrenoceptor fusion. *Biochim Biophys Acta* **1813**(8): 1511-1524.

Kebede M, Alquier T, Latour MG, Semache M, Tremblay C and Poitout V (2008) The fatty acid receptor GPR40 plays a role in insulin secretion in vivo after high-fat feeding. *Diabetes* **57**(9): 2432-2437.

Kebede M, Ferdaoussi M, Mancini A, Alquier T, Kulkarni RN, Walker MD and Poitout V (2012) Glucose activates free fatty acid receptor 1 gene transcription via phosphatidylinositol-3-kinase-dependent O-GlcNAcylation of pancreas-duodenum homeobox-1. *Proc Natl Acad Sci U S A* **109**(7): 2376-2381.

Kenakin T (1995) Agonist-receptor efficacy. I: Mechanisms of efficacy and receptor promiscuity. *Trends Pharmacol Sci* **16**(6): 188-192.

Kenakin T (2001) Inverse, protean, and ligand-selective agonism: matters of receptor conformation. *FASEB J* **15**(3): 598-611.

Kendall MR and Hupfeld CJ (2008) FTY720, a sphingosine-1-phosphate receptor modulator, reverses high-fat diet-induced weight gain, insulin resistance and adipose tissue inflammation in C57BL/6 mice. *Diabetes Obes Metab* **10**(9): 802-805.

Keppler A, Gendreizig S, Gronemeyer T, Pick H, Vogel H and Johnsson K (2003) A general method for the covalent labeling of fusion proteins with small molecules in vivo. *Nat Biotechnol* **21**(1): 86-89.

Kerppola TK (2008) Bimolecular fluorescence complementation (BiFC) analysis as a probe of protein interactions in living cells. *Annu Rev Biophys* **37**: 465-487.

Khairallah RJ, Kim J, O'Shea KM, O'Connell KA, Brown BH, Galvao T, Daneault C, Des Rosiers C, Polster BM, Hoppel CL and Stanley WC (2012) Improved mitochondrial function with diet-induced increase in either docosahexaenoic acid or arachidonic acid in membrane phospholipids. *PLoS One* **7**(3): e34402.

Khan SM, Sleno R, Gora S, Zylbergold P, Laverdure JP, Labbe JC, Miller GJ and Hebert TE (2013) The expanding roles of Gbetagamma subunits in G protein-coupled receptor signaling and drug action. *Pharmacol Rev* **65**(2): 545-577.

Kilpatrick LE, Briddon SJ, Hill SJ and Holliday ND (2010) Quantitative analysis of neuropeptide Y receptor association with beta-arrestin2 measured by bimolecular fluorescence complementation. *Br J Pharmacol* **160**(4): 892-906.

Kilpatrick LE, Briddon SJ and Holliday ND (2012) Fluorescence correlation spectroscopy, combined with bimolecular fluorescence complementation, reveals the effects of beta-arrestin complexes and endocytic targeting on the membrane mobility of neuropeptide Y receptors. *Biochim Biophys Acta* **1823**(6): 1068-1081.

Kim CM, Dion SB and Benovic JL (1993) Mechanism of beta-adrenergic receptor kinase activation by G proteins. *J Biol Chem* **268**(21): 15412-15418.

Kim HS, Hwang YC, Koo SH, Park KS, Lee MS, Kim KW and Lee MK (2013a) PPAR-gamma activation increases insulin secretion through the up-regulation of the free fatty acid receptor GPR40 in pancreatic beta-cells. *PLoS One* **8**(1): e50128.

Kim J, Ahn S, Rajagopal K and Lefkowitz RJ (2009) Independent beta-arrestin2 and Gq/protein kinase Czeta pathways for ERK stimulated by angiotensin type 1A receptors in vascular smooth muscle cells converge on transactivation of the epidermal growth factor receptor. *J Biol Chem* **284**(18): 11953-11962.

Kim J, Li Y and Watkins BA (2011) Endocannabinoid signaling and energy metabolism: a target for dietary intervention. *Nutrition* **27**(6): 624-632.

Kim J, Li Y and Watkins BA (2013b) Fat to treat fat: Emerging relationship between dietary PUFA, endocannabinoids, and obesity. *Prostaglandins Other Lipid Mediat*.

Kim YM and Benovic JL (2002) Differential roles of arrestin-2 interaction with clathrin and adaptor protein 2 in G protein-coupled receptor trafficking. *J Biol Chem* **277**(34): 30760-30768.

Kimura M, Takatsuki A and Yamaguchi I (1994) Blasticidin S deaminase gene from Aspergillus terreus (BSD): a new drug resistance gene for transfection of mammalian cells. *Biochim Biophys Acta* **1219**(3): 653-659.

Kinnamon SC (2012) Taste receptor signalling - from tongues to lungs. *Acta Physiol (Oxf)* **204**(2): 158-168.

Kniazeff J, Bessis AS, Maurel D, Ansanay H, Prezeau L and Pin JP (2004) Closed state of both binding domains of homodimeric mGlu receptors is required for full activity. *Nat Struct Mol Biol* **11**(8): 706-713.

Kobilka BK, Kobilka TS, Daniel K, Regan JW, Caron MG and Lefkowitz RJ (1988) Chimeric alpha 2-,beta 2-adrenergic receptors: delineation of domains involved in effector coupling and ligand binding specificity. *Science* **240**(4857): 1310-1316.

Kolakowski LF, Jr. (1994) GCRDb: a G-protein-coupled receptor database. *Receptors Channels* **2**(1): 1-7.

Kong G, Penn R and Benovic JL (1994) A beta-adrenergic receptor kinase dominant negative mutant attenuates desensitization of the beta 2-adrenergic receptor. *J Biol Chem* **269**(18): 13084-13087.

Kostenis E, Conklin BR and Wess J (1997) Molecular basis of receptor/G protein coupling selectivity studied by coexpression of wild type and mutant m2 muscarinic receptors with mutant G alpha(q) subunits. *Biochemistry* **36**(6): 1487-1495.

Kotarsky K, Nilsson NE, Flodgren E, Owman C and Olde B (2003) A human cell surface receptor activated by free fatty acids and thiazolidinedione drugs. *Biochem Biophys Res Commun* **301**(2): 406-410.

Kourtoglou GI (2011) Insulin therapy and exercise. *Diabetes Res Clin Pract* **93 Suppl 1**: S73-77.

Kozma E, Jayasekara PS, Squarcialupi L, Paoletta S, Moro S, Federico S, Spalluto G and Jacobson KA (2013) Fluorescent ligands for adenosine receptors. *Bioorg Med Chem Lett* **23**(1): 26-36.

Krasnoperov V, Lu Y, Buryanovsky L, Neubert TA, Ichtchenko K and Petrenko AG (2002) Post-translational proteolytic processing of the calcium-independent receptor of alpha-latrotoxin (CIRL), a natural chimera of the cell adhesion protein and the G protein-coupled receptor. Role of the G protein-coupled receptor proteolysis site (GPS) motif. *J Biol Chem* **277**(48): 46518-46526.

Kraus S, Benard O, Naor Z and Seger R (2003) c-Src is activated by the epidermal growth factor receptor in a pathway that mediates JNK and ERK activation by gonadotropin-releasing hormone in COS7 cells. *J Biol Chem* **278**(35): 32618-32630.

Krenzel ES, Chen Z and Hamilton JA (2013) Correspondence of Fatty Acid and Drug Binding Sites on Human Serum Albumin: A Two-Dimensional Nuclear Magnetic Resonance Study. *Biochemistry*.

Krilov L, Nguyen A, Miyazaki T, Unson CG, Williams R, Lee NH, Ceryak S and Bouscarel B (2011) Dual mode of glucagon receptor internalization: role of PKCalpha, GRKs and beta-arrestins. *Exp Cell Res* **317**(20): 2981-2994.

Krupnick JG, Goodman OB, Jr., Keen JH and Benovic JL (1997) Arrestin/clathrin interaction. Localization of the clathrin binding domain of nonvisual arrestins to the carboxy terminus. *J Biol Chem* **272**(23): 15011-15016.

Kruse AC, Hu J, Pan AC, Arlow DH, Rosenbaum DM, Rosemond E, Green HF, Liu T, Chae PS, Dror RO, Shaw DE, Weis WI, Wess J and Kobilka BK (2012) Structure and dynamics of the M3 muscarinic acetylcholine receptor. *Nature* **482**(7386): 552-556.

Kuner R, Kohr G, Grunewald S, Eisenhardt G, Bach A and Kornau HC (1999) Role of heteromer formation in GABAB receptor function. *Science* **283**(5398): 74-77.

Kunishima N, Shimada Y, Tsuji Y, Sato T, Yamamoto M, Kumasaka T, Nakanishi S, Jingami H and Morikawa K (2000) Structural basis of glutamate recognition by a dimeric metabotropic glutamate receptor. *Nature* **407**(6807): 971-977.

Kurten RC, Cadena DL and Gill GN (1996) Enhanced degradation of EGF receptors by a sorting nexin, SNX1. *Science* **272**(5264): 1008-1010.

Kuszak AJ, Pitchiaya S, Anand JP, Mosberg HI, Walter NG and Sunahara RK (2009) Purification and functional reconstitution of monomeric mu-opioid receptors: allosteric modulation of agonist binding by Gi2. *J Biol Chem* **284**(39): 26732-26741.

Lagerstrom MC and Schioth HB (2008) Structural diversity of G protein-coupled receptors and significance for drug discovery. *Nat Rev Drug Discov* **7**(4): 339-357.

Lambright DG, Noel JP, Hamm HE and Sigler PB (1994) Structural determinants for activation of the alpha-subunit of a heterotrimeric G protein. *Nature* **369**(6482): 621-628.

Lambright DG, Sondek J, Bohm A, Skiba NP, Hamm HE and Sigler PB (1996) The 2.0 A crystal structure of a heterotrimeric G protein. *Nature* **379**(6563): 311-319.

Lan H, Hoos LM, Liu L, Tetzloff G, Hu W, Abbondanzo SJ, Vassileva G, Gustafson EL, Hedrick JA and Davis HR (2008) Lack of FFAR1/GPR40 does not protect mice from high-fat diet-induced metabolic disease. *Diabetes* **57**(11): 2999-3006.

Lan H, Liu Y, Bell MI, Gurevich VV and Neve KA (2009) A dopamine D2 receptor mutant capable of G protein-mediated signaling but deficient in arrestin binding. *Mol Pharmacol* **75**(1): 113-123.

Lane JR, Powney B, Wise A, Rees S and Milligan G (2008) G protein coupling and ligand selectivity of the D2L and D3 dopamine receptors. *J Pharmacol Exp Ther* **325**(1): 319-330.

Laporte SA, Oakley RH, Holt JA, Barak LS and Caron MG (2000) The interaction of beta-arrestin with the AP-2 adaptor is required for the clustering of beta 2-adrenergic receptor into clathrin-coated pits. *J Biol Chem* **275**(30): 23120-23126.

Laporte SA, Oakley RH, Zhang J, Holt JA, Ferguson SS, Caron MG and Barak LS (1999) The beta2-adrenergic receptor/betaarrestin complex recruits the clathrin adaptor AP-2 during endocytosis. *Proc Natl Acad Sci U S A* **96**(7): 3712-3717.

Latour MG, Alquier T, Oseid E, Tremblay C, Jetton TL, Luo J, Lin DC and Poitout V (2007) GPR40 is necessary but not sufficient for fatty acid stimulation of insulin secretion in vivo. *Diabetes* **56**(4): 1087-1094.

Lauffer LM, Iakoubov R and Brubaker PL (2009) GPR119 is essential for oleoylethanolamide-induced glucagon-like peptide-1 secretion from the intestinal enteroendocrine L-cell. *Diabetes* **58**(5): 1058-1066.

Le Poul E, Loison C, Struyf S, Springael JY, Lannoy V, Decobecq ME, Brezillon S, Dupriez V, Vassart G, Van Damme J, Parmentier M and Detheux M (2003) Functional characterization of human receptors for short chain fatty acids and their role in polymorphonuclear cell activation. *J Biol Chem* **278**(28): 25481-25489.

Leach K, Sexton PM and Christopoulos A (2011) Quantification of allosteric interactions at G protein-coupled receptors using radioligand binding assays. *Curr Protoc Pharmacol* **Chapter 1**: Unit 1 22.

Lebon G, Warne T, Edwards PC, Bennett K, Langmead CJ, Leslie AG and Tate CG (2011) Agonist-bound adenosine A2A receptor structures reveal common features of GPCR activation. *Nature* **474**(7352): 521-525.

Lee SP, So CH, Rashid AJ, Varghese G, Cheng R, Lanca AJ, O'Dowd BF and George SR (2004) Dopamine D1 and D2 receptor Co-activation generates a novel phospholipase C-mediated calcium signal. *J Biol Chem* **279**(34): 35671-35678.

Lee T, Schwandner R, Swaminath G, Weiszmann J, Cardozo M, Greenberg J, Jaeckel P, Ge H, Wang Y, Jiao X, Liu J, Kayser F, Tian H and Li Y (2008) Identification and functional characterization of allosteric agonists for the G protein-coupled receptor FFA2. *Mol Pharmacol* **74**(6): 1599-1609.

Lehmann JM, Moore LB, Smith-Oliver TA, Wilkison WO, Willson TM and Kliewer SA (1995) An antidiabetic thiazolidinedione is a high affinity ligand for peroxisome proliferator-activated receptor gamma (PPAR gamma). *J Biol Chem* **270**(22): 12953-12956.

Leifke E, Naik H, Wu J, Viswanathan P, Demanno D, Kipnes M and Vakilynejad M (2012) A multiple-ascending-dose study to evaluate safety, pharmacokinetics, and pharmacodynamics of a novel GPR40 agonist, TAK-875, in subjects with type 2 diabetes. *Clin Pharmacol Ther* **92**(1): 29-39.

Leonelli M, Graciano MF and Britto LR (2011) TRP channels, omega-3 fatty acids, and oxidative stress in neurodegeneration: from the cell membrane to intracellular cross-links. *Braz J Med Biol Res* **44**(11): 1088-1096.

Li J, Xiang B, Su W, Zhang X, Huang Y and Ma L (2003) Agonist-induced formation of opioid receptor-G protein-coupled receptor kinase (GRK)-G beta gamma complex on membrane is required for GRK2 function in vivo. *J Biol Chem* **278**(32): 30219-30226.

Li Y, Kokrashvili Z, Mosinger B and Margolskee RF (2013) Gustducin couples fatty acid receptors to GLP-1 release in colon. *Am J Physiol Endocrinol Metab*.

Liao W, Nguyen MT, Yoshizaki T, Favelyukis S, Patsouris D, Imamura T, Verma IM and Olefsky JM (2007) Suppression of PPAR-gamma attenuates insulin-stimulated glucose uptake by affecting both GLUT1 and GLUT4 in 3T3-L1 adipocytes. *Am J Physiol Endocrinol Metab* **293**(1): E219-227.

Lin D, Guo Q, Luo J, Zhang J, Nguyen K, Chen M, Tran T, Dransfield PJ, Brown SP, Houze J, Vimolratana M, Jiao XY, Wang Y, Birdsall NJ and Swaminath G (2012) Identification and Pharmacological Characterization of Multiple Allosteric Binding Sites on the FFA1 Receptor. *Mol Pharmacol*.

Lin DC, Zhang J, Zhuang R, Li F, Nguyen K, Chen M, Tran T, Lopez E, Lu JY, Li XN, Tang L, Tonn GR, Swaminath G, Reagan JD, Chen JL, Tian H, Lin YJ, Houze JB and Luo J (2011) AMG 837: a novel GPR40/FFA1 agonist that enhances insulin secretion and lowers glucose levels in rodents. *PLoS One* **6**(11): e27270.

Liou AP, Lu X, Sei Y, Zhao X, Pechhold S, Carrero RJ, Raybould HE and Wank S (2011) The G-protein-coupled receptor GPR40 directly mediates long-chain fatty acid-induced secretion of cholecystokinin. *Gastroenterology* **140**(3): 903-912.

Lisenbee CS, Dong M and Miller LJ (2005) Paired cysteine mutagenesis to establish the pattern of disulfide bonds in the functional intact secretin receptor. *J Biol Chem* **280**(13): 12330-12338.

Litosch I (2012) Negative feedback regulation of Gq signaling by protein kinase C is disrupted by diacylglycerol kinase zeta in COS-7 cells. *Biochem Biophys Res Commun* **417**(3): 956-960.

Liu D, Wang L, Meng Q, Kuang H and Liu X (2012a) G-protein coupled receptor 120 is involved in glucose metabolism in fat cells. *Cell Mol Biol (Noisy-le-grand)* **Suppl.58**: OL1757-1762.

Liu J, Conklin BR, Blin N, Yun J and Wess J (1995) Identification of a receptor/G-protein contact site critical for signaling specificity and G-protein activation. *Proc Natl Acad Sci U S A* **92**(25): 11642-11646.

Liu W, Chun E, Thompson AA, Chubukov P, Xu F, Katritch V, Han GW, Roth CB, Heitman LH, AP IJ, Cherezov V and Stevens RC (2012b) Structural basis for allosteric regulation of GPCRs by sodium ions. *Science* **337**(6091): 232-236.

Liu W, Eilers M, Patel AB and Smith SO (2004) Helix packing moments reveal diversity and conservation in membrane protein structure. *J Mol Biol* **337**(3): 713-729.

Lodeiro M, Theodoropoulou M, Pardo M, Casanueva FF and Camina JP (2009) c-Src regulates Akt signaling in response to ghrelin via beta-arrestin signaling-independent and -dependent mechanisms. *PLoS ONE* **4**(3): e4686.

Lohse MJ, Benovic JL, Codina J, Caron MG and Lefkowitz RJ (1990) beta-Arrestin: a protein that regulates beta-adrenergic receptor function. *Science* **248**(4962): 1547-1550.

Lohse MJ, Nuber S and Hoffmann C (2012) Fluorescence/bioluminescence resonance energy transfer techniques to study G-protein-coupled receptor activation and signaling. *Pharmacol Rev* **64**(2): 299-336.

Lu H, Koshkin V, Allister EM, Gyulkhandanyan AV and Wheeler MB (2010) Molecular and metabolic evidence for mitochondrial defects associated with beta-cell dysfunction in a mouse model of type 2 diabetes. *Diabetes* **59**(2): 448-459.

Luo J, Swaminath G, Brown SP, Zhang J, Guo Q, Chen M, Nguyen K, Tran T, Miao L, Dransfield PJ, Vimolratana M, Houze JB, Wong S, Toteva M, Shan B, Li F, Zhuang R and Lin DC (2012) A Potent class of GPR40 full agonists engages the enteroinsular axis to promote glucose control in rodents. *PLoS One* **7**(10): e46300.

Luttrell DK and Luttrell LM (2004) Not so strange bedfellows: G-protein-coupled receptors and Src family kinases. *Oncogene* **23**(48): 7969-7978.

Luttrell LM, Ferguson SS, Daaka Y, Miller WE, Maudsley S, Della Rocca GJ, Lin F, Kawakatsu H, Owada K, Luttrell DK, Caron MG and Lefkowitz RJ (1999) Beta-arrestin-dependent formation of beta2 adrenergic receptor-Src protein kinase complexes. *Science* **283**(5402): 655-661.

Luttrell LM, Roudabush FL, Choy EW, Miller WE, Field ME, Pierce KL and Lefkowitz RJ (2001) Activation and targeting of extracellular signal-regulated kinases by beta-arrestin scaffolds. *Proc Natl Acad Sci U S A* **98**(5): 2449-2454.

Ma J, Novack A, Nashashibi I, Pham P, Rabbat CJ, Song J, Shi DF, Zhao Z, Choi YJ and Chen X (2010) Aryl GPR120 receptor agonists and uses there of. *International Patent WO2010/048207*.

MacDonald ML, Lamerdin J, Owens S, Keon BH, Bilter GK, Shang Z, Huang Z, Yu H, Dias J, Minami T, Michnick SW and Westwick JK (2006) Identifying off-target effects and hidden phenotypes of drugs in human cells. *Nat Chem Biol* **2**(6): 329-337.

Madonna R and De Caterina R (2011) Cellular and molecular mechanisms of vascular injury in diabetes--part I: pathways of vascular disease in diabetes. *Vascul Pharmacol* **54**(3-6): 68-74.

Maggio R, Vogel Z and Wess J (1993) Coexpression studies with mutant muscarinic/adrenergic receptors provide evidence for intermolecular "cross-talk" between G-protein-linked receptors. *Proc Natl Acad Sci U S A* **90**(7): 3103-3107.

Malbon CC (2004) Frizzleds: new members of the superfamily of G-protein-coupled receptors. *Front Biosci* **9**: 1048-1058.

Malecz N, Bambino T, Bencsik M and Nissenson RA (1998) Identification of phosphorylation sites in the G protein-coupled receptor for parathyroid hormone. Receptor phosphorylation is not required for agonist-induced internalization. *Mol Endocrinol* **12**(12): 1846-1856.

Manglik A, Kruse AC, Kobilka TS, Thian FS, Mathiesen JM, Sunahara RK, Pardo L, Weis WI, Kobilka BK and Granier S (2012) Crystal structure of the micro-opioid receptor bound to a morphinan antagonist. *Nature* **485**(7398): 321-326.

Marchese A, Chen C, Kim YM and Benovic JL (2003) The ins and outs of G protein-coupled receptor trafficking. *Trends in Biochemical Sciences* **28**(7): 369-376.

Margeta-Mitrovic M, Jan YN and Jan LY (2000) A trafficking checkpoint controls GABA(B) receptor heterodimerization. *Neuron* **27**(1): 97-106.

Marie J, Richard E, Pruneau D, Paquet JL, Siatka C, Larguier R, Ponce C, Vassault P, Groblewski T, Maigret B and Bonnafous JC (2001) Control of conformational equilibria in the human B2 bradykinin receptor. Modeling of nonpeptidic ligand action and comparison to the rhodopsin structure. *J Biol Chem* **276**(44): 41100-41111.

Marion S, Oakley RH, Kim KM, Caron MG and Barak LS (2006) A beta-arrestin binding determinant common to the second intracellular loops of rhodopsin family G protein-coupled receptors. *J Biol Chem* **281**(5): 2932-2938.

Maruyama T, Kanaji T, Nakade S, Kanno T and Mikoshiba K (1997) 2APB, 2-aminoethoxydiphenyl borate, a membrane-penetrable modulator of Ins(1,4,5)P3-induced Ca2+ release. *J Biochem* **122**(3): 498-505.

Matsuda-Nagasumi K, Takami-Esaki R, Iwachidow K, Yasuhara Y, Tanaka H, Ogi K, Nakata M, Yano T, Hinuma S, Taketomi S, Odaka H and Kaisho Y (2013) Lack of GPR40/FFAR1 does not induce diabetes even under insulin resistance condition. *Diabetes Obes Metab* **15**(6): 538-545.

Matsumura S, Eguchi A, Mizushige T, Kitabayashi N, Tsuzuki S, Inoue K and Fushiki T (2009) Colocalization of GPR120 with phospholipase-Cbeta2 and alpha-gustducin in the taste bud cells in mice. *Neurosci Lett* **450**(2): 186-190.

Matsumura S, Mizushige T, Yoneda T, Iwanaga T, Tsuzuki S, Inoue K and Fushiki T (2007) GPR expression in the rat taste bud relating to fatty acid sensing. *Biomedical Research-Tokyo* **28**(1): 49-55.

Matta JA, Miyares RL and Ahern GP (2007) TRPV1 is a novel target for omega-3 polyunsaturated fatty acids. *J Physiol* **578**(Pt 2): 397-411.

Maurel D, Comps-Agrar L, Brock C, Rives ML, Bourrier E, Ayoub MA, Bazin H, Tinel N, Durroux T, Prezeau L, Trinquet E and Pin JP (2008) Cell-surface protein-protein interaction analysis with time-resolved FRET and snap-tag technologies: application to GPCR oligomerization. *Nat Methods* **5**(6): 561-567.

May LT, Briddon SJ and Hill SJ (2010) Antagonist selective modulation of adenosine A1 and A3 receptor pharmacology by the food dye Brilliant Black BN: evidence for allosteric interactions. *Mol Pharmacol* **77**(4): 678-686.

May LT, Bridge LJ, Stoddart LA, Briddon SJ and Hill SJ (2011) Allosteric interactions across native adenosine-A3 receptor homodimers: quantification using single-cell ligand-binding kinetics. *FASEB J* **25**(10): 3465-3476.

May LT, Leach K, Sexton PM and Christopoulos A (2007) Allosteric modulation of G protein-coupled receptors. *Annu Rev Pharmacol Toxicol* **47**: 1-51.

McDonald PH, Chow CW, Miller WE, Laporte SA, Field ME, Lin FT, Davis RJ and Lefkowitz RJ (2000) Beta-arrestin 2: a receptor-regulated MAPK scaffold for the activation of JNK3. *Science* **290**(5496): 1574-1577.

Michalik L, Auwerx J, Berger JP, Chatterjee VK, Glass CK, Gonzalez FJ, Grimaldi PA, Kadowaki T, Lazar MA, O'Rahilly S, Palmer CN, Plutzky J, Reddy JK, Spiegelman BM, Staels B and Wahli W (2006) International Union of Pharmacology. LXI. Peroxisome proliferator-activated receptors. *Pharmacol Rev* **58**(4): 726-741.

Middleton RJ, Briddon SJ, Cordeaux Y, Yates AS, Dale CL, George MW, Baker JG, Hill SJ and Kellam B (2007) New fluorescent adenosine A1-receptor agonists that allow quantification of ligand-receptor interactions in microdomains of single living cells. *J Med Chem* **50**(4): 782-793.

Mieczkowska A, Basle MF, Chappard D and Mabilleau G (2012) Thiazolidinediones induce osteocyte apoptosis by a G protein-coupled receptor 40-dependent mechanism. *J Biol Chem* **287**(28): 23517-23526.

Miller WE, Maudsley S, Ahn S, Khan KD, Luttrell LM and Lefkowitz RJ (2000) beta-arrestin1 interacts with the catalytic domain of the tyrosine kinase c-SRC. Role of beta-

arrestin1-dependent targeting of c-SRC in receptor endocytosis. *J Biol Chem* **275**(15): 11312-11319.

Milligan G (2009) G protein-coupled receptor hetero-dimerization: contribution to pharmacology and function. *Br J Pharmacol* **158**(1): 5-14.

Milligan G and Bouvier M (2005) Methods to monitor the quaternary structure of G protein-coupled receptors. *FEBS J* **272**(12): 2914-2925.

Mitchell DC, Niu SL and Litman BJ (2012) Quantifying the differential effects of DHA and DPA on the early events in visual signal transduction. *Chem Phys Lipids* **165**(4): 393-400.

Monnot C, Bihoreau C, Conchon S, Curnow KM, Corvol P and Clauser E (1996) Polar residues in the transmembrane domains of the type 1 angiotensin II receptor are required for binding and coupling. Reconstitution of the binding site by co-expression of two deficient mutants. *J Biol Chem* **271**(3): 1507-1513.

Montiel M, Quesada J and Jimenez E (2004) Activation of second messenger-dependent protein kinases induces muscarinic acetylcholine receptor desensitization in rat thyroid epithelial cells. *Mol Cell Endocrinol* **223**(1-2): 35-41.

Moore K, Zhang Q, Murgolo N, Hosted T and Duffy R (2009) Cloning, expression, and pharmacological characterization of the GPR120 free fatty acid receptor from cynomolgus monkey: comparison with human GPR120 splice variants. *Comp Biochem Physiol B Biochem Mol Biol* **154**(4): 419-426.

Moore RH, Sadovnikoff N, Hoffenberg S, Liu S, Woodford P, Angelides K, Trial JA, Carsrud ND, Dickey BF and Knoll BJ (1995) Ligand-stimulated beta 2-adrenergic receptor internalization via the constitutive endocytic pathway into rab5-containing endosomes. *J Cell Sci* **108 (Pt 9)**: 2983-2991.

Morgan NG and Dhayal S (2009) G-protein coupled receptors mediating long chain fatty acid signalling in the pancreatic beta-cell. *Biochem Pharmacol* **78**(12): 1419-1427.

Morgensztern D and McLeod HL (2005) PI3K/Akt/mTOR pathway as a target for cancer therapy. *Anticancer Drugs* **16**(8): 797-803.

Moro O, Lameh J, Hogger P and Sadee W (1993a) Hydrophobic amino acid in the i2 loop plays a key role in receptor-G protein coupling. *J Biol Chem* **268**(30): 22273-22276.

Moro O, Lameh J and Sadee W (1993b) Serine- and threonine-rich domain regulates internalization of muscarinic cholinergic receptors. *J Biol Chem* **268**(10): 6862-6865.

Moro O, Shockley MS, Lameh J and Sadee W (1994) Overlapping multi-site domains of the muscarinic cholinergic Hm1 receptor involved in signal transduction and sequestration. *J Biol Chem* **269**(9): 6651-6655.

Morrison DK and Davis RJ (2003) Regulation of MAP kinase signaling modules by scaffold proteins in mammals. *Annu Rev Cell Dev Biol* **19**: 91-118.

Mudaliar S and Edelman SV (2001) Insulin therapy in type 2 diabetes. *Endocrinol Metab Clin North Am* **30**(4): 935-982.

Mukherjee RS, McBride EW, Beinborn M, Dunlap K and Kopin AS (2006) Point mutations in either subunit of the GABAB receptor confer constitutive activity to the heterodimer. *Mol Pharmacol* **70**(4): 1406-1413.

Mulsant P, Gatignol A, Dalens M and Tiraby G (1988) Phleomycin resistance as a dominant selectable marker in CHO cells. *Somat Cell Mol Genet* **14**(3): 243-252.

Mundell SJ, Luo J, Benovic JL, Conley PB and Poole AW (2006) Distinct clathrin-coated pits sort different G protein-coupled receptor cargo. *Traffic* **7**(10): 1420-1431.

Mundell SJ, Matharu AL, Nisar S, Palmer TM, Benovic JL and Kelly E (2010) Deletion of the distal COOH-terminus of the A2B adenosine receptor switches internalization to an arrestin- and clathrin-independent pathway and inhibits recycling. *Br J Pharmacol* **159**(3): 518-533.

Nagai T, Ibata K, Park ES, Kubota M, Mikoshiba K and Miyawaki A (2002) A variant of yellow fluorescent protein with fast and efficient maturation for cell-biological applications. *Nat Biotechnol* **20**(1): 87-90.

Nagasaki H, Kondo T, Fuchigami M, Hashimoto H, Sugimura Y, Ozaki N, Arima H, Ota A, Oiso Y and Hamada Y (2012) Inflammatory changes in adipose tissue enhance expression of GPR84, a medium-chain fatty acid receptor: TNFalpha enhances GPR84 expression in adipocytes. *FEBS Lett* **586**(4): 368-372.

Nagasumi K, Esaki R, Iwachidow K, Yasuhara Y, Ogi K, Tanaka H, Nakata M, Yano T, Shimakawa K, Taketomi S, Takeuchi K, Odaka H and Kaisho Y (2009) Overexpression of GPR40 in pancreatic beta-cells augments glucose-stimulated insulin secretion and improves glucose tolerance in normal and diabetic mice. *Diabetes* **58**(5): 1067-1076.

Nakamoto K, Nishinaka T, Matsumoto K, Kasuya F, Mankura M, Koyama Y and Tokuyama S (2012) Involvement of the long-chain fatty acid receptor GPR40 as a novel pain regulatory system. *Brain Res* **1432**: 74-83.

Nakamura K, Hipkin RW and Ascoli M (1998a) The agonist-induced phosphorylation of the rat follitropin receptor maps to the first and third intracellular loops. *Mol Endocrinol* **12**(4): 580-591.

Nakamura K, Krupnick JG, Benovic JL and Ascoli M (1998b) Signaling and phosphorylation-impaired mutants of the rat follitropin receptor reveal an activation- and phosphorylation-independent but arrestin-dependent pathway for internalization. *J Biol Chem* **273**(38): 24346-24354.

Naslund E, Gutniak M, Skogar S, Rossner S and Hellstrom PM (1998) Glucagon-like peptide 1 increases the period of postprandial satiety and slows gastric emptying in obese men. *Am J Clin Nutr* **68**(3): 525-530.

Neary NM, Small CJ, Druce MR, Park AJ, Ellis SM, Semjonous NM, Dakin CL, Filipsson K, Wang F, Kent AS, Frost GS, Ghatei MA and Bloom SR (2005) Peptide YY3-36 and glucagon-like peptide-17-36 inhibit food intake additively. *Endocrinology* **146**(12): 5120-5127.

Negoro N, Sasaki S, Mikami S, Ito M, Tsujihata Y, Ito R, Suzuki M, Takeuchi K, Suzuki N, Miyazaki J, Santou T, Odani T, Kanzaki N, Funami M, Morohashi A, Nonaka M, Matsunaga S, Yasuma T and Momose Y (2012) Optimization of (2,3-dihydro-1-benzofuran-3-yl)acetic acids: discovery of a non-free fatty acid-like, highly bioavailable G protein-coupled receptor 40/free fatty acid receptor 1 agonist as a glucose-dependent insulinotropic agent. *J Med Chem* **55**(8): 3960-3974.

Newman Z, Malik P, Wu TY, Ochoa C, Watsa N and Lindgren C (2007) Endocannabinoids mediate muscarine-induced synaptic depression at the vertebrate neuromuscular junction. *Eur J Neurosci* **25**(6): 1619-1630.

Nguyen T and Lau DC (2012) The obesity epidemic and its impact on hypertension. *Can J Cardiol* **28**(3): 326-333.

Nicholls SJ and Uno K (2012) Peroxisome proliferator-activated receptor (PPAR alpha/gamma) agonists as a potential target to reduce cardiovascular risk in diabetes. *Diab Vasc Dis Res* **9**(2): 89-94.

Nilsson NE, Kotarsky K, Owman C and Olde B (2003) Identification of a free fatty acid receptor, FFA2R, expressed on leukocytes and activated by short-chain fatty acids. *Biochem Biophys Res Commun* **303**(4): 1047-1052.

Nisar S, Kelly E, Cullen PJ and Mundell SJ (2010) Regulation of P2Y1 receptor traffic by sorting Nexin 1 is retromer independent. *Traffic* **11**(4): 508-519.

Nissen SE and Wolski K (2007) Effect of rosiglitazone on the risk of myocardial infarction and death from cardiovascular causes. *N Engl J Med* **356**(24): 2457-2471.

Nobles KN, Xiao K, Ahn S, Shukla AK, Lam CM, Rajagopal S, Strachan RT, Huang TY, Bressler EA, Hara MR, Shenoy SK, Gygi SP and Lefkowitz RJ (2011) Distinct phosphorylation sites on the beta(2)-adrenergic receptor establish a barcode that encodes differential functions of beta-arrestin. *Sci Signal* **4**(185): ra51.

Noel JP, Hamm HE and Sigler PB (1993) The 2.2 A crystal structure of transducin-alpha complexed with GTP gamma S. *Nature* **366**(6456): 654-663.

Norris PC and Dennis EA (2012) Omega-3 fatty acids cause dramatic changes in TLR4 and purinergic eicosanoid signaling. *Proc Natl Acad Sci U S A* **109**(22): 8517-8522.

Nygaard R, Frimurer TM, Holst B, Rosenkilde MM and Schwartz TW (2009) Ligand binding and micro-switches in 7TM receptor structures. *Trends Pharmacol Sci* **30**(5): 249-259.

Oakley RH, Laporte SA, Holt JA, Barak LS and Caron MG (1999) Association of beta-arrestin with G protein-coupled receptors during clathrin-mediated endocytosis dictates the profile of receptor resensitization. *J Biol Chem* **274**(45): 32248-32257.

Oakley RH, Laporte SA, Holt JA, Caron MG and Barak LS (2000) Differential affinities of visual arrestin, beta arrestin1, and beta arrestin2 for G protein-coupled receptors delineate two major classes of receptors. *J Biol Chem* **275**(22): 17201-17210.

Ogawa T, Hirose H, Miyashita K, Saito I and Saruta T (2005) GPR40 gene Arg211His polymorphism may contribute to the variation of insulin secretory capacity in Japanese men. *Metab-Clin Exp* **54**(3): 296-299.

Ogden CL, Carroll MD, Curtin LR, McDowell MA, Tabak CJ and Flegal KM (2006) Prevalence of overweight and obesity in the United States, 1999-2004. *JAMA-J Am Med Assoc* **295**(13): 1549-1555.

Oh da Y, Talukdar S, Bae EJ, Imamura T, Morinaga H, Fan W, Li P, Lu WJ, Watkins SM and Olefsky JM (2010) GPR120 Is an Omega-3 Fatty Acid Receptor Mediating Potent Anti-inflammatory and Insulin-Sensitizing Effects. *Cell* **142**(5): 687-698.

Oh DY, Talukdar S, Bae EJ, Imamura T, Morinaga H, Fan W, Li P, Lu WJ, Watkins SM and Olefsky JM (2010) GPR120 Is an Omega-3 Fatty Acid Receptor Mediating Potent Anti-inflammatory and Insulin-Sensitizing Effects. *Cell* **142**(5): 687-698.

Oldham WM and Hamm HE (2008) Heterotrimeric G protein activation by G-protein-coupled receptors. *Nat Rev Mol Cell Biol* **9**(1): 60-71.

Orban T, Huang CC, Homan KT, Jastrzebska B, Tesmer JJ and Palczewski K (2012) Substrate-Induced Changes in the Dynamics of Rhodopsin Kinase (G Protein-Coupled Receptor Kinase 1). *Biochemistry*.

Overington JP, Al-Lazikani B and Hopkins AL (2006) How many drug targets are there? *Nat Rev Drug Discov* **5**(12): 993-996.

Overton HA, Babbs AJ, Doel SM, Fyfe MC, Gardner LS, Griffin G, Jackson HC, Procter MJ, Rasamison CM, Tang-Christensen M, Widdowson PS, Williams GM and Reynet C (2006) Deorphanization of a G protein-coupled receptor for oleoylethanolamide and its use in the discovery of small-molecule hypophagic agents. *Cell Metab* **3**(3): 167-175.

Padgett CL and Slesinger PA (2010) GABAB receptor coupling to G-proteins and ion channels. *Adv Pharmacol* **58**: 123-147.

Pagotto U, Marsicano G, Cota D, Lutz B and Pasquali R (2006) The emerging role of the endocannabinoid system in endocrine regulation and energy balance. *Endocr Rev* **27**(1): 73-100.

Palczewski K, Kumasaka T, Hori T, Behnke CA, Motoshima H, Fox BA, Le Trong I, Teller DC, Okada T, Stenkamp RE, Yamamoto M and Miyano M (2000) Crystal structure of rhodopsin: A G protein-coupled receptor. *Science* **289**(5480): 739-745.

Pandey P, Seshacharyulu P, Das S, Rachagani S, Ponnusamy MP, Yan Y, Johansson SL, Datta K, Fong Lin M and Batra SK (2013) Impaired expression of protein phosphatase 2A subunits enhances metastatic potential of human prostate cancer cells through activation of AKT pathway. *Br J Cancer*.

Park JH, Scheerer P, Hofmann KP, Choe HW and Ernst OP (2008) Crystal structure of the ligand-free G-protein-coupled receptor opsin. *Nature* **454**(7201): 183-187.

Parker HE, Habib AM, Rogers GJ, Gribble FM and Reimann F (2009) Nutrient-dependent secretion of glucose-dependent insulinotropic polypeptide from primary murine K cells. *Diabetologia* **52**(2): 289-298.

Patel AB, Crocker E, Reeves PJ, Getmanova EV, Eilers M, Khorana HG and Smith SO (2005) Changes in interhelical hydrogen bonding upon rhodopsin activation. *J Mol Biol* **347**(4): 803-812.

Pedelacq JD, Cabantous S, Tran T, Terwilliger TC and Waldo GS (2006) Engineering and characterization of a superfolder green fluorescent protein. *Nat Biotechnol* **24**(1): 79-88.

Pellissier LP, Barthet G, Gaven F, Cassier E, Trinquet E, Pin JP, Marin P, Dumuis A, Bockaert J, Baneres JL and Claeysen S (2011) G protein activation by serotonin type 4 receptor dimers: evidence that turning on two protomers is more efficient. *J Biol Chem*.

Pellissier LP, Sallander J, Campillo M, Gaven F, Queffeulou E, Pillot M, Dumuis A, Claeysen S, Bockaert J and Pardo L (2009) Conformational toggle switches implicated in basal constitutive and agonist-induced activated states of 5-hydroxytryptamine-4 receptors. *Mol Pharmacol* **75**(4): 982-990.

Penela P, Ribas C and Mayor F, Jr. (2003) Mechanisms of regulation of the expression and function of G protein-coupled receptor kinases. *Cell Signal* **15**(11): 973-981.

Penn RB, Pronin AN and Benovic JL (2000) Regulation of G protein-coupled receptor kinases. *Trends Cardiovasc Med* **10**(2): 81-89.

Percherancier Y, Berchiche YA, Slight I, Volkmer-Engert R, Tamamura H, Fujii N, Bouvier M and Heveker N (2005) Bioluminescence resonance energy transfer reveals ligand-induced conformational changes in CXCR4 homo- and heterodimers. *J Biol Chem* **280**(11): 9895-9903.

Perfetti R, Zhou J, Doyle ME and Egan JM (2000) Glucagon-like peptide-1 induces cell proliferation and pancreatic-duodenum homeobox-1 expression and increases endocrine cell mass in the pancreas of old, glucose-intolerant rats. *Endocrinology* **141**(12): 4600-4605.

Petit JM, Guiu B, Duvillard L, Jooste V, Brindisi MC, Athias A, Bouillet B, Habchi M, Cottet V, Gambert P, Hillon P, Cercueil JP and Verges B (2012) Increased erythrocytes n-3 and n-6 polyunsaturated fatty acids is significantly associated with a lower prevalence of steatosis in patients with type 2 diabetes. *Clin Nutr* **31**(4): 520-525.

Philip F, Sengupta P and Scarlata S (2007) Signaling through a G Protein-coupled receptor and its corresponding G protein follows a stoichiometrically limited model. *J Biol Chem* **282**(26): 19203-19216.

Pippig S, Andexinger S and Lohse MJ (1995) Sequestration and recycling of beta 2-adrenergic receptors permit receptor resensitization. *Mol Pharmacol* **47**(4): 666-676.

Pitcher JA, Freedman NJ and Lefkowitz RJ (1998) G protein-coupled receptor kinases. *Annu Rev Biochem* **67**: 653-692.

Pitcher JA, Payne ES, Csortos C, DePaoli-Roach AA and Lefkowitz RJ (1995) The G-protein-coupled receptor phosphatase: a protein phosphatase type 2A with a distinct subcellular distribution and substrate specificity. *Proc Natl Acad Sci U S A* **92**(18): 8343-8347.

Poitout V, Amyot J, Semache M, Zarrouki B, Hagman D and Fontes G (2009) Glucolipotoxicity of the pancreatic beta cell. *Biochim Biophys Acta* **1801**(3): 289-298.

Polizio AH, Chinchilla P, Chen X, Manning DR and Riobo NA (2011) Sonic Hedgehog activates the GTPases Rac1 and RhoA in a Gli-independent manner through coupling of smoothened to Gi proteins. *Sci Signal* **4**(200): pt7.

Porter RK and Brand MD (1995) Mitochondrial proton conductance and H+/O ratio are independent of electron transport rate in isolated hepatocytes. *Biochem J* **310 (Pt 2)**: 379-382.

Potter RM, Maestas DC, Cimino DF and Prossnitz ER (2006) Regulation of N-formyl peptide receptor signaling and trafficking by individual carboxyl-terminal serine and threonine residues. *J Immunol* **176**(9): 5418-5425.

Pournaras DJ, Aasheim ET, Bueter M, Ahmed AR, Welbourn R, Olbers T and le Roux CW (2012) Effect of bypassing the proximal gut on gut hormones involved with glycemic control and weight loss. *Surg Obes Relat Dis* **8**(4): 371-374.

Pouwels KB and van Grootheest K (2012) The rosiglitazone decision process at FDA and EMA. What should we learn? *Int J Risk Saf Med* **24**(2): 73-80.

Pramanik A, Olsson M, Langel U, Bartfai T and Rigler R (2001) Fluorescence correlation spectroscopy detects galanin receptor diversity on insulinoma cells. *Biochemistry* **40**(36): 10839-10845.

Pramanik A and Rigler R (2001) Ligand-receptor interactions in the membrane of cultured cells monitored by fluorescence correlation spectroscopy. *Biol Chem* **382**(3): 371-378.

Prentki M and Nolan CJ (2006) Islet beta cell failure in type 2 diabetes. *J Clin Invest* **116**(7): 1802-1812.

Qin K, Dong C, Wu G and Lambert NA (2011) Inactive-state preassembly of G(q)-coupled receptors and G(q) heterotrimers. *Nat Chem Biol* **7**(10): 740-747.

Ramasamy R, Yan SF and Schmidt AM (2011) Receptor for AGE (RAGE): signaling mechanisms in the pathogenesis of diabetes and its complications. *Ann N Y Acad Sci* **1243**: 88-102.

Ramsden CE, Zamora D, Leelarthaepin B, Majchrzak-Hong SF, Faurot KR, Suchindran CM, Ringel A, Davis JM and Hibbeln JR (2013) Use of dietary linoleic acid for secondary prevention of coronary heart disease and death: evaluation of recovered data from the Sydney Diet Heart Study and updated meta-analysis. *BMJ* **346**: e8707.

Rasmussen SG, Choi HJ, Fung JJ, Pardon E, Casarosa P, Chae PS, Devree BT, Rosenbaum DM, Thian FS, Kobilka TS, Schnapp A, Konetzki I, Sunahara RK, Gellman SH, Pautsch A, Steyaert J, Weis WI and Kobilka BK (2011a) Structure of a nanobody-stabilized active state of the beta(2) adrenoceptor. *Nature* **469**(7329): 175-180.

Rasmussen SG, DeVree BT, Zou Y, Kruse AC, Chung KY, Kobilka TS, Thian FS, Chae PS, Pardon E, Calinski D, Mathiesen JM, Shah ST, Lyons JA, Caffrey M, Gellman SH, Steyaert J, Skiniotis G, Weis WI, Sunahara RK and Kobilka BK (2011b) Crystal structure of the beta2 adrenergic receptor-Gs protein complex. *Nature* **477**(7366): 549-555.

Rasmussen SG, Jensen AD, Liapakis G, Ghanouni P, Javitch JA and Gether U (1999) Mutation of a highly conserved aspartic acid in the beta2 adrenergic receptor: constitutive activation, structural instability, and conformational rearrangement of transmembrane segment 6. *Mol Pharmacol* **56**(1): 175-184.

Redinger RN (2009) Fat storage and the biology of energy expenditure. *Transl Res* **154**(2): 52-60.

Reimann F, Habib AM, Tolhurst G, Parker HE, Rogers GJ and Gribble FM (2008) Glucose sensing in L cells: a primary cell study. *Cell Metab* **8**(6): 532-539.

Remedi MS and Nichols CG (2008) Chronic antidiabetic sulfonylureas in vivo: reversible effects on mouse pancreatic beta-cells. *PLoS Med* **5**(10): e206.

Rennie KL and Jebb SA (2005) Prevalence of obesity in Great Britain. *Obes Rev* **6**(1): 11-12.

Richardson RM, Kim C, Benovic JL and Hosey MM (1993) Phosphorylation and desensitization of human m2 muscarinic cholinergic receptors by two isoforms of the beta-adrenergic receptor kinase. *J Biol Chem* **268**(18): 13650-13656.

Rivero-Muller A, Chou YY, Ji I, Lajic S, Hanyaloglu AC, Jonas K, Rahman N, Ji TH and Huhtaniemi I (2010) Rescue of defective G protein-coupled receptor function in vivo by intermolecular cooperation. *Proc Natl Acad Sci U S A* **107**(5): 2319-2324.

Roberts LD, Murray AJ, Menassa D, Ashmore T, Nicholls AW and Griffin JL (2011) The contrasting roles of PPARdelta and PPARgamma in regulating the metabolic switch between oxidation and storage of fats in white adipose tissue. *Genome Biol* **12**(8): R75.

Rodriguez C, Gonzalez-Diez M, Badimon L and Martinez-Gonzalez J (2009) Sphingosine-1-phosphate: A bioactive lipid that confers high-density lipoprotein with vasculoprotection mediated by nitric oxide and prostacyclin. *Thromb Haemost* **101**(4): 665-673.

Rondard P, Huang S, Monnier C, Tu H, Blanchard B, Oueslati N, Malhaire F, Li Y, Trinquet E, Labesse G, Pin JP and Liu J (2008) Functioning of the dimeric GABA(B) receptor extracellular domain revealed by glycan wedge scanning. *EMBO J* **27**(9): 1321-1332.

Rose RH, Briddon SJ and Hill SJ (2012) A novel fluorescent histamine H(1) receptor antagonist demonstrates the advantage of using fluorescence correlation spectroscopy to study the binding of lipophilic ligands. *Br J Pharmacol* **165**(6): 1789-1800.

Rose RH, Briddon SJ and Holliday ND (2010) Bimolecular fluorescence complementation: lighting up seven transmembrane domain receptor signalling networks. *Br J Pharmacol* **159**(4): 738-750.

Rosen H, Gonzalez-Cabrera PJ, Sanna MG and Brown S (2009) Sphingosine 1-phosphate receptor signaling. *Annu Rev Biochem* **78**: 743-768.

Rosenbaum DM, Cherezov V, Hanson MA, Rasmussen SG, Thian FS, Kobilka TS, Choi HJ, Yao XJ, Weis WI, Stevens RC and Kobilka BK (2007) GPCR engineering yields high-resolution structural insights into beta2-adrenergic receptor function. *Science* **318**(5854): 1266-1273.

Rovati GE, Capra V and Neubig RR (2007) The highly conserved DRY motif of class A G protein-coupled receptors: beyond the ground state. *Mol Pharmacol* **71**(4): 959-964.

Rozenfeld R and Devi LA (2007) Receptor heterodimerization leads to a switch in signaling: beta-arrestin2-mediated ERK activation by mu-delta opioid receptor heterodimers. *FASEB J* **21**(10): 2455-2465.

Rozenfeld R and Devi LA (2011) Exploring a role for heteromerization in GPCR signalling specificity. *Biochem J* **433**(1): 11-18.

Rucker D, Padwal R, Li SK, Curioni C and Lau DC (2007) Long term pharmacotherapy for obesity and overweight: updated meta-analysis. *BMJ* **335**(7631): 1194-1199.

Sabin MA, Stewart CE, Crowne EC, Turner SJ, Hunt LP, Welsh GI, Grohmann MJ, Holly JM and Shield JP (2007) Fatty acid-induced defects in insulin signalling, in myotubes derived from children, are related to ceramide production from palmitate rather than the accumulation of intramyocellular lipid. *J Cell Physiol* **211**(1): 244-252.

Saha S, New LS, Ho HK, Chui WK and Chan EC (2010) Investigation of the role of the thiazolidinedione ring of troglitazone in inducing hepatotoxicity. *Toxicol Lett* **192**(2): 141-149.

Sakamoto J, Kimura H, Moriyama S, Odaka H, Momose Y, Sugiyama Y and Sawada H (2000) Activation of human peroxisome proliferator-activated receptor (PPAR) subtypes by pioglitazone. *Biochem Biophys Res Commun* **278**(3): 704-711.

Salom D, Lodowski DT, Stenkamp RE, Le Trong I, Golczak M, Jastrzebska B, Harris T, Ballesteros JA and Palczewski K (2006) Crystal structure of a photoactivated deprotonated intermediate of rhodopsin. *Proc Natl Acad Sci U S A* **103**(44): 16123-16128.

Salvado L, Serrano-Marco L, Barroso E, Palomer X and Vazquez-Carrera M (2012) Targeting PPARbeta/delta for the treatment of type 2 diabetes mellitus. *Expert Opin Ther Targets* **16**(2): 209-223.

Samama P, Cotecchia S, Costa T and Lefkowitz RJ (1993) A mutation-induced activated state of the beta 2-adrenergic receptor. Extending the ternary complex model. *J Biol Chem* **268**(7): 4625-4636.

Sambrook J and Russell DW (2001) Molecular Cloning. *CSHL Press*.

Sanchez-Laorden BL, Jimenez-Cervantes C and Garcia-Borron JC (2007) Regulation of human melanocortin 1 receptor signaling and trafficking by Thr-308 and Ser-316 and its alteration in variant alleles associated with red hair and skin cancer. *J Biol Chem* **282**(5): 3241-3251.

Sasaki S, Kitamura S, Negoro N, Suzuki M, Tsujihata Y, Suzuki N, Santou T, Kanzaki N, Harada M, Tanaka Y, Kobayashi M, Tada N, Funami M, Tanaka T, Yamamoto Y, Fukatsu K, Yasuma T and Momose Y (2011) Design, synthesis, and biological activity of potent and orally available G protein-coupled receptor 40 agonists. *J Med Chem* **54**(5): 1365-1378.

Sato K, Awasaki Y, Kandori H, Tanakamaru ZY, Nagai H, Baron D and Yamamoto M (2011) Suppressive effects of acid-forming diet against the tumorigenic potential of pioglitazone hydrochloride in the urinary bladder of male rats. *Toxicol Appl Pharmacol* **251**(3): 234-244.

Sawzdargo M, George SR, Nguyen T, Xu S, Kolakowski LF and O'Dowd BF (1997) A cluster of four novel human G protein-coupled receptor genes occurring in close proximity to CD22 gene on chromosome 19q13.1. *Biochem Biophys Res Commun* **239**(2): 543-547.

Scarselli M, Li B, Kim SK and Wess J (2007) Multiple residues in the second extracellular loop are critical for M3 muscarinic acetylcholine receptor activation. *J Biol Chem* **282**(10): 7385-7396.

Scheen AJ (2013) GLP-1 receptor agonists or DPP-4 inhibitors: How to guide the clinician? *Ann Endocrinol (Paris)*.

Scheer A, Costa T, Fanelli F, De Benedetti PG, Mhaouty-Kodja S, Abuin L, Nenniger-Tosato M and Cotecchia S (2000) Mutational analysis of the highly conserved arginine within the Glu/Asp-Arg-Tyr motif of the alpha(1b)-adrenergic receptor: effects on receptor isomerization and activation. *Mol Pharmacol* **57**(2): 219-231.

Scheerer P, Park JH, Hildebrand PW, Kim YJ, Krauss N, Choe HW, Hofmann KP and Ernst OP (2008) Crystal structure of opsin in its G-protein-interacting conformation. *Nature* **455**(7212): 497-502.

Schneider EH, Schnell D, Strasser A, Dove S and Seifert R (2010) Impact of the DRY motif and the missing "ionic lock" on constitutive activity and G-protein coupling of the human histamine H4 receptor. *J Pharmacol Exp Ther* **333**(2): 382-392.

Schottenfeld D, Beebe-Dimmer JL, Buffler PA and Omenn GS (2013) Current perspective on the global and United States cancer burden attributable to lifestyle and environmental risk factors. *Annu Rev Public Health* **34**: 97-117.

Schroder R, Janssen N, Schmidt J, Kebig A, Merten N, Hennen S, Muller A, Blattermann S, Mohr-Andra M, Zahn S, Wenzel J, Smith NJ, Gomeza J, Drewke C, Milligan G, Mohr K

and Kostenis E (2010) Deconvolution of complex G protein-coupled receptor signaling in live cells using dynamic mass redistribution measurements. *Nat Biotechnol* **28**(9): 943-949.

Schwartz TW, Frimurer TM, Holst B, Rosenkilde MM and Elling CE (2006) Molecular mechanism of 7TM receptor activation--a global toggle switch model. *Annu Rev Pharmacol Toxicol* **46**: 481-519.

Schwartz TW, Perlman S, Rosenkilde MM and Hjorth SA (1997) How receptor mutagenesis may confirm or confuse receptor classification. *Ann N Y Acad Sci* **812**: 71-84.

Seljeset S and Siehler S (2012) Receptor-specific regulation of ERK1/2 activation by members of the "free fatty acid receptor" family. *J Recept Signal Transduct Res* **32**(4): 196-201.

Senogles SE, Heimert TL, Odife ER and Quasney MW (2004) A region of the third intracellular loop of the short form of the D2 dopamine receptor dictates Gi coupling specificity. *J Biol Chem* **279**(3): 1601-1606.

Shah NR and Braverman ER (2012) Measuring adiposity in patients: the utility of body mass index (BMI), percent body fat, and leptin. *PLoS One* **7**(4): e33308.

Sheikh SP, Vilardarga JP, Baranski TJ, Lichtarge O, Iiri T, Meng EC, Nissenson RA and Bourne HR (1999) Similar structures and shared switch mechanisms of the beta2-adrenoceptor and the parathyroid hormone receptor. Zn(II) bridges between helices III and VI block activation. *J Biol Chem* **274**(24): 17033-17041.

Shenoy SK and Lefkowitz RJ (2003) Multifaceted roles of beta-arrestins in the regulation of seven-membrane-spanning receptor trafficking and signalling. *Biochem J* **375**(Pt 3): 503-515.

Shenoy SK, McDonald PH, Kohout TA and Lefkowitz RJ (2001) Regulation of receptor fate by ubiquitination of activated beta 2-adrenergic receptor and beta-arrestin. *Science* **294**(5545): 1307-1313.

Shenoy SK, Modi AS, Shukla AK, Xiao K, Berthouze M, Ahn S, Wilkinson KD, Miller WE and Lefkowitz RJ (2009) Beta-arrestin-dependent signaling and trafficking of 7-transmembrane receptors is reciprocally regulated by the deubiquitinase USP33 and the E3 ligase Mdm2. *Proc Natl Acad Sci U S A* **106**(16): 6650-6655.

Shi L and Javitch JA (2004) The second extracellular loop of the dopamine D2 receptor lines the binding-site crevice. *Proc Natl Acad Sci U S A* **101**(2): 440-445.

Shimpukade B, Hudson BD, Hovgaard CK, Milligan G and Ulven T (2012) Discovery of a potent and selective GPR120 agonist. *J Med Chem* **55**(9): 4511-4515.

Shiraishi J, Tanizawa H, Fujita M, Kawakami S and Bungo T (2011) Localization of hypothalamic insulin receptor in neonatal chicks: evidence for insulinergic system control of feeding behavior. *Neurosci Lett* **491**(3): 177-180.

Simon MI, Strathmann MP and Gautam N (1991) Diversity of G proteins in signal transduction. *Science* **252**(5007): 802-808.

Simonds WF (1999) G protein regulation of adenylate cyclase. *Trends Pharmacol Sci* **20**(2): 66-73.

Simonds WF, Butrynski JE, Gautam N, Unson CG and Spiegel AM (1991) G-protein beta gamma dimers. Membrane targeting requires subunit coexpression and intact gamma C-A-A-X domain. *J Biol Chem* **266**(9): 5363-5366.

Simpson KA, Martin NM and Bloom SR (2009) Hypothalamic regulation of food intake and clinical therapeutic applications. *Arq Bras Endocrinol Metabol* **53**(2): 120-128.

Singh N, Pydi SP, Upadhyaya J and Chelikani P (2011) Structural basis of activation of bitter taste receptor T2R1 and comparison with Class A G-protein-coupled receptors (GPCRs). *J Biol Chem* **286**(41): 36032-36041.

Smith NJ, Stoddart LA, Devine NM, Jenkins L and Milligan G (2009) The action and mode of binding of thiazolidinedione ligands at free fatty acid receptor 1. *J Biol Chem* **284**(26): 17527-17539.

Soga T, Ohishi T, Matsui T, Saito T, Matsumoto M, Takasaki J, Matsumoto S, Kamohara M, Hiyama H, Yoshida S, Momose K, Ueda Y, Matsushime H, Kobori M and Furuichi K (2005) Lysophosphatidylcholine enhances glucose-dependent insulin secretion via an orphan G-protein-coupled receptor. *Biochem Biophys Res Commun* **326**(4): 744-751.

Sohy D, Yano H, de Nadai P, Urizar E, Guillabert A, Javitch JA, Parmentier M and Springael JY (2009) Hetero-oligomerization of CCR2, CCR5, and CXCR4 and the protean effects of "selective" antagonists. *J Biol Chem* **284**(45): 31270-31279.

Sondek J, Bohm A, Lambright DG, Hamm HE and Sigler PB (1996) Crystal structure of a G-protein beta gamma dimer at 2.1A resolution. *Nature* **379**(6563): 369-374.

Soto-Guzman A, Robledo T, Lopez-Perez M and Salazar EP (2008) Oleic acid induces ERK1/2 activation and AP-1 DNA binding activity through a mechanism involving Src kinase and EGFR transactivation in breast cancer cells. *Mol Cell Endocrinol* **294**(1-2): 81-91.

Southern PJ and Berg P (1982) Transformation of mammalian cells to antibiotic resistance with a bacterial gene under control of the SV40 early region promoter. *J Mol Appl Genet* **1**(4): 327-341.

Stanley S, Wynne K and Bloom S (2004) Gastrointestinal satiety signals III. Glucagon-like peptide 1, oxyntomodulin, peptide YY, and pancreatic polypeptide. *Am J Physiol Gastrointest Liver Physiol* **286**(5): G693-697.

Stanley WC, Dabkowski ER, Ribeiro RF, Jr. and O'Connell KA (2012) Dietary fat and heart failure: moving from lipotoxicity to lipoprotection. *Circ Res* **110**(5): 764-776.

Steneberg P, Rubins N, Bartoov-Shifman R, Walker MD and Edlund H (2005) The FFA receptor GPR40 links hyperinsulinemia, hepatic steatosis, and impaired glucose homeostasis in mouse. *Cell Metab* **1**(4): 245-258.

Stephenson RP (1956) A modification of receptor theory. *Br J Pharmacol Chemother* **11**(4): 379-393.

Stoddart LA, Brown AJ and Milligan G (2007) Uncovering the pharmacology of the G protein-coupled receptor GPR40: high apparent constitutive activity in guanosine 5'-O-(3-[35S]thio)triphosphate binding studies reflects binding of an endogenous agonist. *Mol Pharmacol* **71**(4): 994-1005.

Stoddart LA, Smith NJ and Milligan G (2008) International Union of Pharmacology. LXXI. Free Fatty Acid Receptors FFA1,-2, and-3: Pharmacology and Pathophysiological Functions. *Pharmacological Reviews* **60**(4): 405-417.

Stoddart LA, Vernall AJ, Denman JL, Briddon SJ, Kellam B and Hill SJ (2012) Fragment screening at adenosine-A(3) receptors in living cells using a fluorescence-based binding assay. *Chem Biol* **19**(9): 1105-1115.

Strader CD, Sigal IS, Candelore MR, Rands E, Hill WS and Dixon RA (1988) Conserved aspartic acid residues 79 and 113 of the beta-adrenergic receptor have different roles in receptor function. *J Biol Chem* **263**(21): 10267-10271.

Sugden MC and Holness MJ (2008) Role of nuclear receptors in the modulation of insulin secretion in lipid-induced insulin resistance. *Biochem Soc Trans* **36**(Pt 5): 891-900.

Sum CS, Tikhonova IG, Costanzi S and Gershengorn MC (2009) Two arginine-glutamate ionic locks near the extracellular surface of FFAR1 gate receptor activation. *J Biol Chem* **284**(6): 3529-3536.

Sum CS, Tikhonova IG, Neumann S, Engel S, Raaka BM, Costanzi S and Gershengorn MC (2007) Identification of residues important for agonist recognition and activation in GPR40. *J Biol Chem* **282**(40): 29248-29255.

Sun F, Yu K, Yang Z, Wu S, Zhang Y, Shi L, Ji L and Zhan S (2012) Impact of GLP-1 receptor agonists on major gastrointestinal disorders for type 2 diabetes mellitus: a mixed treatment comparison meta-analysis. *Exp Diabetes Res* **2012**: 230624.

Sun Q, Hirasawa A, Hara T, Kimura I, Adachi T, Awaji T, Ishiguro M, Suzuki T, Miyata N and Tsujimoto G (2010) Structure-activity relationships of GPR120 agonists based on a docking simulation. *Mol Pharmacol*.

Suzuki M, Takaishi S, Nagasaki M, Onozawa Y, Iino I, Maeda H, Komai T and Oda T (2013) Medium-chain Fatty Acid-sensing Receptor, GPR84, Is a Proinflammatory Receptor. *J Biol Chem* **288**(15): 10684-10691.

Suzuki T, Igari S, Hirasawa A, Hata M, Ishiguro M, Fujieda H, Itoh Y, Hirano T, Nakagawa H, Ogura M, Makishima M, Tsujimoto G and Miyata N (2008) Identification of G protein-coupled receptor 120-selective agonists derived from PPARgamma agonists. *J Med Chem* **51**(23): 7640-7644.

Sykaras AG, Demenis C, Case RM, McLaughlin JT and Smith CP (2012) Duodenal enteroendocrine I-cells contain mRNA transcripts encoding key endocannabinoid and fatty acid receptors. *PLoS One* **7**(8): e42373.

Takei K, McPherson PS, Schmid SL and De Camilli P (1995) Tubular membrane invaginations coated by dynamin rings are induced by GTP-gamma S in nerve terminals. *Nature* **374**(6518): 186-190.

Takeuchi M, Hirasawa A, Hara T, Kimura I, Hirano T, Suzuki T, Miyata N, Awaji T, Ishiguro M and Tsujimoto G (2013) FFA1-selective agonistic activity based on docking simulation using FFA1 and GPR120 homology models. *Br J Pharmacol* **168**(7): 1570-1583.

Talsania T, Anini Y, Siu S, Drucker DJ and Brubaker PL (2005) Peripheral exendin-4 and peptide YY(3-36) synergistically reduce food intake through different mechanisms in mice. *Endocrinology* **146**(9): 3748-3756.

Talukdar S, Olefsky JM and Osborn O (2011) Targeting GPR120 and other fatty acid-sensing GPCRs ameliorates insulin resistance and inflammatory diseases. *Trends Pharmacol Sci* **32**(9): 543-550.

Tan CP, Feng Y, Zhou YP, Eiermann GJ, Petrov A, Zhou C, Lin S, Salituro G, Meinke P, Mosley R, Akiyama TE, Einstein M, Kumar S, Berger JP, Mills SG, Thornberry NA, Yang L and Howard AD (2008) Selective small-molecule agonists of G protein-coupled receptor 40 promote glucose-dependent insulin secretion and reduce blood glucose in mice. *Diabetes* **57**(8): 2211-2219.

Tanaka T, Katsuma S, Adachi T, Koshimizu TA, Hirasawa A and Tsujimoto G (2008a) Free fatty acids induce cholecystokinin secretion through GPR120. *Naunyn Schmiedebergs Arch Pharmacol* **377**(4-6): 523-527.

Tanaka T, Yano T, Adachi T, Koshimizu TA, Hirasawa A and Tsujimoto G (2008b) Cloning and characterization of the rat free fatty acid receptor GPR120: in vivo effect of the natural ligand on GLP-1 secretion and proliferation of pancreatic beta cells. *Naunyn Schmiedebergs Arch Pharmacol* **377**(4-6): 515-522.

Taneera J, Lang S, Sharma A, Fadista J, Zhou Y, Ahlqvist E, Jonsson A, Lyssenko V, Vikman P, Hansson O, Parikh H, Korsgren O, Soni A, Krus U, Zhang E, Jing XJ, Esguerra JL, Wollheim CB, Salehi A, Rosengren A, Renstrom E and Groop L (2012) A systems genetics approach identifies genes and pathways for type 2 diabetes in human islets. *Cell Metab* **16**(1): 122-134.

Tazoe H, Otomo Y, Karaki S, Kato I, Fukami Y, Terasaki M and Kuwahara A (2009) Expression of short-chain fatty acid receptor GPR41 in the human colon. *Biomed Res* **30**(3): 149-156.

Thompson D and Whistler JL (2011) Dopamine D(3) receptors are down-regulated following heterologous endocytosis by a specific interaction with G protein-coupled receptor-associated sorting protein-1. *J Biol Chem* **286**(2): 1598-1608.

Thorens B (1995) Glucagon-like peptide-1 and control of insulin secretion. *Diabete Metab* **21**(5): 311-318.

Tigerholm J, Borjesson SI, Lundberg L, Elinder F and Fransen E (2012) Dampening of hyperexcitability in CA1 pyramidal neurons by polyunsaturated fatty acids acting on voltage-gated ion channels. *PLoS One* **7**(9): e44388.

Tikhonova IG, Sum CS, Neumann S, Engel S, Raaka BM, Costanzi S and Gershengorn MC (2008) Discovery of novel agonists and antagonists of the free fatty acid receptor 1 (FFAR1) using virtual screening. *J Med Chem* **51**(3): 625-633.

Tikhonova IG, Sum CS, Neumann S, Thomas CJ, Raaka BM, Costanzi S and Gershengorn MC (2007) Bidirectional, iterative approach to the structural delineation of the functional "chemoprint" in GPR40 for agonist recognition. *J Med Chem* **50**(13): 2981-2989.

Toft-Nielsen MB, Madsbad S and Holst JJ (1999) Continuous subcutaneous infusion of glucagon-like peptide 1 lowers plasma glucose and reduces appetite in type 2 diabetic patients. *Diabetes Care* **22**(7): 1137-1143.

Tsao PI and von Zastrow M (2000) Type-specific sorting of G protein-coupled receptors after endocytosis. *J Biol Chem* **275**(15): 11130-11140.

Tsuga H, Kameyama K, Haga T, Kurose H and Nagao T (1994) Sequestration of muscarinic acetylcholine receptor m2 subtypes. Facilitation by G protein-coupled receptor

kinase (GRK2) and attenuation by a dominant-negative mutant of GRK2. *J Biol Chem* **269**(51): 32522-32527.

Tsujihata Y, Ito R, Suzuki M, Harada A, Negoro N, Yasuma T, Momose Y and Takeuchi K (2011) TAK-875, an orally available G protein-coupled receptor 40/free fatty acid receptor 1 agonist, enhances glucose-dependent insulin secretion and improves both postprandial and fasting hyperglycemia in type 2 diabetic rats. *J Pharmacol Exp Ther* **339**(1): 228-237.

Turton MD, O'Shea D, Gunn I, Beak SA, Edwards CM, Meeran K, Choi SJ, Taylor GM, Heath MM, Lambert PD, Wilding JP, Smith DM, Ghatei MA, Herbert J and Bloom SR (1996) A role for glucagon-like peptide-1 in the central regulation of feeding. *Nature* **379**(6560): 69-72.

Unick JL, Beavers D, Bond DS, Clark JM, Jakicic JM, Kitabchi AE, Knowler WC, Wadden TA, Wagenknecht LE and Wing RR (2013) The long-term effectiveness of a lifestyle intervention in severely obese individuals. *Am J Med* **126**(3): 236-242, 242 e231-232.

Valiquette M, Parent S, Loisel TP and Bouvier M (1995) Mutation of tyrosine-141 inhibits insulin-promoted tyrosine phosphorylation and increased responsiveness of the human beta 2-adrenergic receptor. *EMBO J* **14**(22): 5542-5549.

Vanderheyden V, Devogelaere B, Missiaen L, De Smedt H, Bultynck G and Parys JB (2009) Regulation of inositol 1,4,5-trisphosphate-induced Ca2+ release by reversible phosphorylation and dephosphorylation. *Biochim Biophys Acta* **1793**(6): 959-970.

Venkatakrishnan AJ, Deupi X, Lebon G, Tate CG, Schertler GF and Babu MM (2013) Molecular signatures of G-protein-coupled receptors. *Nature* **494**(7436): 185-194.

Vernall AJ, Stoddart LA, Briddon SJ, Hill SJ and Kellam B (2012) Highly potent and selective fluorescent antagonists of the human adenosine A(3) receptor based on the 1,2,4-triazolo[4,3-a]quinoxalin-1-one scaffold. *J Med Chem* **55**(4): 1771-1782.

Vettor R, Granzotto M, De Stefani D, Trevellin E, Rossato M, Farina MG, Milan G, Pilon C, Nigro A, Federspil G, Vigneri R, Vitiello L, Rizzuto R, Baratta R and Frittitta L (2008) Loss-of-function mutation of the GPR40 gene associates with abnormal stimulated insulin secretion by acting on intracellular calcium mobilization. *J Clin Endocrinol Metab* **93**(9): 3541-3550.

Vilsboll T, Christensen M, Junker AE, Knop FK and Gluud LL (2012) Effects of glucagon-like peptide-1 receptor agonists on weight loss: systematic review and meta-analyses of randomised controlled trials. *BMJ* **344**: d7771.

Virtue S, Masoodi M, Velagapudi V, Tan CY, Dale M, Suorti T, Slawik M, Blount M, Burling K, Campbell M, Eguchi N, Medina-Gomez G, Sethi JK, Oresic M, Urade Y, Griffin JL and Vidal-Puig A (2012) Lipocalin prostaglandin D synthase and PPARgamma2 coordinate to regulate carbohydrate and lipid metabolism in vivo. *PLoS One* **7**(7): e39512.

Vogelstein B and Gillespie D (1979) Preparative and analytical purification of DNA from agarose. *Proc Natl Acad Sci U S A* **76**(2): 615-619.

Waldhoer M, Fong J, Jones RM, Lunzer MM, Sharma SK, Kostenis E, Portoghese PS and Whistler JL (2005) A heterodimer-selective agonist shows in vivo relevance of G protein-coupled receptor dimers. *Proc Natl Acad Sci U S A* **102**(25): 9050-9055.

Wall MA, Coleman DE, Lee E, Iniguez-Lluhi JA, Posner BA, Gilman AG and Sprang SR (1995) The structure of the G protein heterotrimer Gi alpha 1 beta 1 gamma 2. *Cell* **83**(6): 1047-1058.

Wang D, Sun X, Bohn LM and Sadee W (2005) Opioid receptor homo- and heterodimerization in living cells by quantitative bioluminescence resonance energy transfer. *Mol Pharmacol* **67**(6): 2173-2184.

Wang S, Hashemi T, Fried S, Clemmons AL and Hawes BE (1998) Differential intracellular signaling of the GalR1 and GalR2 galanin receptor subtypes. *Biochemistry* **37**(19): 6711-6717.

Wang XH, Chen SF, Jin HM and Hu RM (2009) Differential analyses of angiogenesis and expression of growth factors in micro- and macrovascular endothelial cells of type 2 diabetic rats. *Life Sci* **84**(7-8): 240-249.

Warne T, Serrano-Vega MJ, Baker JG, Moukhametzianov R, Edwards PC, Henderson R, Leslie AG, Tate CG and Schertler GF (2008) Structure of a beta1-adrenergic G-protein-coupled receptor. *Nature* **454**(7203): 486-491.

Watson SJ, Brown AJ and Holliday N (2012) Differential Signalling by Splice Variants of the Human Free Fatty Acid Receptor, GPR120. *Mol Pharmacol*.

Wauquier F, Philippe C, Leotoing L, Mercier S, Davicco MJ, Lebecque P, Guicheux J, Pilet P, Miot-Noirault E, Poitout V, Alquier T, Coxam V and Wittrant Y (2013) The free fatty acid receptor G protein-coupled receptor 40 (GPR40) protects from bone loss through inhibition of osteoclast differentiation. *J Biol Chem* **288**(9): 6542-6551.

Wellen KE and Thompson CB (2012) A two-way street: reciprocal regulation of metabolism and signalling. *Nat Rev Mol Cell Biol* **13**(4): 270-276.

White JF, Grodnitzky J, Louis JM, Trinh LB, Shiloach J, Gutierrez J, Northup JK and Grisshammer R (2007) Dimerization of the class A G protein-coupled neurotensin receptor NTS1 alters G protein interaction. *Proc Natl Acad Sci U S A* **104**(29): 12199-12204.

White JH, Wise A, Main MJ, Green A, Fraser NJ, Disney GH, Barnes AA, Emson P, Foord SM and Marshall FH (1998) Heterodimerization is required for the formation of a functional GABA(B) receptor. *Nature* **396**(6712): 679-682.

Whorton MR, Bokoch MP, Rasmussen SG, Huang B, Zare RN, Kobilka B and Sunahara RK (2007) A monomeric G protein-coupled receptor isolated in a high-density lipoprotein particle efficiently activates its G protein. *Proc Natl Acad Sci U S A* **104**(18): 7682-7687.

Whorton MR, Jastrzebska B, Park PS, Fotiadis D, Engel A, Palczewski K and Sunahara RK (2008) Efficient coupling of transducin to monomeric rhodopsin in a phospholipid bilayer. *J Biol Chem* **283**(7): 4387-4394.

Wild S, Roglic G, Green A, Sicree R and King H (2004) Global prevalence of diabetes - Estimates for the year 2000 and projections for 2030. *Diabetes Care* **27**(5): 1047-1053.

Williams JA, Batten SE, Harris M, Rockett BD, Shaikh SR, Stillwell W and Wassall SR (2012) Docosahexaenoic and eicosapentaenoic acids segregate differently between raft and nonraft domains. *Biophys J* **103**(2): 228-237.

Wise A, Jupe SC and Rees S (2004) The identification of ligands at orphan G-protein coupled receptors. *Annu Rev Pharmacol Toxicol* **44**: 43-66.

Wolfe BL, Marchese A and Trejo J (2007) Ubiquitination differentially regulates clathrin-dependent internalization of protease-activated receptor-1. *J Cell Biol* **177**(5): 905-916.

Wu B, Chien EY, Mol CD, Fenalti G, Liu W, Katritch V, Abagyan R, Brooun A, Wells P, Bi FC, Hamel DJ, Kuhn P, Handel TM, Cherezov V and Stevens RC (2010) Structures of the CXCR4 chemokine GPCR with small-molecule and cyclic peptide antagonists. *Science* **330**(6007): 1066-1071.

Wu G, Krupnick JG, Benovic JL and Lanier SM (1997) Interaction of arrestins with intracellular domains of muscarinic and alpha2-adrenergic receptors. *J Biol Chem* **272**(28): 17836-17842.

Wu H, Wacker D, Mileni M, Katritch V, Han GW, Vardy E, Liu W, Thompson AA, Huang XP, Carroll FI, Mascarella SW, Westkaemper RB, Mosier PD, Roth BL, Cherezov V and Stevens RC (2012) Structure of the human kappa-opioid receptor in complex with JDTic. *Nature* **485**(7398): 327-332.

Xiao K, Sun J, Kim J, Rajagopal S, Zhai B, Villen J, Haas W, Kovacs JJ, Shukla AK, Hara MR, Hernandez M, Lachmann A, Zhao S, Lin Y, Cheng Y, Mizuno K, Ma'ayan A, Gygi SP and Lefkowitz RJ (2010) Global phosphorylation analysis of beta-arrestin-mediated signaling downstream of a seven transmembrane receptor (7TMR). *Proc Natl Acad Sci U S A* **107**(34): 15299-15304.

Xiong Y, Miyamoto N, Shibata K, Valasek MA, Motoike T, Kedzierski RM and Yanagisawa M (2004) Short-chain fatty acids stimulate leptin production in adipocytes through the G protein-coupled receptor GPR41. *Proc Natl Acad Sci U S A* **101**(4): 1045-1050.

Xiong Y, Swaminath G, Cao Q, Yang L, Guo Q, Salomonis H, Lu J, Houze JB, Dransfield PJ, Wang Y, Liu JJ, Wong S, Schwandner R, Steger F, Baribault H, Liu L, Coberly S, Miao L, Zhang J, Lin DC and Schwarz M (2013) Activation of FFA1 mediates GLP-1 secretion in mice. Evidence for allosterism at FFA1. *Mol Cell Endocrinol* **369**(1-2): 119-129.

Yan L, Bai XL, Fang ZF, Che LQ, Xu SY and Wu D (2013) Effect of different dietary omega-3/omega-6 fatty acid ratios on reproduction in male rats. *Lipids Health Dis* **12**: 33.

Yaney GC and Corkey BE (2003) Fatty acid metabolism and insulin secretion in pancreatic beta cells. *Diabetologia* **46**(10): 1297-1312.

Yao F, Svensjo T, Winkler T, Lu M, Eriksson C and Eriksson E (1998) Tetracycline repressor, tetR, rather than the tetR-mammalian cell transcription factor fusion derivatives, regulates inducible gene expression in mammalian cells. *Hum Gene Ther* **9**(13): 1939-1950.

Yip PK, Pizzasegola C, Gladman S, Biggio ML, Marino M, Jayasinghe M, Ullah F, Dyall SC, Malaspina A, Bendotti C and Michael-Titus A (2013) The omega-3 Fatty Acid eicosapentaenoic Acid accelerates disease progression in a model of amyotrophic lateral sclerosis. *PLoS One* **8**(4): e61626.

Yun SP, Ryu JM, Jang MW and Han HJ (2011) Interaction of profilin-1 and F-actin via a beta-arrestin-1/JNK signaling pathway involved in prostaglandin E(2)-induced human mesenchymal stem cells migration and proliferation. *J Cell Physiol* **226**(2): 559-571.

Zhang J, Barak LS, Anborgh PH, Laporte SA, Caron MG and Ferguson SS (1999) Cellular trafficking of G protein-coupled receptor/beta-arrestin endocytic complexes. *J Biol Chem* **274**(16): 10999-11006.

Zhang J, Ferguson SS, Barak LS, Menard L and Caron MG (1996) Dynamin and beta-arrestin reveal distinct mechanisms for G protein-coupled receptor internalization. *J Biol Chem* **271**(31): 18302-18305.

Zhang L, Bijker MS and Herzog H (2011a) The neuropeptide Y system: pathophysiological and therapeutic implications in obesity and cancer. *Pharmacol Ther* **131**(1): 91-113.

Zhang L, Keung W, Samokhvalov V, Wang W and Lopaschuk GD (2010a) Role of fatty acid uptake and fatty acid beta-oxidation in mediating insulin resistance in heart and skeletal muscle. *Biochim Biophys Acta* **1801**(1): 1-22.

Zhang T, Yan Z, Sromek A, Knapp BI, Scrimale T, Bidlack JM and Neumeyer JL (2011b) Aminothiazolomorphinans with mixed kappa and mu opioid activity. *J Med Chem* **54**(6): 1903-1913.

Zhang X, Yan G, Li Y, Zhu W and Wang H (2010b) DC260126, a small-molecule antagonist of GPR40, improves insulin tolerance but not glucose tolerance in obese Zucker rats. *Biomed Pharmacother* **64**(9): 647-651.

Zhou C, Tang C, Chang E, Ge M, Lin S, Cline E, Tan CP, Feng Y, Zhou YP, Eiermann GJ, Petrov A, Salituro G, Meinke P, Mosley R, Akiyama TE, Einstein M, Kumar S, Berger J, Howard AD, Thornberry N, Mills SG and Yang L (2010) Discovery of 5-aryloxy-2,4-thiazolidinediones as potent GPR40 agonists. *Bioorg Med Chem Lett* **20**(3): 1298-1301.

Zimmerman B, Simaan M, Akoume MY, Houri N, Chevallier S, Seguela P and Laporte SA (2011) Role of ssarrestins in bradykinin B2 receptor-mediated signalling. *Cell Signal* **23**(4): 648-659.

Zoudilova M, Kumar P, Ge L, Wang P, Bokoch GM and DeFea KA (2007) Beta-arrestin-dependent regulation of the cofilin pathway downstream of protease-activated receptor-2. *J Biol Chem* **282**(28): 20634-20646.

Zurn A, Zabel U, Vilardaga JP, Schindelin H, Lohse MJ and Hoffmann C (2009) Fluorescence resonance energy transfer analysis of alpha 2a-adrenergic receptor activation reveals distinct agonist-specific conformational changes. *Mol Pharmacol* **75**(3): 534-541.